2015

ROBUST FAULT ANALYSIS FOR PERMANENT MAGNET DC MOTOR IN SAFETY CRITICAL APPLICATIONS

Abed, Wathiq

http://hdl.handle.net/10026.1/3550

COPYRIGHT NOTICE

ROBUST FAULT ANALYSIS FOR PERMANENT MAGNET DC MOTOR IN SAFETY CRITICAL APPLICATIONS

By

Wathiq Rafa Abed

A thesis submitted to Plymouth University

In partial fulfilment for the degree of

DOCTOR OF PHILOSOPHY

PLYMOUTH UNIVERSITY

2015

Abstract

Robust fault analysis (FA) including the diagnosis of faults and predicting their level of severity is necessary to optimise maintenance and improve reliability of Aircraft. Early diagnosis of faults that might occur in the supervised process renders it possible to perform important preventative actions.

The proposed diagnostic models were validated in two experimental tests. The first test concerned a single localised and generalised roller element bearing fault in a permanent magnet brushless DC (PMBLDC) motor. Rolling element bearing defect is one of the main reasons for breakdown in electrical machines. Vibration and current are analysed under stationary and non-stationary load and speed conditions, for a variety of bearing fault severities, and for both local and global bearing faults.

The second test examined the case of an unbalance rotor due to blade faults in a thruster, motor based on a permanent magnet brushed DC (PMBDC) motor. A variety of blade fault conditions were investigated, over a wide range of rotation speeds. The test used both discrete wavelet transform (DWT) to extract the useful features, and then feature reduction techniques to avoid redundant features. This reduces computation requirements and the time taken for classification by the application of an orthogonal fuzzy neighbourhood discriminant analysis (OFNDA) approach.

The real time monitoring of motor operating conditions is an advanced technique that presents the real performance of the motor, so that the dynamic recurrent neural network (DRNN) proposed predicts the conditions of components and classifies the different faults under different operating conditions. The results obtained from real time simulation demonstrate the effectiveness and reliability of the proposed methodology in accurately classifying faults and predicting levels of fault severity.

TABLE OF CONTENTS

CHAPTER 1: Introduction

CHAPTER 2: Background and Summary of Previous Work on Fault Diagnosis and Condition Monitoring

CHAPTER 3: Permanent Magnet DC Motor Characteristics

CHAPTER 5: PMDC Motor Faults Analysis under Stationary and Non-Stationary Operating Conditions

CHAPTER 6: Features Extraction and Dimensionality Reduction

CHAPTER 7: Fault Classification Based Dynamic Neural Network

CHAPTER 8: Results and Discussion

CHAPTER 9: Conclusion and Recommendations for Future Research

Appendices

List of Figures

Chapter 1

Chapter 2

Chapter 3

Chapter 4

Chapter 5

Chapter 6

Chapter 7

Chapter 8

Appendices

List of Tables

Chapter 7

Chapter 8

Appendices

List of Abbreviations

ACO	Ant colony optimisation
AI	Artificial intelligence
ANFIS	Adaptive Neuro Fuzzy Inference Systems
DFT	Discrete fourier transform
DIS	Data independent selection
DWT	Discrete wavelet transform
DNN	Dynamic neural network
DRNN	Dynamic recurrent neural network
EA	Envelope analysis
EKF	Extended Kalman filter
EMD	Empirical mode decomposition
EN	Elman network
FIR	Finite impulse response
FE	Finite element
FFT	Fast Fourier transform
FFNN	Feed-forward neural network
FLS	Fuzzy Logic system
GA	Genetic Algorithm
IIF	Infinite impulse response
HT	Hilbert transform
KF	Kalman filter
LDA	Linear discriminate analysis
MCSA	Motor current signature analysis
MDL	Minimum description length
MLP	Multilayer perceptron
MOSFET	Metal oxide semiconductor field effect transistor
NARX	Nonlinear autoregressive classifier with exogenous data
NDR	Nonlinear dimensionality reduction
NN	Neural Network
PCA	Principle component analysis
PMSM	Permanent magnet synchronous motor
PWM	Pulse width modulation
OFNDA	Orthogonal fuzzy neighbourhood discriminant analysis
PMBLDC	Permanent magnet brushless direct current
PMBDC	Permanent magnet brushed direct current
PMDC	Permanent magnet direct current
PSO	Particle swarm optimisation
RBF	Radial basis function
RNN	Recurrent neural network
STD	Stander deviation
STFT	Short time Fourier transform
SVM	Support vector machines
TDNN	Time delay neural network
USVs	Unmanned surface vehicles
UUV	Unmanned underwater vehicle
WVD	Wigner-Ville distribution
WPT	Wavelet packet transform
WT	Wavelet transform

ACKNOWLEDGEMENTS

First, I would like to thank all mighty Allah who blessed and inspired me with the strength, confidence and determination needed for the completion of my research project.

It is my pleasure to express sincere thanks to my supervisors, Dr. Sanjay Sharma and Prof. Robert Sutton for their assistance, encouragement, guidance, criticism and support throughout the present research project. I am also grateful for them for letting me develop my own ideas.

I would like to acknowledge the Iraqi Ministry of Higher Education and Scientific Research for the scholarship that provided the financial support for this PhD project.

Many thanks to the staff at the School Office, led by the Barbara Fuller who I am convinced can solve just about any problem us students seem to come up against.

Thanks are extended to the staff at the graduate school office. Lucy Cheetham (my first contact at the university before I was here), Francesca Niedzielski, Carole Watson, Sarah Kearns and Prof. Mick Fuller have likewise provided me with much appreciated assistance.

I am very grateful for the encouragement and support of my father Rafa Abed, my mother Khairiyah Mohammed, my brothers and sisters for a lifetime of support and encouragement. I am extremely grateful to my wife Shymma Yaseen and my children, Zahraa, Sajjad and Tiba, for their support, continuous encouragement, patience, and lovely smiles that can relieve any kind of tiredness.

I also wish to thank Amit Motwani, Andy Animmalia, Kayode Owa, Tomasz Szyrowski and all my colleagues and friends in AMS group at Plymouth University, for their support and our valuable discussions

Authors' Declaration

At no time during the registration for the degree of Doctor of Philosophy has the author been registered for any other University award without prior agreement of the Graduate Committee.

Word count of main body of thesis: 39,084

Wathiq Abed

 20 March 2015

CHAPTER 1

Introduction

"The chapter presents the Problem Statement for this research project, outlines the aims and objectives, and presents the structure of the thesis"

1.1   Problem Statement

Condition monitoring and fault diagnosis of electrical machines are necessary to optimise maintenance and improve reliability levels, especially in critical application, as shown in Figure 1.1. Electrical machines are subjected to a wide variety of abnormal operating conditions, and early diagnosis of faults that might occur in the supervised process renders it possible to perform important preventative actions. Moreover, it allows one to avoid heavy economic losses involved in stopped production, and the replacement of elements and parts. This has led to the study and development of concepts of modern fault diagnostics and condition monitoring (Tavner 2008).

Faults that occur in electrical machines can be divided into two categories: electrical and mechanical faults, as will be explained in Chapter 2. Although a variety of techniques have been proposed for electrical machinery fault condition monitoring and fault diagnosis, all these methods have limitations and more effective methods are needed to develop the reliability of diagnostics (see appendix A-1).

The high power density, high efficiency, long operating life, high torque to inertia and high efficiency of the permanent magnet DC (PMDC) motor have led to its use in applications for which the high reliability of the machine is a key-feature (Wenping et al. 2012). PMBLDC motors are essential components in electro-mechanical actuators (EMA) and cabin pressure control of aircraft, due to advantages (Villani et al. 2012 and Jose 2010). The proposed fault diagnosis approach will be implemented for permanent magnet brushless DC (PMBLDC) motor and for thrust motor blade faults, both in operations based on a PMBDC motor.

PMBLDC motors are essential components in electro-mechanical actuators (EMA) and cabin pressure control of aircraft, due to advantages such as high efficiency, long operating life and high torque to inertia ratio (Villani et al. 2012). Industrial systems are dynamic and non-linear in nature, and hence during their identification it seems desirable to employ the models which can represent the dynamic of the system. Non-stationary operating conditions represent the most common PMBLDC motor applications and almost all of the available literatures in the field of electrical motor diagnostics assume that the motor is operating at a constant speed (Rajagopalan 2006).

Thrust motors based on a permanent magnet brushed (PMDC) motor are typically used in the propulsion systems of small electric-powered boats, such as USVs. USVs are now being employed by the scientific, offshore and naval sectors to perform a multitude of different tasks. As a consequence of their success, these sectors are now demanding longer mission lengths coupled with increasing vehicle autonomy. Furthermore, PMDC motors are most commonly used in variable speed and torque applications such as antenna positioning, medical equipment agricultural equipment, door openers (Jacek 2013) and nuclear power plants (Krishnan 2010).

There are essentially four main distinct fault diagnosis approaches soft computing, signal processing, physics-based models and hybrid methods (Sobhani and Khorasani 2009) that one could investigate, as will be discussed in Chapter 2. The main purpose of this chapter is to present the motivations behind this project, to list the aims and objectives of the project, as given in **Section 1.2,** and the main contributions of the thesis to existing knowledge, see **Section 1.3**. Poster and paper presentations were given at relevant conferences and several papers have been published, as detailed in **Section 1.4.** Finally, **Section 1.5** provides a brief overview of the thesis structure.
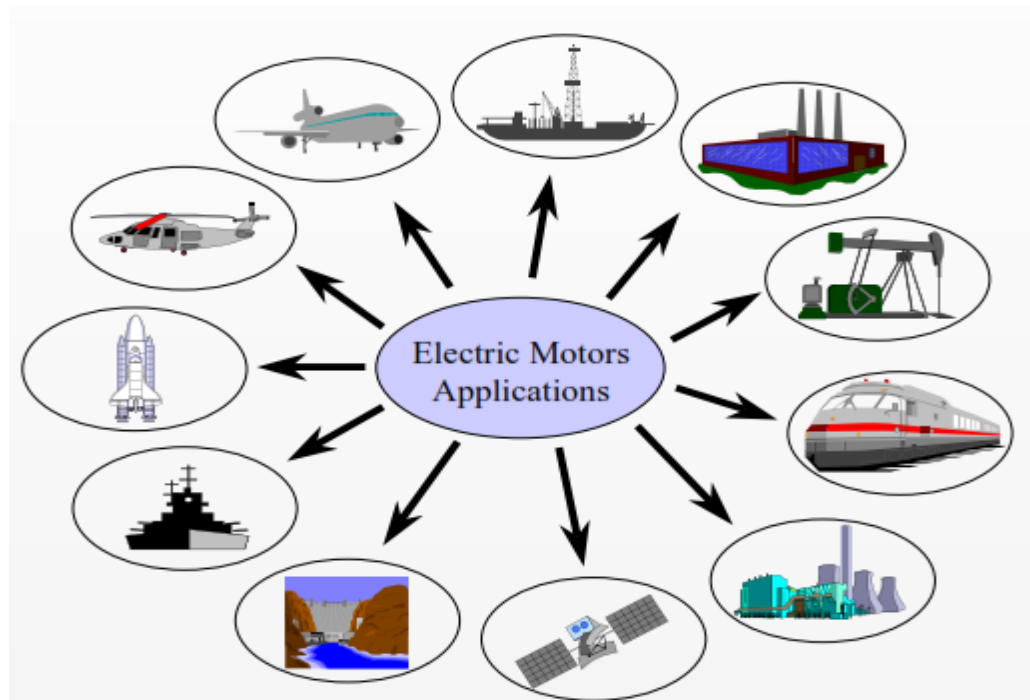
Figure 1.1 Electrical motor applications (Toliyat 2002). Permission to reproduce this figure has been granted by Hamid Toliyat

1.2 Aim and Objectives of The Research

The aim of this work is to develop a new fault analysis (FA) scheme for PMDC motor used in high performance applications that can accurately detect faults and provide useful information about the detected faults. For this purpose, a robust FA approach for rolling element bearing and blades faults, under a variety of operating conditions including speed and load, has been proposed.

The proposed diagnostic procedures used in this thesis include three main stages, as illustrated in Figure 1.2. In the first stage, the data (current and vibration) are collected and then discrete wavelet transform (DWT) is optimised then used to extract the useful features in time and frequency domains.

In the second stage, the features are reduced to remove redundancy and to decrease the training time. An inaccurate reduction feature tool may remove useful information and will jeopardise the overall performance, and thus the feature reduction stage represents the critical stage in the diagnosis process. The final stage is fault classification using dynamic neural network (DRNN).
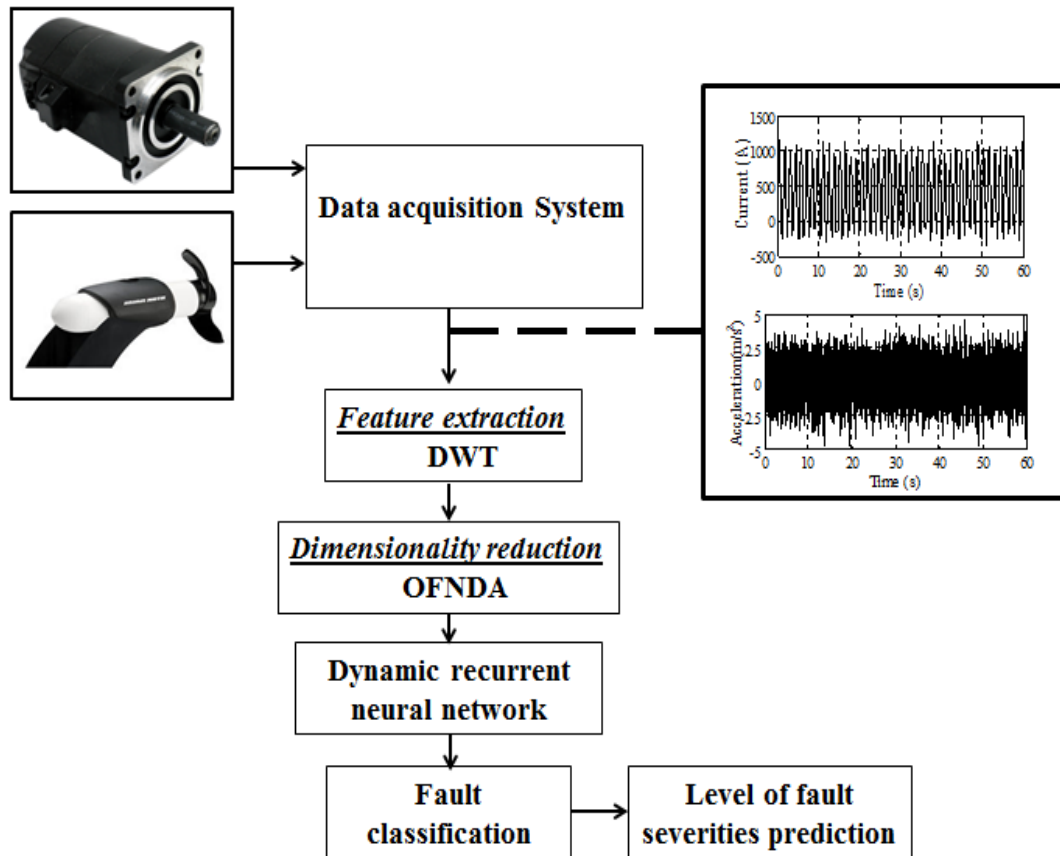
Figure 1.2 The proposed fault diagnosis process

To achieve this aim the following objectives are identified:-

➢ To investigate experimentally the characteristic effects of rolling element bearing faults in the stator currents and raw vibration signals of a PMBLDC motor operating

under various speeds and loads conditions. To achieve this, the various PMBLDC motor rolling element bearing faults, such as single localised faults (inner race; outer race; ball faults) and generalised bearing faults (corrosion) are replicated in a laboratory and their effect on the spectrum of the motor current and vibration studied. This helps in better understanding the behaviour of bearing defects in PMBLDC motors (Chapter 4).

➢ To validate the proposed approach, unbalanced rotors due to blades faults, and their effect on the motor current and vibration spectrums are presented, under different operation speeds (Chapter 4).

➢ To increase fault diagnosis reliability, especially for critical applications, the current signal has been used together with the vibration signal as another fault indicator (Chapter 5).

➢ To develop a features extraction tool suitable for machinery fault diagnosis. The most significant features are crucially important for pattern recognition problems. To extract the useful information, DWT a signal analysis method that provides the time and frequency information of the signal was applied (chapter 6).

➢ To reduce additional computational time for fault classification. An accurate dimensionality reduction tool is needed to select the most informative features from the general feature set. In this, orthogonal fuzzy neighbourhood discriminant analysis (OFNDA) is implemented as a new approach for feature reduction; it works to maximise the distance between features belonging to different classes, while minimise the distance between features in the same class, taking into account the contribution of the samples to the different classes (chapter 6).

➤ To develop a new and robust FA algorithm under stationary and non-stationary operating conditions. A DRNN have been implemented for fault detection and diagnosis, and fault severity prediction. With this kind of the network an approach based on the feedback from outputs has to be applied to the input (Chapter 7).

1.3 Major Contributions to Knowledge

As has been established in previous discussions, effective fault detection is very important for PMDC motor applications. The research performed in this work addresses rolling element bearings in PMBLDC motors, and unbalanced mechanical load in PMBDC motors (thrust motor), and proposes a robust FA system to detect and diagnose rolling element bearing faults and unbalanced mechanical loads for PMDC motors (brushed and brushless) working under different operating conditions. The main contributions of this research to the field of electrical machine condition monitoring are summarised as follows (see Figure 1.3):

➤ Set up an experimental test for the PMBLDC motor, operating under healthy and different rolling element bearing fault conditions (localised and generalised), and analyse the performances of the motor under stationary and variable loads and speed conditions. Set up an experiment to test PMBDC motors for blade faults.

➤ Overcome the limitations of vibration signal especially in low speed conditions, because the energy generated from bearing defects might not show any important change in signature and thus become undetectable. Stator current was implemented together with vibration signal under stationary and non-stationary operating conditions, using current as fault indicator will not increasing cost because current sensor already included in electrical protection system. (Chapters 4 and 5).

➤ In designing a reliable and accurate diagnosis technique, it is critical to find a set of redundant features to reduce additional computation and time taken for classification. Therefore, an accurate dimensionality reduction tool is needed to remove redundant features. Additionally the total classification time can be reduced using dimension reduction techniques. OFNDA is suggested for feature reduction. There are no accounts in the literature of using the intelligent features of OFNDA for feature reduction in the fault diagnosis of an electrical motor (Chapter 6).

➤ Algorithms for DRNN have been developed and proposed, allowing improved fault prediction accuracy of condition monitoring systems (see Chapter 7). Both the fault location and fault severity prediction can be identified with this intelligent diagnosis approach.
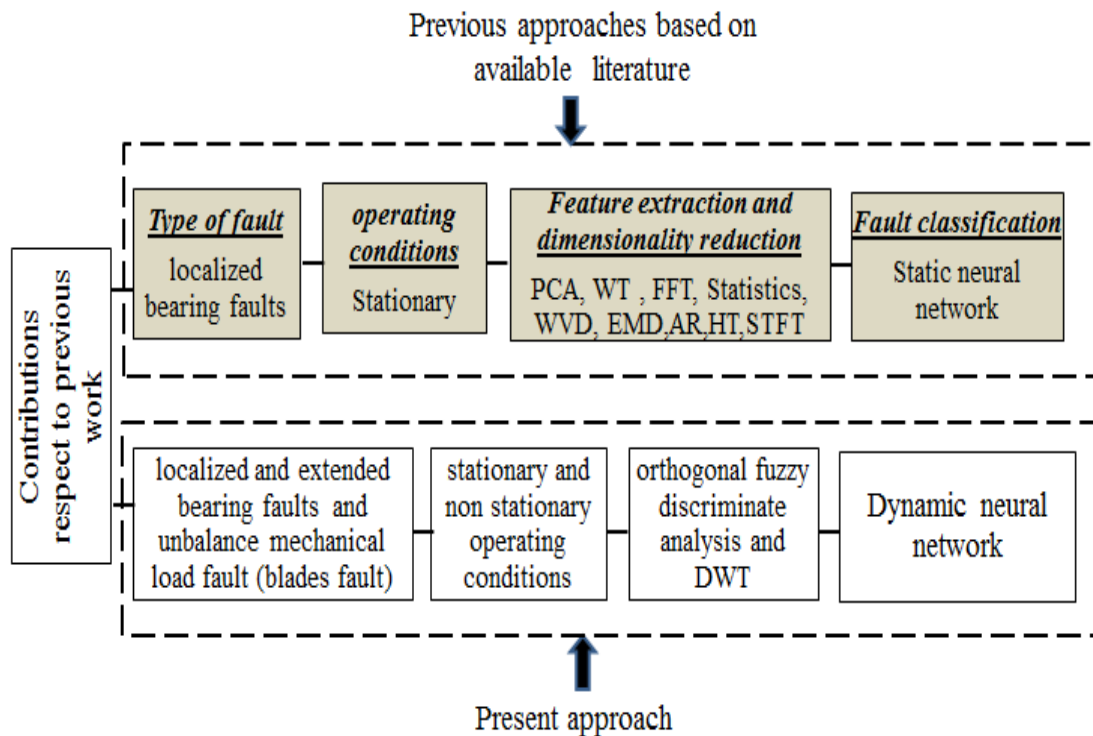
Figure 1.3 Contributions to knowledge in present fault analysis approach

1.4 List of Publications

The results of the work have been presented in journals and conferences papers. Another journal and a conference paper are expected after the completion of the thesis.

❖ **Journal Papers**

1- Abed W, Sharma SK, Sutton R, and Amit Motwani (2015). 'A robust bearing fault detection and diagnosis technique for brushless DC motors under non-stationary operating conditions' *Journal of Control, Automation and Electrical Systems*, doi: 10.1007/s40313-015-0173-7.

2- Abed W, Sharma SK, Sutton R (2015)'Neural network fault diagnosis of a trolling motor based on feature reduction techniques for an unmanned surface vehicle', Proceedings of the Institution of Mechanical Engineers, Part I: Journal of Systems and Control Engineering doi: 10.1007/s40313-015-0173-7.

3- Abed W, Sharma SK, Sutton R 'Unmanned marine vehicle thruster fault diagnosis', submitted for special issue of the *International Journal of Adaptive Control and Signal Procession*

❖ **Conferences Papers and Technical Report**

4- Abed W, Sharma SK, Sutton R. (2013) 'Fault diagnosis of brushless DC motor for an aircraft actuator using a neural wavelet network' *Proceedings of the 1st IET Control and Automation Conference*, Conference Aston Lakeside Centre, Birmingham, UK, 4 - 5 June, pp.1-6, doi: org/10.1049/cp.2013.0020.

5- Abed W Sharma SK, Sutton R. (2014) 'Intelligent Fault Diagnosis of an Unmanned Underwater Vehicle Electric Thruster Motor', *the Global Event for Undersea Defence and Technology (UDT)*, Liverpool, UK, 10-12 June.

6- Abed W, Sharma SK, Sutton R. (2104) 'Diagnosis of bearing fault of brushless DC motor based on dynamic neural network and orthogonal fuzzy neighborhood discriminant analysis', *10th International Conference of the United Kingdom, Automatic Control Council (UKACC)*, Loughborough University, UK, 9 - 11 July, pp. 378-382,doi: 10.1109/CONTROL.2014.6915170.

7- Abed W, Sharma SK, Sutton R.(2015)'Corrosion Fault Diagnosis on Rolling Element Bearing under variable load and speed conditions *' , 9th IFAC Symposium on Control of Power and Energy Systems (CPES)*, New Delhi, India, 9-11 December.

8- Abed W. (2012). 'Hardware Interface for Trolling Motor', Technical Notes, *Autonomous Marine Systems (AMS),* Plymouth University.

❖ Invited Talks and Poster Presentations

In addition to the peer reviewed publications, the work described in this thesis has also been presented on the following occasions.

9- Abed W, Sharma SK, Sutton R. (2013). 'Fault diagnosis of trolling motor based on unmanned surface vehicle using neural network', Plymouth Marine Laboratory Conference, 28th November, Plymouth, UK.

10- Abed W. (2014) 'Robust Fault analysis Technique for Permanent Magnet DC Motor In safety Critical Applications', United Kingdom Automatic Control Council (UKACC) day. London. 23rd October, available online at: http://ukacc. group. shef. ac.uk/?page_id=570.

11- Abed W, (2012).'Fault Diagnosis of Aircraft Actuator Drives using Wavelet Neural Networks', The Postgraduate Society Annual Conference, Plymouth University, UK, 26th June.

12- Abed W, (2012). 'Inter turn Fault Diagnosis of Brushless DC motor For Aircraft Actuator Using Intelligent Techniques', The Postgraduate Society Conference Series, Plymouth University, 21st Nov.

13- Abed W,(2014)'A new approach to intelligent fault diagnosis of bearing in brushless DC motor under non-stationary operating conditions', Iraqi Cultural Attaché, Plymouth University, 13 March.

14- Abed W, (2014) 'Application of Dynamic Neural Network for Bearing Fault Diagnosis of BLDC Motor in Aircraft', Postgraduate Society Conference, Plymouth University, 19th March.

❖ Training Courses

1- PhD student workshop. United Kingdom Automatic Control Council (UKACC), Loughborough University, UK, 8th July 2014.

2- Learning and Teaching for General Teaching Associates Course (GTA), Plymouth, University, UK, 2012.

3- Learning and Teaching for General Teaching Associates Course; Learning and Teaching for Postgraduate Certificate in Academic Practice (PGCAP), Plymouth University, UK, 2013.

1.5 Thesis Structure

The content of this thesis is organised into nine chapters (see Figure 1.4).

Chapter 1 provides a brief introduction to fault diagnosis. This chapter also summarises the thesis aim and objectives, its main of contributions to current knowledge and a list of related publications.

Chapter 2 presents the literature review of previous research into fault detection and diagnosis techniques, as well as data processing, feature subset selection and fault classification.

Chapter 3 introduces the both types of PMDC motor. Firstly, the symptoms and mechanisms of electrical and mechanical faults in the PMDC motor are presented. Secondly, the main fault diagnosis techniques of electrical machines are described.

Chapter 4 describes the experimental setup design for validating the proposed schemas. The experiments include building a test rig for rolling element bearings with both types of bearing fault (single local and generalised). The motor was tested under stationary and non-stationary operating conditions, and with different levels of fault severity. To validate the fault diagnosis approach, a second experiment was setup, to diagnosis unbalanced mechanical loads (thruster motor blades faults) under a wide range of rotation speeds.

Chapter 5 introduces raw vibration and current measurements as indicator for detection and diagnosis in roller bearings and unbalance mechanical load faults. The acquired data is presented in time and frequency domains, to exam the effects of faults on motor performance.

Chapter 6 discusses different signal processing techniques in time, frequency and time-frequency domain. A DWT as feature extraction approach is presented, to extract the

useful features from the motor vibration and current signals. Before application, the DWT wavelet function and level are optimised. A new feature reduction approach in terms of electrical motor fault diagnosis has been proposed for dimensionality reduction, to eliminate irrelevant features that affect diagnosis accuracy.

Chapter 7 develops a dynamic neural network (DNN) for PMDC motor fault classification and level of fault severity prediction. A DRNN is fed by OFNDA features for training, testing and validation purposes. A mean squared error cost function is computed and desired outputs. The training of the network consists of finding a set of weights that minimise this cost function.

Chapter 8 presents the results of the proposed features extraction, dimensionality reduction and fault classification approaches, with accompanying discussion. Comparisons are also made with popular methods of feature reduction and fault classification, to evaluate the capability and effectiveness of the proposed techniques in real situations.

Chapter 9 presents the general conclusions drawn from this research, and proposes ideas for potential future work.
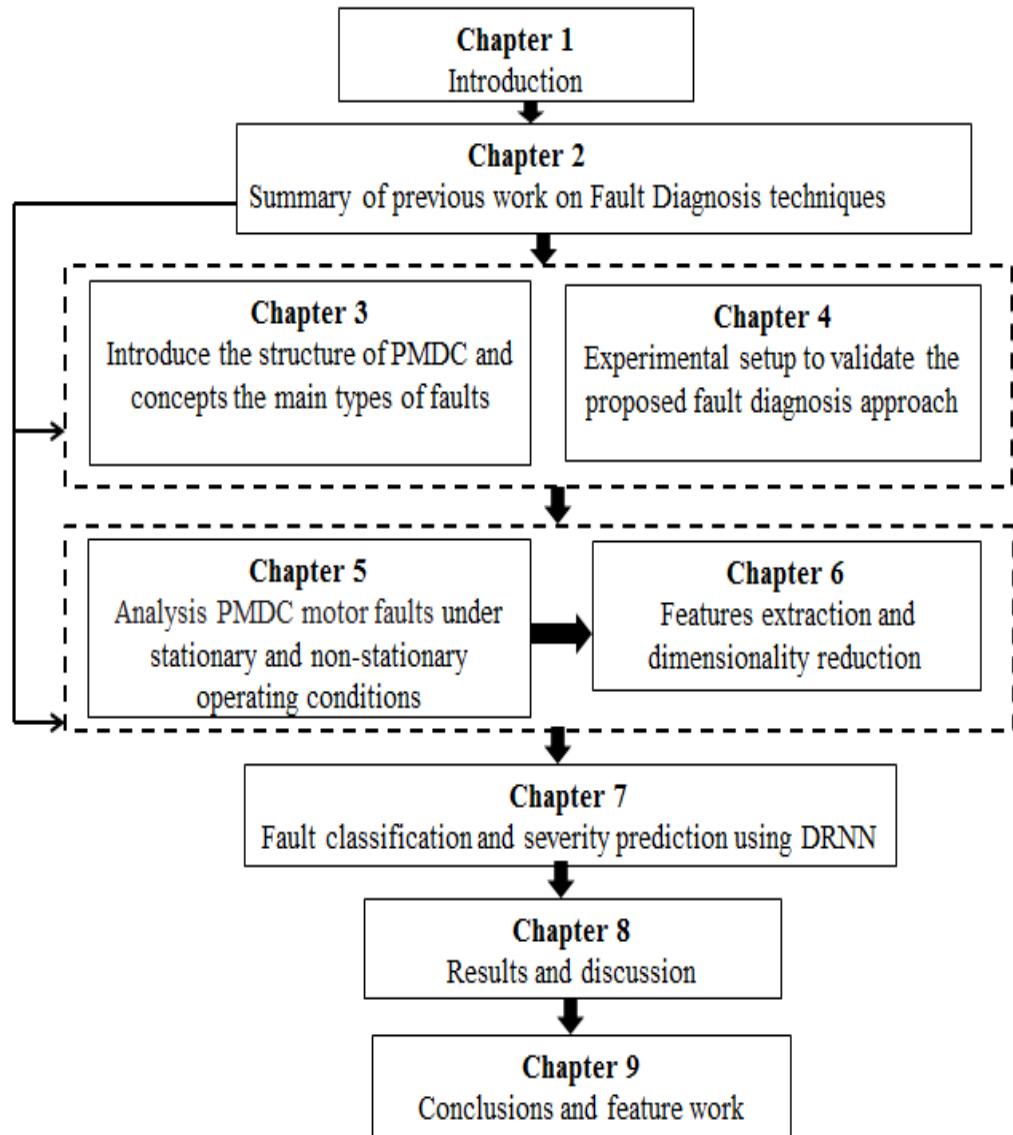
Figure 1.4 Structure of the thesis

CHAPTER 2

Literature Review

"This chapter presents a general review of the literature on electrical machine fault detection and isolation especially in critical applications. It emphasises the artificial intelligent techniques that are most commonly used for rolling element bearings and unbalanced mechanical load in PMDC motor"

2.1 Introduction

The manufacturers and users of electrical machines initially relied on simple protections such as over-current, over-voltage, and earth fault. Over time the tasks performed by these machines have grown more and more complex. It has now become very important to diagnose faults at their very inception, as unscheduled machine downtime can upset deadlines and cause heavy financial losses.

In general a failure, as opposed to a fault, is defined as '*a permanent interruption of a system's ability to perform a required function under specified operating conditions*' and it is a much more severe concept than a fault (Isermann 2006). The concept of fault diagnosis consists of the following three essential task models (Patan 2008):

➢ Fault detection (FD): detection of the occurrence of faults in the system that lead to undesired or intolerable behaviour of the whole system.

➢ Fault Detection and Diagnosis (FDD): detection and localisation of faults.

➢ Fault analysis (FA): determination of the type, cause and severity of faults, and prediction of possible future faults and the time frames in which these could develop,

using available data and knowledge about the behaviour of the diagnosed process, either mathematical, quantitative or qualitative.

FA of PMBDC motor is a challenging problem and has not been fully explored. The literature shows there is still a gap between FA theory and its application. Thus this thesis attempts to fill the gap by developing FA algorithms for PMDC motor. In researching pathways towards safe and reliable operations, a number of literature reviews on electrical machine fault diagnosis have been published, for example (Subhasis. et al. (2005), Yao and Toliyat (2012), Lee et al. (2014) and Henao et al. (2014).

In this research both types of rolling element bearing fault in the PMBLDC motor are presented, under a variety of operating conditions ranging from constant loads and speeds to continuous transient operation. This involves recognising the bearing and fault signatures produced in a PMBLDC motor, and estimating the severity of the fault both under stationary and non-stationary operating conditions, as well as validating the diagnosis approach with other types of fault and machines; unbalanced mechanical loads of PMBDC motor are considered.

Many fault diagnosis techniques are implemented to diagnose motor faults and each technique has its advantages and disadvantages. The proper selection of fault indicators, feature extraction techniques and dimensionality reduction tools, together with the fault classification algorithm, will overcome the challenges of accurate FA.

This chapter is divided into four further sections. Section 2.2 will give an overview of the common faults in electrical motors. Section 2.3 will present a summary of previous work that is related to recent developments in electrical motor FA. Section 2.4 will discuss the main condition monitoring indicators. Finally, section 2.5 presents conclusions drawn from this literature review.

2.2 The Basic Concepts of Fault Diagnosis Techniques

There are many reasons for fault occurrence. Some are due to errors in manufacturing, changes in environment and control action errors by humans, any of which may bring the system out of its operating point. (Schröder 2006). It is important to be able to detect faults while they are still developing and this is called incipient failure detection. A timely warning that can be followed by maintenance can avoid catastrophic failures and costly long down times. Undetected, these faults will have an effect on the system performance and lead to failure.

A typical fault diagnosis process consists of two stages: the residual generation and the residual evaluation. In the residual generation stage, a residual generator is designed to make its output robust against unknown inputs and system disturbances, while at the same time being sensitive to the fault. In the residual evaluation stage, the residual is processed to alert the operator to the fault and, further, to isolate it (Zhou et al. 2012).

For robust fault diagnosis purposes, the following conditions are needed (Dunn 2002):

➢ The need to improve accuracy in failure prediction.

➢ The need for an overall view of equipment condition.

➢ The need to reduce the cost of condition monitoring.

➢ The need to improve system reliability.

Many techniques have been implemented for electrical motor fault detection and diagnosis, such as artificial intelligence (AI), signal processing, model based and hybrid techniques, as shown in Figure 2.1. The strengths and drawbacks of each technique are discussed, based on literature reviews.

```
                    ┌─────────────────────────────────┐
                    │     Fault diagnosis methods     │
                    └─────────────────────────────────┘
                                    │
        ┌──────────────┬────────────┴─────────────┬──────────────┐
        ▼              ▼                           ▼              ▼
  ┌───────────┐  ┌───────────┐           ┌───────────┐  ┌───────────┐
  │Artificial │  │  Model    │           │  Signal   │  │  Hybrid   │
  │intelligence│  │  based    │           │processing │  │techniques │
  └───────────┘  └───────────┘           └───────────┘  └───────────┘
        │              │                       │              │
        ▼              ▼                       ▼              ▼
  ┌───────────┐  ┌───────────┐           ┌───────────┐  ┌───────────┐
  │  Neural   │  │ Parameter │           │Time domain│  │ Combined  │
  │  network  │  │estimation │           │  feature  │  │several methods│
  └───────────┘  └───────────┘           └───────────┘  └───────────┘
        │              │                       │
        ▼              ▼                       ▼
  ┌───────────┐  ┌───────────┐           ┌───────────┐
  │Fuzzy logic│  │  Parity   │           │ Frequency │
  │           │  │ relation  │           │domain feature│
  └───────────┘  └───────────┘           └───────────┘
        │              │                       │
        ▼              ▼                       ▼
  ┌───────────┐  ┌───────────┐           ┌───────────┐
  │  Genetic  │  │ Observers │           │Time – frequency│
  │algorithms │  │           │           │domain feature│
  └───────────┘  └───────────┘           └───────────┘
        │
        ▼
  ┌───────────┐
  │Expert system│
  └───────────┘
```
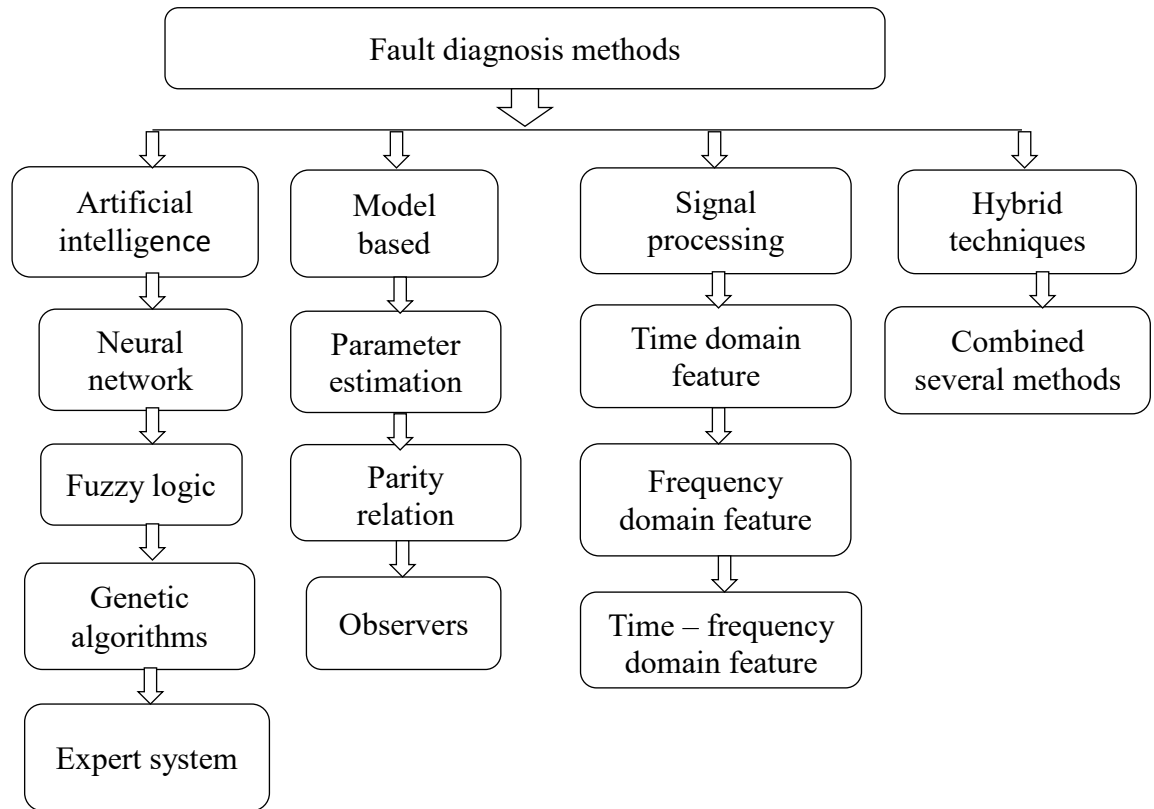
Figure 2.1 The main condition monitoring and fault diagnosis techniques

2.2.1 **Artificial intelligence techniques**

Recently, AI has been introduced as an accurate approach for condition monitoring and fault diagnosis purposes, where accurate mathematical models are difficult to develop. AI aims to generate classifying expressions simple enough to be understood easily by humans (Sun et al. 2014).

In this section a brief description of various AI techniques such as expert systems, on fuzzy logic system (FLS) (Lemos et al. 2013), neural network (NN), genetic algorithm (GA), adaptive neuro fuzzy inference systems (ANFIS) (Yilmaz and Ayaz 2009) and support vector machines (SVM) are discussed and applications of AI for electric motor fault diagnostics are considered.

Among the various pattern recognition approaches for condition monitoring and fault diagnosis of electrical machinery, NN have been commonly used, with the ability to

classify conditions based on training patterns from samples (Walker et al. 2014, Yang et al. 2013). Basically, a NN consists of a layer of input nodes, one or more layers of hidden nodes, one layer of output nodes, and connecting weights

An NN is an effective motor fault detection method while avoiding the need for a mathematical model. In addition, an NN can recognise patterns even at high noise levels (Ding et al. 2013). Different NN architectures have been developed for fault diagnosis purposes, including the FFNN (Ziaja et al. 2014), the Kohonen network (Germen et al. 2014), the radial basis function (RBF) network (Zarei et al. 2014) and Probabilistic neural network (PNN) (Li et al. 2014).

Mahammed and Hiyama (2011) compared FFNN, RBF network, Elman network (EN) and ANFIS methods for induction motor bearing fault diagnosis in order to select the optimal fault diagnosis method for the most commonly found inner race faults. From the comparison they found FFNN gives fewer validation errors for outer race and ball defects, while EN gives a better performance in contrast to validation errors, and FFNN and EN are the best static NN structures for rolling element bearing fault classification.

However, these techniques ignored the dynamic behaviour of electric motor, most industrial systems are dynamic and nonlinear in nature, and hence during their identification it seems desirable to employ the models which can represent the dynamics of the system. Recently great attention has been paid to the development of DNN due to their capabilities for modelling nonlinear dynamical systems.

In real-life applications there are several circumstances where the motor is never operating at a constant speed or with a constant load, such as in automotive and aircraft applications (Sadough et al. 2014). Hyun et al. (2010) and Yusuf et al. (2009) have shown that DNNs are an attractive method for fault diagnosis in electrical machines. They allow improved fault prediction accuracy. In addition, to learn the dynamics of

complicated nonlinear systems, DNN are more provide the capability which conventional static NN cannot model (Xuhong and Yigang 2005).

Unmanned surface vehicles (USVs) are now being employed by the scientific, offshore and naval sectors to perform a multitude of different tasks. As a consequence of their success, these sectors are now demanding longer mission lengths coupled with increasing vehicle autonomy. With an escalation in autonomy comes the need for higher reliability in such vehicles in order for them to better cope with unexpected events. Hence there is a growing interest in the use of fault detection and diagnostic techniques in unmanned underwater vehicle (UUV). The thruster of the UUV is one of the most common and important sources of faults, and it always has a direct effect on the control performance (Qian and Daqi 2009)

Hai et al. (2014) designed a petri-based recurrent neural network (RNN) to improve robustness in response to nonlinear characteristics of an open frame underwater vehicle. A threshold was used to regulate training and learning, and an online training algorithm was developed based on a gradient descent method. The results showed that the computational efficiency was improved and a faster convergence speed was obtained.

Ah Chung and Back (1994) reviewed a number of DNN that have been introduced by a number of researches. DNN can be represented as FFNN with layered dynamic neurons. It is done by introducing a linear dynamic system (Cho et al. 2010, Mohammadi et al. 2011) composed of dynamic neurons. In dynamic neurons, there is a finite impulse response (FIR) filter after the activation function that generates a dynamic mapping between the input and output of the neuron. NN of the dynamic type are discussed in detail in Chapter 6.

Similarly, Sina et al. (2014) used DNN but with infinite impulse response (IIR), as shown in Figure 2.2, to diagnose fault in a dual spool turbo fan engine in the aircraft.

The proposed fault diagnosis schemes consist of multiple DNN corresponding to various operating modes of the healthy and faulty engine conditions. Using the residuals that are generated by measuring the difference of each network output and measuring engine output, various criteria were established for accomplishing the fault diagnosis task that is, addressing the problem of fault detection and isolation of the system components.

Embedded linguistic knowledge and approximate reasoning capability represent the advantages of FLS as a fault diagnosis technique. The FLS method is based on the theory of fuzzy sets, which are an extension of binary sets and able to take in partial memberships that range between 0 and 1.
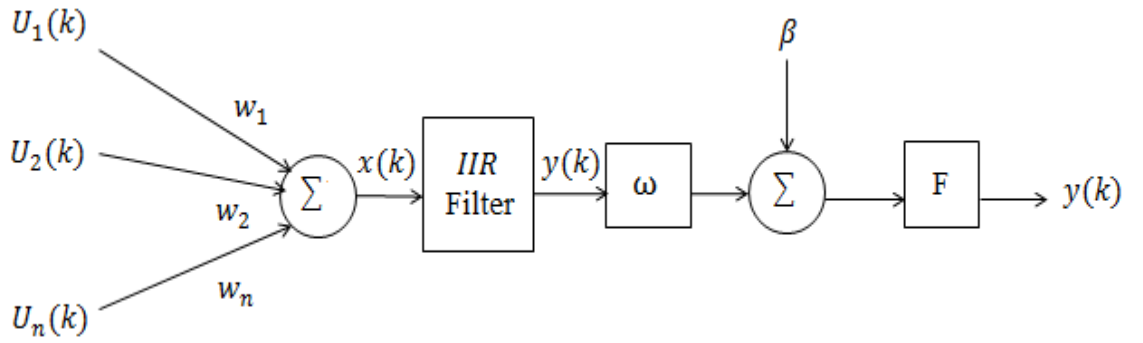
Figure 2.2 Dynamic neuron structures

Unlike NN, FLS models tend to a rule explosion, for instance, the number of rules increases exponentially if the number of variables or fuzzy sets per variable increases, making it complicated to identify the whole model from the knowledge of an expert only. Different automated techniques have been used recently for optimising fuzzy models, including NN and GA (Abdusslam 2012).

Lemos et al. (2013) suggested an adaptive fault diagnosis technique for dynamic systems and tested an FLS classifier offline and applied in real time. The FLS approach

allows quick detection of small faults, as the adaptive FLS threshold takes care of modelling errors.

However, FLS rules should be optimally designed to obtain robust diagnostics techniques and sometimes it is difficult to properly establish the FLS forecasting inference rules (Qing et al. 2013). Wen (2011) compared FLS and NN based FDD approaches for electrical motors and found that an FLS approach is capable of modelling a complex problem, employing an if-then type of expert rules and linguistic variables to capture directly the qualitative aspects of the human reasoning process involved. However it is difficult to tune the membership functions and the fuzzy rule.
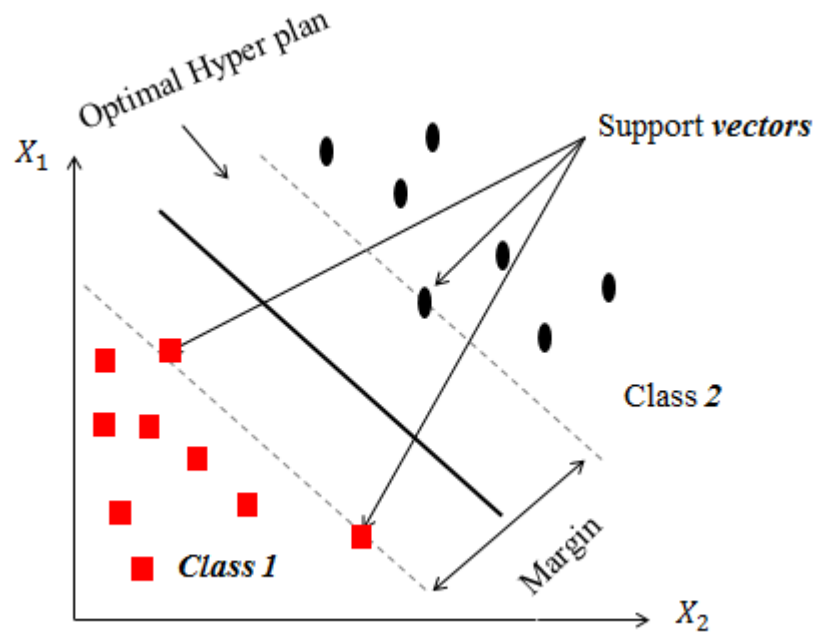
Figure 2.3 Support vectors machine classifier

Meanwhile, a NN based technique allows an accurate solution to a particular fault problem, without the need for knowledge about the faulty system. However, the main NN drawback is related to the fact that the exact architecture of the NN to be used is not known in advance On the other hand, an SVM is an effective tool for motor fault classification based on statistical learning theory, due to its good generalization abilities

(Ahmadi et al. 2014). The standard SVM is based on binary classification problems to determine a linear boundary between the two different classes, by maximising the distance of the nearest data to the boundary in each class, as shown in Figure 2.3. The nearest data points are known as support vectors.

Yizhuo et al. (2009) proposed an approach to diagnose rolling bearing faults based on nonlinear dimensionality reduction (NDR) and SVM for fault classification. In this approach time and frequency domain features were extracted from the original signal and then fed into a feature reduction tool to generate low dimension.

The results proved that NRD provides better performance than linear dimensionality reduction. However, an SVM requires rigorous tuning of kernel parameters and the process of optimising generates a large amount of calculation. Furthermore, SVM has high complexity and needs a wide range of data, and the traditional SVM is unusable with dynamic data (Xiao et al. 2013).

To deal with non-stationary vibration signals, Wavelet transform (WT) is presented as an effective feature extraction and denoising tool. Bin et al. (2011) and Kankar et al. (2011) used two criteria for selecting the best WT features. The first one uses maximum energy to shannon entropy ratio and the second one is based on maximum relative wavelet energy. These features are then used to feed machine learning approaches (NN, SVM) and a self-organising map.

On this basis, Khan and Rahman (2009) have developed a novel fault diagnosis technique for permanent magnet synchronous motor (PMSM) using wavelet packet transform (WPT) to process the line current to obtain features in the time and frequency domain, and used these as inputs to a three layer FFNN. The results showed the ability of the proposed technique to diagnose faults for on line implementation.

In designing a reliable and accurate diagnosis system based on NN techniques, it is critical to eliminate redundant features to reduce additional computational time for classification. Different feature reduction methods, such as kernel principle component analysis (KPCA) (Zhang, Y et al. 2013) and linear discriminate analysis (LDA) Xiaohang et al. (2013) have been used to reduce feature redundancy. Further discussion of feature reduction approaches will be presented in Chapter 5.

2.2.2 Model-based techniques

Model-based fault diagnosis can be defined as the detection and isolation of faults in the system based on a comparison of the system's available measurements with information represented by a model (Changning and Gang 2010). As illustrated in Figure 2.4, model-based techniques consist of the detection of faults in the technical process, including actuators, components and sensors, by measuring the available input and output variables $x(t)$ and $y(t)$. The detection methods generate residuals r, parameter estimates θ, or state estimates x, which are called features. By comparison with the normal features, changes in features are detected.

Model-based approaches have been implemented for fault diagnosis tasks, by attempting to match a mathematical model to a comprehensive model that would include effects due to abnormal conditions such as unbalance or misalignment, to produce the overall response of the system (Yan et al. 2014). Basic process model-based methods are: parity equations (Moseler et al. 1999), parameter estimation (Progovac et al. 2014) and output observers (Liu 2010). Owing to the simultaneous problem of fault detection and control of UUV, Davoodi et al. (2013) developed a dynamic observer. A single model was designed represent in both the control and a detector, where the detector is the dynamic observer and the controller is a state feedback controller based on the dynamic observer.
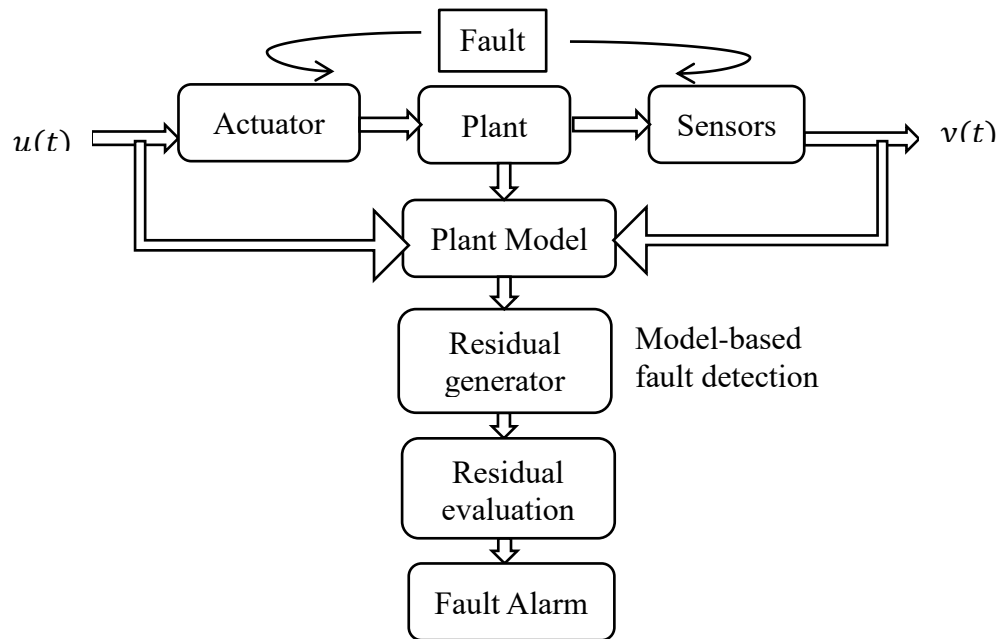
Figure 2.4 Scheme for the model-based fault detection (Isermann 2011),permission to reproduce this figure has been granted by springer science and business media

The parity relation is sometimes called consistency relation, or analytical redundancy relation. It directly checks the consistency between the system model and measured system outputs, and is thus the most realistic fault detection method. The main idea of this method is illustrated in Figure 2.5. The residual is based on parity relations, with u denoting the control signal input.
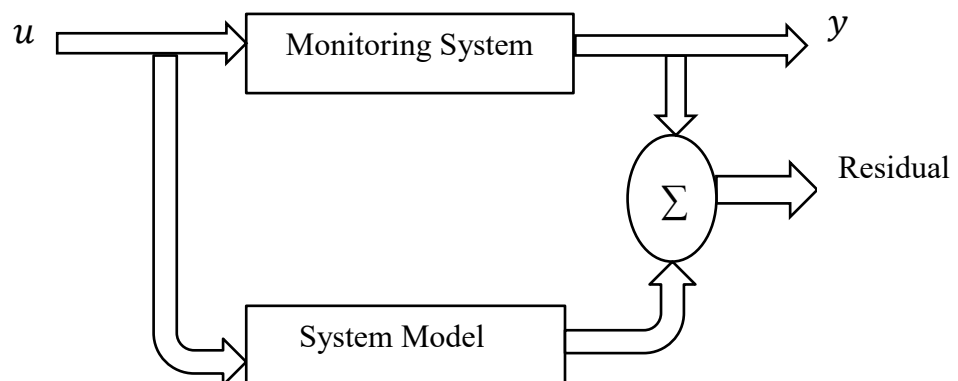
Figure 2.5 Parity relation based residual generation

The system can be modelled as follows (Shen et al. 2014):

$$y(k + 1) = AX(k) + Bu(k) + \gamma(k) \tag{2.2}$$

$$y(k) = CX(k) + Du(k) + v(k) \tag{2.3}$$

where:

$AX(k), y(k), X(k)$ represent the process input, output and state variable respectively, while $\gamma(k)$ and $v(k)$ represent the noise sequences that are assumed to be normally distributed and statistically independent of $x(k)$ and $u(k)$.

Parity relation is a reliable and fast diagnosis method. It has a simple structure, is robust to disturbances and is sensitive enough to anticipate faults (Isermann 2005). Fully decoupled parity equation for fault diagnosis was proposed by Chan et al. (2006) for dynamic systems with known linear and unknown nonlinear characteristics.

The residuals generated from the fully decoupled parity equation can be used for fault estimation using the recursive least squares method, and the results show that the proposed method can be implemented to detect, isolate and identify faults in a simulated DC motor.

Christophe et al. (2002) compared parity relation and observer based methods, and found that parity residual is generated by computing on-line the known part of this equation. The major drawback of this approach is that the residuals are computed using time derivatives for the measured variables. To make the residuals usable in a noisy environment, filtering procedures and post treatments must be used, while observers are dynamical systems that allow the outputs of the process to be estimated. An observer based residual is a combination of the estimation error on the outputs.

The closed-loop structure makes these residuals more robust with respect to noise and perturbations. The synthesis of an observer may be difficult to carry out for some nonlinear systems because the gain matrices must fulfil many constraints. Moreover, this method does not give an explicit formulation of the sensitivity of the residual to faults.

For the parameter estimation approach, the extended Kalman filter (EKF) technique estimates and tunes the parameters of the model to detect faults; changes of the model parameters identify the abnormal operating condition of the actual system (Nakhaeinejad et al. 2011). In addition Alessandri et al. (1999) proposed to diagnose propeller faults in UUV. The method based on EKF was presented for residual filtering.

Olivier et al. (2012) presented a new practical implementation of the Kalman filter (KF) in association with pattern recognition to estimate and predict unknown states in order to detect failure appearance. Also, errors in fault detection and isolation in physical systems can be reduced if uncertainties can be considered. In a general way, this prediction allows prevention of possible system damage by evaluation of operating mode evolution toward a fault.

In conclusion, model-based approaches are based on mathematical models of the system. The requirement of mathematical models of the plant can lead to several difficulties in the implementation of these approaches, for instance due to factors such as system complexity, high dimensionality, nonlinearities and parametric uncertainties (Angelo et al. 2014). In addition, model based techniques provide satisfactory results only when plants exhibit linear behaviour or when the modelling errors can be kept within acceptable limits; accurate mathematical models are needed with low behavioural complexity (Merzouki et al. 2013).

2.2.3 Signal Processing Techniques

A key aspect of a robust FDD is proper signal conditioning and processing. Advanced signal processing capability based on vibration analysis, current analysis, etc. is now available for motor fault diagnosis and condition monitoring purposes. Signal processing techniques are applied to the measured sensor signals in order to generate features or parameters (e.g. amplitudes of frequency components associated with faults) which are sensitive to the presence or absence of specific faults, so that fault decision techniques can then be implemented (Gritli 2014).

One of the most frequently used fault detection methods is the motor current signature analysis (MCSA) approach; it is a non-invasive and low cost effective approach and can be used for simultaneous multi-fault detection. It directly identifies changes in the harmonic content of the motor line current when a fault occurs (Immovilli et al. 2013) using the fast Fourier transform (FFT) and the short fast fourier transform (STFT).

Lau and Ngan (2010) used MCSA with wavelet packet transform to diagnose outer race faults. The results showed that fault severity will increase the distortion of the current waveform. In the experiment, similar waveform distortions were obtained with different motors; the bearings being used were the same.

Subsequently, WPT integrating FFT approaches have been tested and found to be effective for identification of the exact frequency content being distorted. Finally, the root mean square (RMS) value of the WPT coefficient has revealed that there were some correlations between the node number and the RMS value frequency content being distorted. But the frequencies associated with this type of fault depend on the particular conditions of the motor. Additionally the performance of the MCSA technique is degraded by the increment of the load directly modifying the amplitude of the fault indicator (Ovedo et al. 2011).

According to the literature review, MCSA does not always achieve good results, especially during non-stationary operating conditions when variation of the fault characteristics is not constant. A new approach has been implemented by Jun et al. (2013) to diagnose unbalanced mechanical loads in PMSM under non-stationary conditions, based on Park's vector approach and DWT.

Simulations were carried out in the PMSM drive system based on MATLAB/Simulink, and fault indicators are successfully extracted from the square of the stator current Park's vector using DWT. The simulation results show that the proposed method can effectively detect mechanical unbalance faults under non-stationary operating conditions. However, the fundamental components caused by asymmetry of power supply, will be present in the stator current spectrum, and consequently Park's vector spectrum will be weak for detecting faults.

Rajagopalan et al. (2005) proposed a new technique to diagnose rotor fault in PMBLDC motor using windowed Fourier ridges for feature extraction. The main limitation of the Windowed Fourier Ridges (WER) algorithm, however, is that it is dependent on the type and length of the window, as it has to be chosen as a trade-off between time and frequency resolution.

Owing to the limitations of the FFT with non-stationary signals such as information losses and there can be difficulties in interpreting the signals when moving from time to frequency domain (Yahia et al. 2014 and Pandya et al. 2014). The STFT is an extension of the FFT that can be used to perform time frequency analyses, and is given by:

$$\text{STFT}(t, f) = \int_{-\infty}^{\infty} x(t + \tau) w(\tau) e^{-2\pi f \tau} \, d\tau \tag{2.4}$$

where x (t) is a signal and w (τ) is the window function. However, these tools do not provide a better resolution for identifying the faults. The FFT is not useful with non-stationary signals and the amplitude of the fault harmonic component is quite small compared with the fundamental amplitude if the fault severity is small. Hence, fault characters are likely to be hidden. The STFT meanwhile has a fixed window and poor time resolution (Zanardelli et al. 2007, Cusido et al. 2008).

WT has been shown to be a powerful tool for dealing with non-stationary vibration signals. Kankar et al. (2011) presented two criteria to select the best wavelet features: the first of these is based on using maximum energy-to-Shannon entropy ratio, whereas the second one is based on maximum relative wavelet energy. Wavelet decomposition can be expressed as:

$$WT(\text{t}, \tau) = \frac{1}{\sqrt{s}} \int_{-\infty}^{\infty} x(t) \varphi^*(\frac{t-u}{s}) \, dt \tag{2.5}$$

where (s, u) are dilation and translation respectively, and φ^* is the Wavelet function scaled by s and time shifted by u.

An advantage of the WT over the STFT is that the wavelet function $\varphi^*(\frac{t-u}{s})$ is scalable. This allows the WT to adapt to a wide range of frequency and temporal resolutions. The discrete wavelet transform, a signal analysis method that provides the time and frequency information of the signal, was applied, which has the ability to explore signal features with different time and frequency resolutions, was used to obtain the best features from the signals.

Qin et al. (2009) compares two popular rolling element bearing diagnostic techniques: Spectrum analysis in bearings characteristic frequency range and enveloping analysis in the high frequency range, using test data from an aircraft engine test rig. The objectives

were to compare the techniques in terms of the time of detection and data requirement, and provide guidance for technology adoption in further field deployment.

 The results demonstrated that enveloping analysis is able to detect bearing defects much earlier than spectrum analysis, but it requires a higher data sampling rate. The bearing defect's characteristic frequency eventually shows up in the low frequency spectrum at the late stage of the failure, and it is modulated by other harmonics such as those due to shaft imbalance.

Cruz and Cardoso (2005) proposed a multiple reference frame method for voltage unbalances or non-stationary conditions. In this method, the positive sequence of the stator currents of a faulty IM is assumed to be the indicator of a healthy machine. Negative-sequence currents were first removed in order to obtain fault current components from the phase currents. The direct quadrature (*dq)* components of the fault current are obtained only after removing the estimated healthy current components.

In real life applications there are several circumstances where the motor is never operating at a constant speed or with a constant load, such as in automotive and aircraft applications (Villa et al. 2012 , Sadough et al. 2014). Rajagopalan et al. (2008) proposed a new quadratic time-frequency representation for PMBLDC motor bearing faults diagnosis operating under variable speed and load conditions. One of the most important advantages of the quadratic distribution is that these distributions do not depend on any parameter similar to the size or type of the window, and provides much better frequency resolution and localisation of energy but these new distributions are too complicated to be implemented in a commercial system, owing to their perceived intense computational time.

Wigner ville distribution (WVD) and the relative crossing information methods were implemented to extract features from vibration signals and then these features were optimised using the ant colony optimisation (ACO) clustering algorithm. Finally, an FLS diagnosis method was proposed for machine fault decision (Li et al. 2013). The experimental results proved that the diagnostic sensitivity using fuzzy diagnosis method based on sequential inference for motor roller bearing diagnosis.

The main challenge of signal processing approaches is that they do not take into account the dynamic behaviour of the system measured signals. To overcome this drawback, analytical redundancy was introduced by Tehrani and Khorasani (2009) where instead of using extra hardware the redundancy is supplied by a mathematical model of the component.

Accordingly, fault diagnosis systems that are based on analytical redundancy are often called model-based fault diagnosis systems. Furthermore, signal processing techniques only use output signals of the motor; hence the influence of an input on an output is not considered. In turn, frequency analysis is time consuming, thus it is not appropriate for on-line fault diagnosis (Ece and Başaran 2011).

2.2.4 Hybrid techniques

Hybrid techniques are a combination of several technique, and have been proposed for FDD (Liu et al. 2009). It is a compromise between system performance and reliability, cost and size. Most recent applications of NN for FDD are presented with other methods, such as NN with PSO (Hui 2010) or with GA (Ziani et al. 2012).

WPT and NN have been implemented by Wen (2011) to diagnose IM stator winding short faults; here, an NN was trained by an improved GA using the stator current as a fault indicator and WPT as the fault classifiers. The line currents under different

conditions are pre-processed using second level WPT. In addition, a model-based approach has been implemented by Lu et al. (2006) in which an NN was trained by torque and speed data to diagnose inverter switch faults. The electric drive model was simulated using MATLAB® and Simulink® to generate representative training data to train the NN, which was used as a fault classifier.

Daqi and Bing (2013) proposed an approach to diagnose continuous, uncertain and unknown fault patterns of the thruster in a UUV using a credit assignment-based fuzzy cerebellar model articulation controller The proposed approach showed an efficient diagnostic accuracy compared with a self-organization map NN.

Mathew et al. (2012) developed fault diagnosis approaches based on estimating the physical parameters of the PMBLDC motor and then used FLS inference for fault diagnosis. Fuzzy rules were formulated to isolate different types of faults. SVM are data-based and are therefore robust to process knowledge; it is based on structural risk minimisation, which enhances generalisation even with a small training data set and it allows accounting for process non-linearity.

Tiwari et al. (2014) present an approach to diagnose bearing point local defects based on statistical features extracted from time vibration signals. These features are used to train and test both neuro fuzzy and SVM based techniques implemented for fault classification. Similarly, Moosavian et al. (2014) developed a method to diagnose unbalanced loads in rotating machines based on signal processing, feature extraction and fault classification, using features extracted by FFT, SVM, and K-nearest neighbour algorithms, respectively for fault classification. An experimental set up was designed and vibration signals were collected with three operating conditions: no load, balanced load and unbalanced load. The results showed the capability of SVM for unbalanced load machine fault diagnosis

Yun et al. (2013) used the combination of spectral kurtosis and SVM to diagnose misalignment of rolling elements. In this approach, SVM parameters are optimised using GA. Furthermore, SVM can be used with NN to diagnose ball bearing faults, and statistical methods are used for dimension feature reduction (Kankar et al. 2011, Patil et al. 2010, and Sharma et al. 2014).

Empirical mode decomposition (EMD) is a signal processing tool used for non-stationary and nonlinear signals. It works based on decomposing a signal into orthogonal components called the intrinsic mode function (IMF). Camarena et al. (2014) combined EMD with an adaptive linear network based frequency estimator and an FFNN based classifier to provide an intelligent methodology for diagnosis: one and two broken rotor bars, bearing, and unbalance mechanical load faults.

By comparing EMD with DWT, DWT is related to Multi resolution analysis, which provides an orthogonal set of multi resolution elements (different levels of approximations). Meanwhile, EMD is a decomposition procedure based on signal features and does not depend on a function basis, EMD provides a set of components called IMF and it shares some similarities with DWT multi resolution analysis, but they are only approximately orthogonal. However, the lack of theoretical framework, which leads to difficulties for the characterisation and evaluation, represents the main drawback of EMD (Niang et al. 2010).

Liu et al. (2012) developed a mathematical model for PMSM under normal and abnormal conditions, and applied Particle swarm optimisation (PSO) for fault detection and identification. Due to its advantages such as simplicity, easy implementation and its fast convergence to the global optimum, PSO has been applied to different fields requiring parameter optimisation in a high dimensional space. However, during the later

stages of the optimisation the lack of diversity of the particles may lead to premature convergence to a local optimum (Wang et al. 2014).

In conclusion, each intelligent technique has its strengths and drawbacks. Hybrid intelligent techniques have been developed for motor condition monitoring and FDD schemes based on combinations of techniques. Previous research results show that combining multiple approaches can result in better performance for many applications.

2.3 Fault Diagnosis Indicators

According to the types of measurements taken, most methods to monitor the condition of electric machines can be categorised into the following groups: vibration (Seshadrinath et al. 2014), acoustic emission (He et al. 2011), electric monitoring such as current (Kim 2009), and rotating speed (Roy et al. 2014). In this section, the major advantages and disadvantages of these methods are reviewed.

Rolling element bearings have a wide range of applications, ranging from rotating machines that permit shafts, to those rotating with the highest precision together with very low friction, provided the bearings have no faults. When a fault develops either in one or all of the raceways of a bearing, stability of the shaft deviates from the intended motion, resulting in the bearing vibration level increasing (Mao and Wu 2011).

Several indicators have been applied for monitoring bearing defect signals, and can be classified into vibration, temperature (Patil et al. 2010) and acoustic measurement (Delgado et al. 2011).Vibration measurement is the most widely used and effective way to detect rolling bearing faults at an early stage and the vibration signal can be measured using accelerometers or vibration velocity transducer sensors (Jiang et al. 2013, Tenconi et al. 2014).

However at low speed, the vibration signal fault is very weak and sometimes it is difficult to distinguish between detection and a diagnosis based on vibration signal as fault indicator, because it is directly related to the mechanical element (Bediaga et al. 2013).

Current analysis is used to detect rolling bearing and unbalanced mechanical load faults in IM. The proposed diagnostics approach was supported in simulation and experiment tests. Furthermore, current analysis can offer significant economic savings and implementation advantages with respect to traditional vibration monitoring for bearing fault detection (Blodt et al. 2005, Faucher 2010).

Gritli et al. (2013) presented a new technique to diagnose unbalanced mechanical loads. The technique is based on motor axial vibration signature analysis and motor radial vibration signature analysis. In order to investigate the drawbacks and advantages of vibration and current signals as rolling element bearing fault indicators, Immovilli et al. (2010) compared these two sensors and found the vibration signal is a robust indicator for rolling element bearing fault diagnosis, and the current signal is useful for diagnosing faults under low speed operating conditions.

Similarly, Frosini and Bassi (2010) proposed an approach for rolling element localised bearing faults (crack and hole in the outer race, deformation of the seal and corrosion) diagnosis using the stator current as an indicator and a NN for fault classification. By contrast, Trajin et al. (2009) compared stator current and mechanical speed as indicators for rolling element bearing fault diagnosis. Indicator efficiency was studied under different operating points.

Barzegaran et al.(2013) used the frequency response of the rated magnetic field as indicator to detect unbalanced input conditions of the flowing current and the short-circuit of stator windings. Both the simulation model and experimental results show that

the field can be utilised for failure identification in electric motors with high accuracy. In addition, the waveforms of the electromagnetic torque, summation of phase voltages and stator current harmonics are also monitored to identify and locate the fault.

Kim et al. (2009) used the stator current, back-electromotive force, and resultant torque waveforms for both healthy and faulty machines for fault indication, and used a winding function theory for analysing the motor waveforms for stator inter-turn faults in a PMBLDC motor. Similarly, stator currents were used for mechanical load fault diagnosis (Rajagopalan et al. 2008).

Owing to initial manufacture and ageing phenomena, an additional undesirable time varying torque is caused by unbalanced mechanical defects. The additional torque will affect the stator and rotor current amplitude and the sideband stator current harmonics that are characteristic of mechanical unbalance defects (Salah et al. 2013).

Furthermore, the photogrammetric approach was implemented by Huang et al. (2014) for monitoring turbine blades damage (both damaged and undamaged blades). In order to control the rotation of the wind turbine blade, a motor was used to spin the blades at controlled angular velocities. Two high speed cameras were set in front of the turbine to tape the video images, to measure the displacement fields by image template matching.

2.4 Chapter Summary

The literature review has covered a variety of topics involving the main electrical and mechanical faults in electrical motors and faults that are related to the particular structure of PMBLDC motors. Previously proposed methods for fault diagnosis have been considered, including recently utilised AI based, signal processing, model-based and hybrid approaches, and feature extraction and feature reduction tools. The review also indicates that the usage of PMDC motor drives is widely increasing in a variety of

industrial and critical applications because their architecture is suitable for any safety critical applications. Thus, the demand for a diagnostics approach is increasing (Jose 2010.

The review in this chapter also indicates that previously proposed methods mainly consider rolling element bearing faults in PMBLDC, and indicates that rolling element bearing defects represent the main source of failure in electrical motors, while the research on bearing fault detection for these motor drives still remains an unexplored area. NNs for electrical motor FA have become prominent due to their ability to reduce dependence on human experts and accurate mathematical models. However, the response of a static network at any time point depends only on the value of the input sequence at that same time point. In real-life applications there are several circumstances where the motor is never operating at a constant speed or with a constant load such as in automotive and aircraft applications.

DNN are more versatile and provide the capability to learn the dynamics of complicated nonlinear systems, which conventional static neural networks cannot model. Based on this review it has been concluded that the following topics need to be developed:

➢ The high power density and high efficiency of the PMDC motor has led to the use of this machine in applications in which high reliability is a key feature, such as aerospace/aircraft actuators, automotive auxiliaries and traction. FA in this type of machine needs to be researched more. Rolling element bearing faults represent the main source of abnormal conditions in electrical machines. However, almost all of the previous research is focused on single localised faults and ignore generalised bearing faults. This work is discussed in Chapter 4.

➢ FA of electrical motors has been dependent on a single indicator of the motor situation. To increase diagnosis, the use of multiple fault indicators for FA has not been addressed well. This work is discussed in Chapter 5.

➢ The development of an accurate feature extraction and dimensionality reduction technique, to extract the useful information for fault decision and to remove redundant features that affect diagnosis accuracy. DWT was proposed for feature extraction that provides the time and frequency information of the signal and orthogonal fuzzy discriminate analysis (OFNDA) was implemented for feature reduction This work is discussed in Chapter 6

➢ Almost all the literature concerns FA stationary operating conditions, and this is not realistic in practical applications. FA under non-stationary operating conditions, especially in critical applications, has not been covered well and DNN has been presented to improve the reliability of the proposed fault diagnosis approach. It allows improving fault prediction accuracy of condition monitoring systems. This work is discussed in Chapter 7.

CHAPTER 3

Permanent Magnet DC Motor Characteristics

"In this chapter, background about PMDC motor characteristics applied to high performance applications is provided, and then common electrical and mechanical faults are described."

3.1 Introduction

The high power density and high efficiency of the PMDC motor have led to its use in applications where the high reliability of the machine is a key-feature (Villani et al. 2012). Redundancy and conservative design techniques have been widely adopted for improving the reliability of PMDC motor against the variety of failures than can occur. However, these techniques are expensive to realise. As an alternative, considerable diagnostic strategies and control schemes can be devised to ensure high reliability.

 In general, a fault can be defined as something that changes the behaviour of the system such that the system no longer satisfies its purpose. There are many reasons related to fault occurrence. Some of these are due to errors in manufacturing, changes in environment and control action errors by humans, any of which may bring the system out of its operating point (Schröder 2006).

FA, as discussed in Chapter 2, is a sequential process involving three steps: feature extraction, reduction and decision-making. Feature extraction is performed by the use of

appropriate signal processing and the decision-making, and is a process to classify the obtained features into different categories.

To facilitate a clearer understanding of the proposed FA schemes, the fundamentals of operation and construction of a PMDC motor are presented in more detail. The main types of PMDC motor and their faults, and the mechanisms by which they induce fault signatures into the machine performance, are also discussed.

3.2 PMDC Motor Fundamentals

In a PMDC motor, the excitation can be produced in an electromagnetic field by a PM such as ceramic, alnico and rare earth varieties instated of an external DC supply (Krishnan 2001). In the construction of electrical machines, PMDC motor bring the following benefits (Ahmed et al. 2014) :

➢ There are no excitation losses, which mean substantial increases in efficiency because no electrical energy is absorbed by the field excitation system.
➢ Permanent magnet excitation has a higher torque and output power per volume than electromagnetic excitation.
➢ The dynamic performance is better than motors with electromagnetic excitation.
➢ PMDC motors are simple in construction and maintenance.

Alternatively, PMDC motor are subjected to limitations, including demagnetization owing to excessive current in the motor winding or overheating Also, the magnets in PMDC motor are limited in air gap flux density. However, with development magnetic material these characteristics are becoming less restrictive for PMDC design (Fitzgerald et al. 2003).

The common types of permanent magnet motor used in industry can be classified as follows:

➢ PMBDC motor, where a permanent magnet provide the excitation.

➢ PMSM where a permanent magnet replace the DC rotor excitation winding.

➢ Line-start PMSM, where synchronous machines are equipped with a squirrel-cage, induction-type rotor winding for line starting. A permanent magnet embedded in the cage synchronises the motor.

➢ Doubly salient PM motors, where switched reluctance motor with permanent magnet is embedded in the stator or rotor side.

3.2.1 PMBLDC motor principles

A PMBLDC motor's physical appearance is supplied by an inverter that converts a DC voltage to three-phase alternating-current voltages, with the frequency corresponding to rotor instant velocity. Owing to PMBLDC motor advantages, such as high efficiency, long operating life and high torque to inertia ratio, the PMBLDC motor is an essential component in aircraft electrical power systems, such as electro mechanical actuators (EMA) of its flight control surfaces and cabin pressure valves (Garcia et al. 2008,).

The construction of a PMBLDC motor is very similar to the AC motor. The stator windings of a PMBLDC motor are similar to those in a poly phase AC motor, and the rotor is composed of one or more permanent magnet (see Figure 3.1). The major difference between the motors is in rotor construction and the addition of rotor position sensors such as encoders or Hall Effect devices.
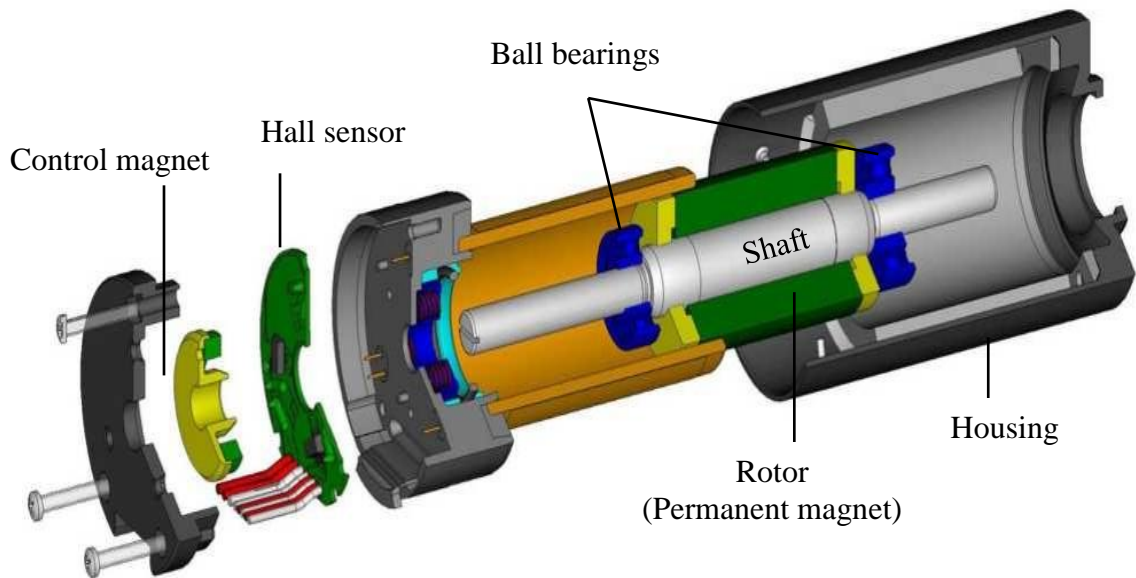
Figure 3.1 PMBLDC motor structure (Maxon motor 2010). Permission to reproduce this figure has been granted by Maxon motor

Table 3.1 Comparison between advantages and disadvantages of PMBLDC motor and conventional DC motor (Jian 2011)

Characteristic	Brushed DC motor	Brushless DC motor
Commutation control	Mechanical contact between brushed and commutator	Electronic commutation using transistors
Rotor position detection	Automatic detection by brushed	By hall sensor, optical encoding
Maintenance	Regular Maintenance needed	Usually no maintenance required
Connection with external circuit	By reverse of the terminal voltage	By rearranging logic sequencer
Electric noise generation	Arcs in the brushes will generate high noise.	Low noise, generation
Power losses and efficiency	Additional electrical and mechanical brush losses	There is no brushes loss
Speed Range	Lower speed range due to Mechanical limitations by the brushes/commutator	Higher speed range
Control Requirements	No controller is required for fixed speed	A controller is always required to keep the motor running

These sensors provide electrical signals the control uses to sequentially energize the three-phase windings to produce maximum rotor torque and desired rotation direction. The advantages and disadvantages of the PMBLDC motor and conventional brushed DC motor are illustrated in Table 3.1 (Yedamale 2003, Hill 2004).

PMBLDC motor drives fall into two principal classes of sinusoidal excited and square wave (trapezoidal excited) motors. Figure 3.2 shows the equivalent circuit for three phase of a PMBLDC motor, the stator winding each with N_s equivalent turns and resistance r_s. The main elements of a PMBLDC motor are the permanent magnet motor, inverter, rectifier, shaft position sensor (Hall sensor, encoder) current detector, and controller (Yan et al. 2014).
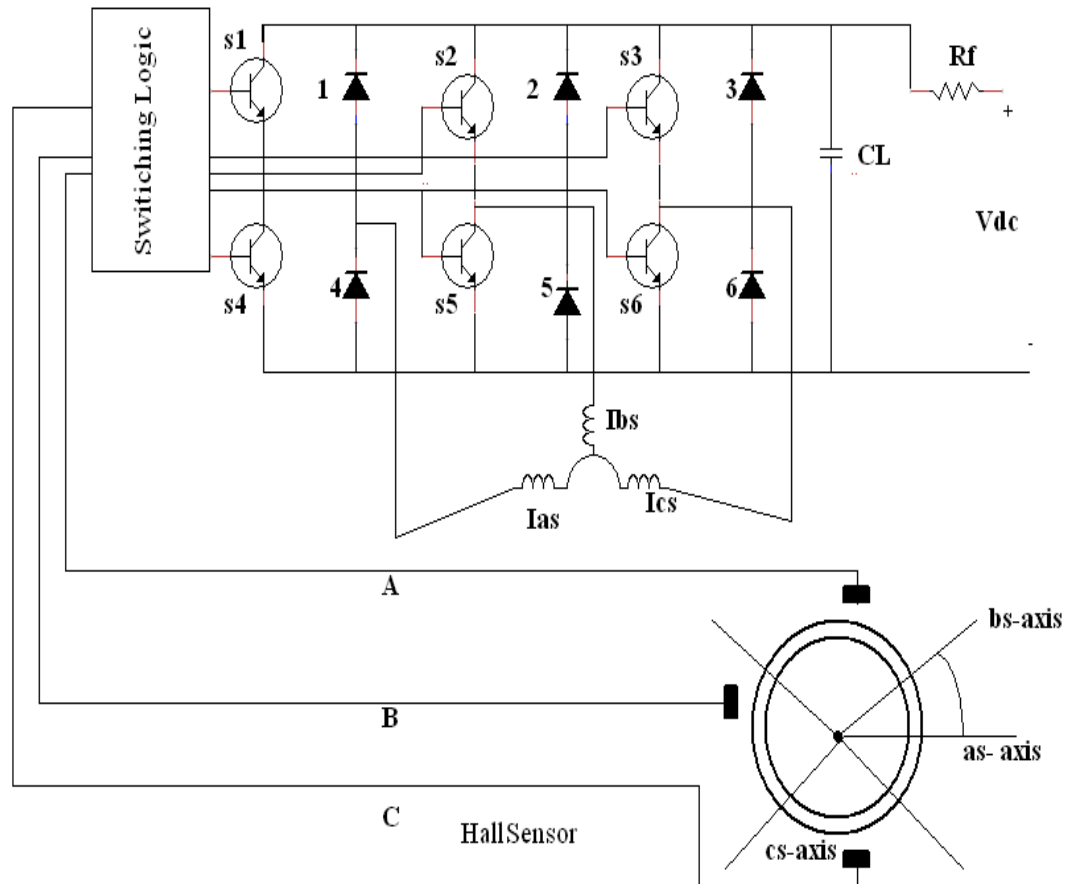
Figure 3.2 Electrical circuit layout of the PMBLDC motor

Many different approaches such as physical, finite element (FE) and quadratic axis (DQ) mathematical models have been implemented for motor modelling. Mohammed et al. (2005) compared between these models and showed that DQ provides an inaccurate model for the PMBLDC motor as it ignores the harmonic effects caused by pole shape and gives a very smooth torque.

The DQ model is based on the assumption that both the winding flux linkage and the working flux distribution are sinusoidal. Mohammed et al. (2006) applied an FE based physical phase variable model and the model was capable of providing information about the location and severity of the short circuit faults. On the other hand a physical phase variable model provides the same accuracy of as an FE model but with much faster simulation speed.

This report undertakes a good compromise between computational complexity and model accuracy, and the model developed here is versatile for representing both the healthy and the faulty condition of the PMBLDC motor. The following assumptions were made while designing the model here (Krishnan 2001).

➢ Voltage drop across the electronic control circuit (diodes, transistors and the connecting wires is negligible)

➢ The cogging torque of the motor is ignored

➢ The induced harmonic in the rotor due to stator harmonic fields is ignored

➢ The iron and stray losses are also neglected

➢ Saturation is neglected

➢ Eddy current and hysteresis losses are neglected

The PMBLDC motor system is defined by the following equations:

$$V_{abc} = I_{abc}.R_{abc} + L_{abc}\frac{dI_{abc}}{dt} + e_{abc} \qquad (3.1)$$

43

$$h_{abc} = L_{abc}.I_{abc} \tag{3.2}$$

$$L_a = L_a = L_c = L_s \tag{3.3}$$

$$L_{ab} = L_{bc} = L_{ca} = L_m \tag{3.4}$$

The stator phase voltage equation is given by:

$$\begin{bmatrix} V_a \\ V_b \\ V_c \end{bmatrix} = \begin{bmatrix} R_a & 0 & 0 \\ 0 & R_a & 0 \\ 0 & 0 & R_a \end{bmatrix} \begin{bmatrix} I_a \\ I_b \\ I_c \end{bmatrix} + \begin{bmatrix} L_s & L_m & L_m \\ L_m & L_s & L_m \\ L_m & L_m & L_s \end{bmatrix} p \begin{bmatrix} I_a \\ I_b \\ I_c \end{bmatrix} + \begin{bmatrix} e_a \\ e_b \\ e_c \end{bmatrix} \tag{3.5}$$

The electromechanical torque generated by the motor is expressed as:

$$T_{em} = J \frac{d_{wr}}{dt} + \beta w_r + T_l \tag{3.6}$$

Speed of motor is proportional to the position of the rotor and given by:

$$\frac{d\theta}{dt} = w_r \tag{3.7}$$

where V_{abc} is three phase voltage, R_{abc} is stator resistance, I_{abc} is three phase stator current, h_{abc} is flux linkage, L_s is self-inductance, L_M is a mutual inductance, L is inductance, T_{em} is an electro mechanical torque, w_r is a rotor speed, θ is an electrical position of the rotor flux, T_l is the load torque and e_{abc} is the back emf.

Figure has been removed due to Copyright restrictions

Figure 3.3 A trapezoidal Back-EMF (Yedamale 2003)

Square wave motors, meanwhile, are also fed with three-phase waveforms shifted by 120°one from another, but these wave shapes are rectangular or trapezoidal. Such a shape is produced when the armature current is precisely synchronised with the rotor's instantaneous position and frequency, as illustrated in Figure 3.3. Sinusoidal excited PMBLDC motor are fed with three-phase sinusoidal waveforms and operate on the principle of a rotating magnetic field, in which all phase windings conduct current at a time.

3.2.2 PMBDC motor principles

PMDC motor are widely used for low power applications and are often the preferred choice when considerations such as freedom from maintenance and operation under adverse conditions are factors (Gieras 2009). The structure of a PMDC motor is based on replacing field winding by a PM located in the stator to generate a magnetic field and armature windings, located in the rotor.

The magnetic field of the PMDC motor is generated by PM so no power is used to create the magnetic field structure as shown in Figure 3.4. The stator magnetic flux remains essentially constant at all levels of armature current and, therefore, the speed with. torque curve of the PM motor is linear over an extended range.

The brushes allow mechanical connection with a set of a commutator, which connects with the armature winding and the current follows to the armature windings through a set of slip rings and brushes that make mechanical connection with commutator. The ideal brush selection offers low voltage loss, no arcing, little commutator wear, and generates little noise. Changes in direction of rotation can be achieved by varying voltage polarity. Figure 3.5 shows the schematic circuit diagram for a PMDC motor.
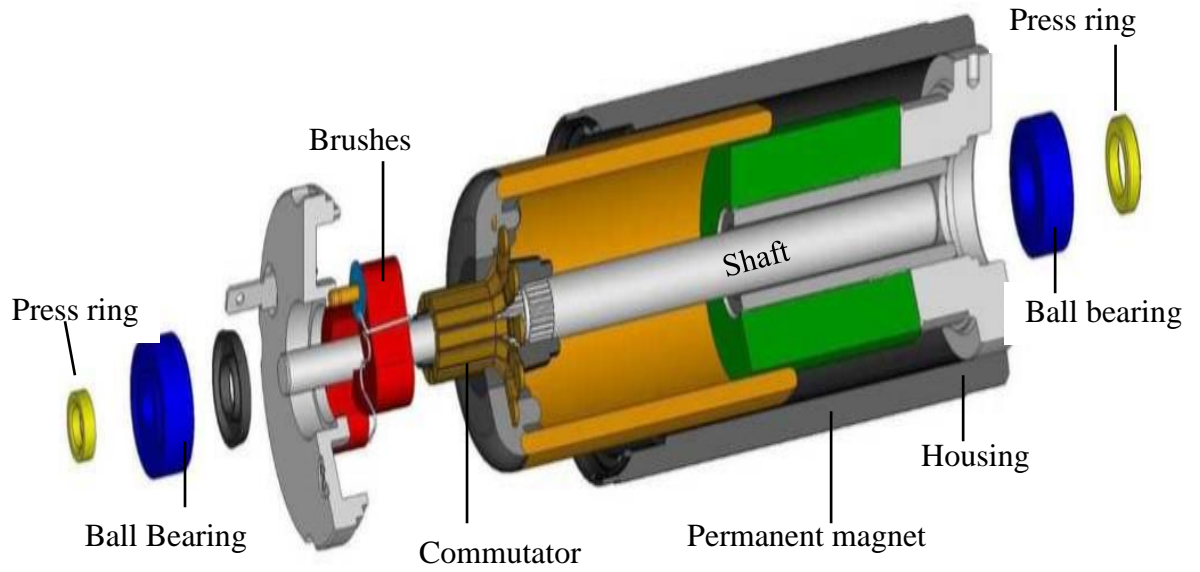
Figure 3.4 PMBDC motor structure Maxon motor (2010). Permission to reproduce this figure has been granted by Maxon motor

Figure has been removed due to Copyright restrictions

Figure 3.5 Equivalent circuits for a PMDC motor (Ivan 2013)

A differential equation for the equivalent circuit can be derived by using Kirchhoff's voltage law around the electrical loop (Joyce et al. 2014).

$$V - V_R - V_L - V_b = 0 \qquad (3.8)$$

The voltage across the resistor can be represented as

$$V_R = i_a R \qquad (3.9)$$

$$V_L = L\frac{di_a}{dt} \qquad (3.10)$$

where L is the inductance of the armature coil R is the resistance and i_a is the armature current. The back electric motive force (back emf) can be written as:

$$V_b = K_a\ \emptyset_d\ W_m \tag{3.11}$$

where $\emptyset_d$ is the net flux, K_a geometric constant and W_m is the rotation speed.

In a PMBDC motor $\emptyset_d$ is constant so that the Eq 3.11 can be reduced to:

$$V_b = K_m\ W_m \tag{3.12}$$

where

$$(K_m\ = K_a\ \emptyset_d) \tag{3.13}$$

Substituting eqns gives the following differential equation

$$V_a = I_a R + L\frac{dI_a}{dt} + K_m\ W_m \tag{3.14}$$

Assuming of the energy balance on the system, the sum of the torques of the motor must equal zero. Therefore,

$$T_d - T_{w'} - T_w - T_m = 0 \tag{3.15}$$

where T_{ed} is the electromagnetic torque, $T_{w'}$ is the torque due to rotational acceleration of the rotor, T_w is the torque produced from the velocity of the rotor, and T_l is the torque of the mechanical load. The electromagnetic torque is proportional to the current through the armature winding and can be written as

$$T_d = K_t i_a \tag{3.16}$$

$$T_{w'} = J\frac{di_a}{dt} \tag{3.17}$$

$$T_w = \delta W_a \tag{3.18}$$

where K_t is the torque constant J is the inertia of the rotor and δ is the damping coefficient associated with the mechanical rotational system of the machine.

3.3 The Main Faults in PMDC Motor

The major internal faults in electrical machines can be classified in two main categories: electrical and mechanical faults, as shown in Figure 3.6 (Spyropoulos and Mitronikas 2013). The reasons why electric motors fail in industry have been commonly reported as follows (Utthiyuung et al. 2002, Bindu and Thomas 2014) :

➢ Exceeding the standard lifetime

➢ Abnormal power, voltage, and current

➢ Overload or unbalanced load

➢ Mechanical, dynamic and thermal stress

➢ Electrical stress from fast switching inverters or unstable ground

➢ Residual stress from manufacturing

➢ Harsh application environment (dust, water leaks, environmental vibration, chemical contamination, high temperature)
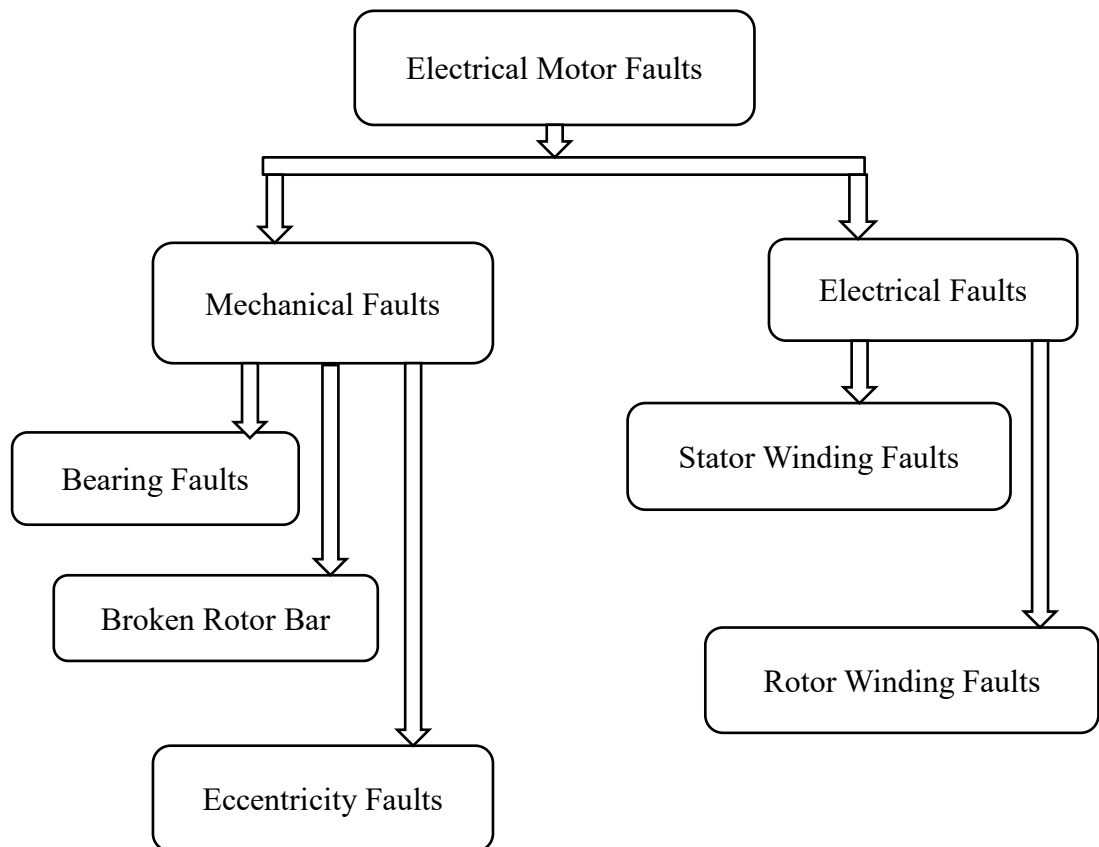
Figure 3.6 The main faults in electrical motors

3.3.1 Electrical faults

Electrical faults are usually influenced by power quality, such as variations of frequency and unbalanced voltage, and can be categorised as stator and rotor winding, inverter, position of sensor faults, and bearing faults.

3.3.1.1 Stator and rotor winding faults

About 21 % of total electrical motor failures are related to stator winding faults (Ojaghi et al. 2013). Stator winding faults are usually related to insulation defects due to electrical voltage, large stresses of electrical voltage, electro-dynamic forces resulting from winding currents, thermal aging from multiple cooling and heating cycles, and mechanical vibrations of internal and external sources. There are different types of stator faults that may occur in a PMBLDC motor drive and the main faults can be classified as: winding short circuit (turn to turn), winding open phase (see Figure 3.7) and inverter switch open or short circuit (Kyung et al. 2014).

As a consequence, the principle effects of a turn-to-turn winding insulation short are that it results in a three phase impedance imbalance in the stator windings. This leads to asymmetries in the phase currents and phase-to-neutral voltages, leading to increased harmonic generation and overall performance degradation (Xiangli et al. 2014). Furthermore, the resultant short circuit between the copper turns causes a significant circulating current to flow in the coil, leading to rapid deterioration and failures (Zouzou et al. 2010).
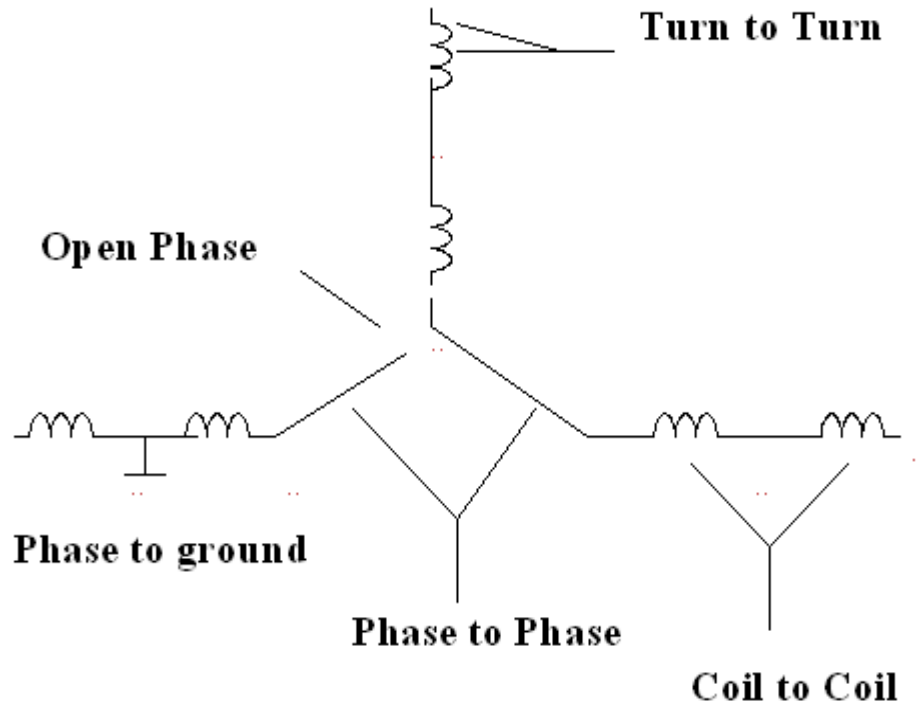
Figure 3.7 Stator winding faults

3.3.1.2 Inverter switch open or short circuit in PMBLDC motor

Three phase inverter systems consist of three H-bridge inverters connected to a common DC power, with capacitor used to drive a motor (Zhu 2008). Inverter power switch faults are subdivided into short circuit and open circuit. In short circuits, in most cases, switch fault occurs due to one of several reasons, such as extra thermal stresses, which could be due to high switching frequency or excessive loading.

Each electronic switch is modelled by a non-linear transistor, which acquires an extremely high value when the switch is open and a very low value when it is closed, so that during faulty operation the resistors that represent the faulty switch are set to a high value. The effect of a power switch open-circuit fault will change the corresponding terminal voltage (Jung et al. 2013).

3.3.1.3 Position of sensor failure in a PMBLDC motor

Electronic commutation of a PMBLDC motor depends on accurate detection of rotor position. There are two main control strategies to determine rotor position. In the first one, optical encoders are used for applications with high resolution requirements. In the second strategy, Hall effect sensors are used for applications at low speeds with low resolution requirements (Tashakori and Ektesabi 2013).

Hall sensors lie stationary, 120 electrical degrees apart, to supply commutation signals to part of the motor. Any misalignment in the Hall sensor with respect to the rotor magnet will cause an error in determining rotor position (Jiancheng et al. 2014). Many factors may cause a breakdown of the Hall effect sensor in PMBLDC motor, including core defects such as corrosion, cracks, residual magnetic fields and core breakage, changes in the bias current, or changes in the orientation of the induced magnetic field in the sensor due to mechanical shocks (Balaban et al. 2009).

3.3.2 Mechanical related faults

Mechanical faults can be related to: rotor eccentricity, broken rotor bar, end ring faults, load faults (unbalance, gearbox fault or general failure in the load part of the drive), or bearing faults.

3.3.2.1 Eccentricity related faults

Machines can fail due to an air gap eccentricity, caused by shaft deflection, inaccurate positioning of the rotor with respect to the stator, worn bearing stator core movement or a bent rotor shaft. There are two types of air gap eccentricity (the static air gap eccentricity and the dynamic air gap eccentricity) (Shakouhi et al. 2012). Furthermore, rotor bending that result in premature failure of blades and other internal components is one of the most serious problems experienced in power plant operations. The problems

often reduce plant availability by limiting generation and increase plant operation and maintenance cost. Extreme rotor bending defect often led to interaction between the turbine's rotor and stationary parts (eccentricity) (Farshad, S et al 2013). In addition, the marine vehicle unbalanced load faults in an electric thruster motor occur when there is damage to marine vehicle propeller blades (Oyvind, 2006).

Eccentricity faults come from unbalance, rotor misalignment, improper mounting, or a bent rotor shaft and producing of an output torque oscillation (unbalanced magnetic pull) and those reduce production efficiency. In addition there are many indication for eccentricity faults including mechanical vibration, temperature ununiformed air-gap, torque increase, and changes in voltage and line current (Torkaman et al. 2014) .

3.3.2.2 Broken rotor bar and end-ring faults

Rotor failures now account for around 5%–10% of total motor failures (Bellini et al. 2008)*.* Broken rotor bar faults as shown in Figure 3.8 can be caused by the thermal stresses due to overload, magnetic stresses caused by electromagnetic forces, inherent stresses due to manufacturing, and mechanical stresses due to the effects of lost laminations, fatigued parts and bearing failure; these are the main reasons of bars breakage occurrence.

Figure has been removed due to Copyright restrictions

Figure 3.8 Broken rotor bar fault (Wen 2011)

3.3.2.3 Unbalanced mechanical load

Most rotating machinery problems can be solved by using the balancing operation, and unbalance is the most common cause of motor vibrations. It reduces the lifespan of various mechanical components of motors, such as bearings, shaft and gears (Moosavian et al. 2014).

Unbalanced mechanical load, as part of the other electrical motor faults, represents 10% of other faults. Stator current time-frequency, torque oscillation and vibration can be used as fault indicators (Martin et al. 2006).

3.3.2.4 Rolling element bearing faults

The bearing rolling element is one of the most common parts in the PMDC motor and its defects one of the most common reasons for failure; it represents about 40 to 50% of all motor faults (see Figure 3.9) (Bianchini et al. 2011, Bediaga et al. 2013, Xiaohang et al. 2014).
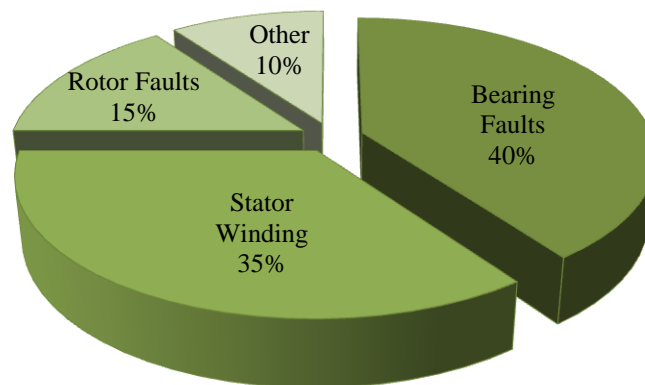
Figure 3.9 The main failure distribution of electrical motors

The bearing structure consists of two rings, inner and outer, as shown in Figure 3.10. A set of balls or rolling elements is placed in raceways rotating inside these rings. Rolling element bearing characteristics are considered in more detail in Chapter 4.

The vibration frequencies to detect these faults are given by:

$$BPFI = \frac{NB}{2}(1 + \frac{BD}{PD}\cos\beta) * f_s \tag{3.19}$$

$$BPFO = \frac{NB}{2}(1 - \frac{BD}{PD}\cos\beta) * f_s \tag{3.20}$$

$$BSF = \frac{Pd}{2}(1 - (\frac{BD}{PD})^2 \cos\beta^2) * f_s \tag{3.21}$$

$$fs = \frac{n}{60} \tag{3.22}$$

where:

fs : Shaft frequency

NB : The number of balls

BD : The ball diameter

Pd : The diameter of the bearing it measured from ball centre to opposite ball centre

β : The contact angle.

$BPFI$: Ball pass frequency inner race

$BPFO$: Ball pass frequency outer race

BSF : Ball Spain frequency
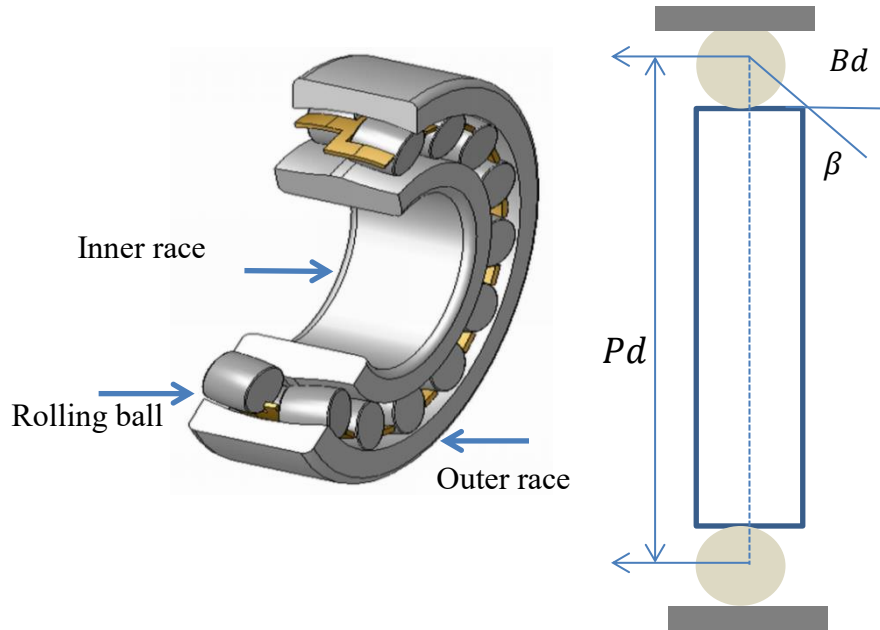
Figure 3.10 Main bearing design parameters

54

Most of the bearings in industrial applications run under non-ideal conditions, such as overloading, misalignment, current fluting and wrong lubrication. These start as marginal defects (Wu et al. 2013). Bearing faults can be classified into two main categories: a single localised defect on the bearing surface, and generalised roughness, where a large area of a bearing's surface has degraded and become irregular (Zhenyu et al. 2009).

Single localised element bearing defects can be classified into three types, inner race, outer race and rolling element defects. The result of such defects is continuing loss of the geometric accuracy of the rolling contact surfaces, and gradual deterioration of bearing function, leading to increased deflection, friction, temperature and vibration.an accelerometer, which is used for vibration measurement, struggles to show the difference between detection and diagnosis using vibration signals, because it is directly related to the mechanical elements (Bediaga et al. 2013).

When a fault occurs on the inner/outer raceway or the rolling element, the interaction between the raceway and rolling elements generates time varying and non-uniform discontinuous forces that drive vibrations. In a single local fault, the contact forces that generate a specific signature in the vibration signal will be discontinuous.

Typical distributed bearing defects include surface roughness, waviness, misaligned races, and off-size rolling elements, which are usually caused by design and manufacturing errors, improper mounting, wear, and corrosion (Choudhury and Tandon 1999). Localised bearing defects include cracks, pits, and spalls on the rolling surfaces, which are usually caused by plastic deformation, and material fatigue. Both distributed and localised bearing faults increase the noise and vibration levels in real-world applications, whereas many distributed faults originate from a localised spelling

(Choudhury 1999). Consequently, in this thesis both types of bearing defect are considered.

Cracks are the most common localised bearing fault, the most common cause being rough treatment such as heavy hammer blows when the bearings are being mounted. The hammer blows can cause fine cracks which can grow and cause fragments of the ring to break-off when the bearing is put into operation. Another common cause of ring cracking is excessive tensile stresses in the rings of a tapered seating or sleeve due to excessive drive-up.

The sources of rolling bearing vibration are the external time varying forces between the components and the transmission mechanism of the machine during the bearings' operation. The contact force between bearing components is continuous under healthy bearing conditions. Therefore, the vibration and stator current signals show a regular signature under different operating conditions, as will be explained in detail in Chapter 5.

The second type of bearing fault is the generalised bearing fault; this work will focuses on the corrosion faults are the second category of bearing faults, denoted as distributed or extended defects. Distributed defects also generate individual signatures in vibration and current signals (Kurfess et al. 2006). Figure 3.11 illustrated the main causes of bearing failure; in the figure corrosion defects represent the most frequent cause of bearing failure, which is lubrication related (Lindh 2003). Dimensional discrepancies are the next most common cause discrepancies, which are a collective term for damage prior to, or during service, due to, e.g., manufacturing flaws, or improper handling during installation, such as forcing the bearing into position with hammer blows, these two mechanisms caused about 90% of all bearing failures.
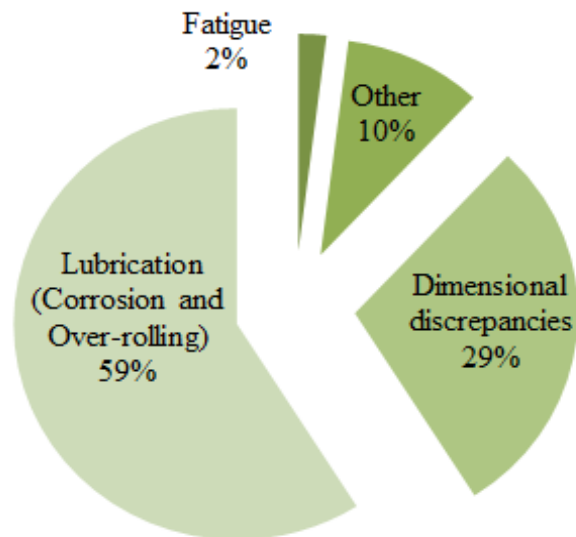
Figure 3.11 The mean reasons for rolling bearing faults

3.4 Chapter Summary

This chapter has briefly reviewed the construction and operation of a PMDC motor. Basic concepts both of brushed and brushless PMDC motor have been introduced. A description of various kinds of mechanical and electrical faults that can occur in a PMDC motor has been presented. The experimental setup and data acquisition are presented in Chapter 4.

CHAPTER 4

Experimental Setup and Data Acquisition

"This chapter introduces the test rig construction and the parameters of measurement associated with incipient fault analysis and identification in a rolling element bearing in a PMBLDC motor and unbalanced mechanical load in PMPDC motors. The manner in which faults are introduced and data acquisitions are described in details"

4.1 Introduction

To validate the proposed fault diagnosis approach, two experiments are presented for the PMDC motor, The first is an experimental setup for rolling element bearing defects of a 1.2kW PMBLDC motor, both of single localised bearing defects and generalised roughness, as shown in Figure 4.1. Several sizes of fault severity were considered for testing purposes.

The second experiment was on blade faults for a trolling motor based on a PMBDC motor. Propellers in the trolling motors are durable but not indestructible. Hard surfaces can damage blades partly or fully and can imbalance the operation of a trolling motor, causing significant damage to the internal parts.

The propulsion system consists of two propellers powered by a set of 24V, 334N Minn Kota Riptide transom mounted saltwater thruster motors. Blade faults in the thruster motor were simulated with four severities, and the current and vibration signals were monitored to diagnose blade faults, which represent unbalanced mechanical load faults.

In this chapter, the framework for preparing the data from both the rolling bearing and blades faults is introduced, including test rigs and electronic components. Various severities of fault are presented

.

<div align="center">(a)   (b)</div>
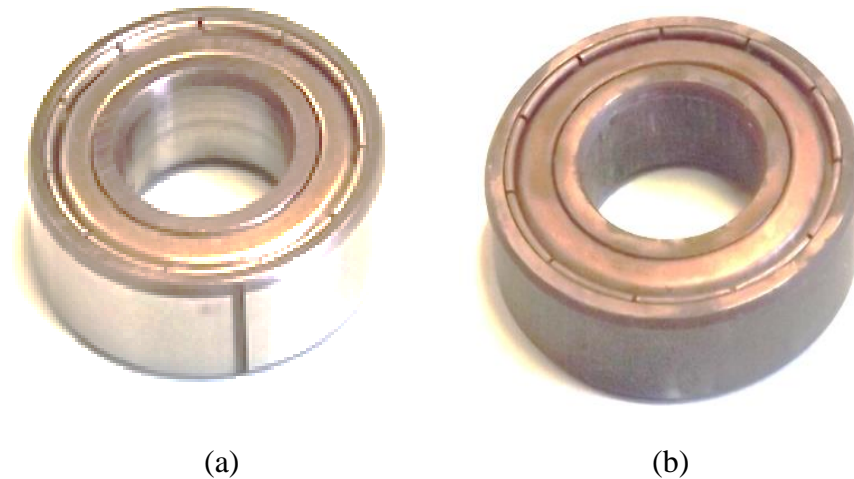
Figure 4.1 Types of bearing faults (a) single localised defect, (b) generalised defect

4.2 Experimental Arrangement for PMBLDC Motor Bearing Fault Diagnosis

Rolling element bearings represent the main source of failures in rotation and are a fundamental part in a wide variety of rotating machines. Abnormalities in their operation will affect the whole machine's performance (Prieto et al. 2011).

The aim of this experiment includes three single localised bearing defects on a bearing surface, namely the inner race, the outer race and the ball defects. These faults were considered in the experiment test. In addition, a generalised roughness over a large area of defect (extended fault) was also considered also for experimental purposes. Most previous related work deals with fault diagnosis under stationary operating conditions.

In this work rolling element bearing faults of a PMBLDC motor were tested under stationary and non-stationary running speeds and load conditions, and the radial

vibration and stator current of motor signals were recorded, and then features were selected from these signals for training a DRNN, which was implemented for fault classification.

The whole experimental setup to acquire bearing normal and fault data is illustrated in Figure 4.2. The setup consisted of a test rig with bearings with normal and abnormal conditions, an accelerometer and current sensors, function generator, DC generator and a load that was changed using variable resistive load, Matlab interface software and data acquisition system (Arduino), which will be explained in detail in the following sections.

A laboratory prototype motor driver has been built to collect bearing fault signals. The overall experimental setup is illustrated in Figure 4.2 (b) and the key specifications of the tested PMBLDC motor are summarised in Tables 4.1 and 4.2. It consists of a 1.2kW, 4000rpm, 50 Hz three phase PMBLDC motor, connected through a flexible coupling (D30 L42 SY) to a DC motor operating as a DC generator and acting as a load. To apply variable loads to the tested motor, the armature circuit of the DC generator is connected to variable resistor banks.

(a)

Function generator   PMBLDC   DC motor with flexible coupling   Variable resistive

DSD806 Digital Drive

Data question
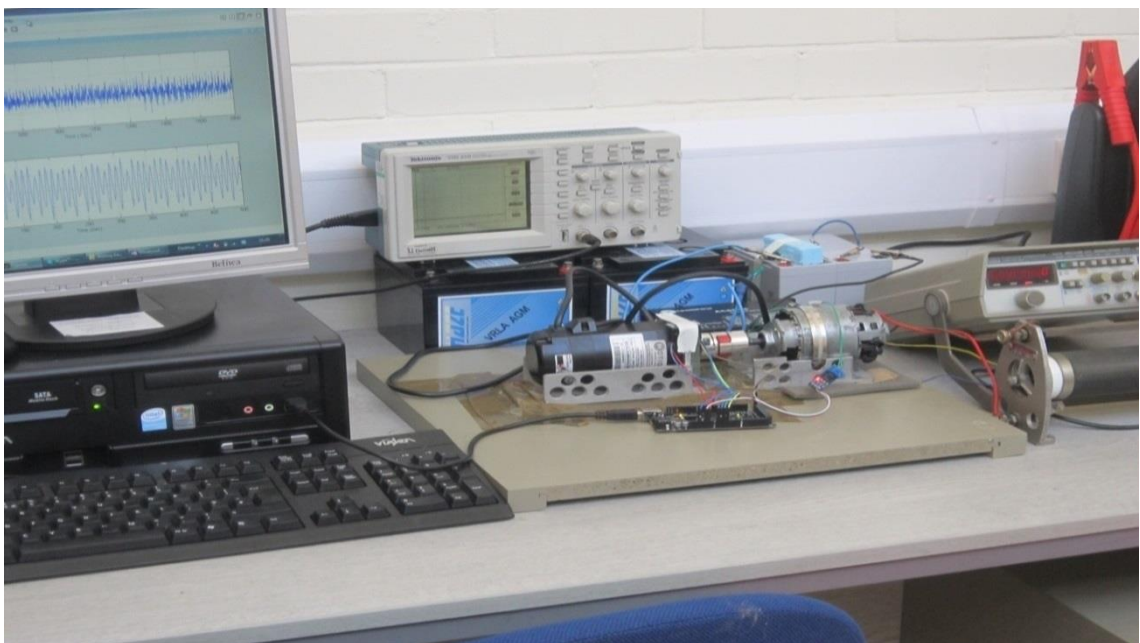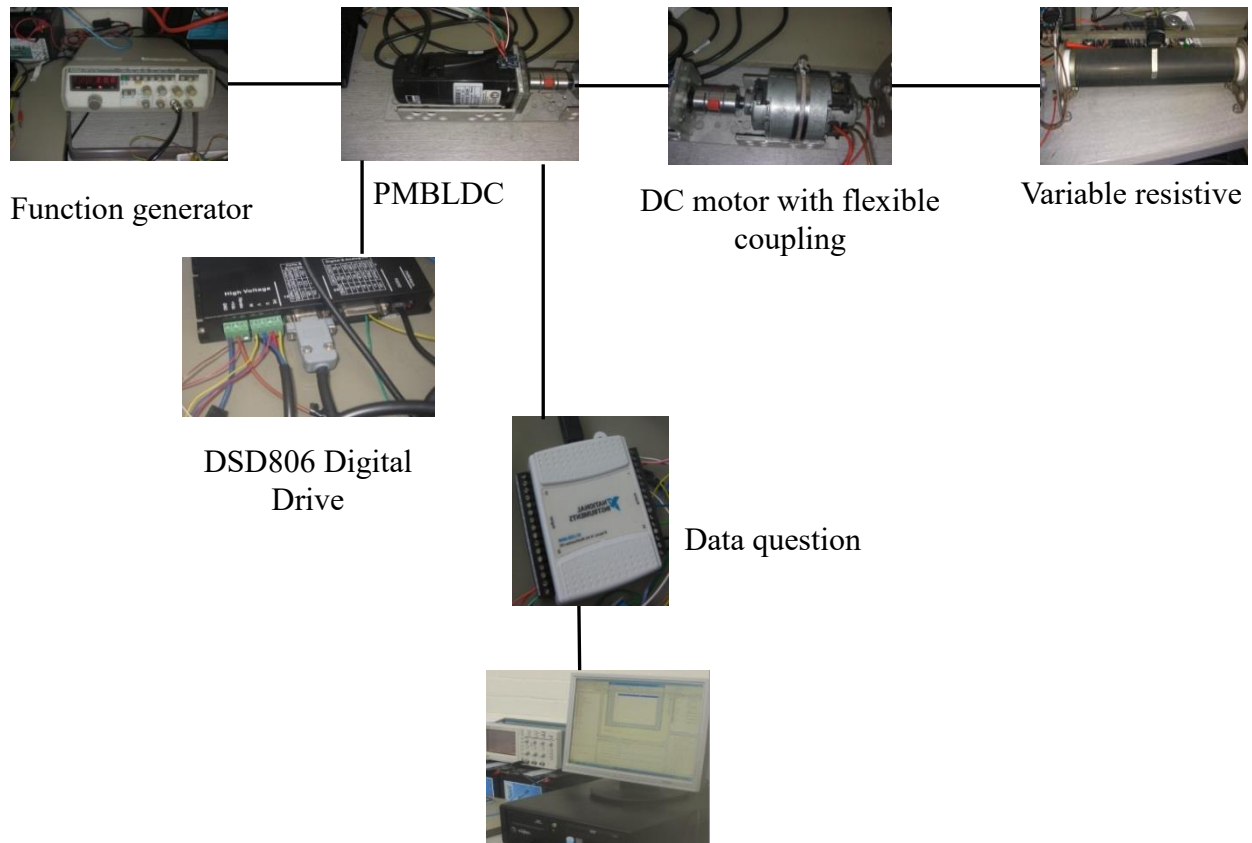
(b)

Figure 4.2 Experiment configurations PMBLDC motor bearing fault: (a) image, (b) schematic

Table 4.1 Parameters of experiment for PMBLDC motor

Parameters	Data
Rated power	400 W
Rated voltage	60 VDC
Rated speed	3000 RPM
Rated torque	1.27 Nm
Torque constant	0.161 Nm/A
Rated current	8.4 A
Inductance	0.59 mH

Table 4.2 Experiment setup requirements

No	Equipment
1	PMBLDC motor
2	Flexible coupling
3	DC motor
4	Motor driver
5	DC power supply (Battery)
6	Function Generator
7	Variable Resistive Load
8	Data acquisition system (Arduino)
9	Current sensor
10	Accelerometer

4.2.1 Test rig construction and components for PMBLDC motor bearing fault diagnosis

The load can be adjusted by changing the resistance rheostat connected to the motor. To emulate a load fluctuation condition, a torque reference is applied to the DC motor that allows increasing or decreasing of the load from 0% up to 100 % of the rated torque of the PMBLDC motor. 180 tests were performed to collect data at normal, abnormal, stationary, non-stationary operating conditions and under different of fault severities.

The PMBLDC motor is driven by an inverter that features an integrated current control loop and provides the electronic commutation necessary to operate the PMBLDC motor. A 24V lead-acid battery was used to supply the PMBLDC motor, through a digital servo drive DSD806. Hall sensors mounted on the rotor shaft provide position control feedback information through a DSD806.

A 3-axis accelerometer (MMA7361) was mounted on the motor bearing housing to collect vibration signals, and three axes of acceleration were measured. Since the accelerometers are usually mounted on the bearing frame, the collected vibration data also contains machinery components vibration.

The contact force between bearing components is continuous under healthy bearing conditions. Therefore, the vibration signal shows a regular signature or characteristic. When a defect or fault occurs on the inner/outer raceway or the rolling element, the interaction between the raceway and rolling elements generate time-varying and non-uniform discontinuous forces that drive vibrations. Additionally a current sensor (ACS714) was used to read the stator current and the load variance using variable resistive load. The experiments were conducted for various load conditions ranging from no load to full load and the rotating speed varied through 600, 900 and 1200 rpm.

4.2.2 Drive user interface system

The operation of the tested drive is controlled by the motor driver model (DSD806) as shown in Figure 4.3 and it is supplied by a DC power supply. DSD806 was developed with 32-bit DSP based on an advanced control algorithm. Their input commands are PUL/DIR signals or ±10V analogue input. A motor driver's characteristics are illustrated in Table 4.3. The DSD806 driver can offer high precision, high speed and high reliability of performance. A DC machine was directly coupled to act as a dynamometer. Since the field circuit of the DC machine was separately excited, an independent DC voltage supply was used to provide the excitation current.

Figure 4.3 DSD806 motor driver (Motion control product LTD 2009)permission to reproduce this figure has been granted by Motion control product LTD

Table 4.3 Features of DSD806 motor driver

no	Features
1	Input voltage: 18VDC – 80VDC
2	Peak current: 18A and continuous current 6A (max.)
3	Self-test function with trapezoidal velocity profile
4	Encoder output
5	Support PUL/DIR and CW/CCW control signals
6	Suitable for 50W-400W servo motors
7	Support clock & direction or ±10V analogue input

4.2.3 Current sensor module ACS712

The ACS712 is an analogue input that provides accurate measurement of AC and DC currents. The main features of the current sensor model ACS721 are 5A range, 5.0 V, single supply operation and low-noise analogy signal path. The device consists of a precise, low-offset, linear Hall circuit with a copper conduction path located near the surface of the die. Applied current flowing through this copper conduction path generates a magnetic field, which the Hall IC converts into a proportional voltage. Device accuracy is optimised through the close proximity of the magnetic signal to the Hall transducer. The output of the device has a positive slope when an increasing current flows through the primary copper conduction path (from pins 1 and 2, to pins 3 and 4). The internal resistance of this conductive path is 1.2 mΩ typically, providing low power losses. Figure 4.4 (a and b) illustrate the board of ACS712 and its schematics respectively.
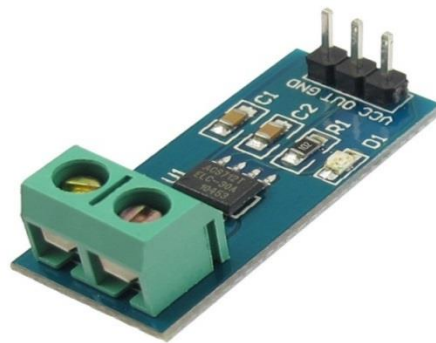
(a)
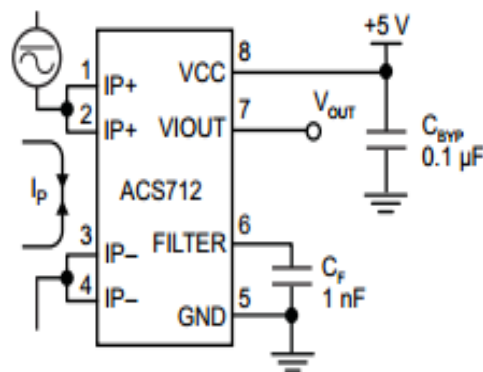
(b)

Figure 4.4 Current Sensor: (a) board and (b) schematic (Allegro Micro Systems 2013), permission to reproduce this figure has been granted by Allegro Micro Systems

4.2.4 Vibration sensor model MMA7361

MMA7361 is a three-axis analogue accelerometer and the main features are Low current consumption: 400 μ A, low voltage operation: 2.2 V – 3.6 V with voltage regulator, signal conditioning with low pass filter, high sensitivity (800 mV/g at 1.5g) and low cost. The MMA7361L includes a sleep mode (3 μ A) that makes it ideal for handheld battery-powered electronics, Figure 4.5 (a and b) illustrate the board of MMA7361 and its schematics.
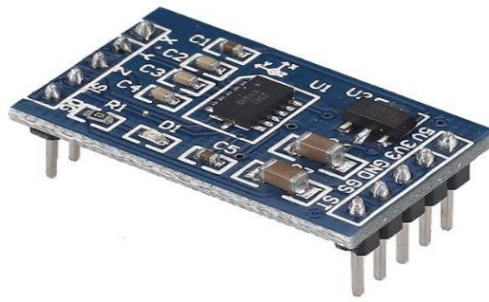
(a)
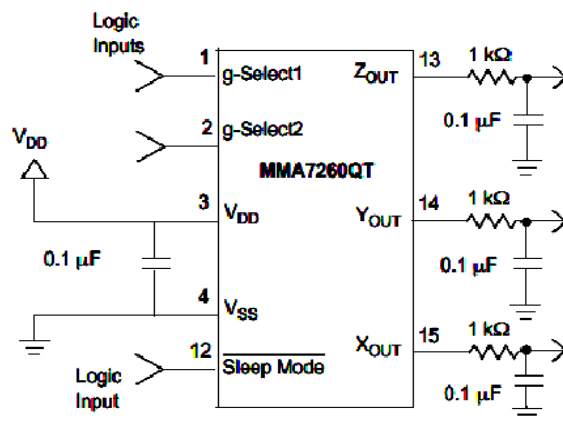
(b)

Figure 4.5 Accelerometer sensor Freescale (2008), permission to reproduce this figure has been granted by Freescale

4.2.5 Data acquisition system

The data acquisition system was designed to acquire radial vibration and stator current signals used for bearing defects on a bearing surface, and a generalised roughness, over a large area of rolling element bearing faults. It consisted of an Arduino omega 2520 model. It can receive input from a variety of sensors and can affect its surroundings by controlling lights, motors, and other actuators. The microcontroller on the board is programmed using the Arduino programming language (based on Wiring) and the Arduino development environment (based on processing), as shown in Figure 4.6 (a).

The Arduino incorporates a 10 bit ADC (analogue-to-digital converter), converting the input voltage range, 0 to 5 volts, to a digital value. Figure 4.6 (b) is a schematic drawing of how the devices are connected to current and vibration sensors. Data acquired from both vibration and current sensors was logged to a Laptop (2.4GHz) at a sampling rate of 300 Hz for 60s periods, so that 18000 data points were logged under healthy operating conditions as well as with the motor running with each type of bearing defect (inner, outer, ball faults and corrosion).

For each of these, the tests were carried out at three different constant speeds (600, 900 and 1200rpm) while varying the load from no-load to 100% of the rated load, and then again at three different constant loads (no load, 50% rated load and 100% rated load) while varying the speed from 600 to 1200 rpm in order to study their possible effects on diagnosis performance. The test motor includes motor in a healthy case, motor with single localised bearing faults and with generalised bearing faults.

Arduino projects can be stand alone or they can communicate with software running on a computer, using Visual Studio in this experiment test system. Visual Studio was implemented to build a data capture interface. Arduino code was implemented to record

as shown in Figure 4.7 and Arduino specification is illustrated in Table 4.4, while the

Matlab 2013a environment was used for analysis.
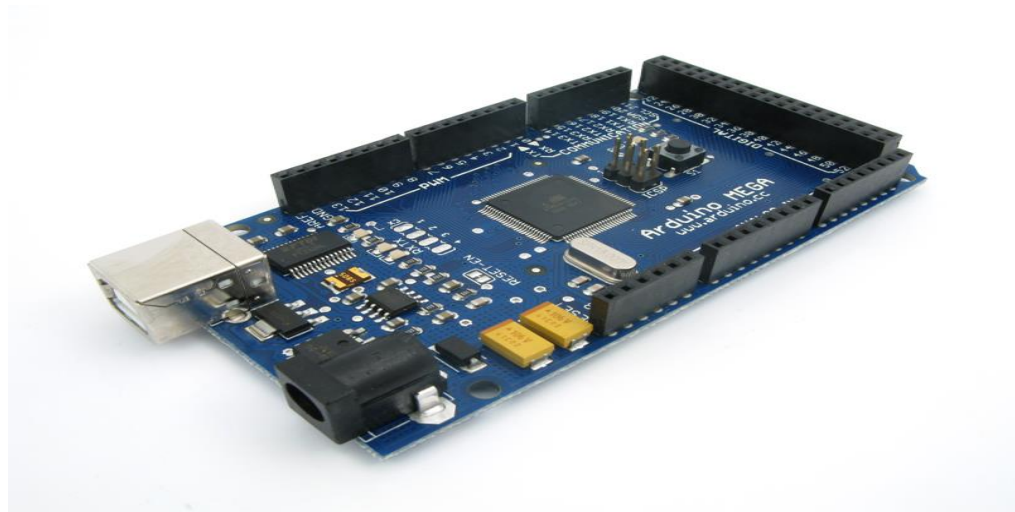
(a)
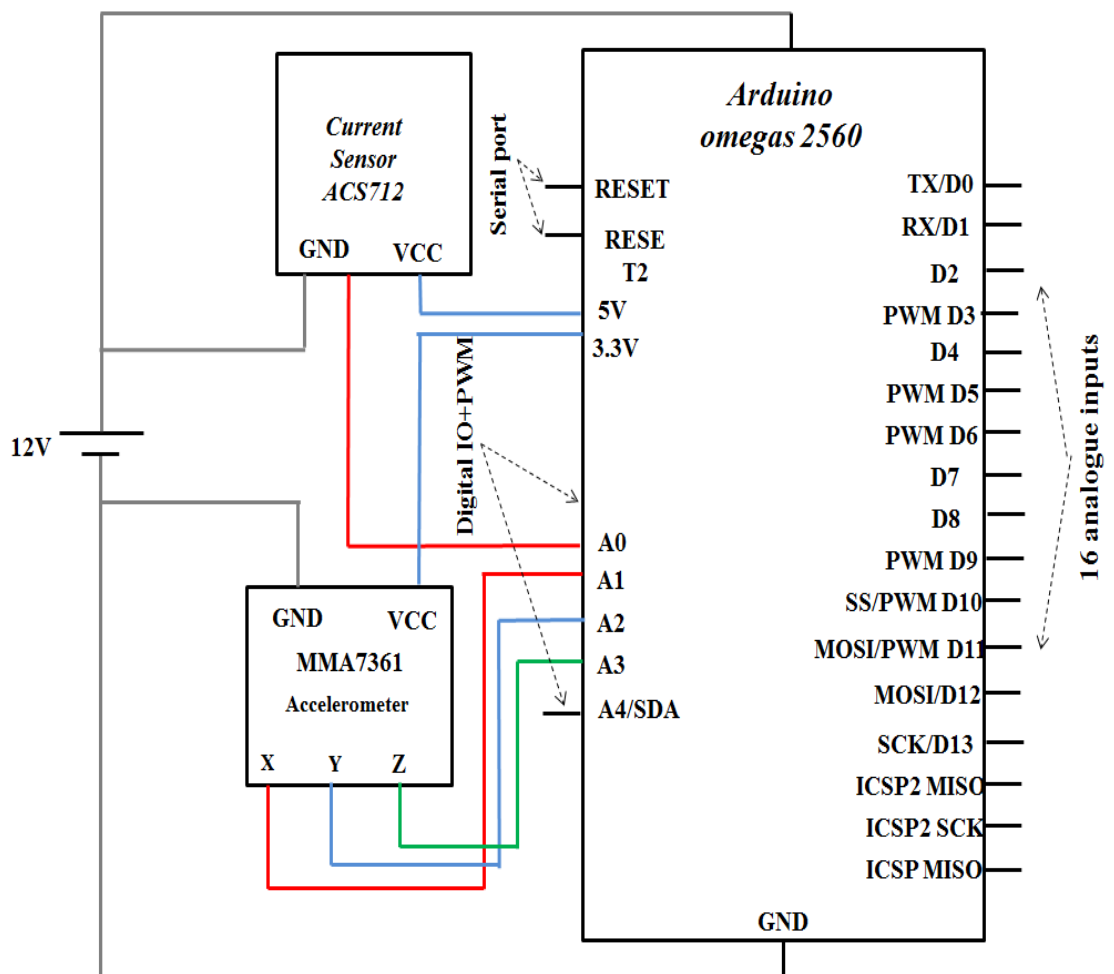
Figure 4.6 Arduino omega 2560 (a) Board image (b) Schematic drawing of Arduino-sensors connection
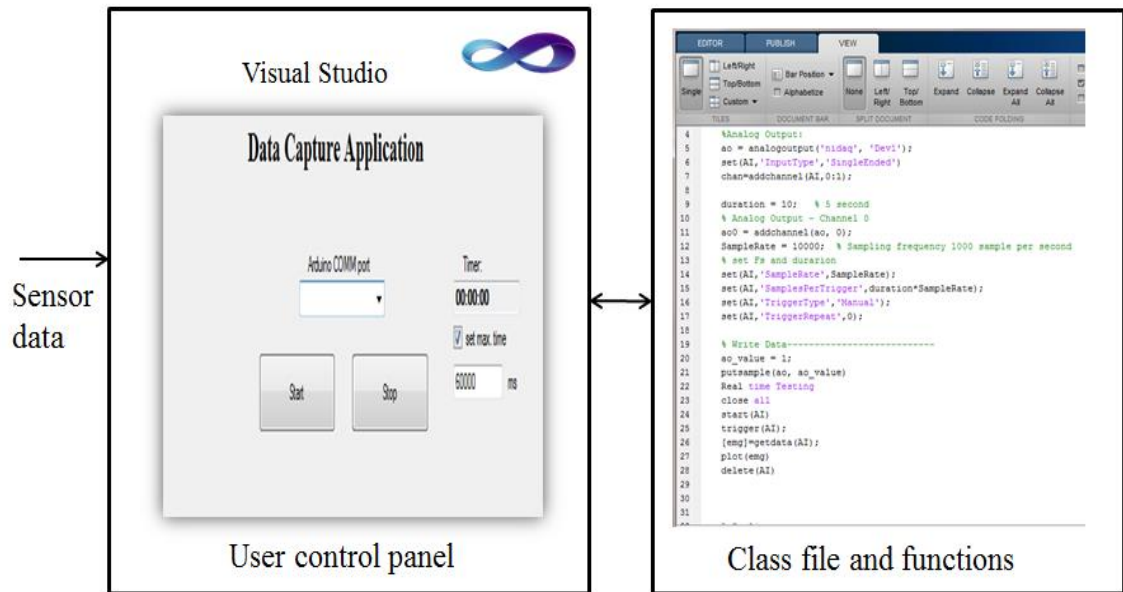
Figure 4.7 Data capture interface

Table 4.4 Arduino omegas 2560 specification

Arduino	Specification
Microcontroller	AT mega 2560
Operating Voltage	5V
Input Voltage	7-12V
Analogue Input Pins	16
Digital I/O Pins	54
DC Current per I/O Pin	40 mA
Dc current sensor for 3.3 v	50 mA
Clock Speed	16 MHz

4.3 Rolling Element Bearings of Single Localised fault

4.3.1 Outer race localised fault

The outer race is mounted in the machine housing and so will not usually rotate. A crack fault was introduced into the outer race with different severities were created using electric spark erosion as shown in Figure 4.8. Data was collected under stationary and non-stationary operating condition as illustrated in Tables 4.5 and 4.6 respectively

(a)

(b)   (c)
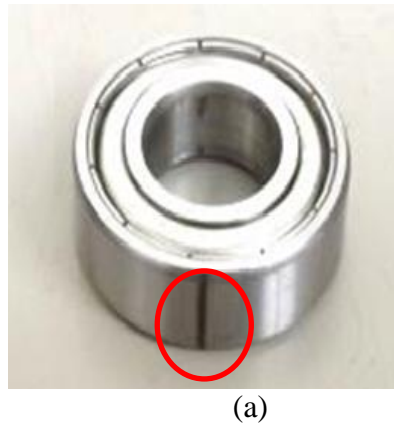
Figure 4.8 Outer race rack fault with different severities: (a) 0.2x1x3 mm, (b) 0.5x1x6 mm and (c) 3x1x9 mm

4.3.2 Inner race localised fault

The inner race is mounted on the shaft of the machine and so will usually be the rotating element. A localised inner race fault was introduced in the same manner to the outer race fault. A crack fault was simulated on the inner race with in three severities, as shown in Figure 4.9.

Table 4.5 Single localised bearing faults under stationary operating conditions

Fault	Fault Severity Width x depth (mm)	Operating condition	
		Load conditions	speed (rpm)
Inner race	1x3x9		
	0.5x1x6	No-load,	600
	0.2x1x3		
Outer race	1x3x9	Full load,	900
	0.5x1x6	Half rated load	1200
	0.2x1x3		
Ball Defects			

Table 4.6 Single local bearing faults under non-stationary operating conditions

Fault	Fault Severity Width x depth (mm)	Operating condition	
		Load conditions	speed (rpm)
Inner race	1x3x9		
	0.5x1x6		600
	0.2x1x3		
Outer race	1x3x9	Variable load	900
	0.5x1x6		1200
	0.2x1x3	Full load	Variable speed
Ball Defects		Half load	
		No load	

(a)

(b)

(c)

Figure 4.9 Outer race crack fault with different severities: (a) 0.2x1x3 mm, (a)0.5x1x6 mm, and (c) 3x1x9 mm

4.3.3 Ball defect

The rolling elements used in rolling bearings are generally ball, roller bearings and tapered roller, as shown in Figure 4.10. The ball bearing transfers the load by point contact with the raceway, so its load-carrying capacity is lower than that of a roller bearing. Rolling bearings are so constructed as to allow the rolling elements to rotate orbitally while also rotating on their own axes at the same time. The rolling elements are usually made of "bearing steel" a type of carbon chromium steel (Emerson bearing 1996).

Figure has been removed due to Copyright restrictions

Figure 4.10 Types of rolling elements bearings (Jens 2014)

4.4 Rolling Element Bearing with Generalised Faults under Laboratory Conditions

A corrosion fault was simulated in the Lab for experimental purposes, using an ultra-sonic device to remove the graze, to study the effect of lubrication on bearing performance, and then using hydrochloric acid (HCL) to simulate faults of four severities, as shown in Figure 4.11.
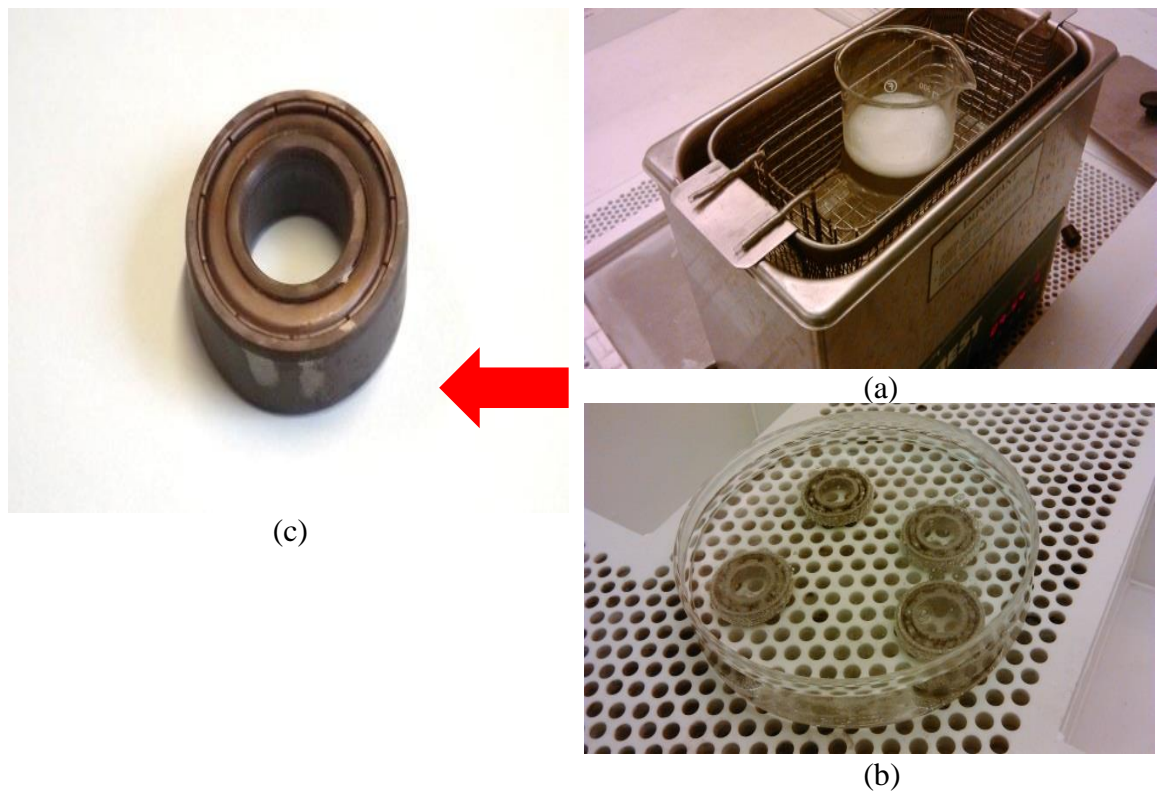
Figure 4.11 Corrosion fault LAB simulator: (a) bearing cleaning, (b) corrosion fault simulator, (c) bearing under corrosion fault
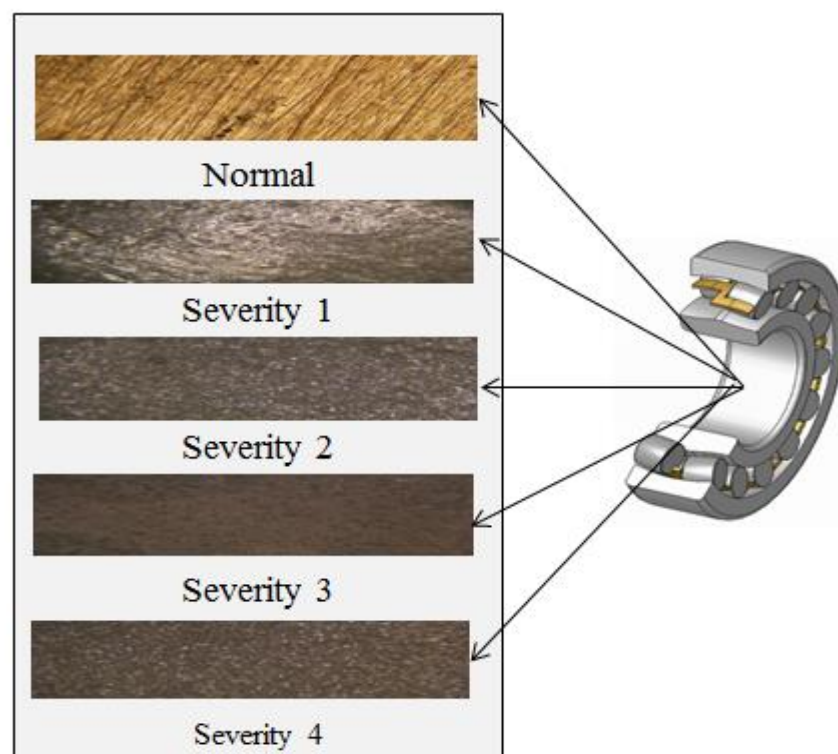
Figure 4.12 Rolling element faults under different severities of corrosion faults

Corrosion faults will form if corrosive material or moisture/water enters the bearing, so that the lubrication no longer provides adequate protection for the steel surfaces of the bearing (see Figure 4.12). It is usually accompanied by increases in the vibration and current signals (Abdusslam 2012).

4.5 Experimental Setup for Thruster Motor Fault Diagnosis

Although modern ship automatic systems are endowed with highly sophisticated subsystems (which are expensive) they also possess manual override facilities in case of emergencies and unforeseen occurrences. However, the luxury of such facilities does not exist on board relatively low cost USVs.

USVs are now being employed by the scientific, offshore and naval sectors to perform a multitude of different tasks with great effect. As a consequence of their success, these sectors are now demanding longer mission lengths, coupled with increasingly more vehicle autonomy.

With an escalation in autonomy comes the need for higher reliability in order for them to better cope with unexpected events. Hence there is a growing interest in the use of fault detection and diagnostic techniques in USVs. At Plymouth University the *Springer* USV has been built and continues to be developed by the Marine and Industrial Dynamic Analysis Research Group (MIDAS).

4.5.1 Test rig construction and components for thruster motor blades fault diagnosis

The propulsion system consists of two propellers powered by a set of 24V, 334N Minn Kota Riptide transom mounted saltwater trolling motors. In common with many USVs, PMBDC motor's is used to provide the means of propulsion, owing to their high efficiency, size and weight.

Thus the timely isolation of faults in a motor will ensure the integrity and safety of a vehicle whilst not adversely affecting the overall system performance. In practice when undertaking a mission, if necessary, a fault detection and diagnosis can be instigated on board a USV whilst at the same time using telemetry to supply its mission control centre with a status report. The objective of this chapter is to devise the experimental setup for the calculation of a PMDC motor based trolling motor. Both motors parameters, including vibration and current under normal and abnormal operating conditions, are collected and used to diagnose blade faults (unbalanced mechanical load).

Propellers in the thruster motors are durable but not indestructible. Hard surfaces can damage blades partly or fully and can imbalance the operation of a trolling motor, causing significant damage to the internal parts. The diagnoses of these faults are thus necessary for the healthy operation of the thruster motors and critical for USV operations. As shown in Figure 4.13, the proposed technique was used to show the behaviour of the motor under normal operating condition and four faulty conditions in 10% (F1), 25% (F2), half (F3) and full cut (F4).
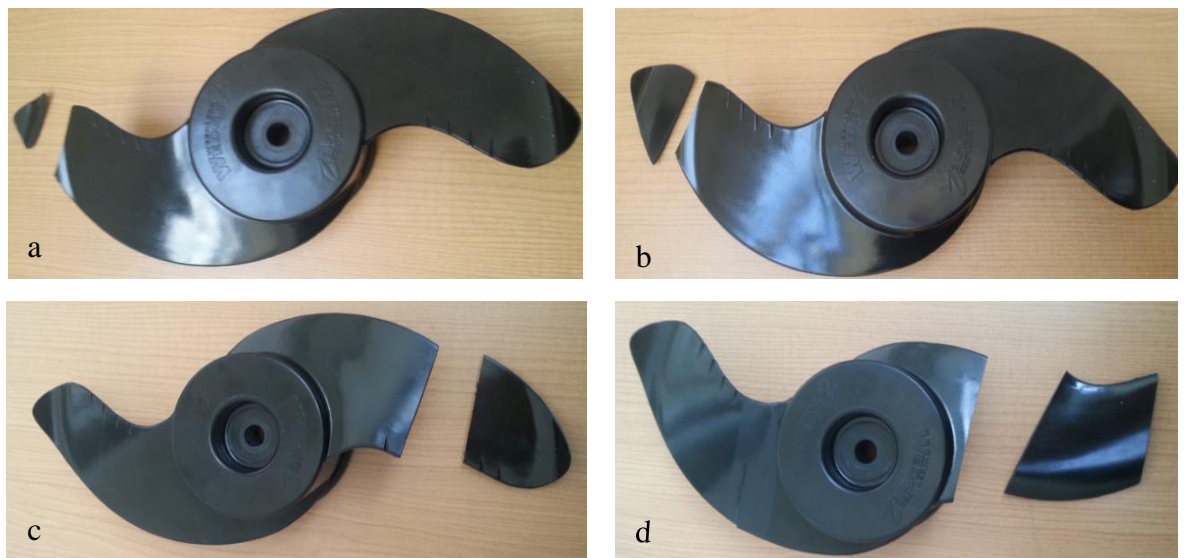
Figure 4.13 Faults in the blades of the thruster motor (a) 10% f and (b) 25%, (c) 50% and (d) full cut

Figure 4.14 (a) shows the laboratory set up for the trolling motor and Figure 4.14 (b) represents its schematic diagram.. A pulse width modulation (PWM) switching technique was used for controlling the speed of the trolling motor by changing the duty cycle of the pulse, as shown in Figure 4.15.
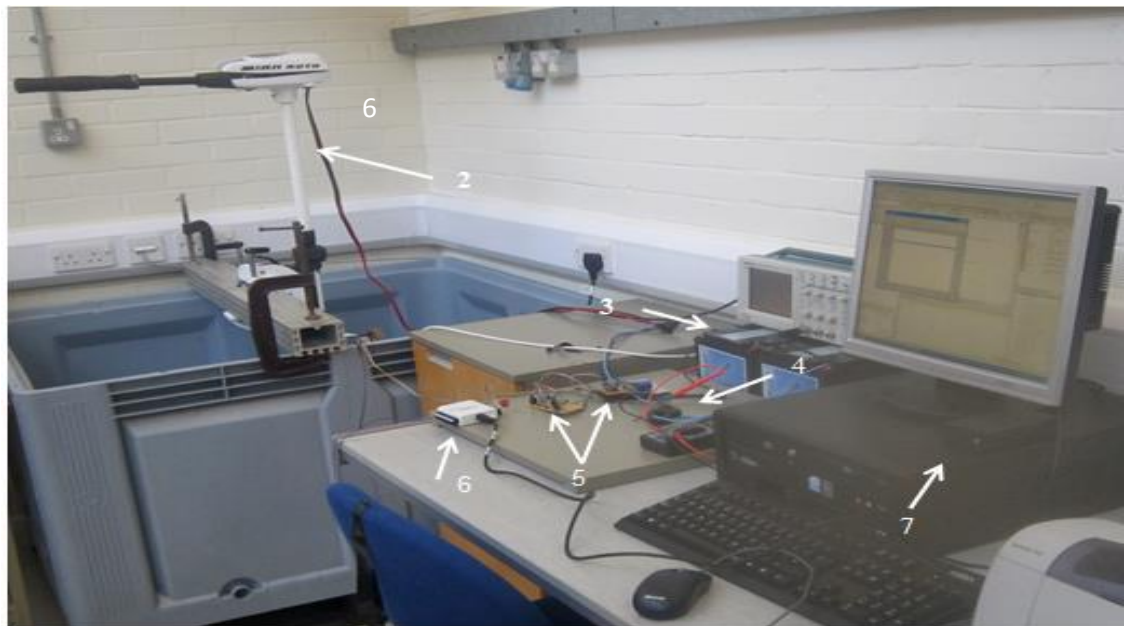
(a)
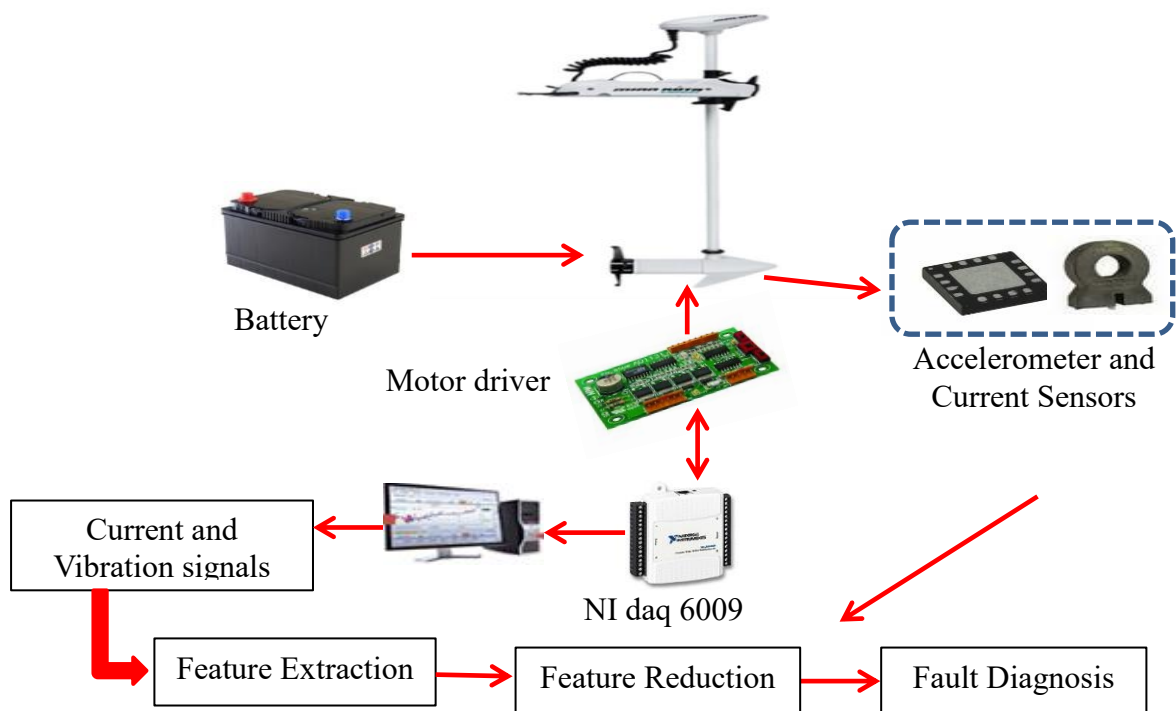
(b)

Figure 4.14 Trolling motor: (a) experimental setup, (b) Schematic of experiment se

A linear current sensor was used to measure the stator current and 3-axis accelerometer (ADXL325) with a full-scale range of ±5 g and bandwidth of 0.5 Hz to 1600 Hz was mounted on the flat surface of the propeller to record the vibration signal. Sensor outputs were logged into a PC via a data acquisition card (NI USB-6009 multifunction I/O device). Matlab was used to change the duty cycle of the PWM signals and the motor was powered by a 24V battery supply.

Data was gathered for five cases: no fault (normal operating conditions), and faults F1–F4, at a sampling rate of 10 kHz for duration of 30 sec,300,000 sample points were obtained for current and vibration at variable rotor speeds.
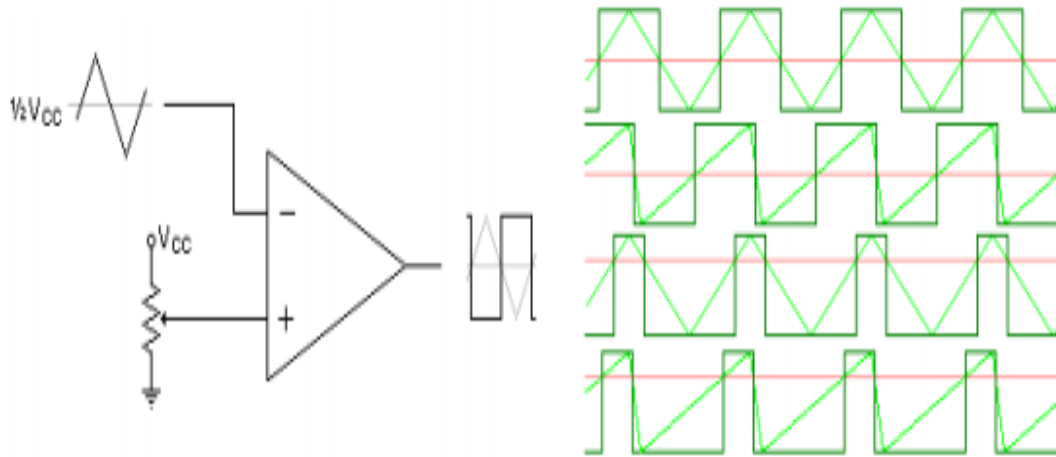
Figure 4.15 PWM Waveforms (Kuphaldt 2009)

4.5.2 Motor driver circuit

The motor drive circuit includes the following components:

An operational amplifier (MCP604) has been used in the circuit driver. This microchip element is suitable for working with low power. MCP604 is implemented to produce a square wave. The high frequency PWM power control system can be realised using semiconductor switches. In this report a metal oxide semiconductor field effect

transistor (MOSFET) driver (TC429) has been used to drive high capacity power MOSFET gates, as shown in Figure 4.16.
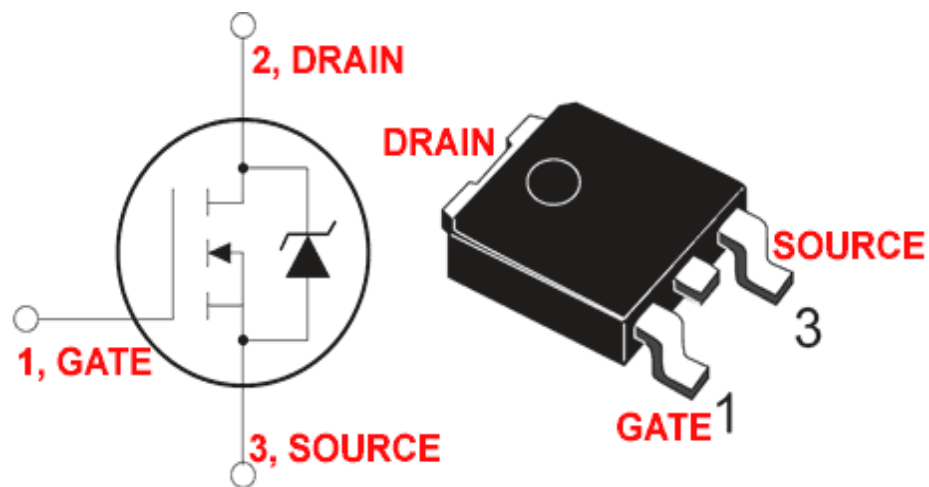
Figure 4.16 MOSFET circuit diagram, (Administrator 2005). Permission to reproduce this figure has been granted by Administrator

When the MOSFET is turned off this causes a voltage spike, so a main capacitor is connected in parallel with the battery to absorb a spike voltage, and when MOSFET turns on again the main capacitor supplies current during the period when the battery current is being re-established.

Diode (1N404) was used to absorb the recoil reverse voltage to protect the MOSFET from high voltage. It must be able to generate voltage signal (0-5) v trough NI DAQ6009. However, the typical voltage signal that a computer generates does not have sufficient current to power the motor, so an amplifier is used to send an amplified signal to the motor by switching MOSFET on and off.

To protect MOSFET from power dissipation and high currents, a heat sink was used in the present circuit. It allows an increase in surface area in contact with air. A voltage regulator was used to supply the required voltage (12v) to the current sensor as shown in Figure 4.17 (a and b) and Figure 4.17 c illustrate the schematic diagram of the motor driver.
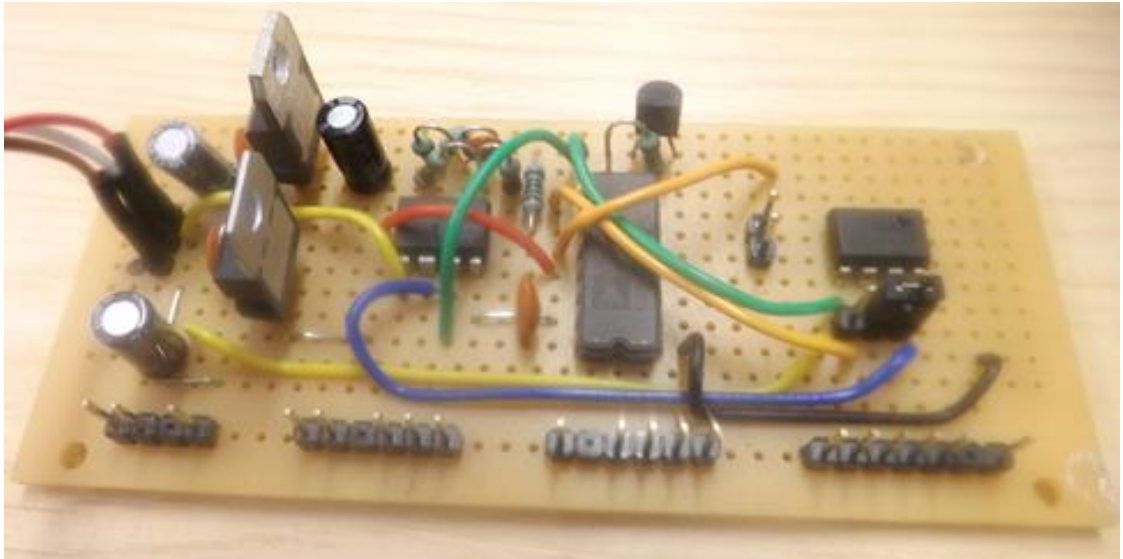
(a)
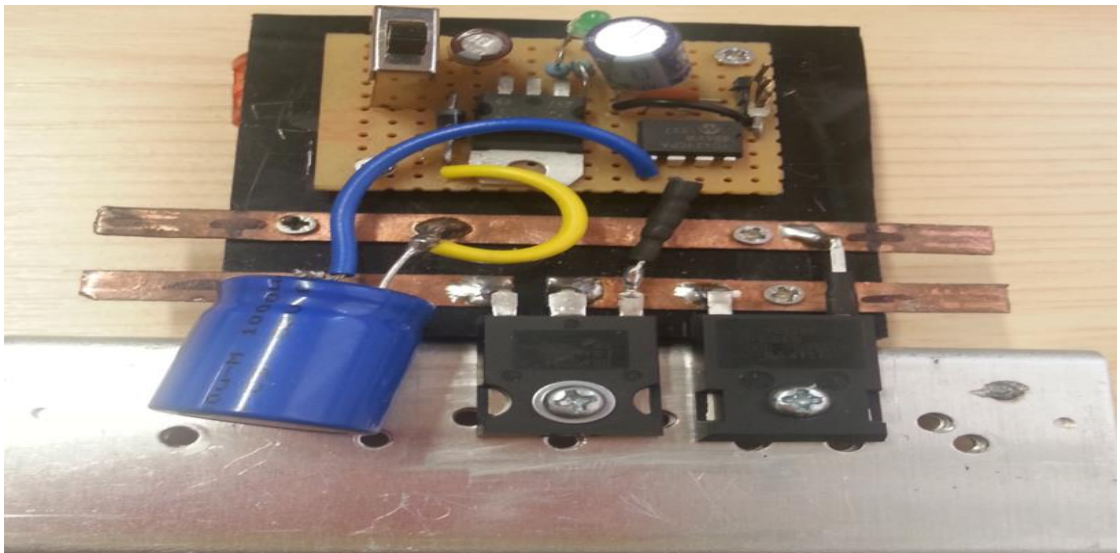
(b)
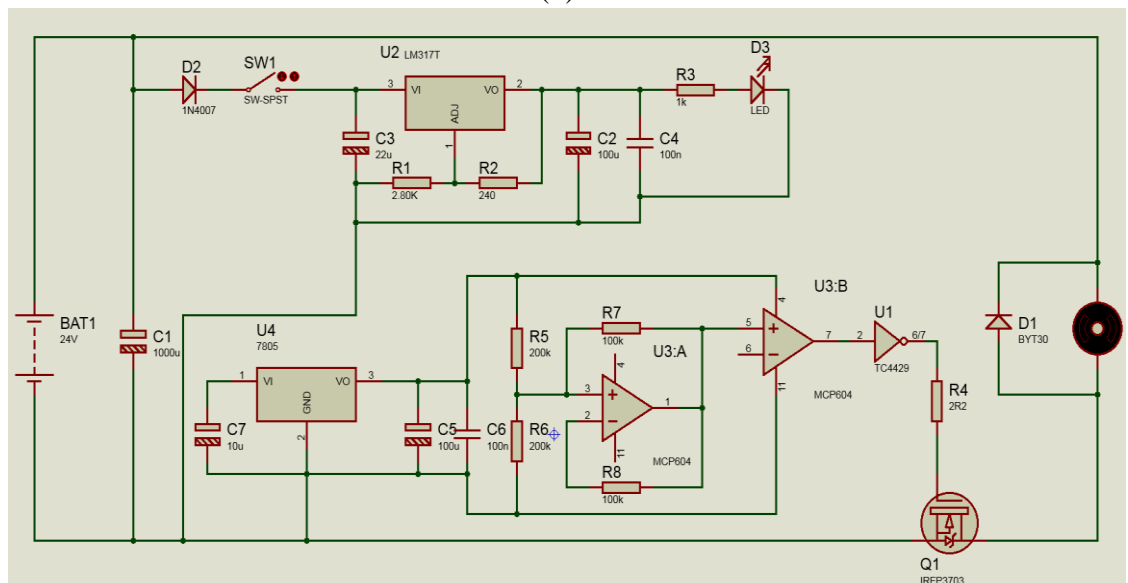
(c)

Figure 4.17 (a) and (b) motor driver boards and (c) circuit diagram of the motor driver

4.5.3 Current sensor

The Honeywell CS series linear current sensor is illustrated in Figure 4.18. The sensing element is assembled in a printed circuit board mountable housing. The combination of the sensor, flux collector, and housing comprises the holder assembly. The main features of *CSLA* are: linear output, AC or DC current sensing, fast response time, minimum energy dissipation, reliable operation, reliable low cost sensing, and an operating temperature range of -25 °C to 85 °C.

Figure has been removed due to Copyright restrictions

Figure 4.18 CSLA Series linear current sensor (Honeywell Inc 2014)

4.5.4 Vibration sensor

For the experimental study, a 3-axis accelerometer (ADXL325) was used, with a minimum full scale range of ± 5 g, sensitivity 174 mv/g and bandwidth 0.5 Hz to 1600 Hz. It was mounted on the motor bearing house to collect vibration signals, with a voltage supply operation between (1.8-3.6) v and supply current 350µA (Analog Devices 2009). Figure 4.19 (a & b) illustrate the accelerometer board and its schematics respectively.

(a)
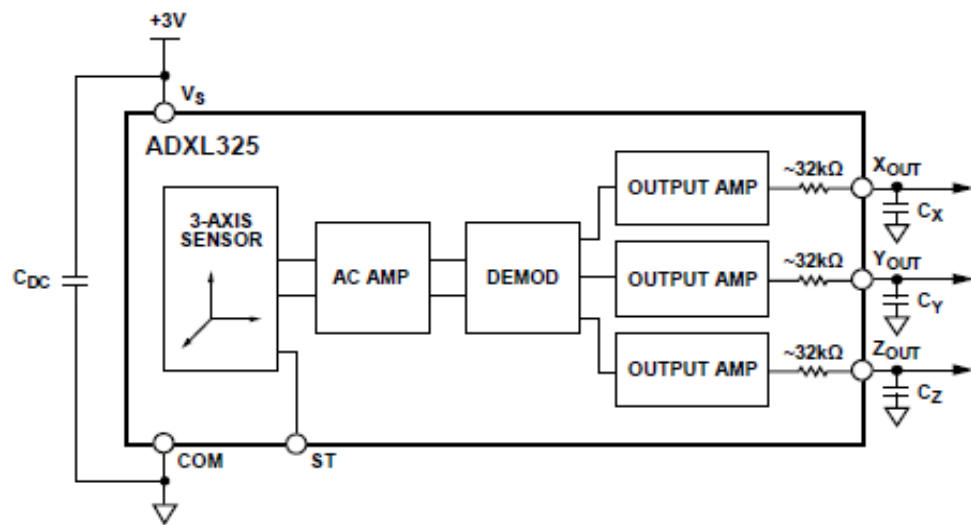
(b)

Figure 4.19 ADXL325 Accelerometer: (a) board, (b) schematics (Analogy devices 2014). Permission to reproduce this figure has been granted by Analogy devices

4.6 Data acquisition system

The Data Acquisition system (DAQ) used: NI-6009 from National Instruments provide the connection to eight single ended analogue input (AI) channels, two analogue output (AO) channels, 12 digital input/output (DIO) channels, and a 32-bit counter with a full-speed USB interface, 0 or 5V, (8.5 mA for outputs) and 1 counter. The LabVIEW software driver was installed and properly configured.

The Data Acquisition Toolbox in MATLAB is needed in order to write and read data to and from a USB-NI 6009 DAQ. These software drivers will ensure and establish a communication link between the computer and the electronic equipment. The 32-bit version of the DAQ Toolbox supports National Instruments devices that can be used with this interface.

The Lab View software driver must be installed and properly configured, as shown in Figure 4.20. In general, data acquisition programming with NI-DAQ involves the following steps:

➢ Initialization needs to specify which ports are being used.

➢ Acquiring data Start AI, not a manual trigger, and extract all data from sensors

➢ Perform read operation from DAQ

➢ Perform write operation from DAQ

➢ Stop and Clear the Task.

To connect sensors to NI-DAQ, a current sensor is connected to an analogue input voltage with port (aio), the accelerometer is connected to the analogue input port with (ai1) and the digital input speed connected to the digital input (ctrl.0); NI-DAQ device is designed to handle maximum signals od 5.0Volt and there is common ground (GND) as detailed in Figure 4.21 (a and b). Moreover the Intel® core i5-2140M computer with central processing unit of 2.40 GHz and 6.0 GB was used in real time implementation.
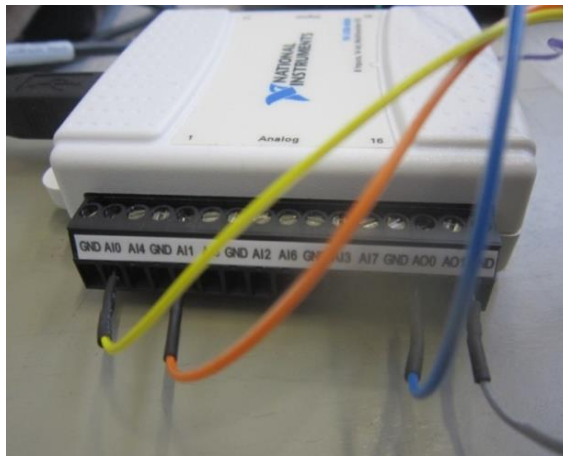
(a)   (b)

Figure 4.20 DAQ connection: (a) analogue input, (b) digital output

Assistant of Lab VIEW 8.0 version was used, and the programming steps are as follows: setting some parameters including the signal type, sampling rate, sampling number and sampling method in a new DAQ Assistant task; transforming the task into a sub VI to generate a graphical code.

Lab VIEW has two main areas in which an application is created. The first area is called the front panel. This is where the architecture of the application is designed. Controls and indicators are placed on the front panel. They are the interactive input and output terminals of the application. Common controls of the front panel include knobs, push 2 buttons, and dials. Common indicators include graphs, slide devices, and digital displays. Figure 4.21 shows the virtual instrument (VI) a block diagram where NI-DAQ card is used to collect and send data.VI allows the user to control the speed of the thruster motor by changing the frequency then collect line current and vibration signals
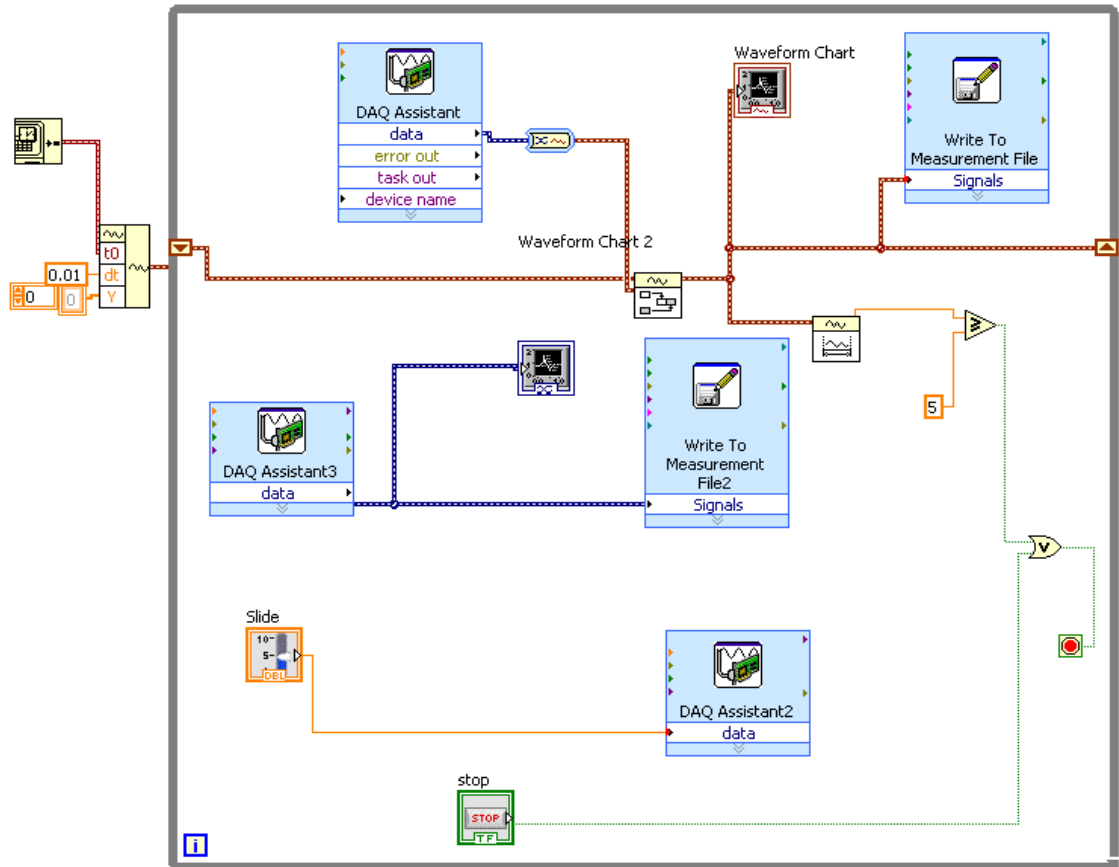
Figure 4.21 Block diagram for interfacing built using LabVIEW and NI-DAQ

4.7 Chapter Summary

This chapter introduced the experiment design and the data acquisition system used to validate the proposed research schema for PMBDC motor rolling element bearing and PMDC motor blades fault diagnosis. The structure of the experiment prototype and details of instruments used have been described. Both single localised and generalised bearing faults were simulated under different degrees of severity to measure the performance of the bearings. Vibration and current signals were collected during the experiment under stationary and non-stationary operating conditions. Also in this chapter, blade faults of thruster motors based on a PMBDC motor were simulated for four levels of fault severity, under stationary operating conditions, and data acquisition for vibration and motor current signals was considered.

CHAPTER 5

PMDC Motor Faults Analysis under Stationary and Non-Stationary Operating Conditions

"This chapter introduces raw vibration and current measurements as indicators for fault detection and diagnosis in roller bearings and unbalance mechanical load faults under stationary and non-stationary operating conditions"

5.1 Introduction

After presenting the experimental set-up in Chapter 4, for both rolling element bearing and thruster motor blades faults, this chapter introduces both stator current and radial vibration signals at different speed and load conditions, to validate the proposed fault diagnosis approach. Localised and generalised roughness bearing faults of PMBLDC motors at different severities of defect are considered. In addition, fault diagnosis of generalised roughness bearing defects is common in industry, but there is a little research in the available literature about this type of faults. However, only a few studies in the available literature have used current and vibration for fault diagnosis

The difficulty of research about generalised roughness or extended faults is that there are no characteristic fault frequencies reflected by the current or vibration signals associated with generalised roughness faults (Immovilli et al. 2009).

This chapter is organised as follows: after the introduction, the ability of stator current and vibration signals for fault indication is presented in section 5.2. The normal characteristics of rolling element bearing are discussed in section 5.3.

Localised bearing faults phenomena under stationary and non-stationary operating conditions are presented in section 5.4; the discussion includes the measured data of cooperation between time waveform and spectrum under stationary operating conditions. Next, generalised roughness (extended) bearing defects under a multitude of fault severities with stationary and non-stationary operating conditions are presented in section 5.5.

To validate the proposed fault diagnosis approach, unbalance mechanical load faults (blades fault) of thruster motors based on BMBDC motor are studied, under different rotation speed conditions. Thruster motor based PMDC motor blades fault analysis will be discussed in section 5.6.

5.2 Vibration and Stator Current Signals Monitoring

Many techniques have been used for rolling element bearing fault diagnosis, and can be classified depending on the type of measurement involved. These can be, for example, vibration, temperature (Patil et al. 2010) or acoustic measurements (Delgado et al. 2011).

Vibration motoring test analysis is an effective tool to determine the level of bearing faults on an electrical machine by measuring the level of vibration of the machine casing (Chiementin et al. 2008, Amar et al. 2014). To determine the rolling bearing faults, an accelerometer vibration analysis is used to measure the vibration characteristic frequencies at a horizontal position to the motor housing.

When a rolling element hits a structural defect in the raceway, a series of vibration pulses will be produced, depending on the location of the defect (e.g. on the outer or inner raceway, or on the rolling element itself). The pulses will contain characteristic frequencies specific to the bearing geometry and operation condition (e.g. rotating speed and variable load) (Jin et al. 2014).

However, vibration can be picked up from other mechanical parts, thus leading to false positives. Furthermore, because vibration signals are related to all the mechanical elements, they only allow for fault detection rather than fault diagnosis. In order to increase fault diagnosis reliability, especially for critical applications, in addition to vibration, the stator current signal can be used as another faults indicator (Trajin et al. 2009). Further, a bearing defect will lead to eccentricity fault, and then electrical parameters magnetic flux and current will affected, so that the current signal can be considered as a bearing fault.

Therefore, a bearing diagnostic technique needs to be designed that is robust enough to differentiate between various vibrations signals, in order to effectively classify faults to overcome false alarms. To increase diagnostics reliability, stator current can also be used to detect bearing faults, stator current sensor are already used as a part of control and protection systems in electric power systems so the use of a current sensor does not necessarily increase the cost of the system. (Bediaga et al. 2013). It has been shown that current signal can be an effective rolling element bearing fault indicator, especially at low motor speeds (Immovilli et al. 2010).

The relation between vibration and current signals caused by bearing faults is presented in two approaches. In the first approach, the vibration at one of the mechanical frequencies characteristic of the defect impacts on the electric machine torque fluctuation, which produces a speed ripple (Immovilli et al. 2009). According to the

second approach, the mechanical vibrations in the air gap due to bearing faults can be considered as slight rotor displacements, which result in instant eccentricities.

Thus, the combined use of both vibration and current signals will provide a more robust fault detection and diagnosis system (Esfahani et al. 2014), and this is the approach used in this work. The relationship of the bearing vibration to the stator current signature can be determined by recalling that any air gap eccentricity produces anomalies in the air gap flux density. Since ball bearings support the rotor, any bearing defect will produce a radial motion between the rotor and stator of the machine.

5.3 Normal Characteristics of Bearing Working Under Stationary Operating Conditions

Ball bearings were used for the study of transducer response to raceway and rolling element defects, respectively. Ratios of tested bearing frequencies to shaft speed were based on experimental data from good bearings. Note that these values may change due to defect effects and vary with operating conditions. In this study, a PMBLDC motor is tested under stationary and non-stationary operating conditions, as mentioned in Chapter 4. The data was calculated as illustrated in Table 5.1.

Table 5.1 Rolling element bearing experimental data description

Bearing defects		No of samples	Dimension	class	Sample per class
Localised bearing defects	Inner race	54336	2	3	18112
	Outer race	54336	2	3	18112
	Ball defects	18112	2	1	18112
Generalised bearing defects	Corrosion	72448	2	4	18112

Figures (5.1 to 5.3) shows the original time wave form and FFT spectral of the stator current and bearing raw vibration signals of a motor operating under normal conditions. The figures represent a motor operating at stationary conditions under no-load, half load and full load, and with 1200 rpm rotational speed; the peaks in this spectrum show the energy distribution at different frequencies.

This fluctuating load leads to a modulated current waveform, as shown in Figure. 5.2. Current waveforms exhibit certain amplitude modulations in line with the torque waveforms. The current flowing through the motor can then be calculated:

$$I = (V_s - V_{emf})/R = (V_s - K_i * \omega)/R \tag{5.1}$$

where V_s is the source voltage and R is the motor electrical resistance; the torque generated by the motor is proportional to the amount of current flowing through the motor:

$$\tau = k_t * I \tag{5.2}$$

where kt is a constant and τ is the torque. At full load the motor has the maximum current flowing through it, thus producing the maximum torque. Whereas, at no load and low speed, motor torque and current will decrease according to the following equation:

$$\text{Mechanical Power } Pm = \tau * \omega \tag{5.3}$$
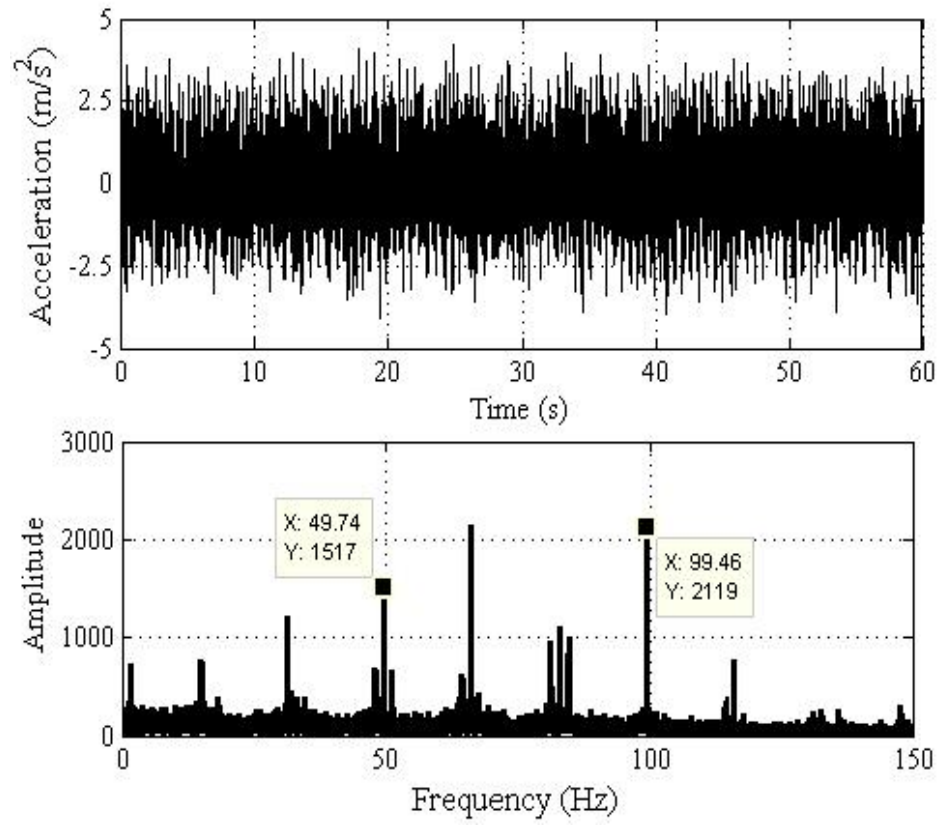
(a)
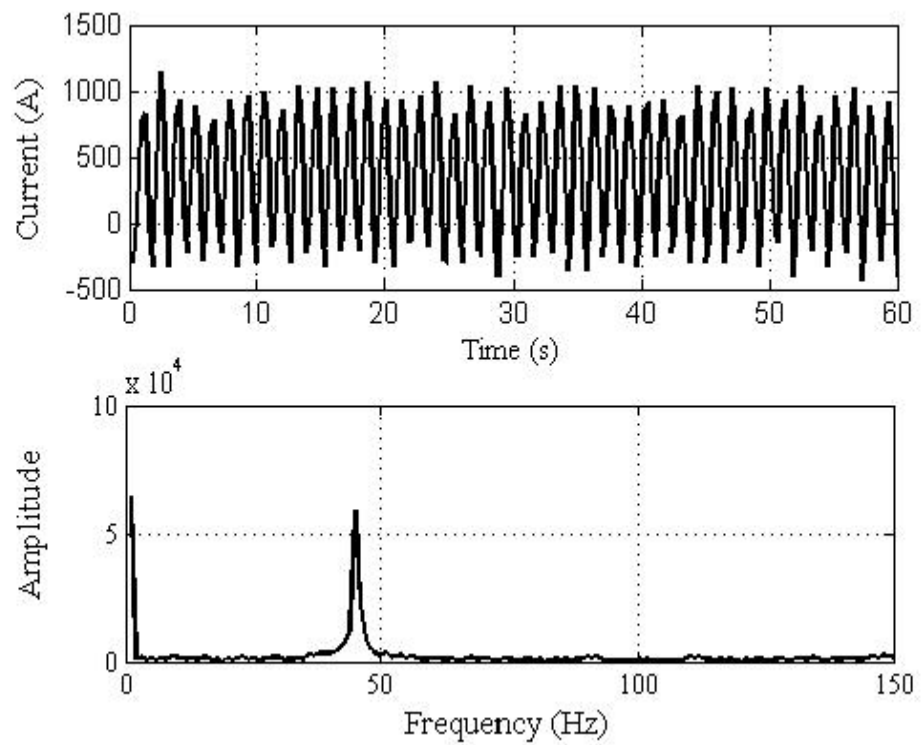
(b)

Figure 5.1 PMBLDC motor (a) raw vibration and (b) stator current at normal and stationary operating conditions (no load and 1200rpm)
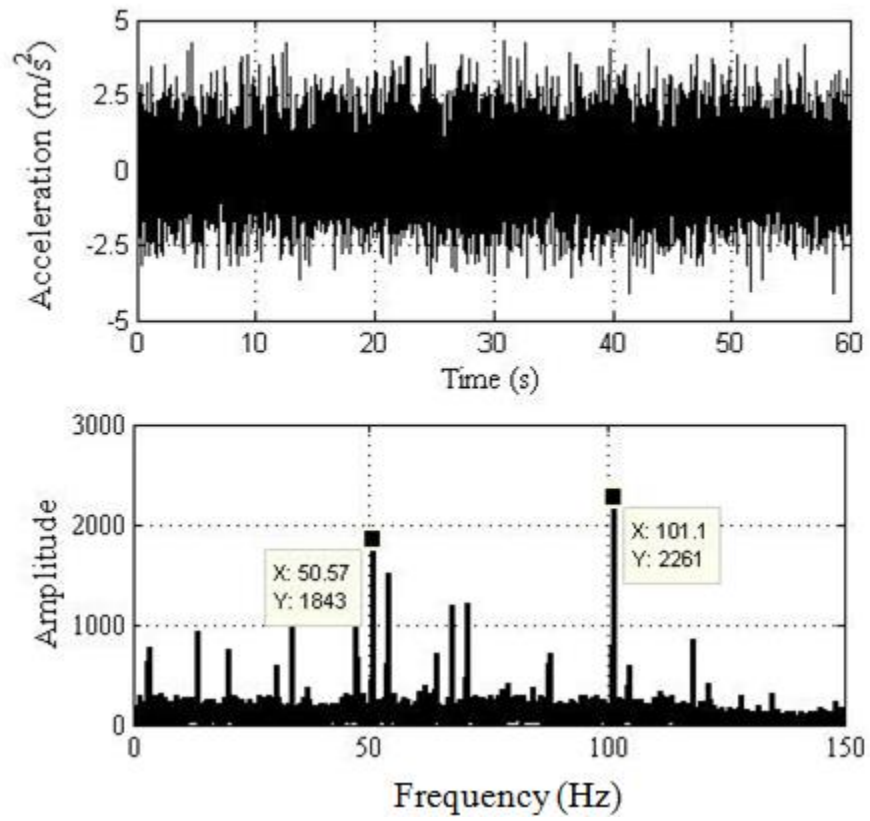
(a)
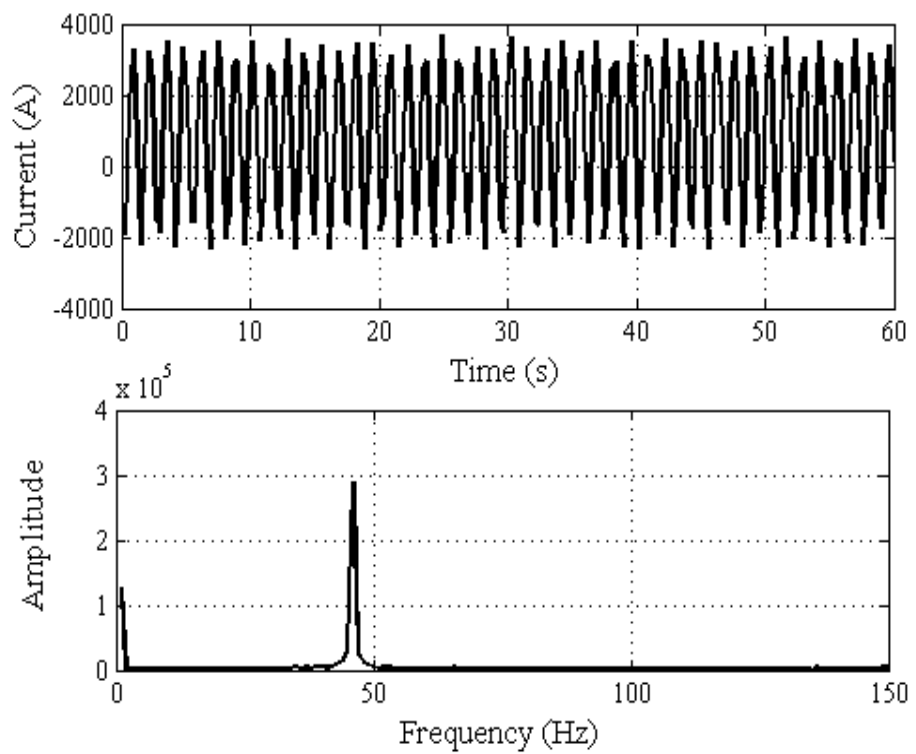
(b)

Figure 5.2 PMBLDC motor (a) raw vibration and (b) stator current at normal and
stationary operating condition (full load and 1200rpm)
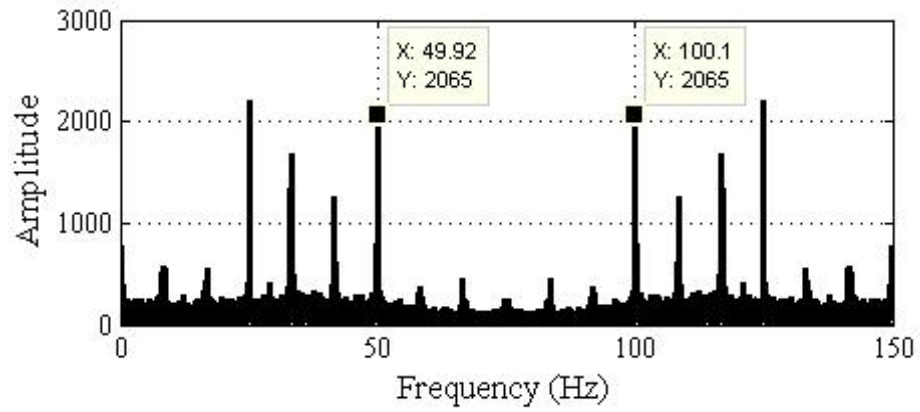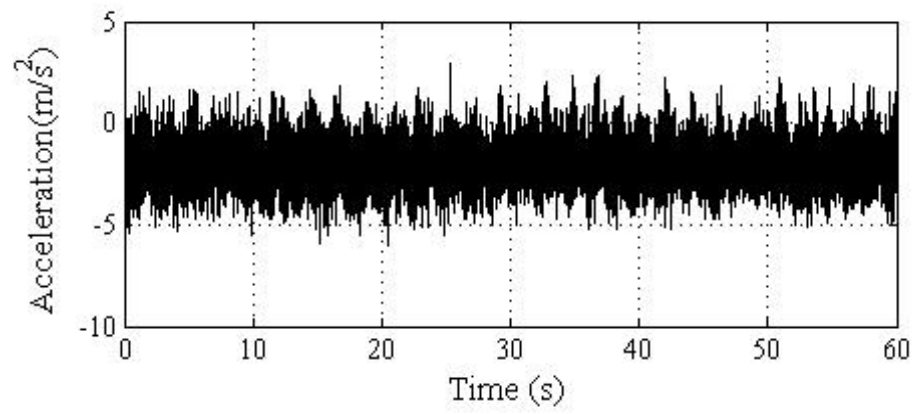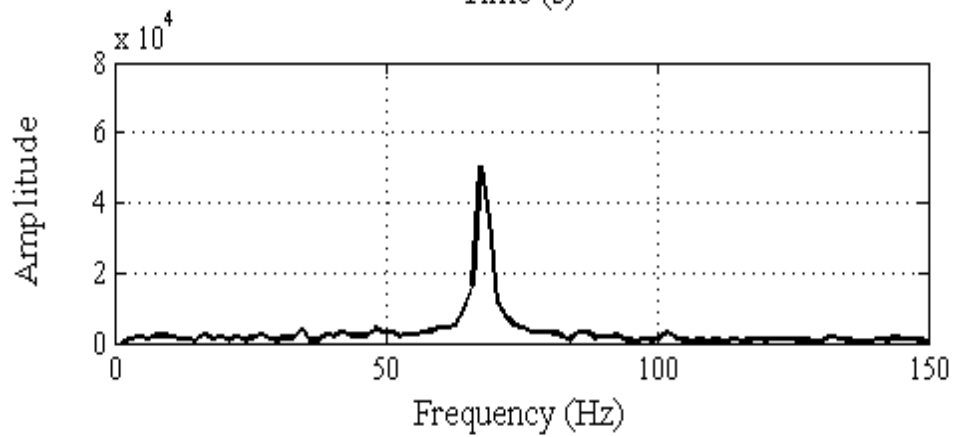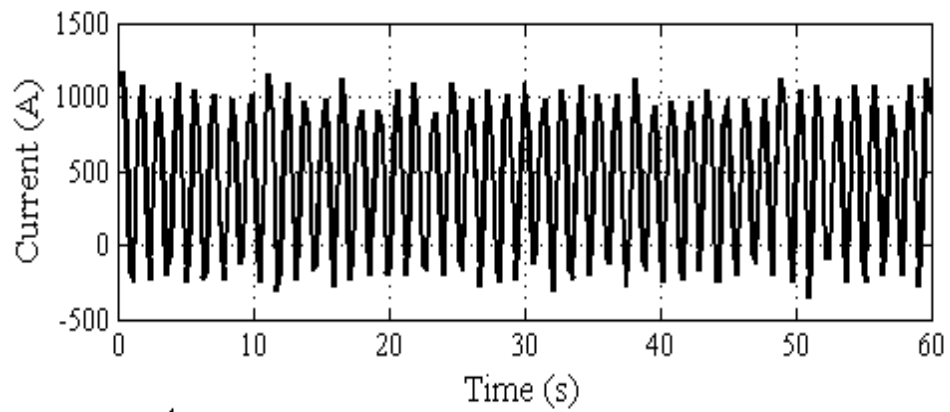
Figure 5.3 PMBLDC motor (a) raw vibration (b) stator current at normal and stationary
operating conditions (half rated load and 1200rpm)

5.4 Bearing Characteristics under Faulty Conditions

Bearing defects can be classified into two categories: single localised bearing defects (inner race, outer race and ball) and generalised roughness defects (extended). Faults in rolling element bearings give impulses as the elements contact the fault and the typical is vibration produced. In this section the behaviour of a PMBLDC motor under rolling element baring faults will be discussed and the effect of stationary and non-stationary speed and load conditions on vibration and current signals will be considered.

5.4.1 Single localised bearing faults under stationary operating conditions

For the single defect on the race, a set of experiments was performed at different speed and load conditions. Frequency calculation is based on the geometric parameters of the actual linear bearing, applied to the kinematic model presented earlier. The experiment used bearing model 6002 ZZ WM1 with number of balls (z)=9; Pd=25mm, BD=3mm, inner diameter 14mm, outer diameter 32mm, ball diameter 3mm, and contact angle assumed β=0, as shown in Figure 5.4.
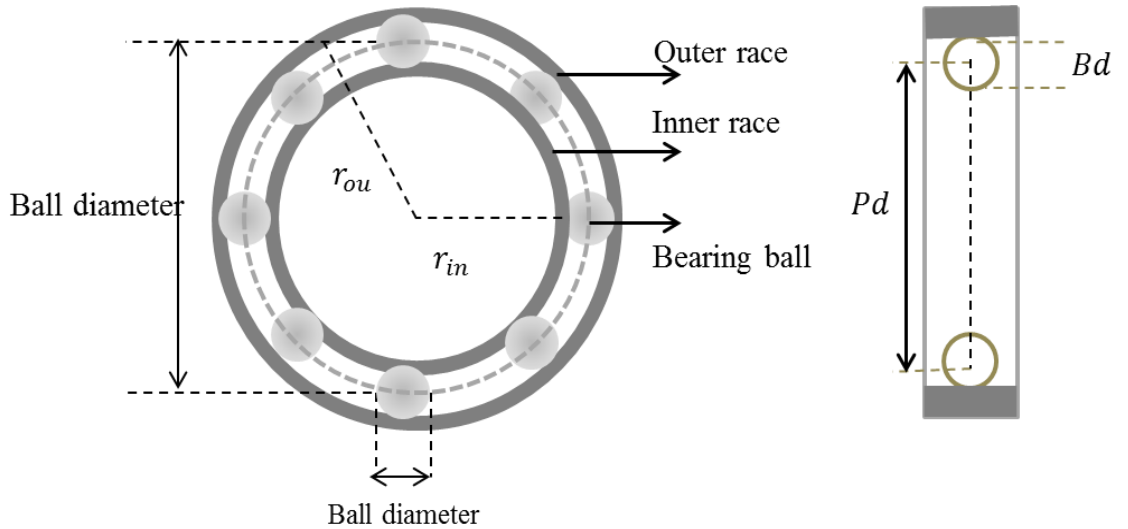
Figure 5.4 Rolling Element bearing component

Table 5.2 Fault classification for all bearings

Fault location	Outer race			Inner race			Ball
Fault location	A (mm)	B (mm)	C (mm)	A (mm)	B (mm)	C (mm)	Spot (mm)
Fault size	3	1	9	3	1	9	0.3
	0.5	1	6	0.5	1	6	
	0.2	1	3	0.2	1	3	

Table 5.3 Bearing defects Frequencies

f_s (Hz)	N (rpm)	BPF0 (Hz)	BPFI (Hz)	BSF (Hz)	ws (rad/s)	wc (rad/s)
5	300	19.8	25.2	20.5	31.4	13.8
10	600	39.6	50.4	41.1	62.8	27.6
15	900	59.4	75.6	61.6	94.2	41.5
20	1200	79.2	100.8	82.13	125.6	55.3

According to equations in Chapter 3 (3.19 - 3.23) the defects frequencies can be calculated as in Table 5.3. Figure 5.5 (a) illustrate the size of an inner race defect (A x B x C) and similarly for the outer race defect Figure 5.5 (b). As mentioned in Chapter 4, there are three severities of inner and outer race faults: 1x3x9 mm, 1x05x6mm and 1x0.2x3mm, as illustrated in Table 5.2. Figures 5.6 and 5.7 show the performance of the PMBLDC motor under inner and outer race cracks, under no-load and 1200rpm rotation speed. The damaged bearing signal produces a series of pulses in time domain vibration signal.

The severity of the outer race fault is much more than the inner race fault; the amplitudes of the performance frequencies are even larger compared to the inner race fault. Generally, the time waveform is very complicated showing the effect of the abnormal situation and the general vibration level of the signal is higher than that of the normal condition.

It can be seen also in Figures 5.6 and 5.7, that the signal from a further distance relative to the position of the faulty bearing has lower vibration amplitudes than the signals from the position where the faulty bearing is placed, and the information contained in the signal can be used for fault detection. Furthermore, the duration of contact between the damage and the ball is very small in comparison to the full measurement time, so that the time waveform figures do not show significant differences between states.
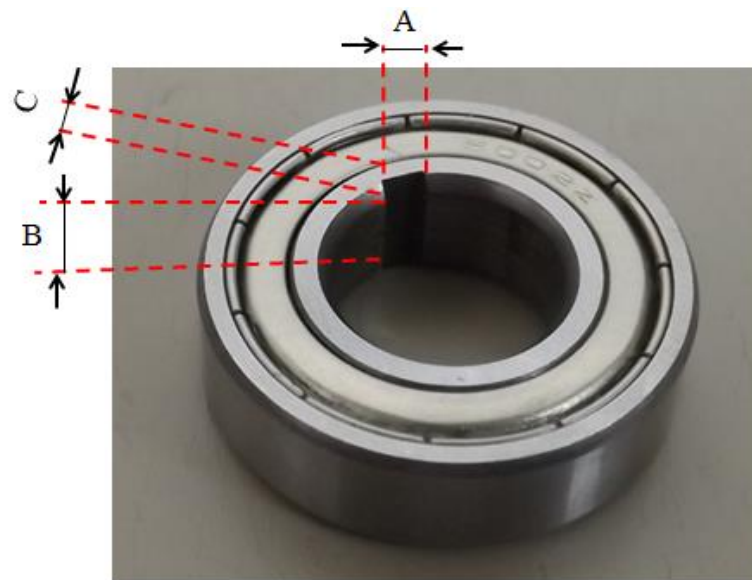
(a)
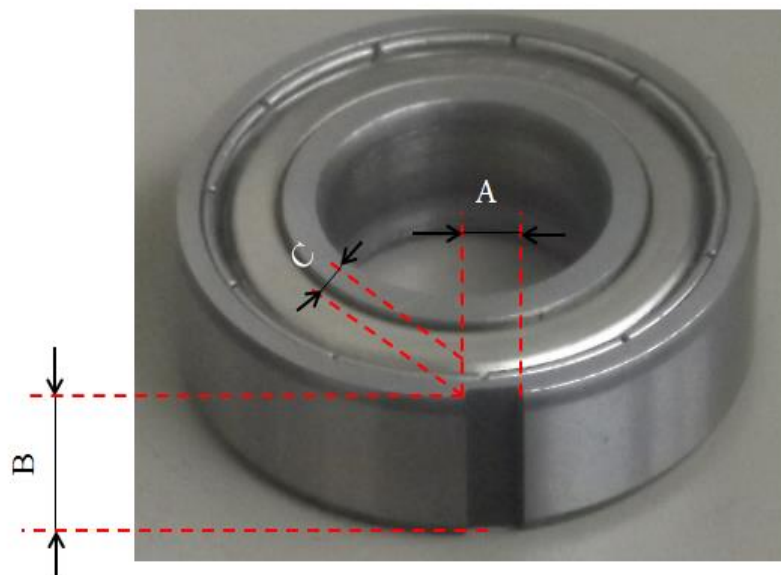
(b)

Figure 5.5 Dimension of outer race defect

The amplitude responses have different pattern depending on the corrupted noise and position of the sensor, and generally the amplitude of the spectrum decreases when load decreases and the maximum coefficient is obtained at low frequency. As bearing fault and radial loads increase, the amplitude of the fault frequency component of vibration signals increase at rotating speeds 600, 900, and 1200 rpm respectively.
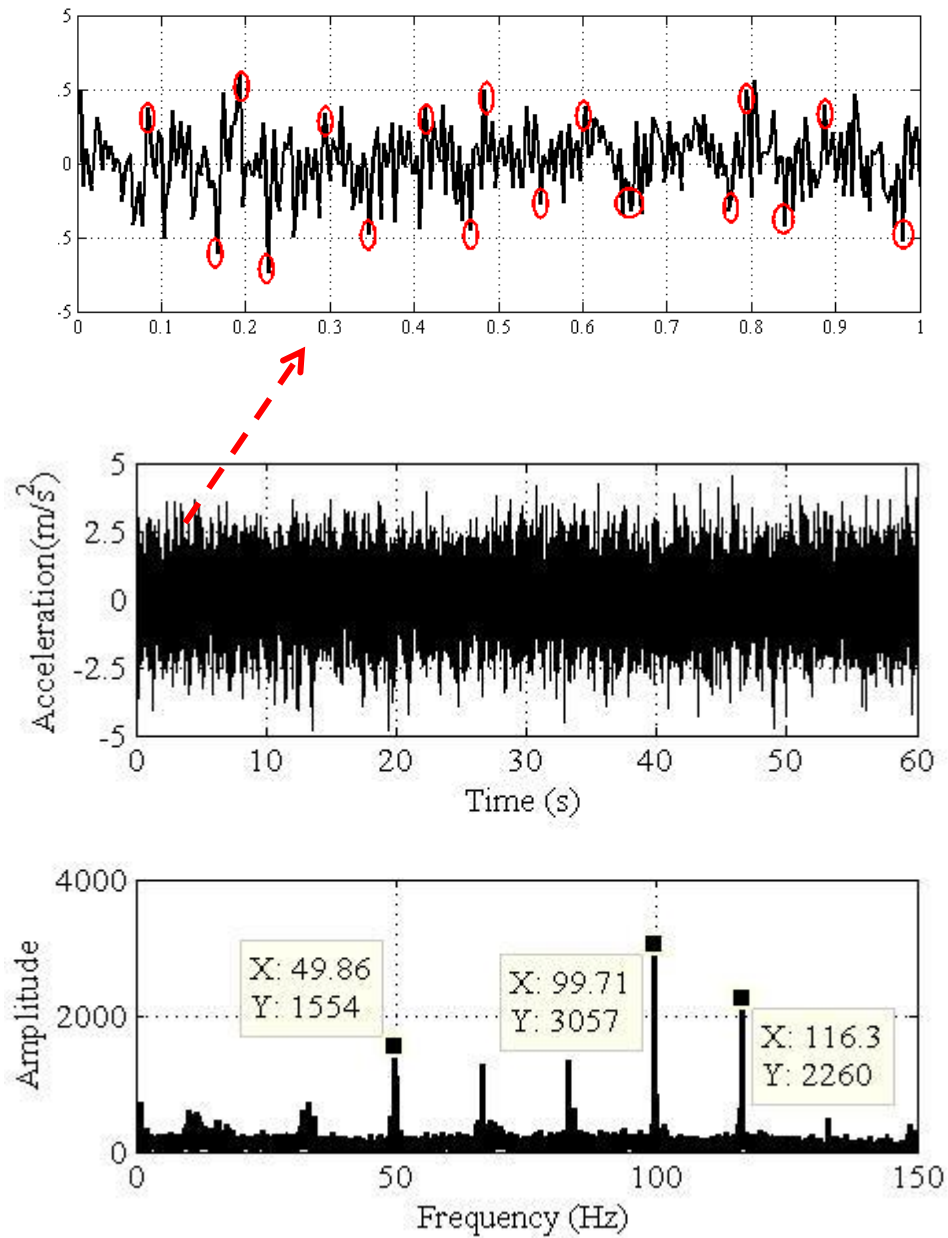
Figure 5.6 Raw vibration time and frequency domain signals under stationary operating conditions: no load and 1200rpm speed with defect size inner 1x3x9 mm

The experiment test data were converted to the frequency domain in order to acquire more fault signs during the signal processing stage. Comparison of normal signals with the signals in Figures 5.6(b) and 5.7(b), when the bearing is operating in faulty cases (inner and outer race defect) indicates the differences in time and frequency domain signals between these two cases. In the frequency domain, the presence of peaks in the vibration spectrum can be used to identify the type of bearing fault; the characteristic frequencies associated with specific faults need to be known and specimen calculations of these are presented in Table 5.2. The initial dominant peak in the spectrum can be easily identified by the difference between the different fault severities spectra.
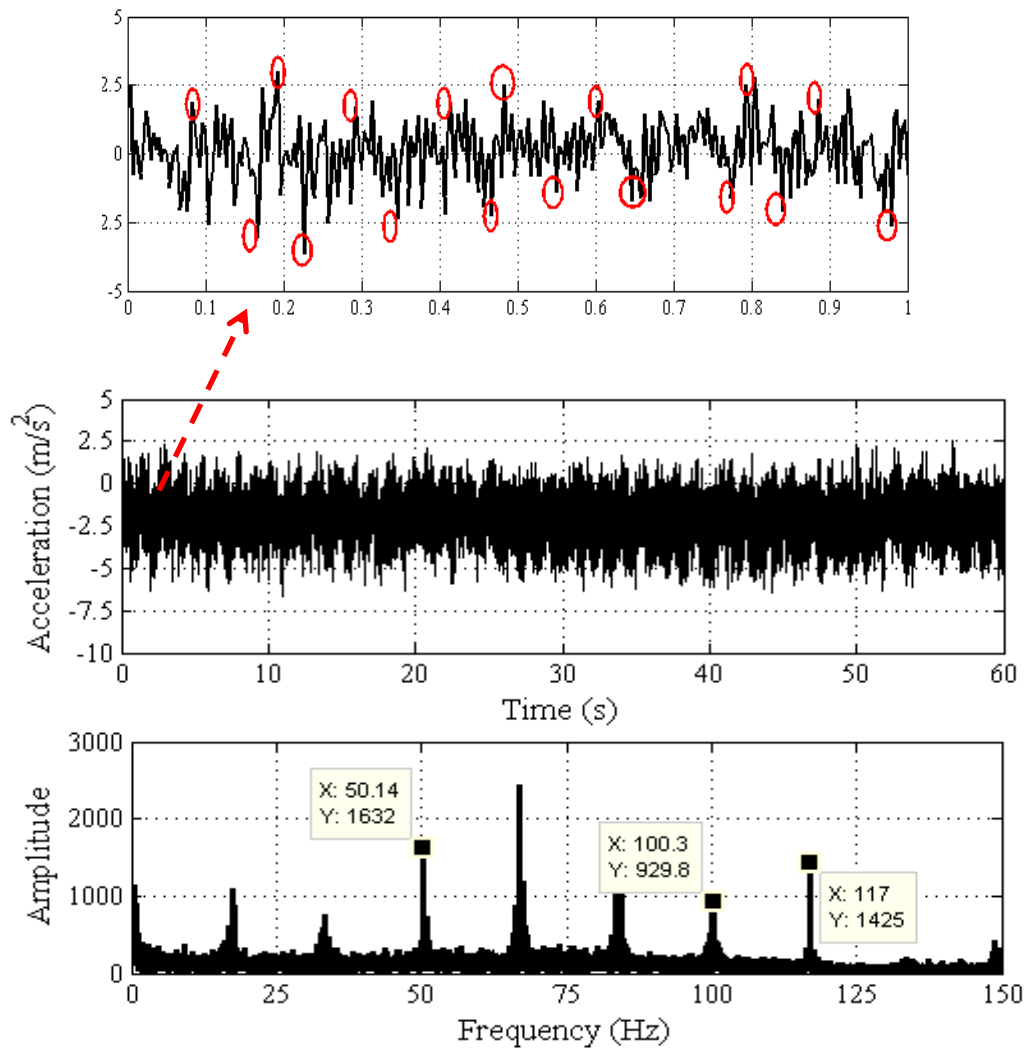
Figure 5.7 Raw vibration time and frequency domain signals under stationary operating conditions: no load and 1200rpm speed with defect size outer 1x3x9 mm

Figures 5.8 and 5.9 shows the comparison between raw vibration signal of the outer race defect spectrum and time waveform under three different severities and no-load, 1200 rpm speed operating conditions. It is unlikely that simply viewing the time-domain signal will detect a fault because the collected data are masked with background noise coming from other components.
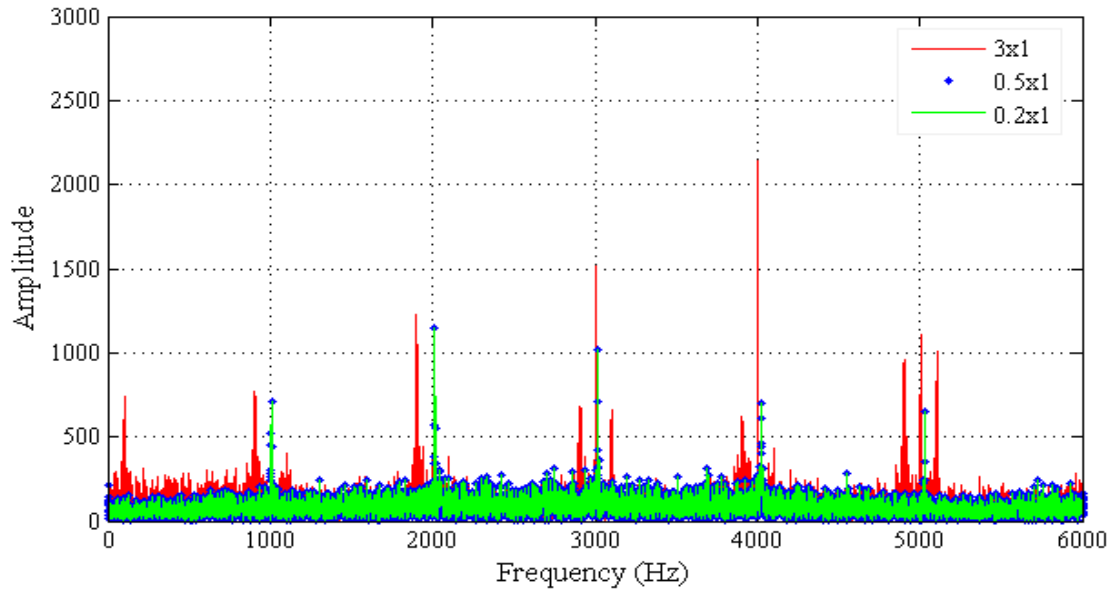
(a)
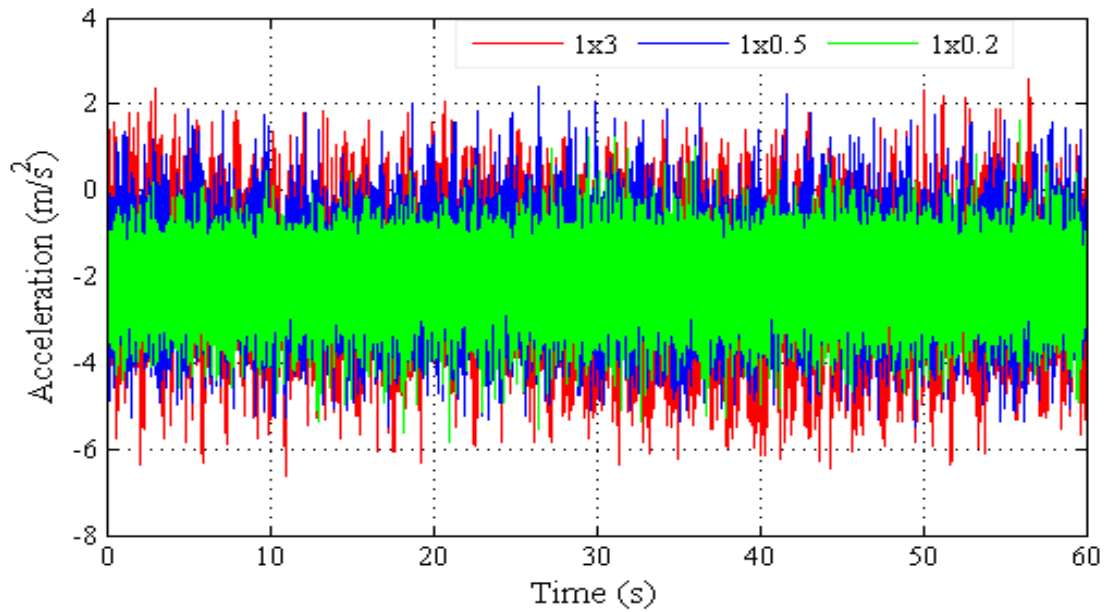
(b)

Figure 5.8 Comparisons between raw vibration signal of the outer race defect (a) spectrum (b) time waveform under three different severities and no-load, 1200 rpm speed operating condition

It can be seen from the vibration and current signals that the amplitude of the spectrum under fault defect is much more than in the fault free case, and generally the amplitude of the spectrum decreases when load decreases. On the other hand, a notch fault was introduced into one of the rolling elements (balls) in a similar way to those introduced earlier to both inner and outer races. A typical vibration waveform and spectrum is shown in Figure 5.10 for a single localised ball defect bearing.
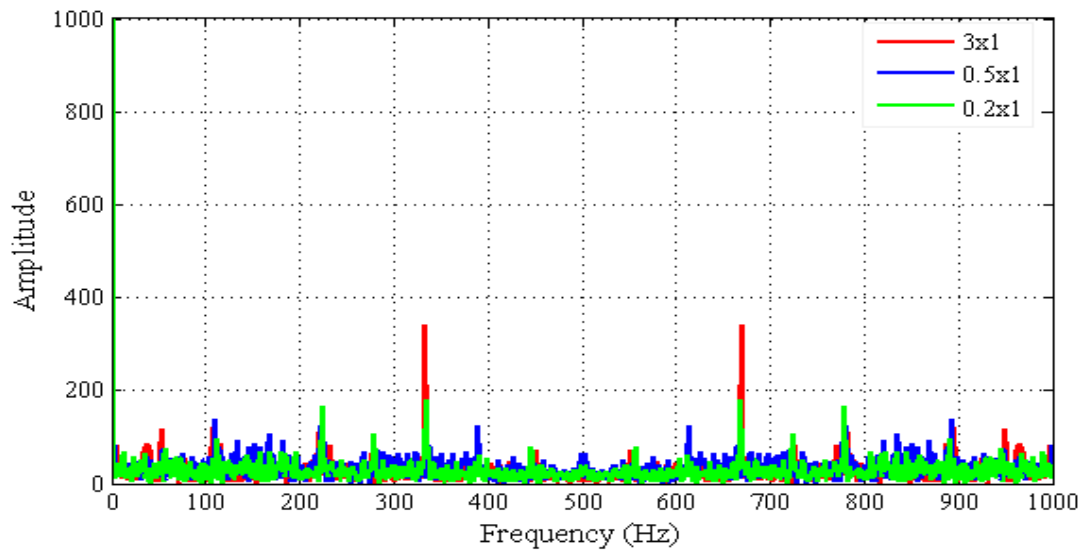
(a)
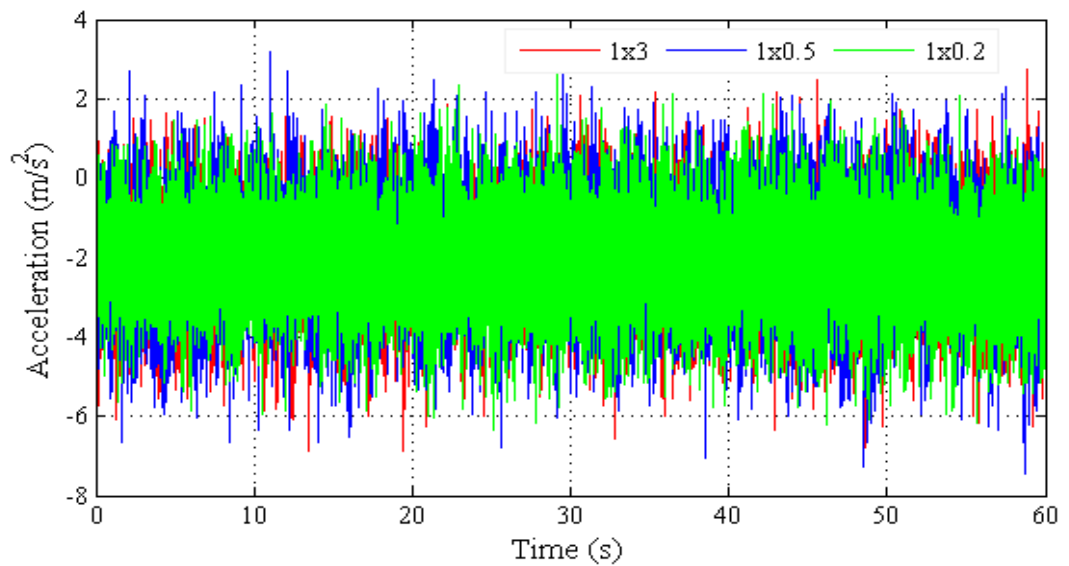
(b)

Figure 5.9 Comparisons between raw vibration signal of the inner race defect
(a) spectrum (b) time waveform under three different severities and
no-load, 1200 rpm speed operating condition
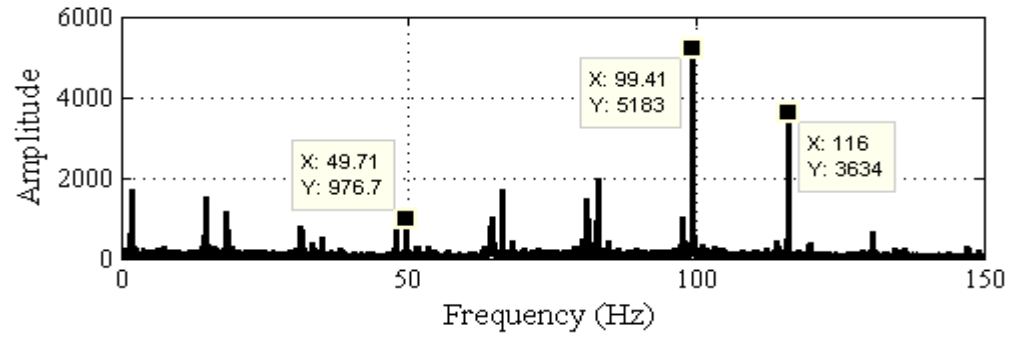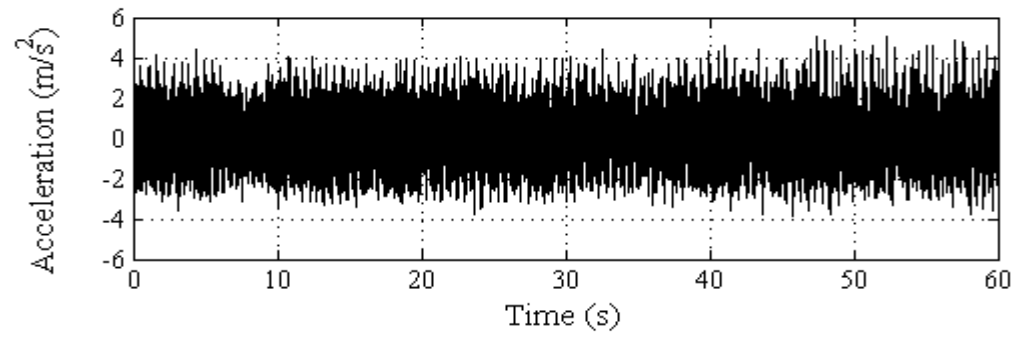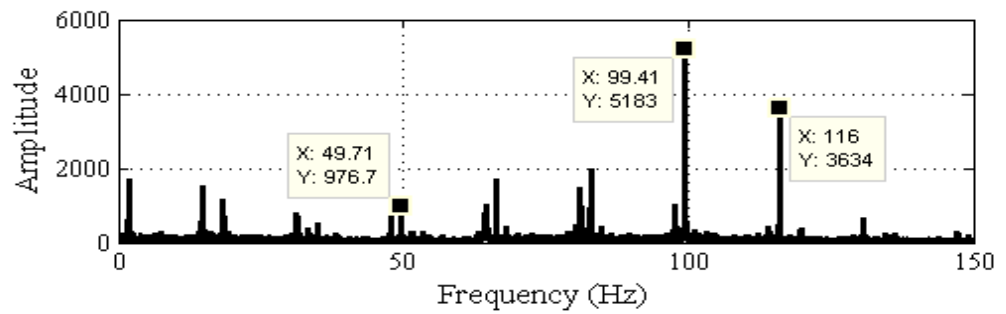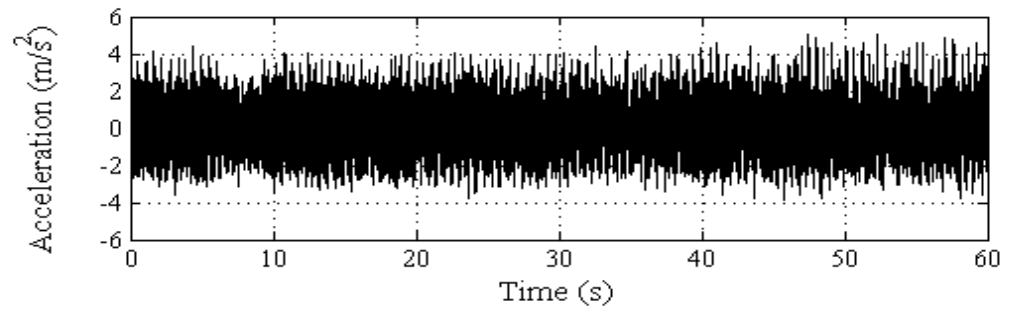
Figure 5.10 Time domain waveform and spectrum of the raw vibration signal for bearing with localised ball defect under stationary operating conditions 1200 rpm speed and (a) no load and (b) half rated load

5.4.2 Single localised bearing faults under non-stationary operating conditions

Due to progress made in engineering, rotating machines are becoming faster and lightweight. They are also required to run at different speeds and loading operating conditions. Diagnosis of faults in such machines will improving the machine's reliability, and is the major focus of industry, which means to gain the maximum working life out of machinery and also minimise maintenance and operating costs.

There are several applications where the motor is never operating at a constant speed or load, such as transient and non-stationary applications. The motor operating in such a non-stationary environment has a non-stationary voltage, current and vibration signal. Current and vibration signals were collected for rolling element bearings with four defects: normal, inner race, outer race and ball defects, under variable load and speed operating conditions. Analysis of non-stationary signals is inherently complicated and sophisticated signal processing techniques are often needed. In the area of fault diagnosis under non-stationary conditions, there has been little work.

In the present work the proposed fault diagnosis approach is tested under non-stationary load and motor speed conditions. The speed varies from 600 rpm to 1200 rpm and the load is varied from full load to 75% and 50% of the rated load, and to no-load. A typical segment of the stator current of a PMBLDC motor operating in such a non-stationary state is shown in Figures (5.11 and 5.12) in which the amplitude of vibration and stator current signals are changing continuously. The figures represent a motor working under full load and variable speed under inner race defects, size (1x0.5x9) mm.
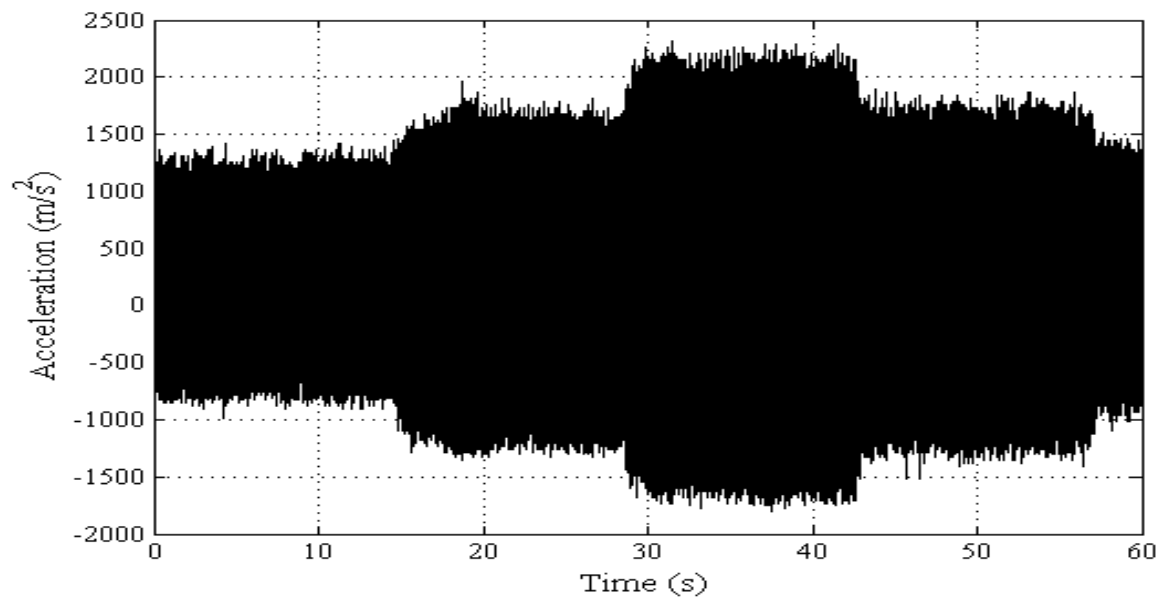
(a)
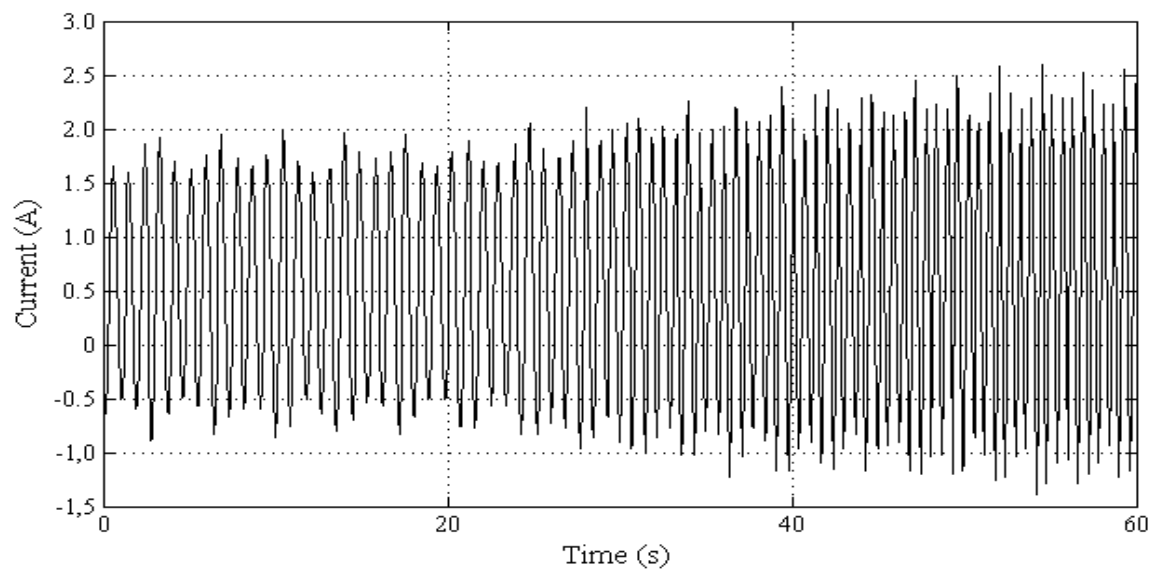
(b)

Figure 5.11 (a) vibration and (b) stator current signal of inner race defect under full load and variable speed conditions
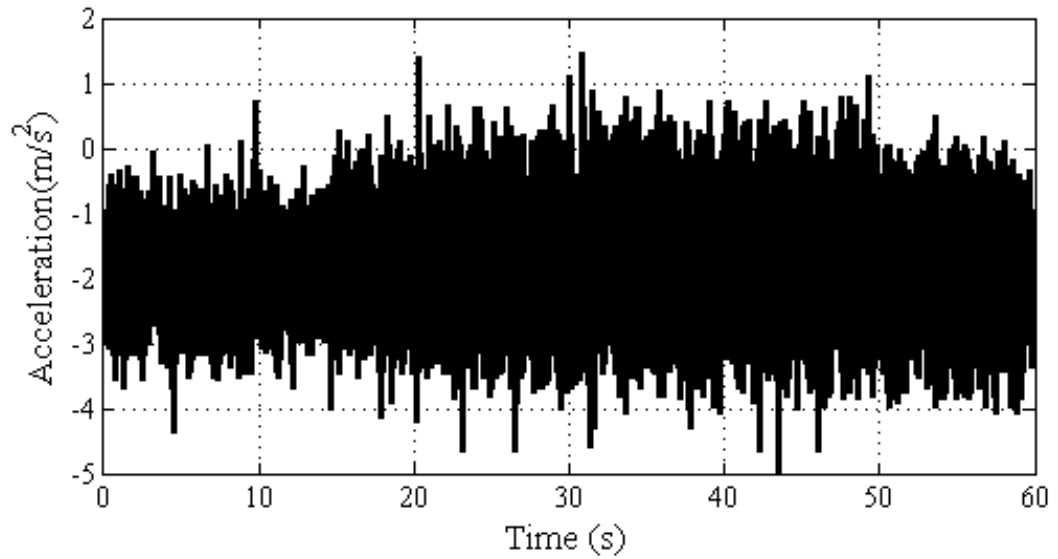
(a)
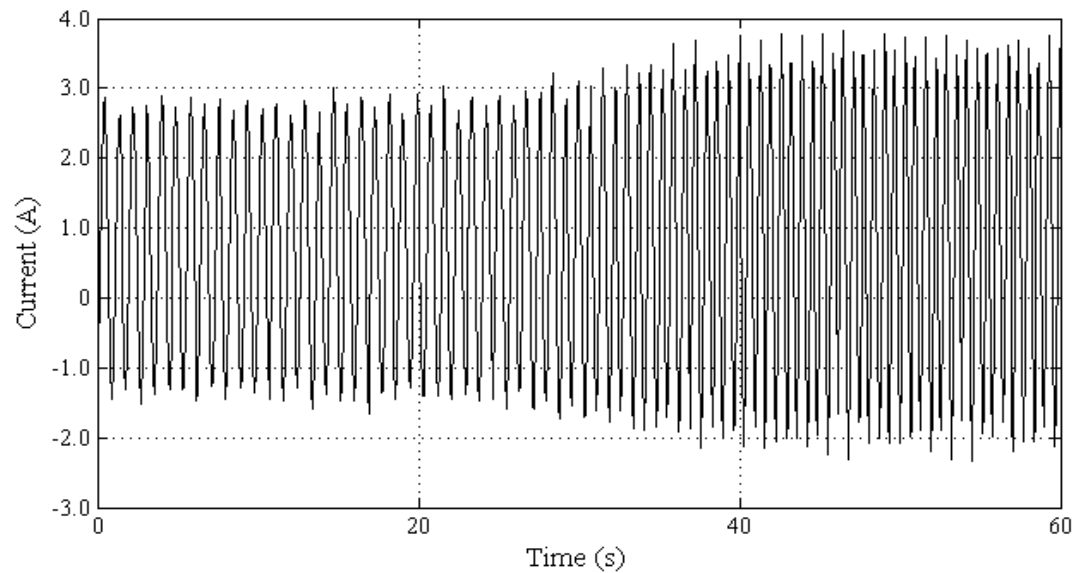
(b)

Figure 5.12 (a) vibration and (b) stator current signal of outer race defect size under full load and variable speed conditions

5.5 Generalised Roughness Bearing Fault Signals under Stationary and Non-stationary Operating Conditions

A corrosion defect is one of generalised roughness in the rolling bearing; the common causes of corrosion include temperature changes, moisture or water. Whenever bearings are put into storage, they should be coated with oil or another preservative, as shown in

Figure 5.13 (a). The consequent vibrations are directly linked to the position of the debris, and therefore they are unlikely to repeat at the same frequency. Thus, it is impossible to analytically define some predictable frequencies to detect in the vibration or current spectra (Sawalhi and Randall 2011).

Image 5.14 (a) shows the bearing surface under different of corrosion defect severities (see also in appendix A). Meanwhile, Figure 5.14 (b) shows the effects of corrosion defects on the different bearing layers). Figure 5.14 shows the vibration waveform and spectrum of corrosion faults with different sizes of severity. It is difficult to isolate a single signature related to the generalised roughness fault, but only a generalised roughness increase of amplitude. A bearing with corrosion defects will produce a vibration signal, due to the products of corrosion that interfere with the balls during the rotation of the shaft.

(a)

(b)
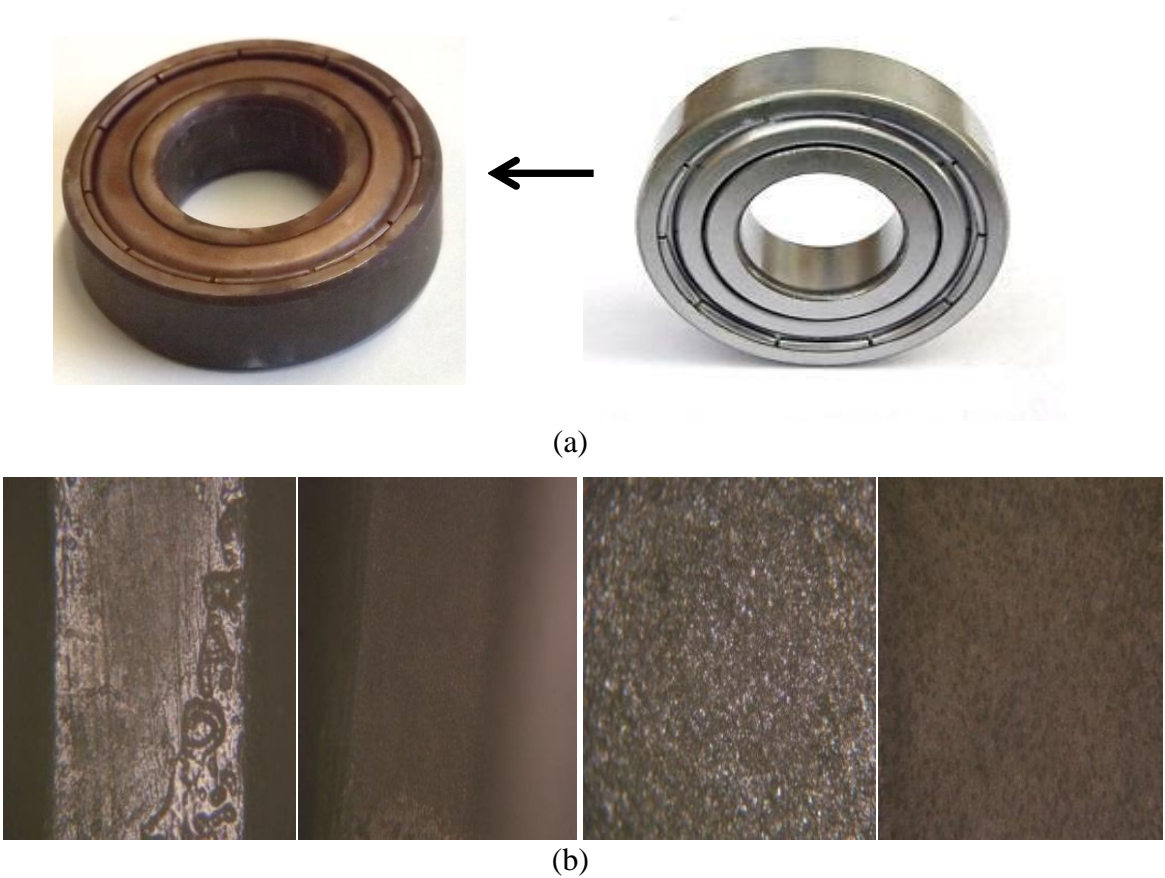
Figure 5.13 Bearing layer with corrosion defect

(a)

(b)

(c)

(d)
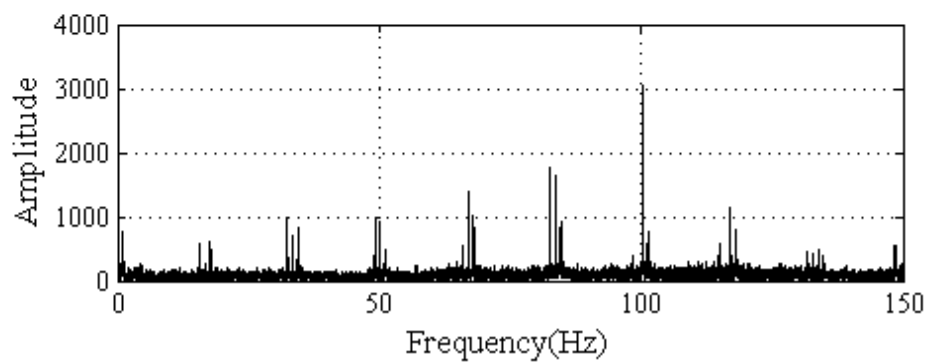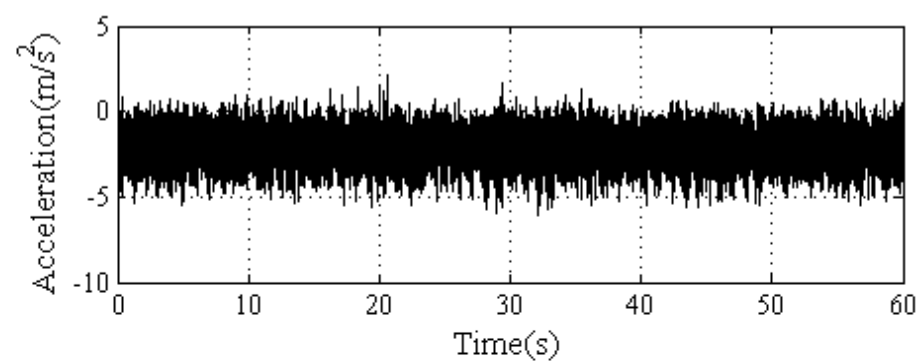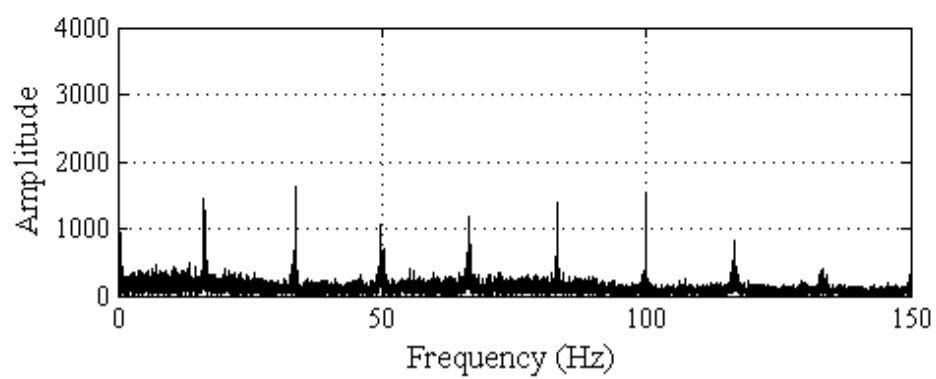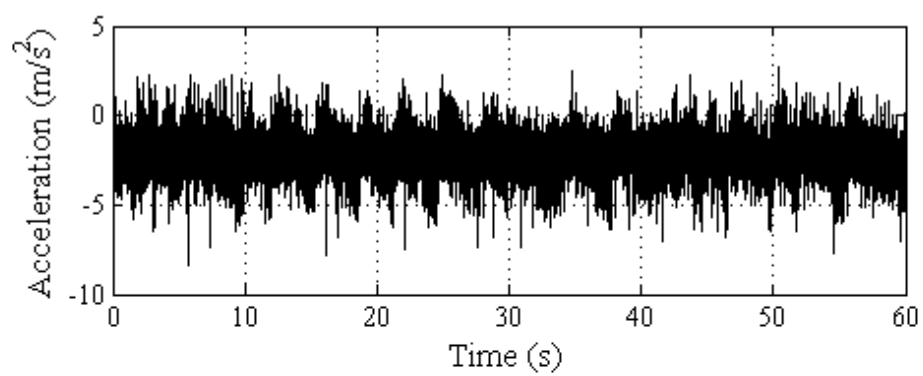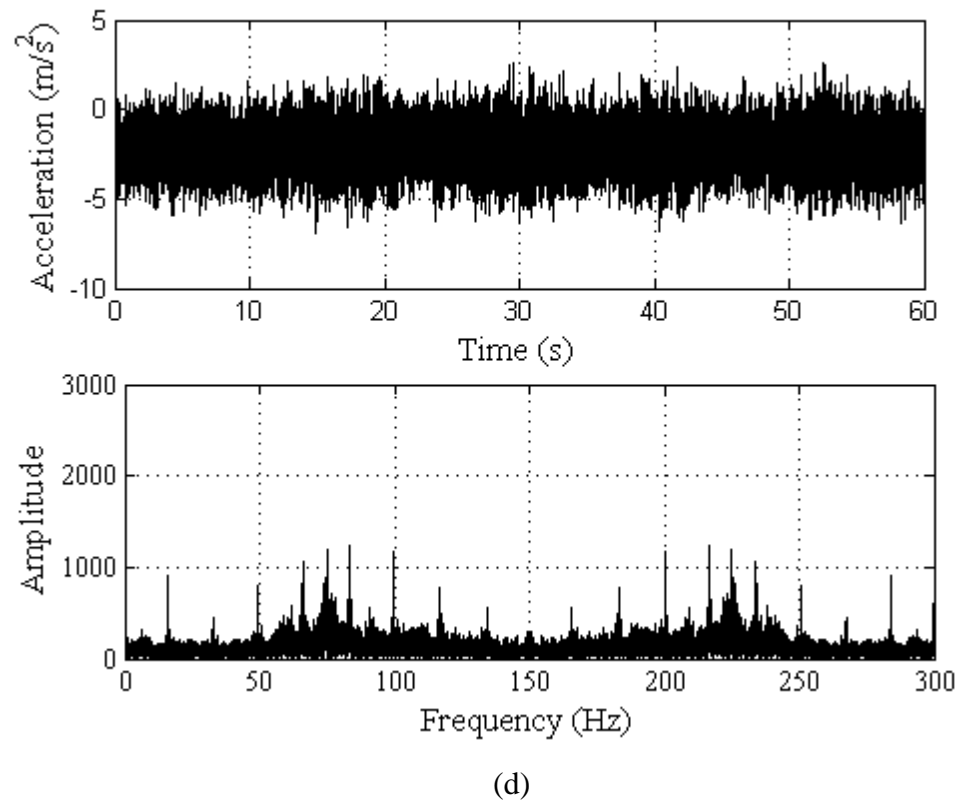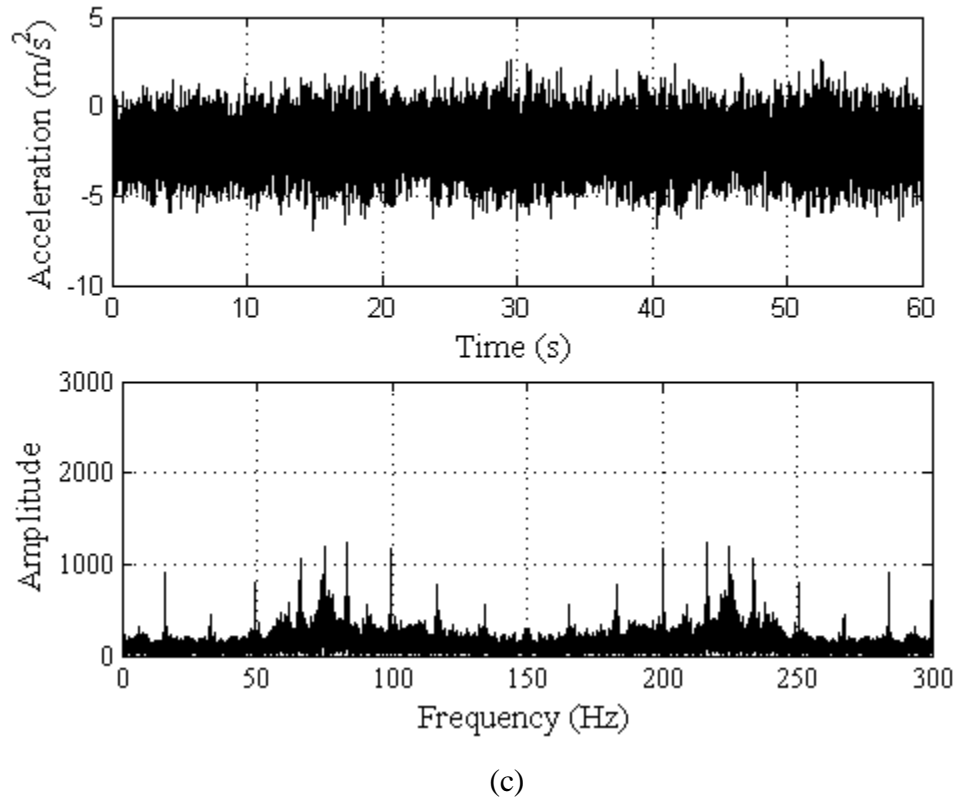
Figure 5.14 Corrosion bearing fault with four severities (a) severity 1, (b) severity 2, (c) severity 3 and (d) severity 4

5.6 Thruster Motor Blades Fault Analysis

There has been growing interest in the use of fault detection and diagnostic techniques in USVs owing to their significant impact on marine operations. As a consequence of their success, these sectors are now demanding longer mission lengths coupled with increasing vehicle autonomy. With an escalation in autonomy comes the need for higher reliability in such vehicles, in order for them to better cope with unexpected events.

In a large number of cases, the present generation of USVs use electric thruster motors as their means of propulsion owing to their high efficiency, size and weight. Thus, the timely isolation of faults in a motor will ensure the integrity and safety of a vehicle while not adversely affecting the overall system performance. This study presents a novel approach to the diagnosis of unbalanced load (blades damage) faults in an electric thruster motor such as is typically found in USV propulsion. The faults were simulated with one of the blades of the trolling motor cut by 10% (F1), by 25% (F2), in half (F3) and fully cut (F4). The proposed technique was used to show the behaviour of the thruster motor under normal operating condition and the four faulty conditions (F1–F4).

Figure 5.15 shows the time domain of the data collected for the raw vibration and line current under four severities of blade fault, and clearly shows the changes in the amplitude based on severity of fault. The change in amplitude in vibration for fault F (4) is nearly 4 times more than fault F1, indicating a more severe fault in the case where the blade of the motor is fully removed. Also, Figure 5.15 also shows the effect on line current amplitude, where variations in the amplitudes are less noticeable compared to the vibration. The data was collected under different rotating speed conditions. MATLAB code was used to change the duty cycle of the PWM signals via the motor driver, to change motor speed. Six data sets were collected, representing motor performance under different speed conditions.

(a)

(b)

(c)

(d)
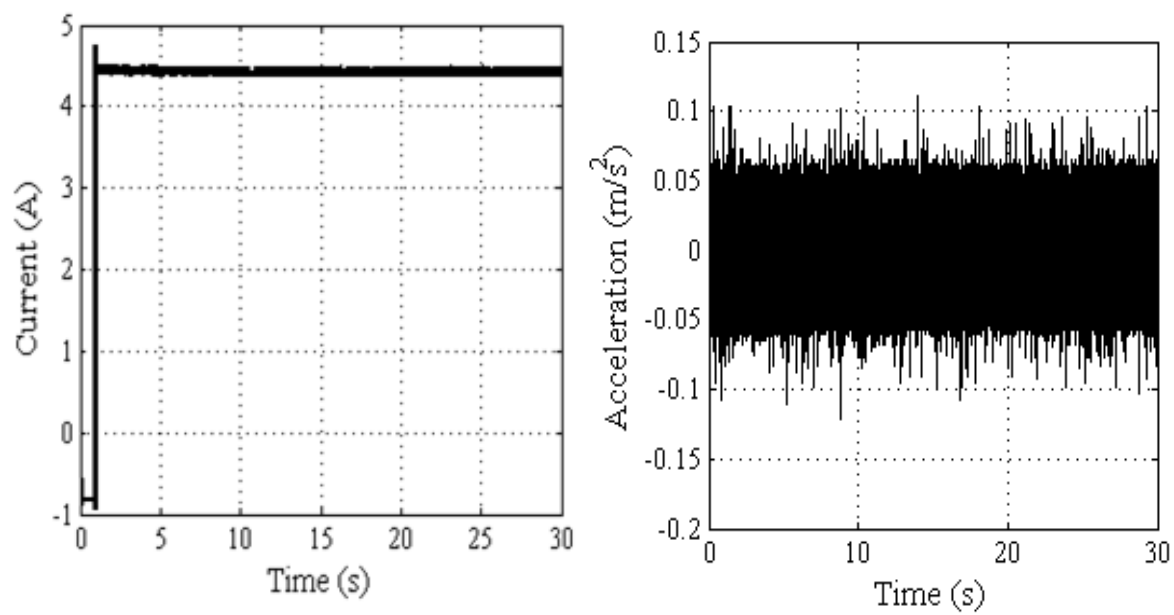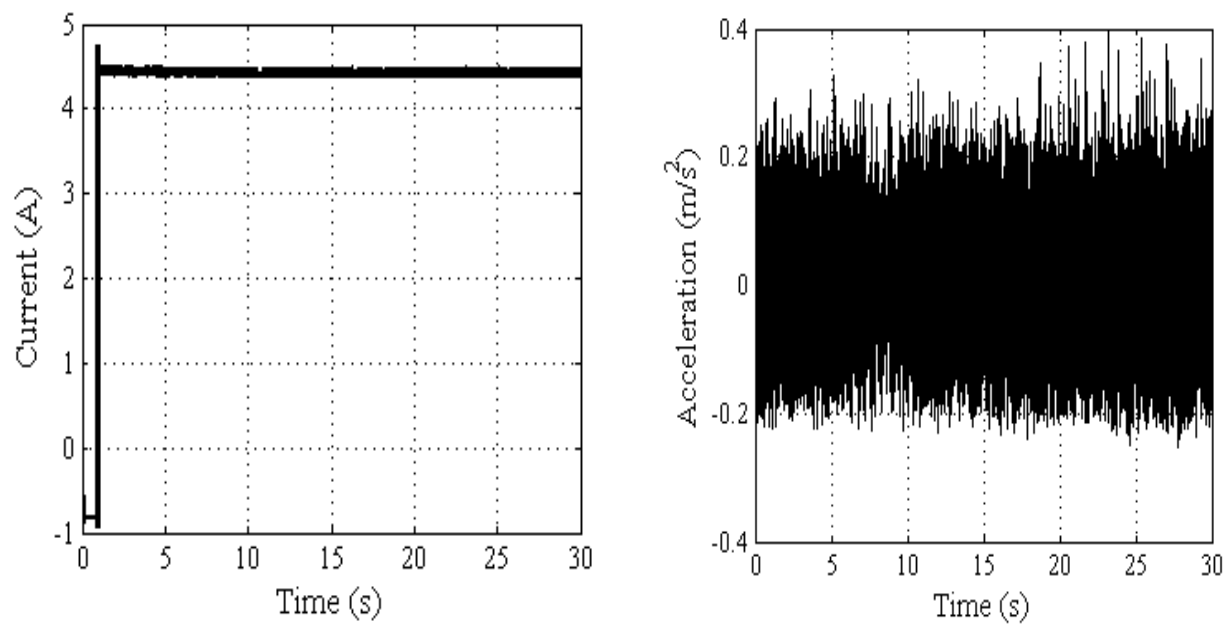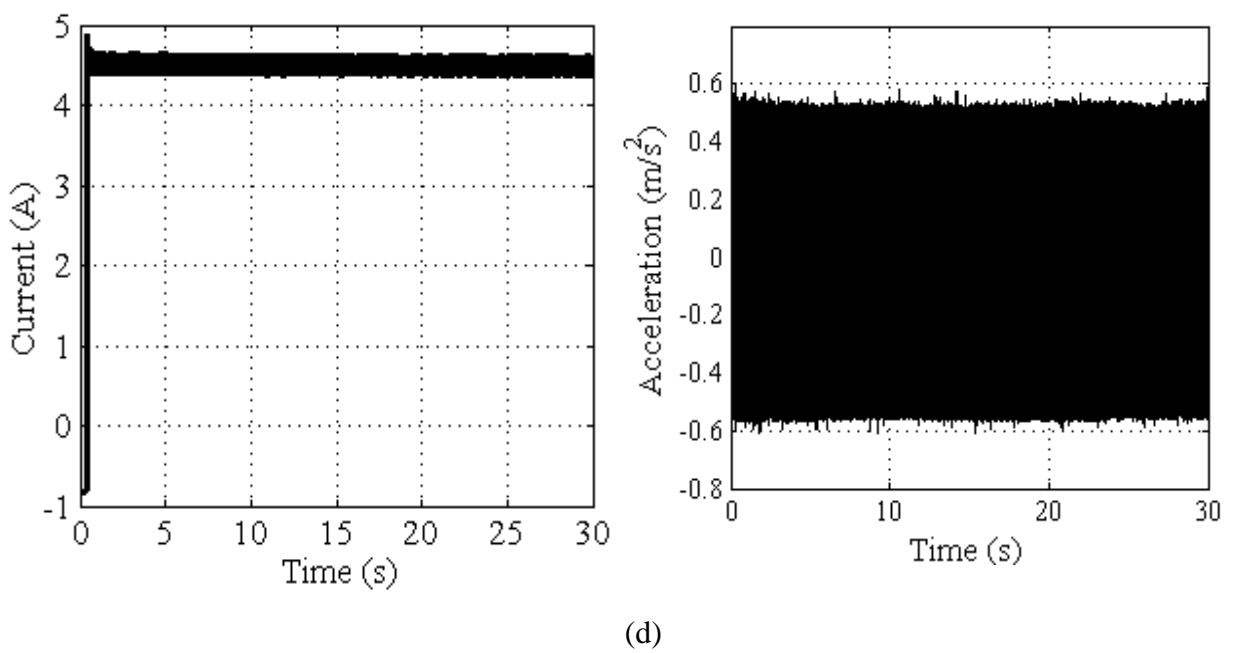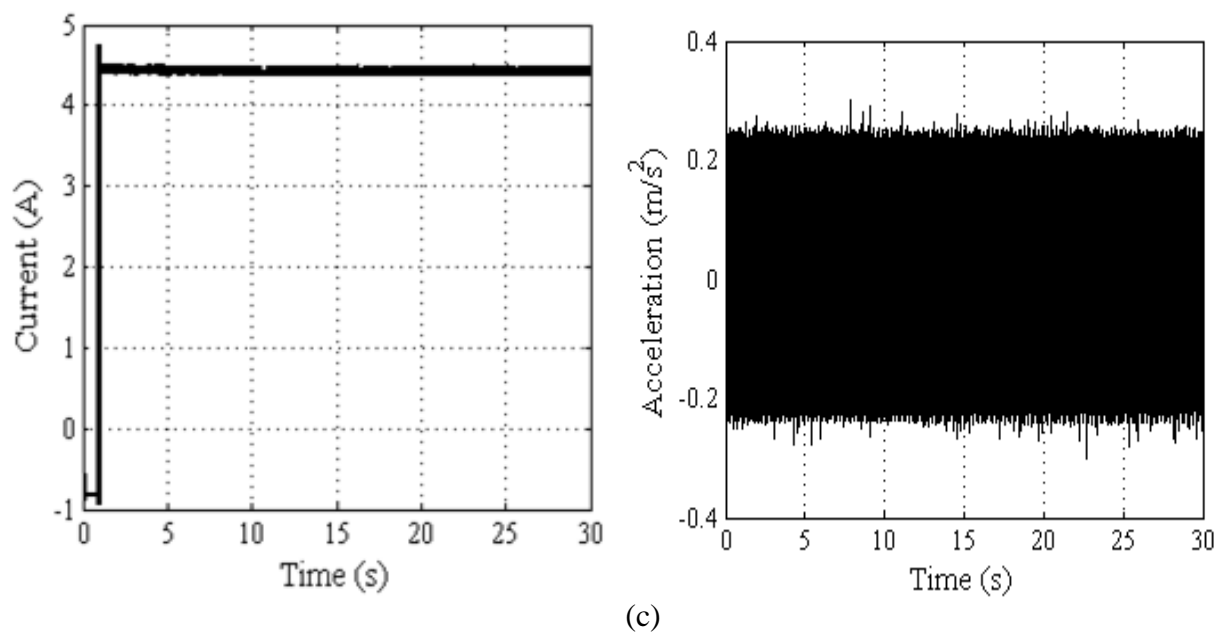
Figure 5.15 Time domain of the raw vibration (left) and current (right) signal under different operating conditions (a) F1, (b) F2, (C) F3 and (d) F4

5.7 Chapter Summary

In this chapter, vibration and current signal have been acquired and plotted in time and frequency domains that represent the following conditions: normal bearing, localised bearing fault: fault on inner race, outer race under different severities, fault in rolling element (ball) , generalised roughness of bearing (corrosion) and blades defects of a thruster motor under different speed conditions. Monitoring based on stator current analysis only needs current sensors. These sensors are often already used for control and protection purposes. Moreover, as for the vibration spectral detector, the stator current indicator needs a low sampling frequency, especially for low supply frequencies.

It can be observed that the experimental data in time and frequency domain cannot produce a reliable fault analysis, especially with a wide range of fault severities and operating conditions. In addition, irrelevant features that affect accuracy and time need to be accounted for in the diagnosis of abnormal conditions.

Owing to the nonlinear operating conditions such as loads, clearance, friction and speeds, which have a distinct influence on the vibration and current signals, it is very difficult to make an accurate evaluation of the working condition of faults through analysis in time or frequency domains only. Furthermore, the bearing fault signature is embedded in the resonance signals, commonly in high frequency bands. The fault-induced signal is often too weak to be detected directly from the resonance signal in its measurement form. Thus, analysing resonance signals allows us to find the key to bearing fault diagnosis.

Chapter six introduces feature extraction and a dimensionality reduction approach to overcome the limitations of the time and frequency analysis of the faults signals proposed in this chapter.

CHAPTER 6

Features Extraction and Dimensionality Reduction

"This chapter discuss tools used for feature extraction and the dimensionality reduction of those features related to specific PMDC motor faults. Vibration and current signals are used to verify the proposed feature extraction and dimensionality reduction tools"

6.1 Introduction

After data collection of the essential sensor signals, features are often extracted and selected to analyse the signals from all these embedded sensors, and to assess the condition of the system by the indirect method. Feature extraction is usually the first step in any pattern recognition system.

Various signal processing techniques have been proposed to extract useful features and to classify fault signals. Existing literature has focused on the steady-state behaviour of faulty drives. In this work both steady and transient operating conditions are investigated in detecting fault phenomena.

Irrelevant features will affect the learning process by increasing the computational cost and sample size, and may lead to over-fitting. In order to increase the robustness of the classifier and to reduce the data processing load, dimensionality reduction is necessary. As such, it is obvious that the main goal of feature subset reduction is to reduce the number of features used in classification, without compromising on accuracy.

This chapter starts first with an introduction to feature extraction techniques (time, frequency and time-frequency), which are presented in section 6.2. Then section 6.3 introduces a general description of WT as a feature extraction tool, the basic mathematical introduction necessary to understand the wavelet transform having been presented. In addition the selection of the optimal mother wavelet and the optimal number of levels of resolution is carried out, using the minimum description length (MDL) data criteria and data independent selection (DIS).

Extraction features for both single localised and generalised bearing faults are reported on in section 6.4, while section 6.5 will introduce DWT to extract features for thruster motor blades faults under different rotating speed conditions. Section 6.6 will introduce the concept of feature projection and dimensionality reduction and section 6.7 presents the proposed dimensionality feature reduction technique OFNDA. Finally, section 6.8 summarises the chapter.

6.2 Features Extraction for PMDC Motor Fault Diagnosis

With the development of modern multi-sensor technology and adaptive signal processing techniques, more features are being extracted for machinery fault diagnosis, applying mutable features that can improve fault diagnosis accuracy. A feature extraction technique is needed for signal processing of recorded time-series signals over a long period of time to obtain suitable feature parameters for fault diagnosis (Olsson 2009).

The process of extracting a suitable feature set is considered as the most important part in a pattern recognition, so that the success of any pattern classification system is based almost entirely on the choice of features used to represent the continuous time waveforms (Jiang et al. 2013). On the other hand, an excessive number of features

increases both of the complexity of data analysis and the time associated with the analysis process (McBain and Timusk 2011).

Corresponding to different signals, the signal analysis method should be properly selected, such that the feature value of signals can be enhanced to improve diagnostic sensitivity. Inaccurate and improper features reduce the overall reliability of fault diagnosis techniques and make them unable to predict actual bearing conditions. Many extraction techniques have been proposed in several domains as shown in Figure 6.1 , including time-domain methods, frequency-domain methods, and time-frequency methods (Mitoma et al. 2008).

```
┌─────────────────────────────────┐
│   Signal Processing technique    │
│      (Features extraction)       │
└─────────────────────────────────┘
```

Time domain	Frequency domain	Time-frequency domain
Statistical features Time synchronous averaging Autoregressive model	Fast Fourier transform Discrete Fourier transform	Wavelet transform Short time Fourier transform Winger distribution
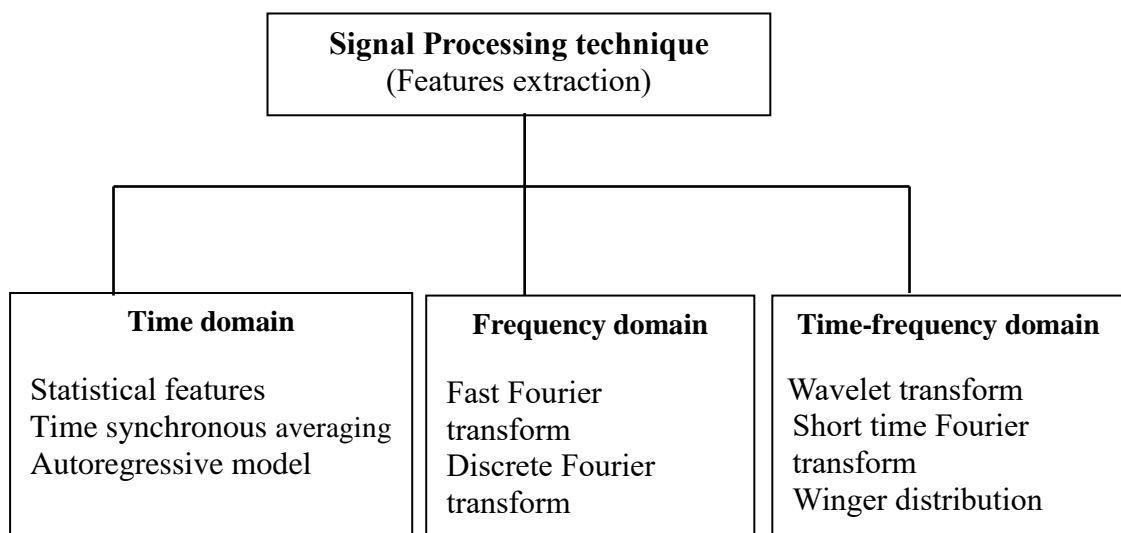
Figure 6.1 Feature extraction techniques

6.2.1 Time domain analysis

Time-domain analysis (TDA) is a useful feature extraction tool for condition monitoring and fault diagnosis of electrical motors. TDA describes the behaviour of the signal as a function of time and can be used to distinguish between good and defective bearings in the time domain signals.

Many TDA techniques have been use TDA for rotating machine fault diagnosis based on signal statistics. A statistical feature such as root mean square (RMS), standard deviation (std), skewness, shape factors and kurtosis represents the traditional TDA features (Doguer and Strackeljan 2009) and these can be defined mathematically as follows (Pandya et al. 2013, Kharche and Kshirsagar 2014):

X_{rms} Value represents the mean energy of the signal but it does not characterise the shape of the signal.

$$X_{rms} = \sqrt{\frac{1}{N}\sum_{i=1}^{N} x(i)^2} \tag{6.2}$$

where N is the number of discrete points and represents the signal from each sampled point.

Peak is the greatest measured amplitude in a signal. Peak is one of the important parameters in acoustic emission analysis. It is represented by the following calculations:

$$X_{Peak\ value} = \frac{1}{2}\big(\max(x(t) - \min(x(t))\big) \tag{6.1}$$

$$X_{std} = \left(\frac{1}{N-1}\sum_{i=1}^{N}(X(i) - \bar{X})^2\right)^{1/2} \tag{6.2}$$

The crest factor or peak-to-average ratio is a measurement of a waveform, calculated from the peak amplitude of the waveform divided by the RMS value of the waveform:

$$Crest\ factor = \frac{XPeak}{Xrms} \tag{6.3}$$

However, Crest Factor and SF are less sensitive to localised bearing faults (Jiang et al. 2014, Pandya et al. 2013).

$$\text{The waveform factors(SF)} = \frac{X_{rms}}{\bar{X}} \tag{6.4}$$

Kurtosis is a statistical moment of probability density function. It is also represented as a square of variance:

$$Kurtosis = \frac{\sqrt{\frac{1}{N}\sum_{i=1}^{N}(X(i)-\bar{X})^3}}{X_{rms}^4} \tag{6.5}$$

Where $\bar{x}$ signal is the mean value of the discrete signal $x(t)$

Skewness represents the measure of the asymmetry of the probability distribution of a real value about its mean, and can be positive or negative.

$$Skewness = \frac{\sqrt{\frac{1}{N}\sum_{i=1}^{N}(X(i)-\bar{X})^3}}{X_{rms}^3} \tag{6.6}$$

Bhavaraju et al. (2010) compared the performance of kurtosis, skewness and standard deviation in bearing faults diagnosis, and the results indicate that kurtosis can give a good indication about the motor situation. TDA is a low cost solution to measuring signals over a wide frequency range. However, it is less sensitive for recognising defects and provides low diagnosing capability (Harris 2013). One main drawback of TDA in detecting defects in bearings is the distortion of the signal from the amount of noise and the interactions from other components. Furthermore, using TDA it is difficult to diagnose specific rotating machine defects at an early stage (Sawalhi 2007).

In addition, the rotational speed varies randomly under non-stationary operating conditions, where both frequency and magnitude of fault components are changed with time in an unpredictable way (Henao et al. 2014). Frequency analysis attempts to overcome TDA disadvantages by detecting faulty signals even at low signal-to-noise ratio conditions by monitoring fault frequencies.

6.2.2 Frequency domain analysis

Frequency domain analysis (FDA) is widely used for rotating machine fault diagnosis. The advantage of frequency-domain compared with TDA is that it has the ability to easily identify and isolate certain frequency components of interest. In addition, for bearing fault diagnosis, the signal from a small fault developing in a roller bearing will be hidden in general bearing noise when applying TDA, but in the FDA there will be a peak in the spectrum at the characteristic fault frequency. The FFT and discrete Fourier transform (DFT) are the most common techniques for transforming a varying time-domain signal into its frequency-domain representation. FFT is used in conventional FDA signature-analysis techniques for conversion of time domain signals into frequency domain signals.

It breaks down a signal into its constitutive sinusoids of different frequencies. In other words, the view of the signal changes from time-based to frequency-based. This technique decomposes a signal into orthogonal basis functions. DFT, meanwhile converts a signal with finite length to the frequency domain (Gritli et al. 2014). The resolution of FFT and DFT can be represented as f_s/N where f_s is the sampling frequency, N is the number of samples, and f_s is the sampling frequency. Mathematically FFT and DFT are given as (Antoni and Randall 2002):

$$FFT[f] = X(f) = \frac{1}{T}\int_{-\infty}^{\infty} X(t)e^{-j2\pi ft}dt \qquad (6.7)$$

$$DFT[f] = \frac{1}{\sqrt{N}}\sum_{i=0}^{N} X(t)e^{-j2\pi ft} \qquad (6.8)$$

where $X(t)$ is a given signal that occurs as a periodic function with period T, and the Fourier series expansion $X(f)$ of $X(t)$ discrete f represents equal spaced frequencies as multiples of the reciprocal of the period T

However, FFT provides information as represented by a component at a certain frequency, and ignores the component in the time domain by applying a windowing function on the signal. Only a portion of the signal is contained in an interval moving window over time, so that the main drawback of FFT is that is the windowing function may distort information from the original signal FFT, when the signal is not suitable under non-stationary conditions (Jayaswal et al. 2010).

On the other hand, Envelope analysis (EA) has the effectiveness of a band-pass analysis method that relies on a suitable choice of narrow band frequencies around the selected resonance (Harmouche et al. 2014) . EA signals are filtered through a band-pass filter and the filtered signal is demodulated with the help of the full wave rectification of Hilbert transform, and then spectrum analysed (Li et al. 2014).

Feng et al. (2015) compared EA with the FFT approach to a vibration signal analysis, and concluded that the FFT is capable of finding distinct faults; it also provides higher performance in damage onset prediction. However, FDA only provides spectral information and there is no information about when this spectral information appears (Gohshi 2012). However, when a single localised bearing fault occurs, the contact between the local defect and its mating surface produces an impulse with a short duration and an approximately exponential damping rate. If the rotational speed is constant, the impulse will repeat at a constant interval (Wang et al. 2014).

Bearings often work in non-stationary conditions (variable speed, variable load). In such operating condition, the impulses do not appear periodically and hence the envelope analysis methods as well as any other techniques based on the assumption of constant rotating speed are no longer applicable. Therefore an alternative time-frequency domain

technique is needed to avoid the drawback of frequency domain features extraction techniques.

6.2.3 Time frequency domain features extraction

Time-frequency analysis (T-FA) is the three-dimensional time, frequency and amplitude representation of a signal, which is suitable to indicate transient events in the signal. T-FA distributions are commonly implemented for rotating machine fault diagnosis and they accurately extract the useful features from a non-stationary signal (Rajagopalan et al. 2006).

To overcome the limitation of FFT methods with non-stationary signals, STFT is a supplementary method. STFT is a basic T-FA that comes from the FFT. It uses a window function to slide on the non-stationary signal and then divide it into several equal-length segments. The inside signal of the segments is supposed to be stationary (Obuchowski et al. 2014). The STFT can be represented as follows:

$$STFT_{w,f}(t,f) = \int_{-\infty}^{\infty} f(t)w(\tau - t)e^{-j2\pi f\tau}d\tau \qquad (6.9)$$

For signal $f(t)$ suppose $w(t - \tau)$ is a window function centred at time t and τ is a time variable. A spectral decomposition is obtained by applying the FFT to the portion of signal viewed through the window $w(t - \tau)$ and all the signal parts outside the window are neglected (Feng et al. 2013) . However, the STFT technique does not provide good energy resolution for a specific point of the data signal, as the length of the window is fixed in each of the data segments of the discrete signal (Peng and Chu 2004). Therefore, STFT is suitable for quasi-stationary signal analysis rather than real non-stationary signal analysis. In order to process non-stationary signals, WVD and EMD have been used for rotating machine fault diagnosis, and provide information about the spectral component and when it occurs (Zhang et al. 2013). WVD has overcome the

limitations of STFT and provided a high resolution in both time and frequency for non-stationary signals. WVD can be defined mathematically as (Climente et al. 2014):

$$X(t,w) = \int_{-\infty}^{\infty} X(t + \frac{\tau}{2}) e^{-jw\tau} d \qquad (6.10)$$

where $X(t)$ is a time signal and w is the frequency

The WVD has certain drawbacks, especially those related to its inherent nature, which causes the interference of the cross term, which may have significant amplitude, and therefore can corrupt the transform space. In practice the vibration signal has multiple components, and may contain the mesh frequency and their harmonic, and occasionally some components called ghost components. The interference among these components may cause complicated results that are difficult to interpret.

Many studies have been done to compare the various signal processing techniques discussed in this section. Choy et al. (2003) made a comparison between WVD and WT; the results showed that WT can provide a more direct quantification, and that combining WVD with other techniques such as WT or EMD will increase its effectiveness for rotating machine fault diagnosis.

To overcome the limitations of STFT and WVD as features extraction techniques, WT has been proposed as one of the powerful T-FA methods. WT has the ability to explore signal features with partial characteristics, and to analyse signals with different time and frequency resolutions. WT has the important and useful ability to detect and recognise stationary, non-stationary, or transitory characteristics of signals, as will be discussed in the next section.

Hocine et al. (2012) and Yan et al. (2014), carried out a review of WT application in electrical machines fault diagnosis. CWT was implemented with vibration signal to

diagnosis bearing fault (Sharma et al. 2014), WPT for stator winding faults (Ping et al. 2013) and DWT for broken rotor bar fault diagnosis (Taher et al. 2014).

6. 3 Wavelet Transform Functions and Approximations

WT is an advanced time and frequency signal processing technique with a growing number of applications in rotating machine fault diagnosis (Bouzida et al. 2011). The windowing of WT is adjusted automatically for low and high frequencies, i.e. it uses short time intervals for high frequency components and long-time intervals for low frequency components.

Thereby, each frequency components gets treated in the same manner without requiring any reinterpretation of the results. This gives much greater compact support when processing non-stationary, transient signals, with higher frequency resolution at low frequency and higher time resolution at high frequency. Compared to the FFT, WT contains a great deal of non-stationary and nonlinear diagnostic information. The theoretical basis for wavelet frequency bandwidth analysis is Parseval's theorem (Chen and Gao 2013). Furthermore, WT has the ability to overcome STFT resolution problems.

In addition, WT uses multi-resolution analysis, and the signals can be decomposed into different frequency bands so that they can be further subject to statistical analyses to obtain feature vectors that represent signal characteristics. WT are inner products of the signal and a family of the wavelets. Let $\vartheta(t)$ be the mother wavelet. The corresponding family of wavelets consists of a series of wavelets, which are generated by dilation and translation from the mother wavelet $\vartheta(t)$ shown as follows:

$$\vartheta_{(a,b)}(t) = \frac{1}{a} X(\frac{t-a}{b})$$

(6.11)

where a is scale factor and b is time location: the factor $\frac{1}{a}$ is used to ensure energy preservation.

The WT of signal $X(t)$ and $w(a,b)$ (the convolution between $X(t)$ and wavelet function) can be represented as the follows:

$$w(a,b) = \int X(t)\vartheta_{a,b}^{*} \, dt \tag{6.12}$$

$w(a,b)$ gives the information of $X(t)$ at different levels of resolution, $\vartheta_{a,b}^{*}$ is the conjugate function of the mother wavelet (Lin and Qu 2000)

The mother wavelet must be compactly supported and satisfied with the admissibility condition.

$$\int_{-\infty}^{\infty} \left. \left| \vartheta^{\wedge}(w) \right|^2 \middle/ |W| \right. \, dw < \infty \tag{6.13}$$

where

$$\vartheta^{\wedge} = \int \vartheta(t) e^{(-jwt)} dt \tag{6.14}$$

Traditionally, the WT can be classified into two main types: continuous and discrete wavelets transform (CWT, DWT). The transaction from continuous to discrete wavelet can be made using $a = a_0^m$, $b = na_0^n b_0$, where n, m are integers and $a_0, b_0 \neq 0$ the limitation of these parameter when $a_0 = 2, b_0 = 1$ leads to the dyadic WT. The time frequency localisation means that more energetic wavelet coefficients are localised. This is useful for feature extraction, denoising and singularity detection and is mostly implemented for transient and non-stationary signals analysis; therefore, it is well suited for the fault location problem in electrical machines.

6.3.1 Discrete wavelet transform for features extraction

To extract the useful information, DWT, a signal analysis method that provides the time and frequency information of the signal was applied. The information that cannot be readily seen in the time domain can be observed in the frequency domain. It has the ability to explore signal features with partial characteristics and analyse signals with different time and frequency resolutions.

In addition, the DWT approach is successfully applied to detect and locate faults, together with identification of the severity of the faults. In DWT the signal is passed through a series of high pass filters (h_n) to analyse the high frequencies, and it is also passed through a series of low pass filters (g_n) to analyse the low frequency components of the signal, as shown in Figure 6.2.

At each decomposition level, the half band filters produce signals spanning only half the frequency band. This doubles the frequency resolution as the uncertainty in frequency is reduced by half with this approach. The time resolution becomes arbitrarily good at high frequencies, while the frequency resolution becomes arbitrarily good at low frequencies.

The correlation between the signal and the wavelet at each level of scaling and shifting is termed the wavelet coefficient. The resolution of the signal, which is a measure of the amount of detail of information in the signal, is changed by the filtering operations, and the scale is changed by changing the size window of signals (Antonino et al. 2013).

$A_o(k)$

$h[n]$ → ↓2 → d_1

$g[n]$ → ↓2 → a_1

Level 2 detail
Coefficients
$\left[\frac{fs}{8} - \frac{fs}{4}\right]$ Hz

$h[n]$ → ↓2 → d_2

$g[n]$ → ↓2 → $a2$

Level 1 detail
Coefficients
$\left[\frac{fs}{16} - \frac{fs}{8}\right]$ Hz

$h[n]$ → ↓2 → d_3

$g[n]$ → ↓2 → $a3$
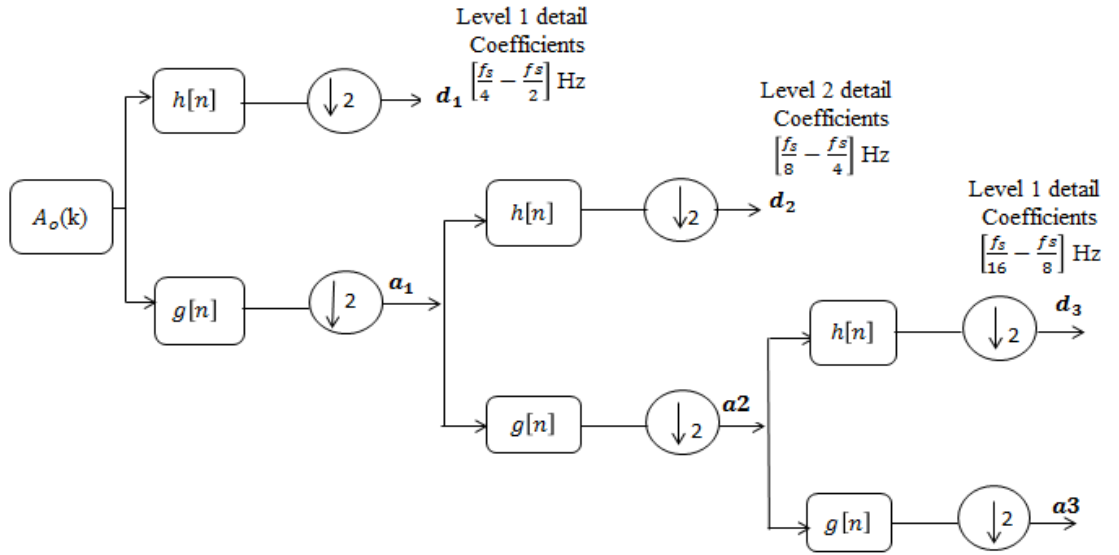
Figure 6.2 A schematic diagram discrete wavelet transforms

Mathematically, the wavelet and scaling functions for a discrete signal $x(t)$ can be represented as the following expressions (Seshadrinath et al. 2014) :

$$x[n] = \sum_m a_{jo,m} \, \emptyset_{jo,m}[n] + \sum_{j=jo}^{j-2} \sum_m d_{j,m} \varphi_{j,m}[n] \tag{6.15}$$

Where $\emptyset[n]$ is the scaling function, $\emptyset_{jo,m}[n] = 2^{2jo/2}\emptyset(2^{jo}n - m)$ is the scaling function at scale 2^{2jo} shifted by m. $a_{jo,m}$ Are the coefficients of approximation at scale 2^{jo}. $\varphi[n]$ is the mother wavelet, $\varphi_{j,k}[n] = 2^{\frac{j}{2}}\varphi(2^{j}n - m)$ is the mother wavelet at a scale of $x = 2^{jo}$ and $N = 2^{j}$ where n is the Number of $X[n]$ sample. The scaling and coefficient level can be given as (Seshadrinath et al. 2014) :

$$\emptyset[n] = \int_{-\infty}^{\infty} x(t) \, \emptyset(t - n)dt \tag{6.16}$$

$$d(j,n) = 2^{j/2} \int_{-\infty}^{\infty} x(t) \, \emptyset(t - n)dt \tag{6.17}$$

The energy of signals (see Figure 6.2) that go through DWT decomposition can be described by:

$$\frac{1}{N}\sum_t |x[t]|^2 = \frac{1}{N_j}\sum_h |cA_{j,h}|^2 + \sum_{j=1}^{J}\sum_{jh} |cD_{j,h}|^2 \qquad (6.18)$$

Some recent studies have successfully applied DWT for different rotating machine faults diagnoses, including localised rolling element bearing faults (Abed et al. 2014), stator winding of a PMBLDC motor, broken rotor bar (Keskes et al. 2013) and rotor eccentricity faults (Yahia et al. 2014). Owing to the ability of the DWT to perform multi-scale analysis of a signal through dilation and translation, it can extract time–frequency features of a signal effectively. Ir can be process a great deal of non-stationary and nonlinear diagnostic information compared with conventional T-FA tools such as STFFT and WVD (Chen and Gao 2013).

6.3.2 Optimal mother wavelet selection

The WT includes a large number of wavelets that one can use for both CWT and DWT analysis. For DWT analysis, examples include orthogonal wavelets, Daubechie (db) and least asymmetric wavelets (sym), and B-spline Biorthogonal (bior) wavelets. For continuous analysis, the CWT includes Morlet (morl), Meyer (meyer) and derivatives of Gaussian (gaus), as shown in Figure 6.3 (Misiti et al. 2014).

Wavelets provide sharper frequency because resolution iterative algorithms for wavelet construction converge faster and the selected mother wavelet should be orthonormal (Weilin et al. 2014). Before the application of the DWT, first we have to select the type of mother wavelet and the number of decomposition levels. Wavelet families (see appendix B) vary in terms of several important properties. The choice of wavelet is dictated by the signal characteristics and the nature of the application.

Various approaches have been developed to optimise mother wavelet selection. Jha et al. (2013) compared between several mother wavelet functions and found that a Daubechie is the optimal mother wavelet for rolling element bearings. Ngui et al. (2013) and Rafiee et al. (2009) have attempted to classify optimisation approaches into qualitative and quantitative approaches.

In qualitative approaches, the selection of a suitable mother wavelet is based on the similarity between the mother wavelet and the signal. However, previous studies also showed that the most similar mother wavelet across the signals is not the proper function for all wavelet-based processing. According to Perrier et al. (1995) mother wavelet are selected based on the following conditions:

➢ To represent the salient features of the disturbances the wavelet function should have a sufficient number of vanishing moments.

➢ To reduce the amount of leakage energy to the adjacent resolution levels the selected wavelet function should have sharp cut off frequencies.

➢ For the same feature of the same signal, the wavelet should provide higher total wavelet energy.

➢ The selected wavelet basis should be orthonormal.

124
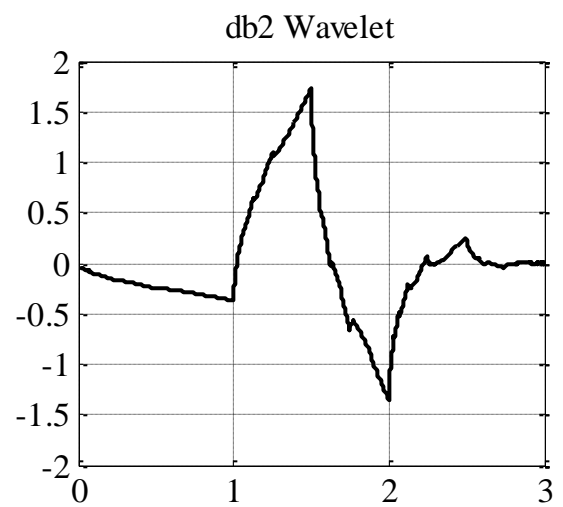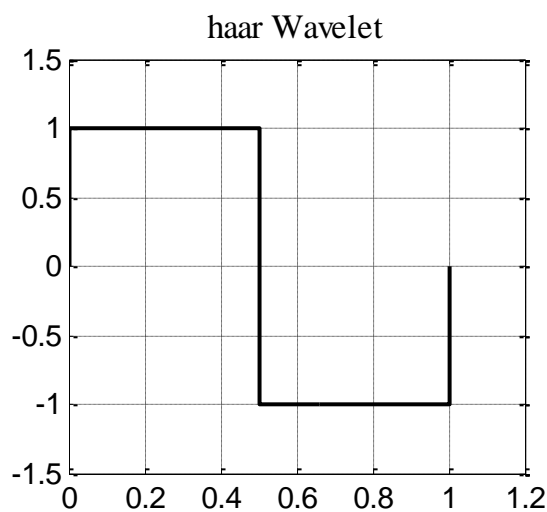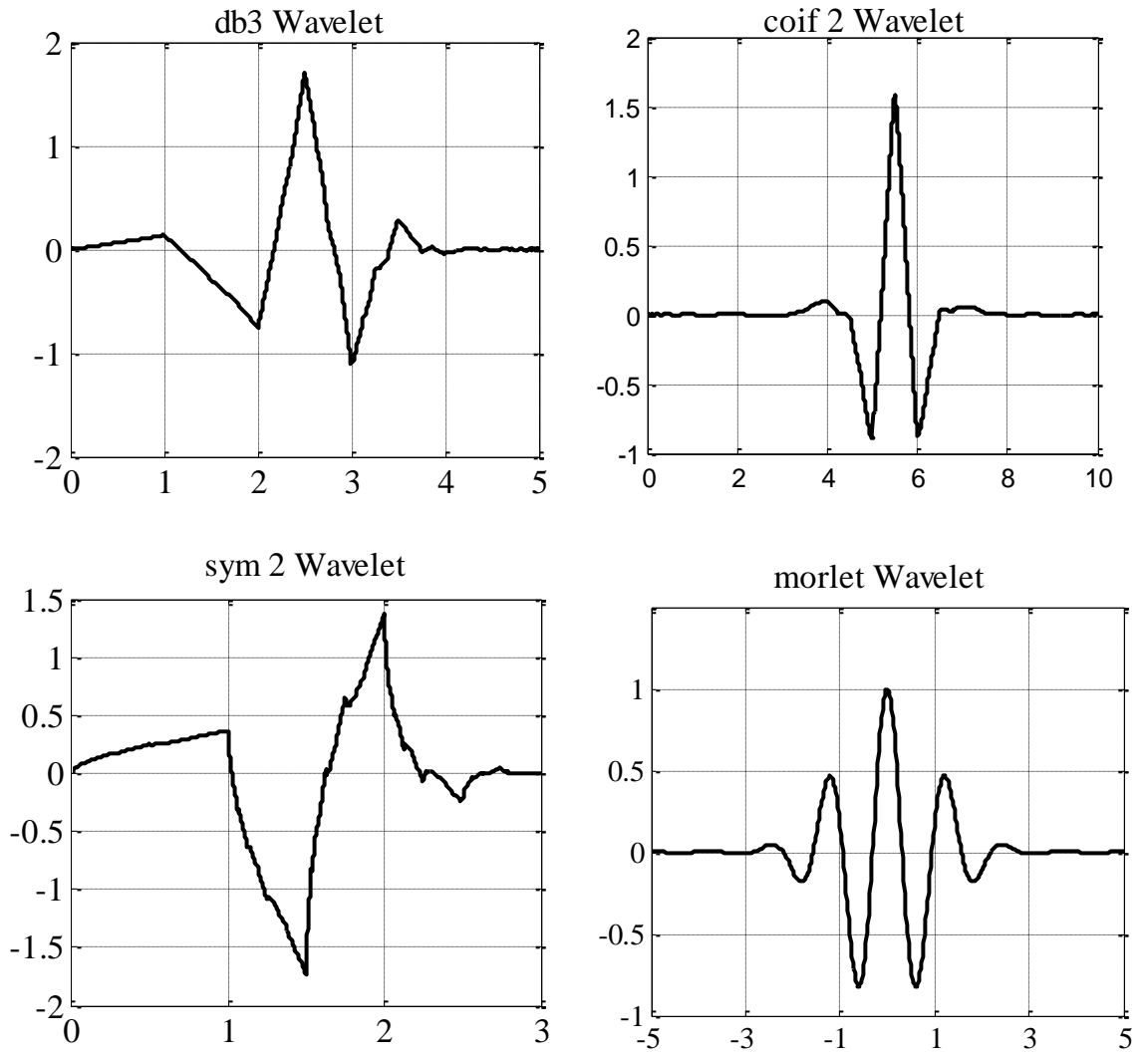
Figure 6.3 Examples of mother wavelet

MDL as a quantitative approach was proposed byHamid and Kawasaki (2002) and Saleh and Rahman (2005) to select an appropriate mother wavelet for remote power protection and power quality monitoring. The MDL criterion aims to achieve a compromise between the number of retained wavelet coefficients and the error of signal reconstruction. In this work, for optimal wavelet analysis selection, the stander deviation (STD) and MDL data criteria are used. The MDL function of index k (number of coefficients to be retained) and n is the (number of wavelet filters).

$$MDL(m, n) = \left\{ \frac{3}{4} m \log N + \frac{N}{2} \log \left\| \hat{a}_n - \hat{a}_n^{(m)} \right\|^2 \right\}$$ (6.19)

where $0 < m < N$, $1 < m < N$, $\hat{a}_n = Wnf$ defined as the vector of the decomposition coefficients of the signal f via the wavelet filter$n$, and $\hat{a}_n^{(m)} = \theta^{(m)} \hat{a}_n$, $= \theta^{(m)} (Wnf)$ represents the vector that contains m nonzero elements, and $\hat{a}_n$ is a hard-threshold operation, that keeps the mTh largest elements of $\hat{a}_n$ in absolute value.

6.3.3. Selection of mother wavelet order and decomposition level

From the previous section, it can be seen that the wavelet transform is constituted by different levels. The maximum level at which to apply the wavelet transform depends on how many data points are contained in a data set, since there is a down-sampling by two operations from one level to the next. The suitable number of levels of decomposition (n) depends on the sampling frequency of the signal being analysed (f_s). For each one of the proposed approaches, it has to be chosen in order to allow the high-level signals (approximation and details) to cover all the range of frequencies along which the sideband component varies during the start up.

The minimum number of decomposition levels necessary for obtaining an approximation signal (a) so that the upper limit of its associated frequency band is under the fundamental frequency (f) (J Antonino et al. 2006). The DIS approach is considered to be optimal for determining wavelet levels. The DIS approach is based on the following steps (Weilin et al. 2014 and Riera et al. 2008):

➤ The number of decomposition levels (nLs) to be adopted depends on the sampling frequency f_s of the signal being analysed. It has to be chosen to allow the high level signals (approximation and details) to cover all the range of frequencies along which the sideband is localised. The sideband components are known as the harmonic components that appear around (left and right) the fundamental frequency components.

> The minimum number of decomposition levels necessary for obtaining an approximation signal so that the upper limit of its associated frequency band is under the fundamental frequency f is described by the following condition:

$$2^{-(nLs+1)}f_s < f \tag{6.20}$$

From this condition, the decomposition level of the approximation signal is the integer nLs:

$$nLs = \text{integer}\left(\frac{\log(f_s/f)}{\log 2}\right) + 2 \tag{6.21}$$

6.4 Feature Extraction of Bearings under Stationary and non-Stationary Operating Conditions

There are several applications where the motor is operating under non-stationary operating conditions (variable speed and load). Actuators and servo motors in the aircraft and transportation industries are examples of non-stationary operations. Detection of faults in such applications is challenging because of the need for complex signal processing techniques.

6.4.1 Features extraction for single localised bearing faults

As mentioned in the previous section, the minimum value of the MDL optimal mother wavelet and STD are used to choose the suitable filter, as illustrated in Table 6.1. Db14 function is selected as the optimal mother wavelet (see Figure 6.4). In this sense, it was observed that, when using a high-order Deubechies wavelet for signal decomposition, the overlapping was smaller than when using a low-order one.

Debauchees are widely used in solving a broad range of problems. They are non-symmetric in waveform, which makes them suitable for approximating the non-symmetric impulse response (Antonino et al. 2006). Different orders of db provide a

library for a user to try out and compare the different results in individual applications (see in appendix C, Table C.1).

Table 6.1 Mother wavelet optimisation based on details of coefficients using DWT

Filter	MDL	STD	Filter	MDL	STD	Filter	MDL	STD
Hear	9.44	265.30	db10	7.354	63.11	Sym5	17.33	62.48
db2	61.88	105.20	db11	5.144	61.98	coif1	33.17	105.90
db3	28.08	67.82	db12	4.664	63.89	coif2	17.84	64.22
db4	15.14	63.30	db13	3.740	63.15	coif3	9.44	63.89
db5	16.18	62.23	db14	2.932	61.85	coif4	3.546	67.81
db6	12.0	63.58	db15	4.093	62.77	demy	2.113	62.64
db7	13.64	63.74	sym2	61.88	105.20	bior1.1	11.17	285.30
db8	13.10	62.36	sym3	28.08	68.04	bior1.3	38.24	70.29
db9	8.668	64.27	Sym4	25.54	64.0	bior1.5	22.75	68.09

In other words, high-order wavelets behave as more ideal filters, a fact that helps to avoid partially the overlapping between frequency bands (Antonino et al. 2006). According to (6.5), f_s =300 sample/s, f =50 Hz, further decomposition of this signal has to be done so that the frequency band [0,] will be decomposed into more bands. Usually, two additional decomposition levels, (i.e., nLs+2) would be adequate for the analysis. In this work nLs = 5 is selected as the decomposition level and the frequency bands of different decomposition levels for fault analysis are provided in Table 6.2.

The energy distributions of the bearing under outer race faults with three severities of defects (0.2x1x3, 0.5x1x6 and 3x1x9) mm, and local bearing defect under stationary operating conditions are summarised in Table 6.3. In the same manner wavelet energy is calculated for inner race and ball defects (see Appendix C, Table C.2)

Table 6.2 frequency bands obtained by decomposition in multilevel

level		Frequency band with sampling frequency $f_s = 300\ sample/s$	Centre frequency (Hz)
J_1	d_1	75-150	225
J_2	d_2	37.5-75	112.5
J_3	d_3	18.75-375	56.25
J_4	d_4	9.37-18.75	28.12
J_5	d_5	4.68- 9.37	14.062
	a_5	0- 4.68	7.03
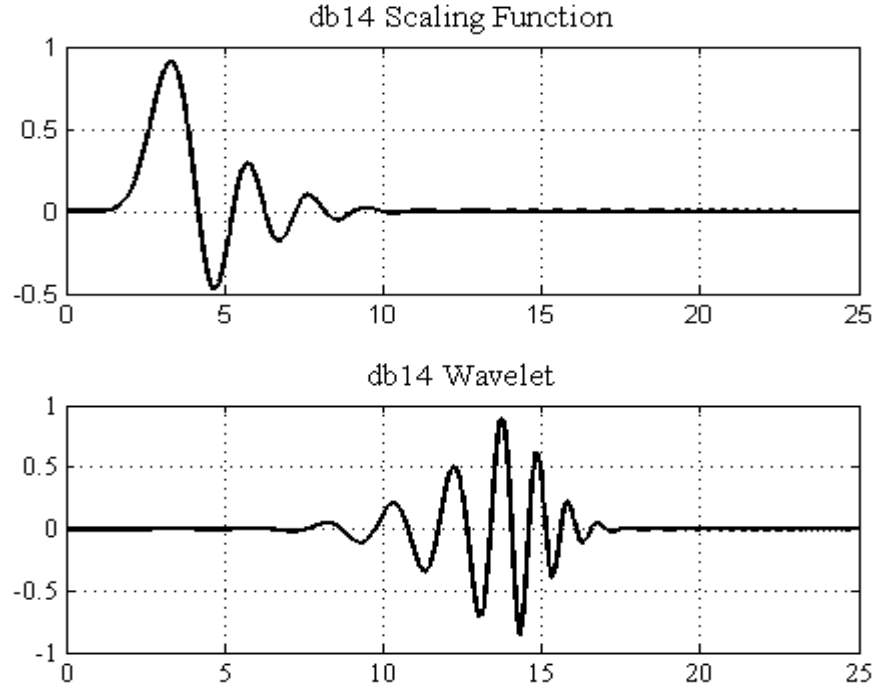
Figure 6.4 db14 filters impulse responses

Mathematically The energy distribution of approximated energy (Ea) and detailed (Ed) can be computed as follows (Wu and Liu 2008):

$$E_a = \frac{1}{N_j} \sum_h |cA|^2 = \frac{\|cA\|^2}{N_j} \tag{6.22}$$

$$E_d = \frac{1}{N_j} \sum_h |cD|^2 = \frac{\|cD\|^2}{N_j} \tag{6.23}$$

where cA and cD are the approxmate and detailed coefficients respectively

Table 6.3 (a to c) showed that the wavelet energy of the details coefficients, D2 and D3 give a good indication about fault severity for no-load and speed 1200 rpm conditions. Wavelet energy (D2, D3) is an increment of 25% and 51% respectively after the fault and is selected to estimate fault severity.

Table 6.3 Energy (J) for different DWT decomposition details and distribution

(a) Outer race with defect size 0.2x1x3mm at different loads (KW) and speeds (rpm) conditions

Load – speed	A	D1	D2	D3	D4	D5
No load-600(rpm)	55.054	0.644	14.243	29.797	0.214	0.048
No load - 900	51.281	3.773	42.182	2.461	0.265	0.040
No load - 1200	49.204	16.261	34.302	0.141	0.057	0.035
Half load -600	58.378	0.691	12.951	27.770	0.169	0.041
Half load -900	50.488	3.895	42.724	2.566	0.279	0.048
Half load -1200	47.137	17.268	35.361	0.139	0.060	0.035
Full load- 600	24.129	0.545	25.390	49.490	0.418	0.028
Full load- 900	5.145	6.818	83.024	4.537	0.453	0.023
Full load- 1200	9.793	31.108	59.053	0.028	0.012	0.006

(b) Outer race with defect size 0.5x1x6mm at different loads (KW) and speeds (rpm) conditions

Load – speed	A	D1	D2	D3	D4	D5
No load-600(rpm)	9.308	1.188	29.392	59.624	0.430	0.058
No load - 900	7.738	6.917	79.841	4.979	0.459	0.073
No load - 1200	6.896	30.602	62.181	0.189	0.088	0.045
Half load -600	28.860	1.011	17.948	51.770	0.341	0.071
Half load -900	23.208	5.860	66.521	3.933	0.412	0.066
Half load -1200	18.966	26.057	54.672	0.177	0.080	0.048
Full load- 600	2.639	0.586	33.837	62.857	0.056	0.025
Full load- 900	8.101	6.508	80.597	4.353	0.423	0.017
Full load- 1200	1.243	34.147	64.555	0.041	0.010	0.004

(c) Outer race with defect size 3x1x9mm at different loads (KW) and speeds (rpm) conditions

Load – speed	A	D1	D2	D3	D4	D5
No load-600(rpm)	11.411	1.198	28.066	58.836	0.427	0.063
No load - 900	9.282	6.798	78.115	5.233	0.074	0.074
No load - 1200	7.844	30.186	61.550	0.276	0.098	0.046
Half load - 600	13.437	1.3189	27.905	56.785	0.484	0.070
Half load- 900	10.364	6.794	77.184	5.121	0.461	0.077
Half load -1200	8.642	28.194	62.768	0.235	0.106	0.055
Full load - 600	2.634	0.571	32.782	63.780	0.161	0.075
Full load - 900	9.26	6.420	79.574	4.316	0.420	0.015
Full load- 1200	2.046	0.582	31.380	65.621	0.346	0.025
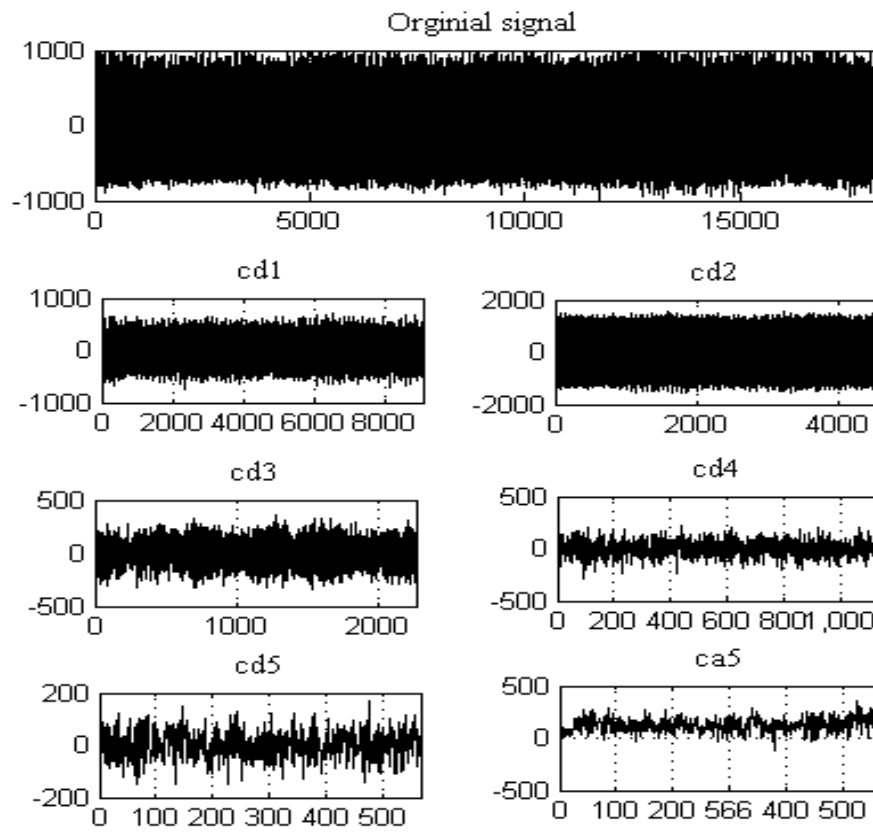
Figure 6.5 DWT decompositions of the vibration signal under normal operation
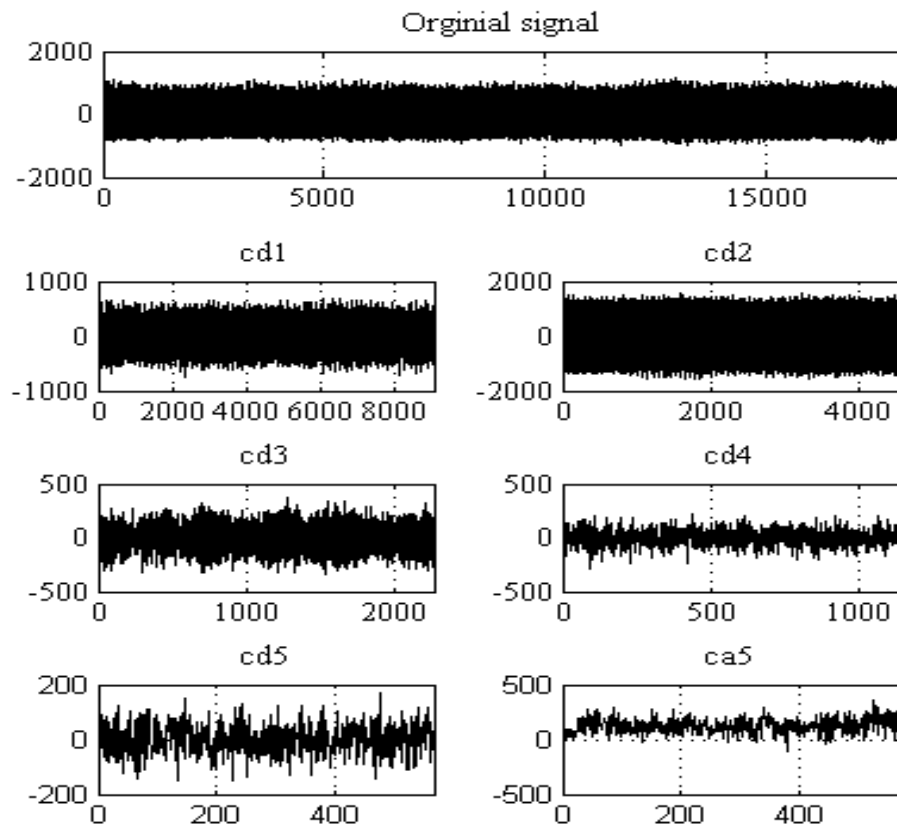
Figure 6.6 DWT decompositions of the current signal under normal operation
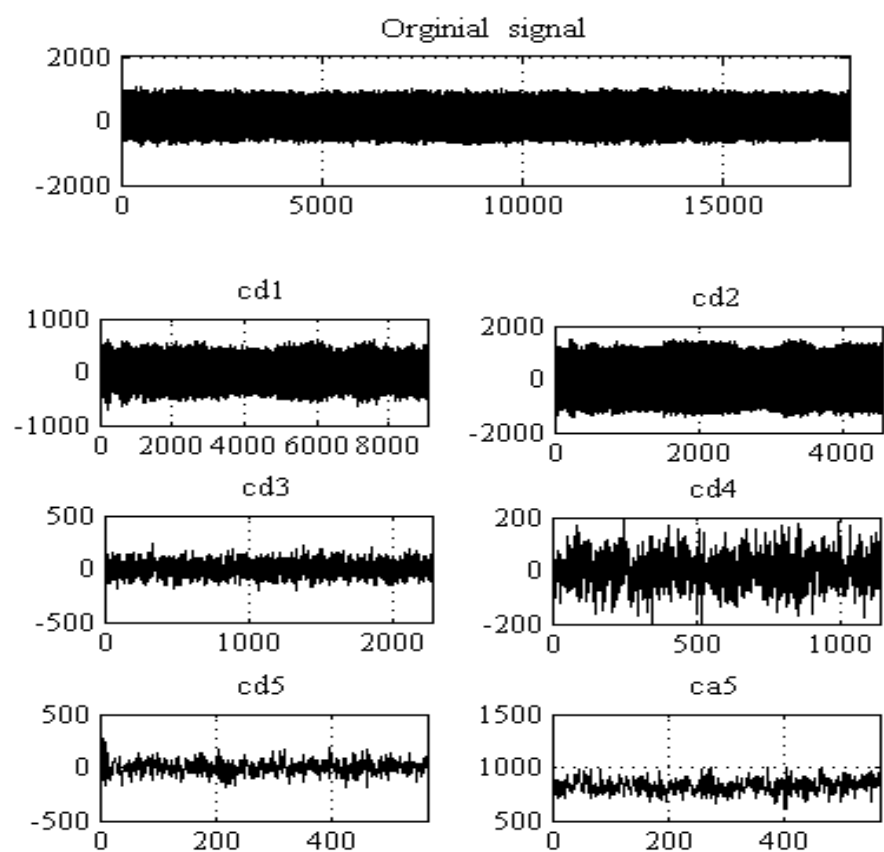
Figure 6.7 DWT decompositions of the vibration signal under fault
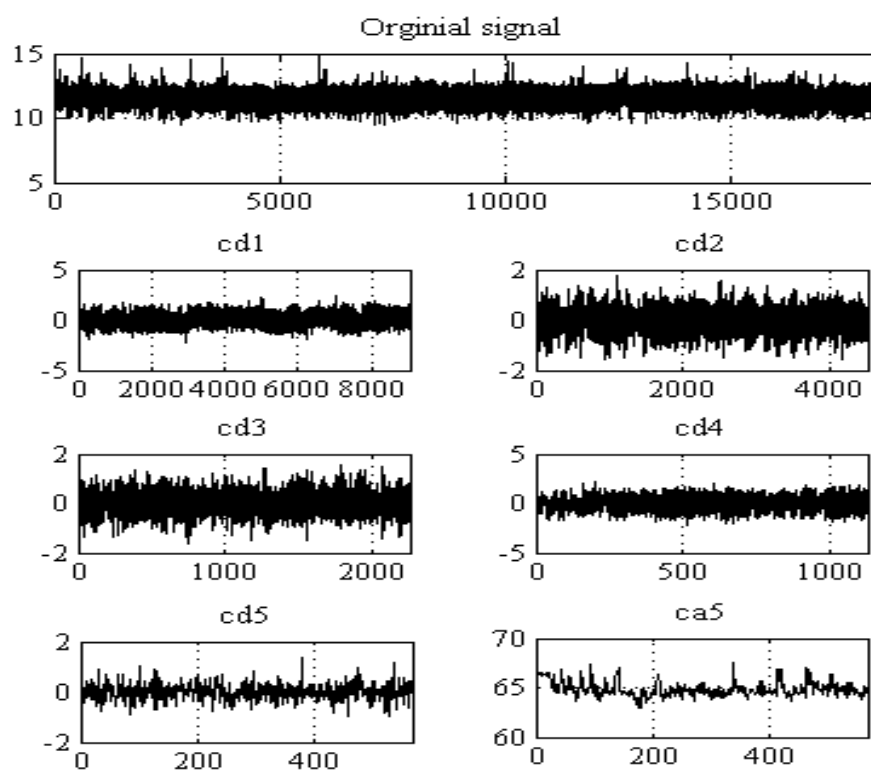
Figure 6.8 DWT decompositions of the current signal under fault

Figures 6.5 and 6.6 show the sampled healthy and faulty stator current and raw vibration signals, The original signal of raw vibration and stator current are plotted at the top of each figure, the signals resulting from the DWT i.e. approximation signal (a) and detail signals (d) with five levels. Figures 6.5 and 6.6 also show the ability of the DWT to discriminate between healthy and faulty cases.

The generated wavelet signal for outer race defects (see Figure 6.5-6.8) after application of DWT can be subjected to qualitative and a quantitative analysis. Qualitative analysis help to obtain information about the determination of the frequency bands through which the fault-related component happens, and from the oscillations in the wavelet signals can determine the type of fault, depending on the characteristic pattern arising.

The wavelet energy decomposition is illustrated in Tables 6.4 and 6.5 showing the comparison of energy distribution for the local bearing faults. It can be seen that level 2 provides an indication about wavelet energy differences between inner outer and ball defects under stationary load and speed conditions.

 On the other hand, once preliminary quantitative analysis of the condition of the machine has been carried out, it is advisable to compute the quantification parameters defined for the corresponding fault, in order to measure the degree of fault in the machine. Similarly for inner race defects, the wavelet energy as listed in appendix C-can be used to predict faults developing under constant and variable speeds and loads conditions, as shown in Figures (6.9 and 6.12).
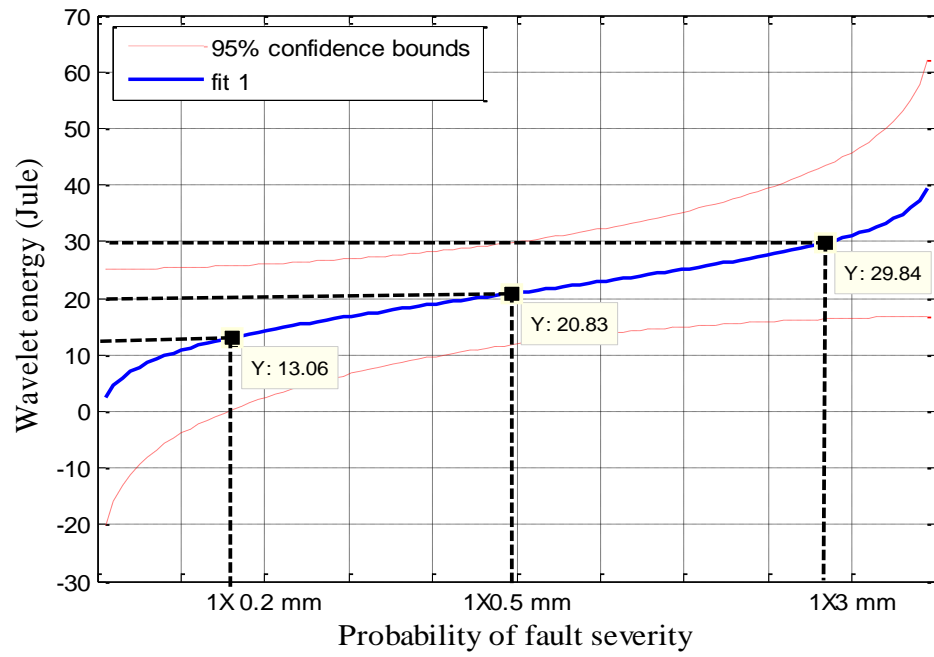
Figure 6.9 Outer fault severities prediction under stationary operating conditions
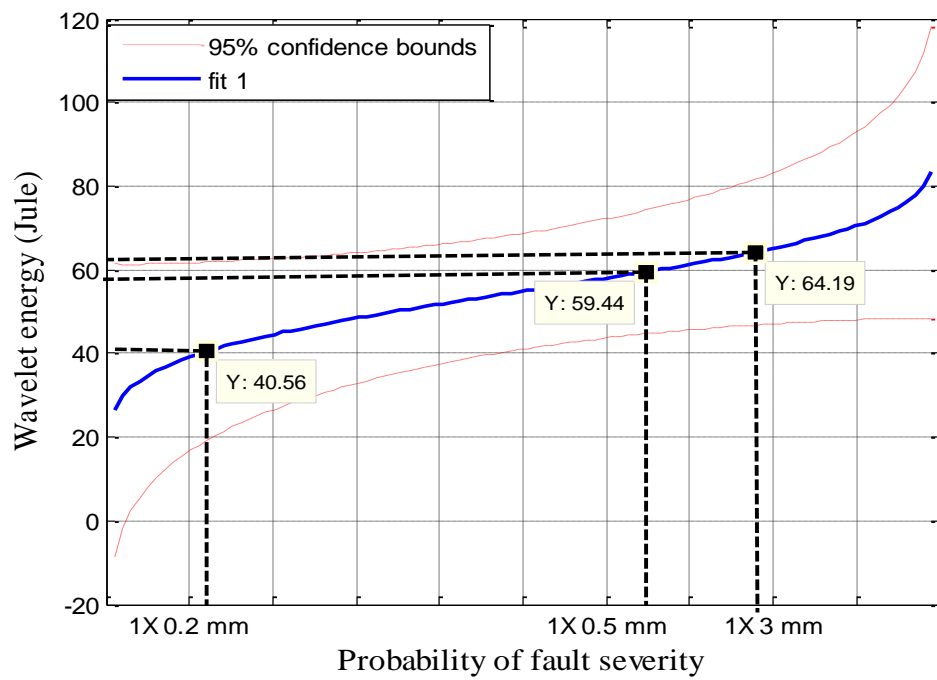
Figure 6.10 Inner fault severities prediction under stationary operating conditions

Table 6.4 Energy (J) for different DWT decomposition details and approximation under variable loads conditions for outer race defect

Speed (rpm)	A	D1	D2	D3	D4	D5
Outer race with defect size 0.2x1x3 mm at variable load conditions						
600	46.902	0.630	17.372	34.902	0.162	0.032
900	38.903	4.471	53.067	3.246	0.283	0.032
1200	31.098	22.977	45.766	0.097	0.040	0.021
Outer race with defect size 0.5x1x6 mm at variable load conditions						
600	10.406	0.805	30.527	57.956	0.275	0.031
900	4.211	6.971	83.895	4.442	0.457	0.024
1200	2.958	34.287	62.673	0.056	0.018	0.009
Outer race with defect size 1x3x9 mm at variable load conditions						
600	6.542	0.924	31.731	60.526	0.241	0.037
900	5.066	7.043	82.724	4.679	0.456	0.035
1200	1.678	33.108	65.135	0.0516	0.017	0.009

Table 6.5 Energy (J) for different DWT decomposition details and approximation under variable speeds conditions for outer race defect

Load	A	D1	D2	D3	D4	D5
Outer race with defect size 0.2x1x3mm at variable speeds conditions						
No load	55.057	5.750	31.156	7.819	0.175	0.043
Half load	7.206	14.789	68.587	9.169	0.232	0.016
Full load	12.975	14.215	62.883	9.646	0.264	0.017
Outer race with defect size 0.5x1x6 mm at variable speeds conditions						
No load	24.354	10.801	52.510	11.939	0.331	0.066
Half load	14.966	11.538	58.813	14.248	0.378	0.057
Full load	1.243	34.147	64.555	0.041	0.010	0.004
Outer race with defect size 1x3x9 mm at variable speeds conditions						
No load	9.463	12.766	62.177	15.129	0.392	0.073
Half load	9.666	12.435	60.939	16.573	0.314	0.074
Full load	1.026	17.327	72.148	9.202	0.284	0.012
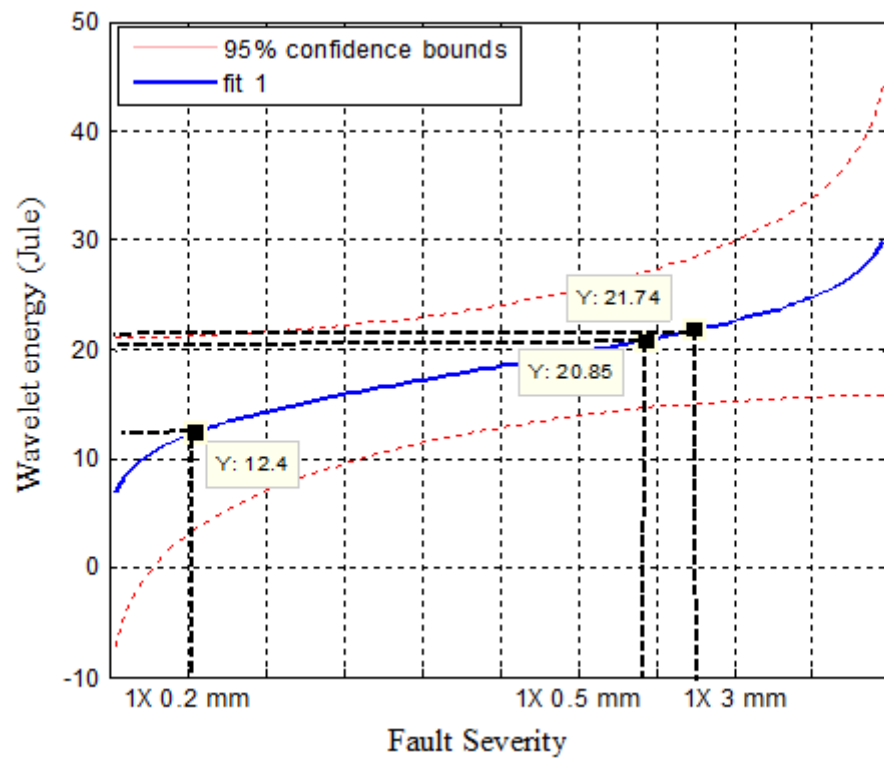
Figure 6.11 Outer fault severities prediction under non-stationary operating conditions
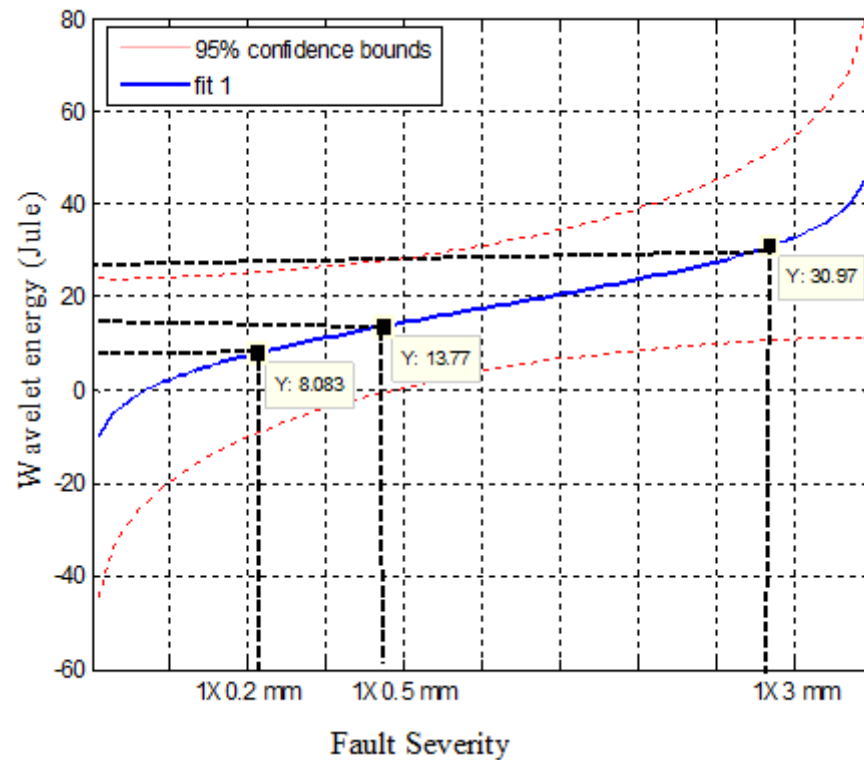
Figure 6.12 Inner fault severities prediction under non-stationary operating condition

6.4.2 Feature extraction for generalised bearing fault

With global (corrosion) bearing faults, a discrete wavelet, Deubechies wavelet db14 is chosen as mother wavelet, with level 5 vibration and current signals, associated with various constant and variable speed and load conditions, with 4 degrees of fault severities.

Table 6.6 Energy (J) for different DWT decomposition details and approximation for corrosion defect severity 1 under stationary loads (KW) and speeds (rpm) conditions

Load – speed(rpm)	A	D1	D2	D3	D4	D5
No load – 600	60.6856	0.3610	6.91921	31.7917	0.2144	0.0352
No load - 900	55.3187	0.4502	43.6514	0.4022	0.0579	0.0259
No load - 1200	52.7298	9.1868	37.8785	0.1269	0.0512	0.0267
Half load -600	1.7344	1.0350	18.5201	76.8586	1.6951	0.1568
Half load -900	78.9946	0.2323	20.5469	0.1803	0.0295	0.0164
Half load -1200	76.5705	4.5070	18.8063	0.0697	0.0277	0.0188
Full load- 600	18.4676	0.0793	17.1227	64.1558	0.1151	0.0596
Full load- 900	0.4713	1.5190	92.7957	5.0405	0.1322	0.0412
Full load- 1200	0.6150	21.704	76.8473	0.6666	0.0963	0.0714

Table 6.7 Wavelet energy for corrosion fault at variable load

Speed	A	D1	D2	D3	D4	D5
Corrosion with defect severity 1 at variable load (KW) conditions						
600	0.8328	1.4615	34.3426	61.8344	1.3838	0.1449
900	13.8217	6.5363	72.5857	6.5147	0.4730	0.0686
1200	0.5688	32.4512	65.9538	0.8414	0.1401	0.0447
Corrosion with defect severity 2 at variable load (KW) conditions						
600	15.8962	1.0811	24.7630	57.6153	0.5097	0.1347
900	13.8217	6.5363	72.5857	6.5147	0.4730	0.0686
1200	13.2113	27.3220	58.5891	0.6559	0.1827	0.0389
Corrosion with defect severity 3 at variable load (KW) condition						
600	0.2338	1.1142	30.8388	66.4733	1.1392	0.2009
900	0.1047	7.3567	85.4630	6.0698	0.9063	0.0995
1200	0.1424	32.0514	66.2188	1.3522	0.1950	0.0403
Corrosion with defect severity 4 at variable load (KW) conditions						
600	2.1932	1.3265	24.8809	70.6931	0.7062	0.2000
900	1.9670	7.3584	83.0121	6.9991	0.5771	0.0863
1200	1.8165	30.1955	67.0309	0.7189	0.1941	0.0441

Table 6.8 Wavelet energy for corrosion fault at variable speed

Load	A	D1	D2	D3	D4	D5
Corrosion with defect severity 1 at variable speeds conditions						
No load	0.9670	14.0017	64.3205	19.8666	0.7350	0.1093
Half load	14.2718	12.6453	66.8833	18.9101	0.4474	0.1141
Full load	1.0113	11.7985	63.8111	22.8135	0.4878	0.0779
Corrosion with defect severity 2 at variable speeds conditions						
No load	0.1542	12.4079	70.0063	16.8279	0.5178	0.0858
Half load	14.2718	12.4261	58.5844	14.3016	0.3535	0.0626
Full load	10.8823	12.2500	56.6147	19.6572	0.5205	0.0753
Corrosion with defect severity 3at variable speeds conditions						
No load	14.4810	10.3872	59.1052	15.5869	0.3696	0.0700
Half load	0.2666	12.2748	68.5494	18.2808	0.5347	0.0937
Full load	0.1065	12.3219	64.4784	22.2255	0.7909	0.0768
Corrosion with defect severity 4 at variable speeds conditions						
No load	2.2477	10.9085	60.9296	25.2633	0.5367	0.1142
Half load	0.7909	11.4275	62.8330	24.4318	0.4280	0.0887
Full load	0.9313	11.2615	57.0982	29.8793	0.6267	0.2029

Similarly to local bearing faults features extraction, the approximated and detailed coefficients are decomposed into 5 levels, as listed in Tables 6.6- 6.8. Figure 6.13 shows the ability of wavelet energy to predict the fault severity.
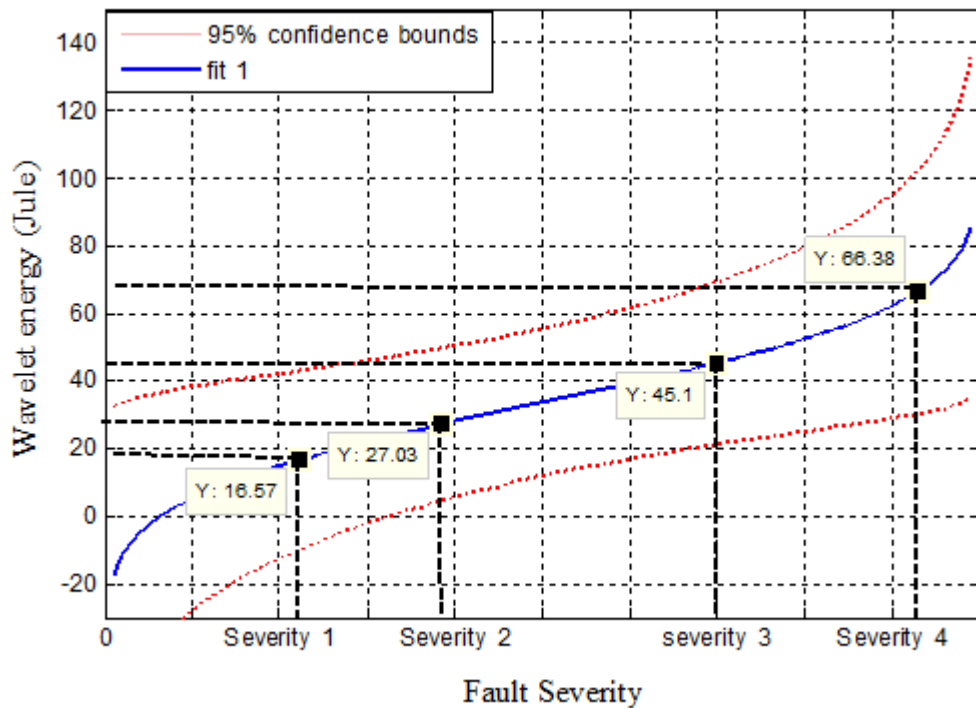
Figure 6.13 Probability of corrosion fault severity

6.5 Feature extraction for Thruster Motor Faults

The same feature extraction procedure can be implemented for unbalanced mechanical load of the thruster motor, as mentioned in Chapter 4. During the experimental setup the data acquisition time is T=30s, with a sampling frequency f_s=3 kHz for all the experiment's tests, and a fundamental frequency of f=50Hz. The measurements are taken at different speed levels, from very low to very high speeds. Wavelet frequency bands are summarised in Table 6.9.

Table 6.9.Wavelet frequency bands

level		Frequency band with sampling frequency $f_s = 3000\ sample/s$	Centre frequency (Hz)
J_1	d_1	750-1500	1125
J_2	d_2	375-750	562.5
J_3	d_3	187.5-375	281.25
J_4	d_4	93.75-187.5	140.62
J_5	d_5	46.87-93.75	70.31
J_6	d_6	23.43-46.87	35.15
J_7	d_7	11.71-23.43	17.57
J_8	d_8	5.85-11.71	8.78
	a_8	0- 5.85	2.92

To optimise the mother wavelet function level of decomposition and function order Eqn 6.18 are implemented and db 12 is selected as the mother wavelet, as illustrated in Table 6.10 and on the basis of Eqn 6.19 nls=8 is chosen as a suitable wavelet level decomposition. Table 6.11 reports DWT decomposition energy at normal and faulty case under different rotation speed conditions.

Table 6.10 Mother wavelet optimisation based on details coefficients using DWT

Filter	MDL	STD	Filter	MDL	STD	Filter	MDL	STD
haar	14.78	1.13	db10	7.13	0.70	sym6	13.10	0.83
db2	15.63	1.11	db11	5.13	0.70	coif1	9.65	1.11
db3	15.67	1.03	db12	5.04	0.67	coif2	13.07	0.93
db4	10.07	0.94	db13	5.89	0.87	coif3	10.27	0.81
db5	9.62	0.87	db14	6.96	0.96	coif4	8.28	0.73
db6	9.88	0.82	sym2	15.63	1.11	demy	9.89	0.97
db7	8.17	0.79	sym3	15.67	1.03	bior1.1	14.7	1.13
db8	7.43	0.75	sym4	11.04	0.95	bior1.3	7.13	1.01
db9	7.23	0.71	sym5	12.58	0.88	bior1.5	11.96	0.89

Table 6.11 DWT decomposition and energy distribution (Joule)

(a) Normal at different speeds

Speed	D1	D2	D3	D4	D5	D6	D7	D8
Max speed	0.0011	0.0012	0.0026	0.0094	0.0045	0.0089	0.0082	0.0066
Speed2	0.0004	0.0004	0.0008	0.0026	0.0019	0.0036	0.0053	0.0058
Speed3	0.0014	0.0011	0.0011	0.0016	0.0013	0.0023	0.0058	0.0058
Speed4	0.0012	0.0015	0.0013	0.0041	0.0012	0.0023	0.0044	0.0057
Speed5	0.0011	0.0016	0.0009	0.0013	0.0012	0.0021	0.0037	0.0058
Low speed	0.0011	0.0015	0.0008	0.0013	0.0013	0.0019	0.0039	0.0056

(b) Faults at speed 1(max speed)

Fault Severity	D1	D2	D3	D4	D5	D6	D7	D8
10%	0.0013	0.0023	0.0090	0.0164	0.0311	0.2132	0.1777	0.0154
25%	0.0019	0.0072	0.0116	0.0137	0.0320	0.1598	0.0865	0.0690
50%	0.0022	0.0087	0.0321	0.0820	0.7618	5.4039	3.7546	0.0066
Full defect	0.0026	0.0130	0.0609	0.1787	1.4362	1.5768	0.8262	0.0192

(c) Faults at speed 2

Fault Severity	D1	D2	D3	D4	D5	D6	D7	D8
10%	0.0013	0.0023	0.0092	0.0156	0.0305	0.2083	0.1819	0.0059
25%	0.0020	0.0074	0.0098	0.0130	0.0316	0.1607	0.0979	0.0272
50%	0.0019	0.0073	0.0273	0.0803	0.7797	5.4388	3.7184	0.0112
Full defect	0.0023	0.0114	0.0534	0.1663	1.3747	1.2753	0.4622	8.0188

(d) Faults at speed 3

Fault Severity	D1	D2	D3	D4	D5	D6	D7	D8
10%	0.0070	0.0053	0.0054	0.0080	0.0121	0.0780	0.1487	0.0177
25%	0.0059	0.0082	0.0139	0.0119	0.0186	0.0961	0.1362	0.0406
50%	0.0054	0.0061	0.0137	0.0386	0.1673	1.5679	3.0805	0.0203
Full defect	0.0058	0.0059	0.0130	0.0459	0.4301	4.2362	9.1805	0.0287

(e) Faults at speed 4

Fault Severity	D1	D2	D3	D4	D5	D6	D7	D8
10%	0.0062	0.0071	0.0058	0.0058	0.0059	0.0237	0.0934	0.0313
25%	0.0055	0.0045	0.0052	0.0056	0.0036	0.0162	0.0518	0.0441
50%	0.0047	0.0055	0.0061	0.0104	0.0441	0.4710	1.8634	0.1833
Full defect	0.0050	0.0060	0.0059	0.0138	0.0889	1.0046	4.7329	0.7504

(f) Faults at Speed 5

Fault severity	D1	D2	D3	D4	D5	D6	D7	D8
10%	0.0058	0.0070	0.0053	0.0026	0.0018	0.0069	0.0268	0.0405
25%	0.0035	0.0034	0.0060	0.0094	0.0072	0.0092	0.0189	0.0530
50%	0.0047	0.0051	0.0047	0.0056	0.0105	0.0857	0.5889	0.4659
Full defect	0.0050	0.0060	0.0059	0.0138	0.0889	1.0046	4.7329	0.7504

(g) Faults at Speed 6 (low speed)

Fault Severity	D1	D2	D3	D4	D5	D6	D7	D8
10%	0.0061	0.0063	0.0046	0.0024	0.0028	0.0029	0.0055	0.0139
25%	0.0043	0.0030	0.0033	0.0051	0.0022	0.0038	0.0116	0.0462
50%	0.0047	0.0054	0.0043	0.0036	0.0035	0.0072	0.0564	0.2077
Full defect	0.0049	0.0057	0.0060	0.0086	0.0064	0.0175	0.1427	0.5667
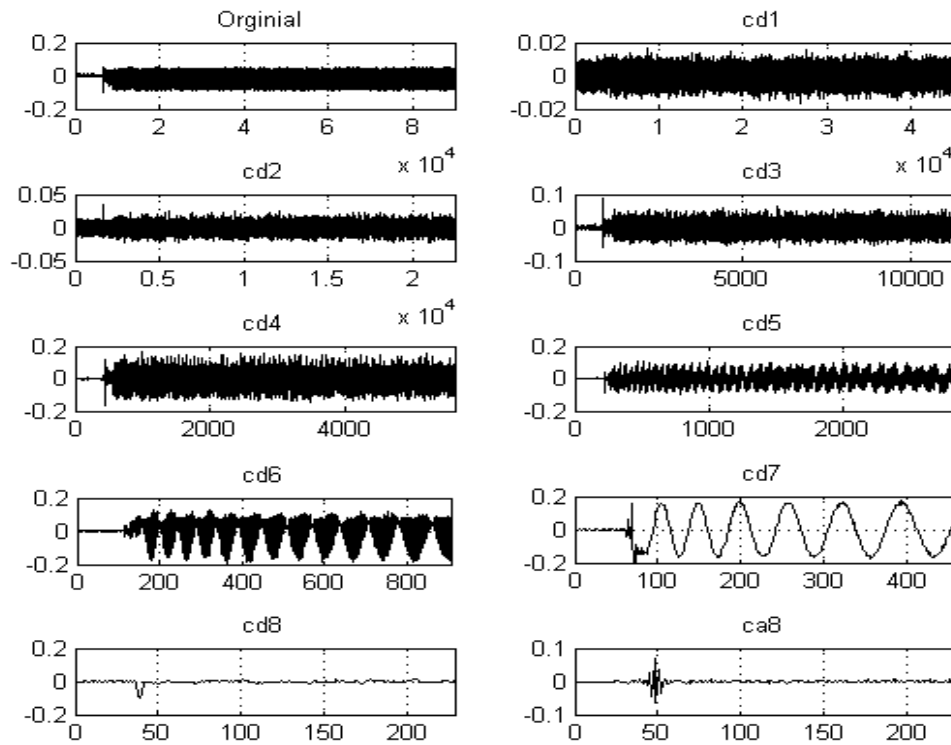
Figure 6.14 DWT decompositions of the thruster motor vibration signal under normal operation
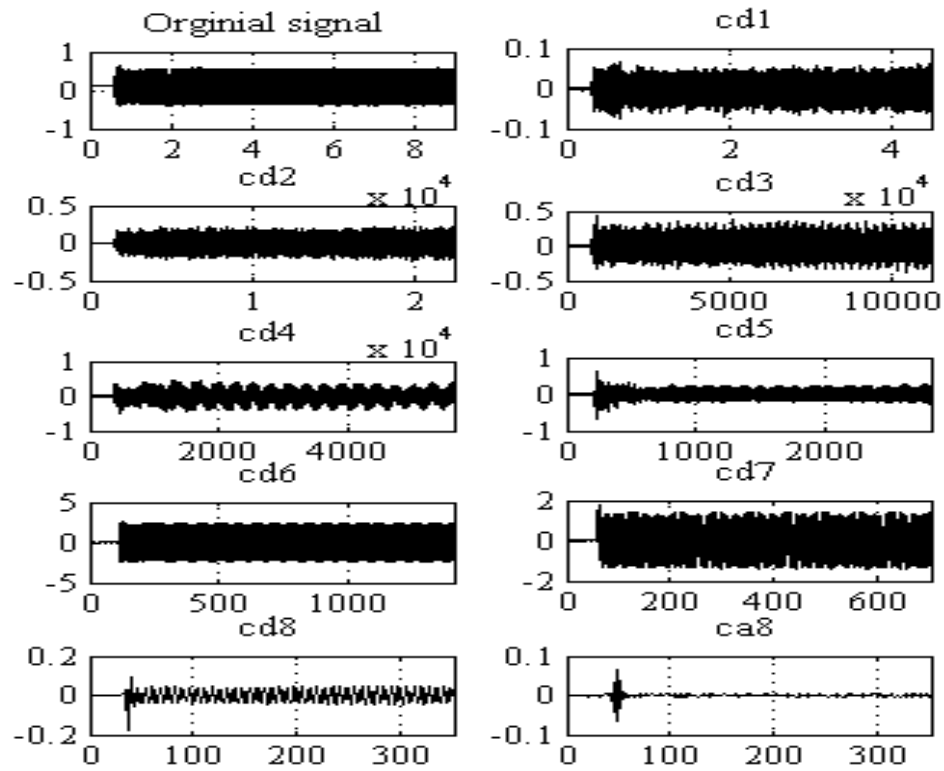
Figure 6.15 DWT decompositions of the thruster motor vibration signal under fault operation

Figures 6.14 and 6.15 show the original signal, details coefficient (d1-d8) approximate coefficient (a8) under normal and corrosion fault conditions, respectively. The DWT representation gives a clear idea about how the original signal is reconstructed using the approximations and details at various levels. As is clear from Figure 6.16, details at level 6 give a good indication about the progress of fault severity, so that it can be used to predict the severity of blade faults, as shown in Figures 6.16 and 6.17.

DWT has been successful in analysing non-stationary signals. However, DWT yields a high dimensional feature vector (Phinyomark et al. 2012) and in some cases the number of features (see Figure 6.18) is relatively larger than the number of training samples. This is usually referred as the 'curse of dimensionality', adversely affecting training and testing speed (Alok et al. 2006). An accurate dimensionality reduction tool is thus needed to remove redundant features information (Prieto et al. 2013).
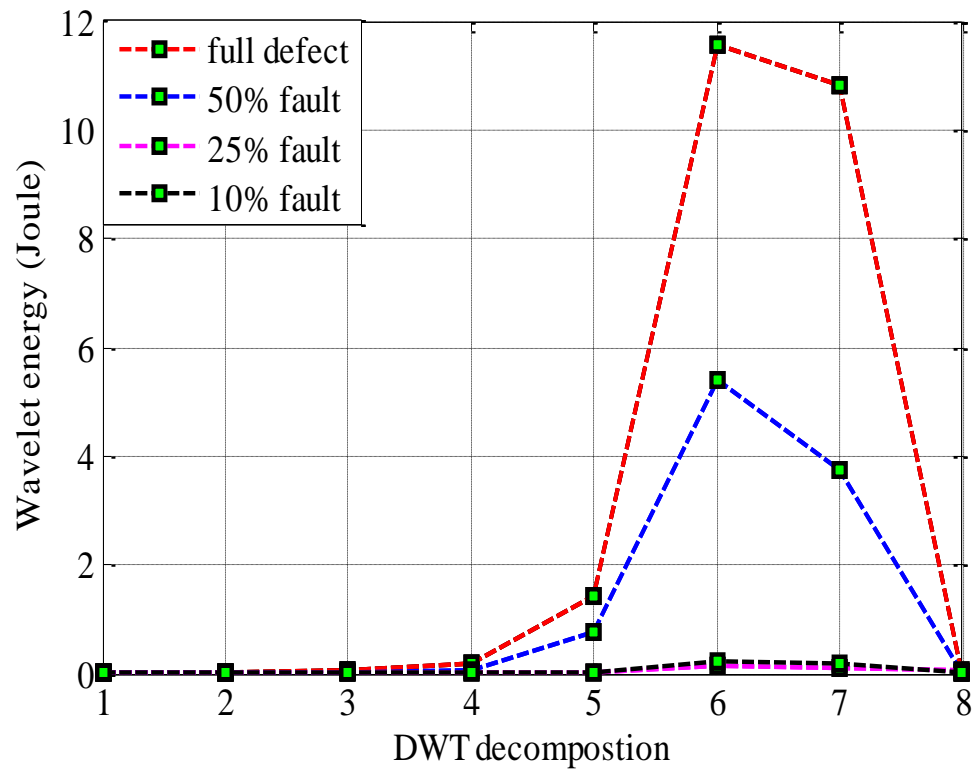
Figure 6.16 Blades F1 faults under high speed
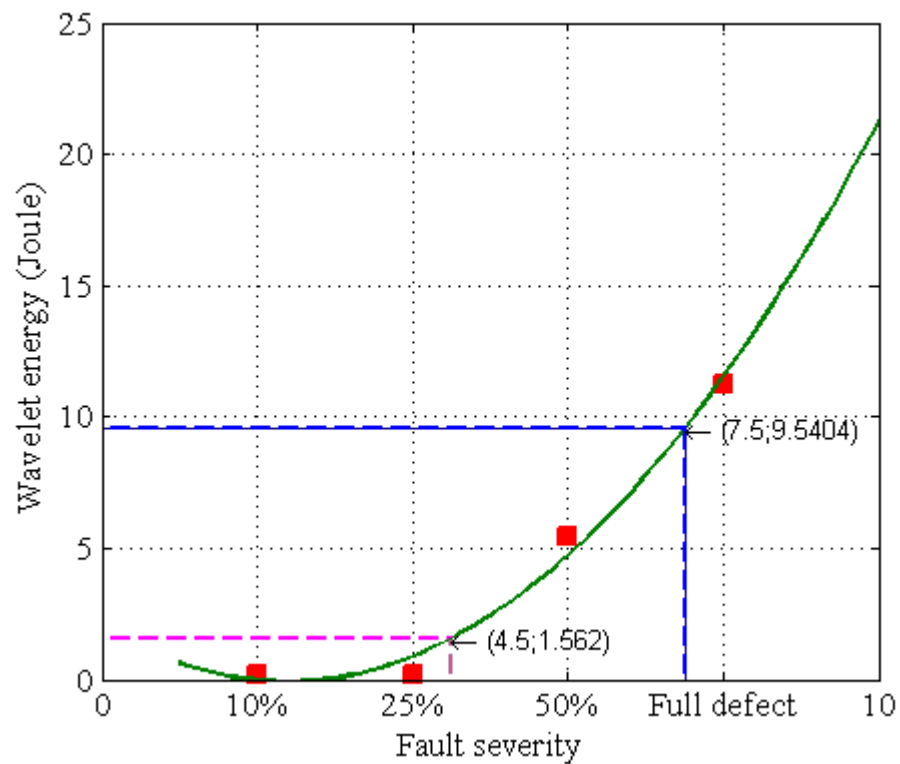
Figure 6.17 Thruster motor blades fault severity prediction under high speed
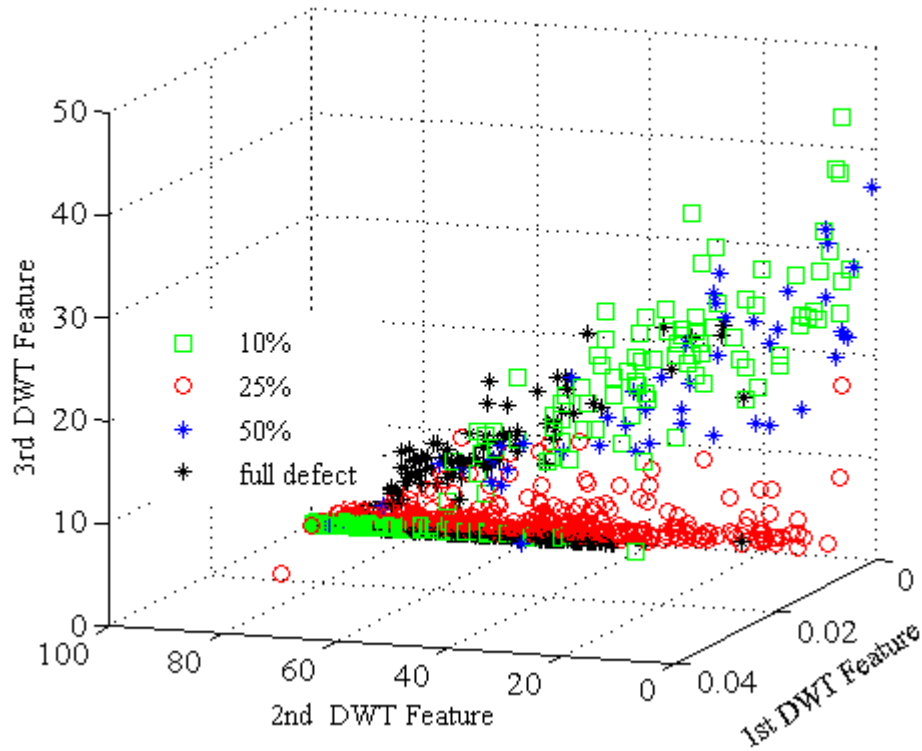
Figure 6.18 Scatter plot of the DWT features

6.6 Feature Projection and Dimensionality Reduction Techniques

Feature projection is an important task in machine learning, for it facilitates classification, compression, and visualization of high-dimensional data by mitigating undesired properties of high-dimensional spaces by removing redundant features information that may lead to over fitting (Biet 2013).

Dimensionality reduction methods can be implemented as methods of feature projection and feature selection. As such, it is obvious that the main goal of feature dimensionality reduction is to reduce the number of features without compromising the quality of classification. Generally, dimension reduction approaches can be classified into linear, and nonlinear as will be discussed in the next two subsections (Cevikalp 2005).

The choice of linear and nonlinear techniques will be determined by the nature of the classification problem. The linear case is the simplest classification problem in which both linear and nonlinear techniques are expected to classify all the data correctly. For

144

nonlinear cases, classes of data can be separated using nonlinear separating planes, where using linear techniques in this case would misclassify a large portion of the data (Chiang et al. 2004).

6.6.1 Linear dimensionality reduction techniques

PCA and LDA are the classic and popular dimensionality reduction methods. PCA is a linear feature reduction techniques used to transfer data to a new orthogonal basis, whose axes are oriented in the directions of the maximum variance of an input data set.

To reduce dimensionality from *d* to *m,* the basic working of a PCA is presented below (Sakthivel et al. 2014):

Step 1: calculate the mean and subtract the sampling mean from each row, as represented in

$$C = \frac{1}{n-1} x_j x_j^T \tag{6.24}$$

$$C_{jk} = \frac{1}{n-1} \sum_{j=1}^{n} \left(x_{ji} - x_i^* \right) \left(x_{jk} - x_k^* \right) \tag{6.25}$$

$$j, k = 1, \dots \dots . p \tag{6.26}$$

where x_j denotes data matrix and n is the matrix dimension.

Step 2: calculate a covariance matrix C as follows:

$$C = \frac{1}{M} \sum_{i=1}^{n} C_{jk} \; C_{jk}{}^T \tag{6.27}$$

Step 3 calculates the eigenvectors and eigenvalues of the matrix C by solving (5):

$$|C - lI| = 0 \tag{6.28}$$

Finally, project the new dataset by multiplying the original data by the covariance matrix. The main drawbacks of PCA is that it works to reduce feature redundancy only, without taking into account the relation of features or variables within the specific class

labels, and this will affect the classification accuracy (Delgado et al. 2011). Furthermore, PCA has the drawback of its limited ability to deal with non-linear behaviour of the data.

LDA is another feature reduction technique that deals with the projection axes on which the distance between data points of the same classes is decreased, and the distance between data points belonging to different classes is increased (Eleyan and Demirel 2007). LDA can produce an optimally discriminant projection by considering the labels of the input data. However, there still exist some drawbacks in LDA.

When the dimension of data is too high and training data is inadequate, LDA cannot find the best projection directions for classification. Moreover, the discriminating power of LDA is also limited in that the dimension of its reduced space cannot be larger than the class number minus one (Jieping et al. 2004). The main difference between LDA and PCA is that the former does data classification whereas PCA does feature classification. In PCA, the shape and location of the original data sets changes when transformed to a different space whilst LDA does not change the location, but only tries to provide more class separation, and draws a decision region between the given classes (Haixian et al. 2014).

6.6.2 Nonlinear dimensionality reduction techniques

Since PCA and LDA are linear, their performances degenerate for nonlinear data where the underlying low-dimensional structure has nonlinear manifolds rather than linear. Over the last decade, a large number of new (nonlinear) techniques for dimensionality reduction have been proposed. Most of these techniques are based on the intuition that data lies on or near a complex low-dimensional manifold that is embedded in the high-

dimensional space. Nonlinear techniques for dimensionality reduction can be classified into three main types (vander et al. 2009).

➢ Techniques that attempt to preserve the global properties of the original data in the low-dimensional representation, such as Kernel PCA.

➢ Techniques that attempt to preserve local properties of the original data in the low-dimensional representation, such as locally linear embedding.

➢ Techniques that perform global alignment of a mixture of linear models, such as locally linear coordination

A new feature reduction approach is proposed in this chapter that has not previously been used for electrical machines fault diagnosis; this will be discussed in next section.

6.7 Orthogonal Fuzzy Discriminate Analysis for Feature Reduction

The feature projection method attempts to determine the best combination of original wavelet coefficients, and additionally, the features reduced are different from the original features. OFNDA is a better technique compared to other feature reduction techniques such as LDA where singularity problems are predominant.

OFNDA has been recently proposed and used in analysis of medical data. Khushaba et al. (2010) present OFNDA for feature reduction as it works to maximise the distance between features belong to different classes (S_b) whilst minimise the distance between features in the same class (S_w) and also taking into account the contribution of the samples to the different classes, as shown in Figure 6.19. OFNDA has been successfully applied here to classify four classes of rolling element bearing defects under constant and variable speed and load conditions. It can be observed from the graph that boundaries between different operating conditions are more distinct in the case of the
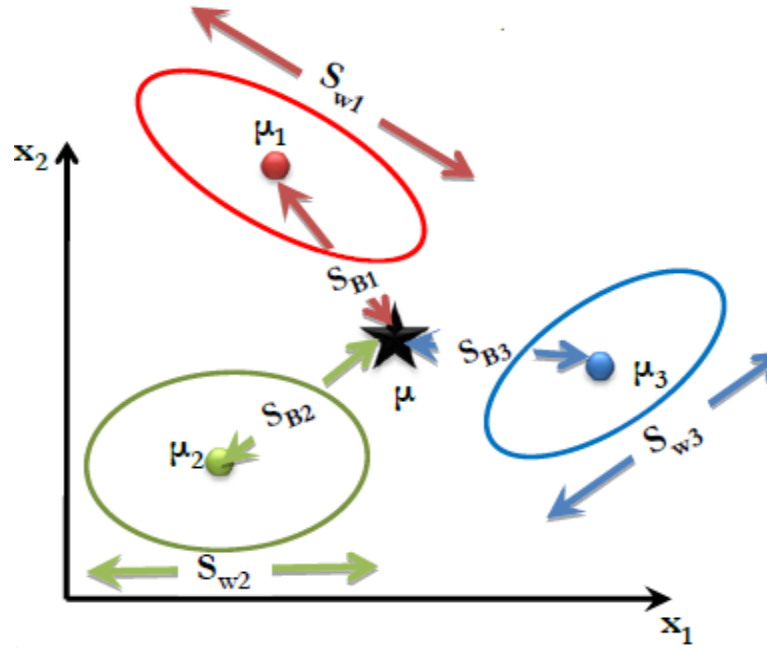
Figure 6.19 The feature space mapping (Farag, 2008) permission to reproduce this figure has been granted by Farag.A

The diagram in Figure 6.20 illustrates the OFNDA process. The first step is to apply principle component analysis to remove any redundancy that may cause singularity, before starting discriminant analysis and keeping all principle components, to prevent the loss of any useful information. The computation of the proposed fuzzy neighbourhood discriminant analysis (FNDA) proceeds by calculating the S_w and S_b as given by:

X_x is the mean of the training samples; this is in turn given as follows:

$$X_x = \frac{\sum_{i=1}^{c} \sum_{k=1}^{l_i} \mu_{ik} X_k}{\sum_{i=1}^{c} \sum_{k=1}^{l_i} \mu_{ik}} \tag{6.29}$$

$$S_W = \sum_{i=1}^{c} \sum_{k=1}^{l_i} \mu_{ik} (K_k - U_i)(X_k - U_i)^T \tag{6.30}$$

. where μ_{ik} is the membership of pattern k in class i, X_k is the K_{th} sample, and U_i is the mean of the patterns that belong to class i, given the universal set $X = \{x1, x2, \ldots, xl\}$, where x is feature vector, $k = 1, 2, \ldots, l$ is the number of samples

$$U_i = \frac{\sum_{k=1}^{l_i} \mu_{ik} X_k}{\sum_{k=1}^{l_i} \mu_{ik}} \tag{6.31}$$

148

$$S_W = \sum_{i=1}^{c} \sum_{k=1}^{l_i} \mu_{ik}\left(K_k X_k{}^T - U_i X_k{}^T - K_k U^T - U_i U_i{}^T\right) \tag{6.32}$$

$$S_W = \sum_{i=1}^{c} \frac{1}{\sum_{j=1}^{li} \mu_{ij}} \sum_{j=1}^{li} \mu_{ij} \left[\sum_{k=1}^{l_i} \mu_{ikK_kX_k}{}^T - \sum_{k=1}^{li} \mu_{ikK_k} \sum_{j=1}^{li} \mu_{ikK_j}{}^T \right] \tag{6.33}$$

This finally simplifies to:

$$\boxed{S_W = \sum_{i=1}^{c} \frac{1}{2 \sum_{j=1}^{li} \mu_{ij}} \sum_{j=1}^{li} \sum_{k=1}^{li} \mu_{ij}\mu_{ik}\left(x_k - x_j \right)\left(x_k - x_j \right)^T} \tag{6.34}$$

$$S_B = \sum_{i=1}^{c} \mu_{ik}(U_i - X_x)(U_i - X_x)^T \tag{6.35}$$

$$S_B = \sum_{i=1}^{c} \sum_{k=1}^{l_i} \mu_{ik}\left(K_k X_k{}^T - U_i X_k{}^T - K_k U^T - U_i U_i{}^T\right) \tag{6.36}$$

$$B = \sum_{k=1}^{li} \mu_{ik} \tag{6.37}$$

$$S_B = \frac{1}{2n}\sum_{i=1}^{c} \sum_{j=1}^{c} B_i B_j \left(\frac{1}{2} U_k U_k - U_j U_k - \frac{1}{2} U_j U_j \right) \tag{6.38}$$

and finally we reach to the last term for SB that is given as

$$\boxed{S_B = \frac{1}{2n}\sum_{j=1}^{li} \sum_{k=1}^{li} B_i B_j \left(U_k - U_j \right)\left(U_k - U \right)^T} \tag{6.39}$$

$$G_{FNDA} = \arg \text{mat } \text{trac}\left(\frac{G^T S_B G}{G^T S_W G}\right) \tag{6.40}$$

Then a QR-decomposition is applied on the resultant matrix to acquire a new transformation matrix Q, that is $G = QR$. In such an equation, Ris an upper triangular matrix and Q is an orthogonal matrix, i.e., one satisfying $Q^T$is the transpose of Q and I is the identity matrix.

$$G = QR \tag{6.41}$$

$$Q = G_{OFNDA} \tag{6.42}$$

G_{FNDA} is the Transformation matrix related to PCA and OFNDA respectively.

$$X(m.n)^* = X(m.n).G_{OFNDA} \tag{6.43}$$

The feature reduction techniques mentioned above were able to reduce drastically the number of wavelet features, originally from 12 to 4, enabling faster computation.

```
┌─────────────────────────────────────┐
│     Wavelet features =X(m. n)       │
└─────────────────────────────────────┘
                 ↓
┌─────────────────────────────────────────┐
│    Select number of reduced features    │
└─────────────────────────────────────────┘
                 ↓
┌────────────────────────────────────────────────┐
│ Pre-processing the selected data to obtain $G_{PCA}$ │
└────────────────────────────────────────────────┘
                 ↓
┌────────────────────────────────────────────────┐
│ Calculate the distance within the class ( $S_W$ ) │
└────────────────────────────────────────────────┘
                 ↓
┌────────────────────────────────────────────────┐
│ Calculate the distance between two classes ($S_B$) │
└────────────────────────────────────────────────┘
                 ↓
┌────────────────────────────────────────────────┐
│ Based on ($S_W$) and ($S_B$),the transformation │
│ Matrix ($G_{FNDA}$) is calculated (see Eq 6.40) │
└────────────────────────────────────────────────┘
                 ↓
┌────────────────────────────────────────────────┐
│   Calculate the transformation matrix  $G$      │
└────────────────────────────────────────────────┘
                 ↓
┌────────────────────────────────────────────────┐
│ Calculate the orthogonal matrix $Q$ (see Eq 6.41) │
└────────────────────────────────────────────────┘
                 ↓
┌────────────────────────────────────────────────┐
│ Project the data with transformation (see Eq 6.43) │
└────────────────────────────────────────────────┘
```

Figure 6.20 The steps of OFNDA performance

6.7.1 Features dimensionality reduction for bearing faults

OFNDA decreases the features extracted using DWT (12 features for bearing fault) to 4 features, which will used in training, validation and testing the DNN in Chapter 7. That represents bearing local and corrosion faults under different severities. OFNDA works to decrease DWT features (18 features in this work) to 4 effective features and ignores the irrelevant features that affect diagnostic accuracy. To evaluate the fault classification performance, the original data was divided into 5 data sets, representing three of the local bearing faults (normal, inner race, outer race, and ball) and the generalised fault (corrosion).

Then, to diagnose fault severity, inner and outer race data sets were divided into three data sets, representing bearing crack fault severities (1x0.2x3, 1x0.5x1x6 and 3x1x9mm); for corrosion faults the data set was divided into four data sets, representing bearing corrosion fault severities. The distribution of OFNDA features is illustrated in Figures (6.21 - 6.24), which used this fault classification.
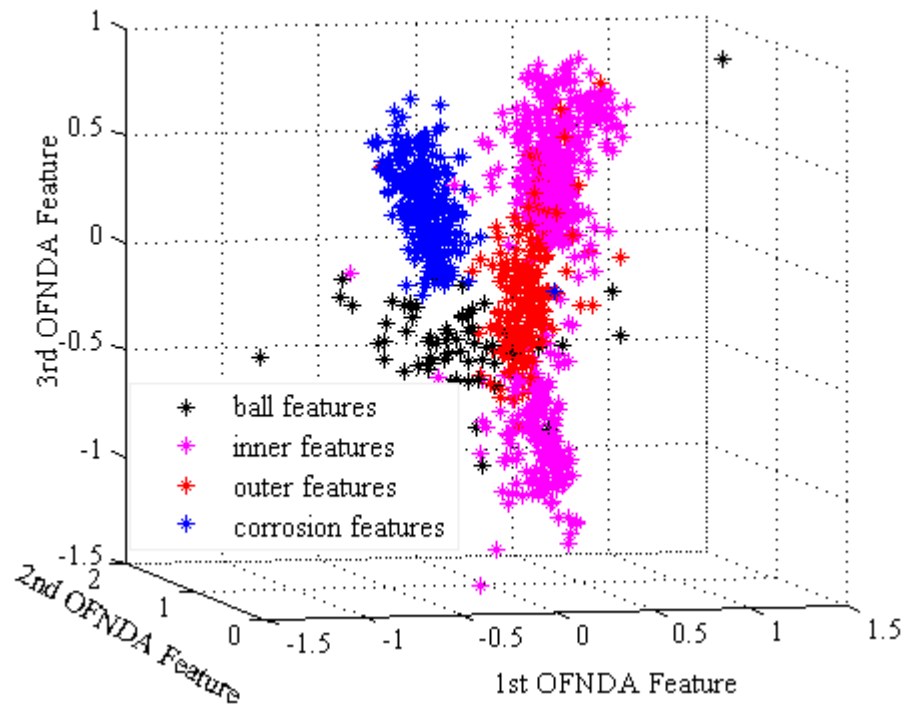
Figure 6.21 Bearing faults OFNDA features for fault classification
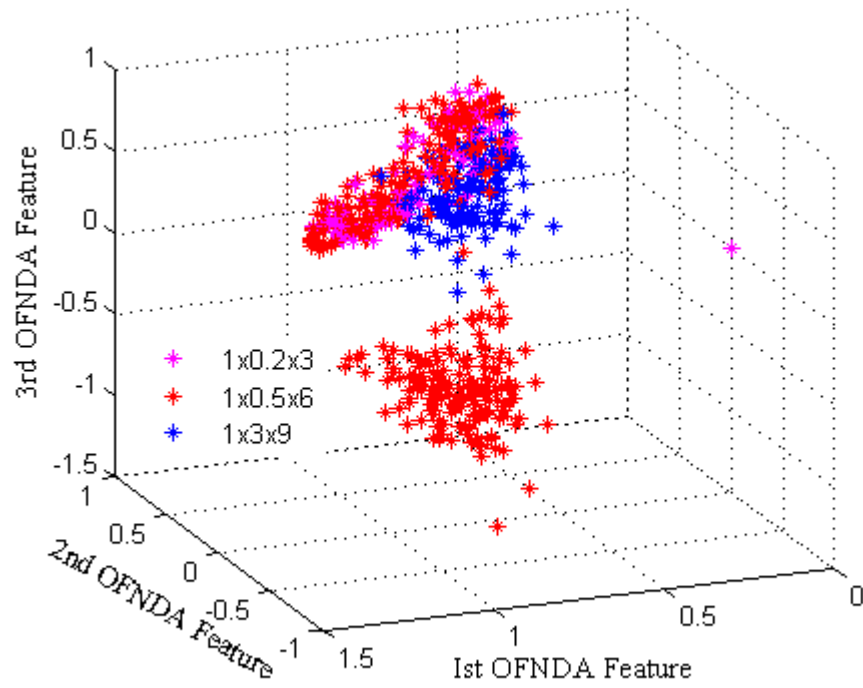
Figure 6.22 OFNDA features under inner fault severities at no load and 1200rpm speed
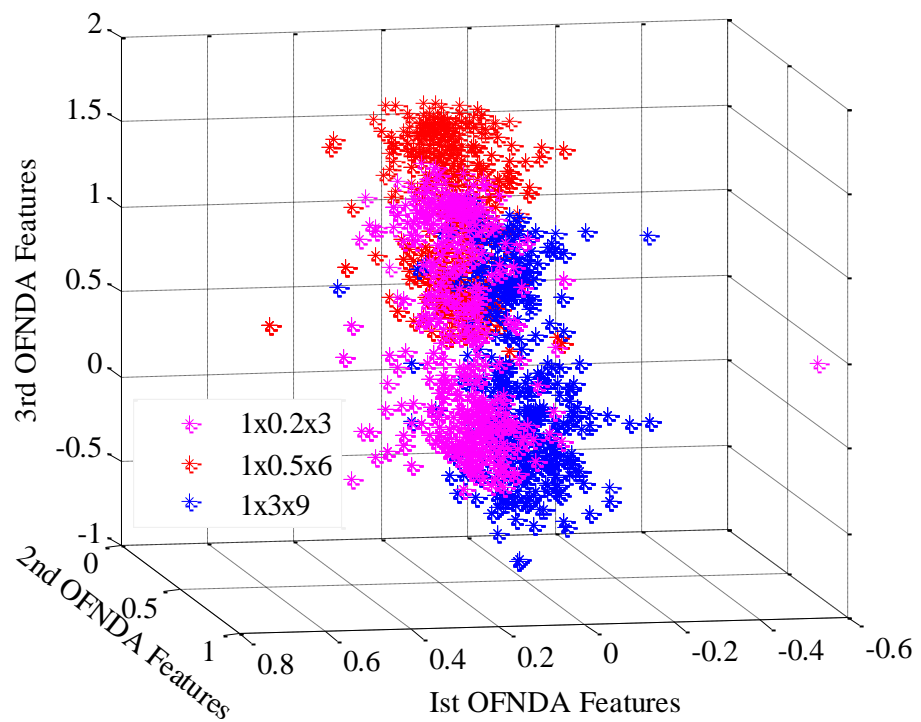
Figure 6.23 OFNDA features under different outer fault severities at no load and 1200rpm speed
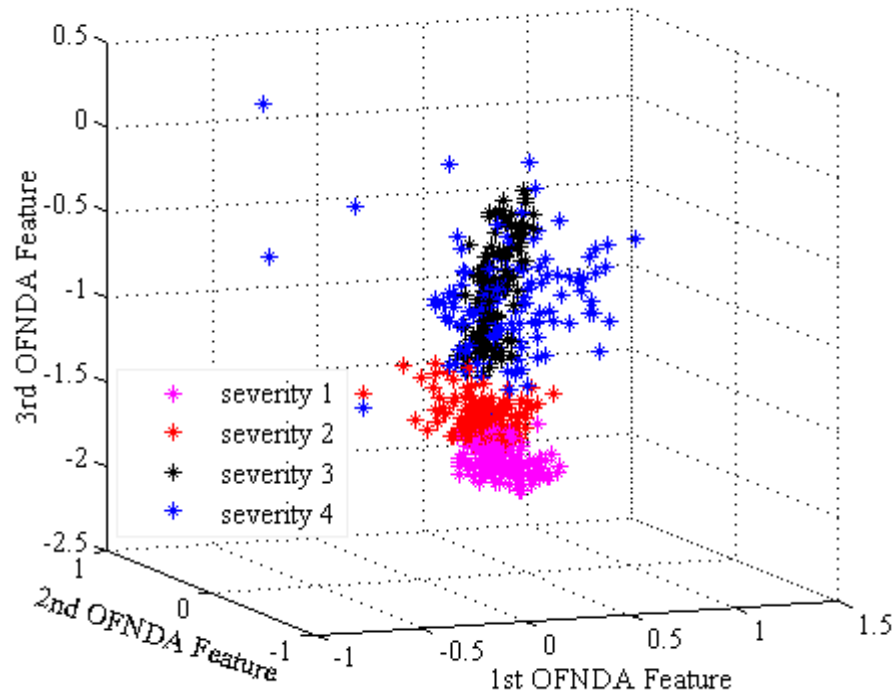
Figure 6.24 OFNDA features under corrosion fault severities at no load and 1200rpm
speed

6.7.2 Features dimensionality reduction for thruster motor faults

A mentioned in section 6.5, (18) feature were extracted using DWT. Then OFNDA was
applied to optimise features and remove irrelevant features that could affect fault
diagnosis performance. OFNDA decreases DWT features to 8 features, as shown in
Figure 6.26. This can be used for fault classification purposes, as will be explained in
the next chapter.
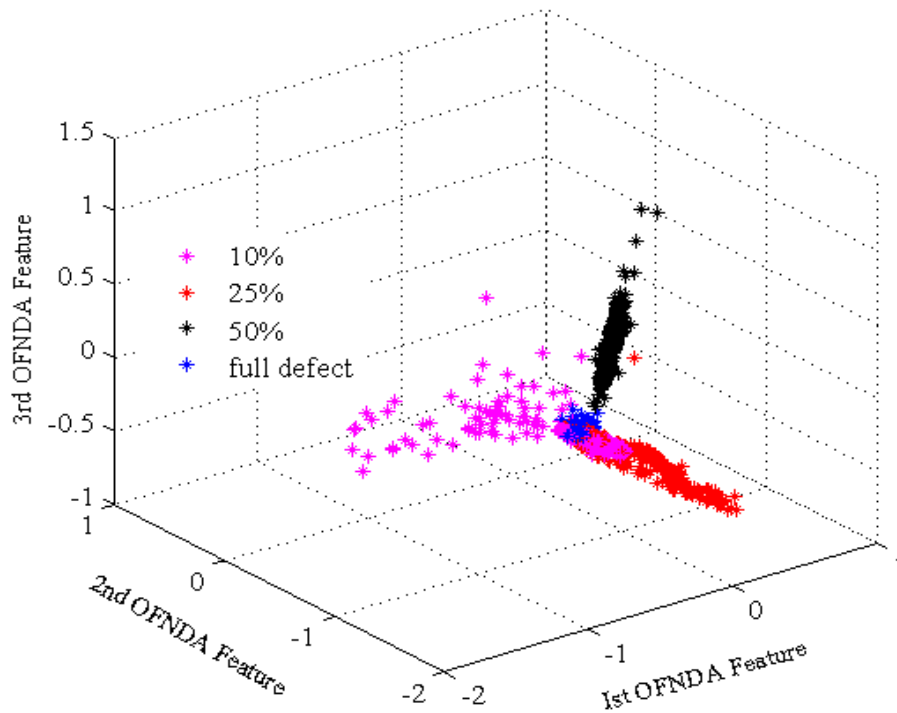
Figure 6.25 OFNDA features under different severities of blades fault

6.8 Chapter Summary

In this chapter, the DWT technique is applied to locate rolling bearing and thruster blade faults based on a permanent magnet dc motor. This technique is based on the analysis of raw vibration and current signals under stationary and non-stationary operating conditions. The approximation and details signals of the fault patterns of the machine are generated, which can be used to predict fault severity. Among different mother wavelet functions and level of decomposition levels, a wavelet filter needs to be optimised. MDL and STD were implemented and DSL was used to optimise the suitable of level of decomposition. DWT was used as an efficient feature extraction method. However, these features alone are not capable of a good fault classification performance. New feature reduction in terms of electrical machine fault diagnosis OFNDA was applied to obtain the best features for fault classification. In the next chapter, OFNDA features will be used for training and testing a dynamic neural network for fault classification.

CHAPTER 7

Fault Classification Based on Dynamic Neural Network

"This chapter introduces dynamic neural network as a method for fault classification and fault severity prediction, based on OFNDA features used for training, validation and testing."

7.1 Introduction

In Chapter 6, different techniques were applied and implemented to extract and optimised useful features from the raw vibration and current signals. In this chapter, NN can be used for fault isolation due to its stability and parallel processing. The solution time for calculating machine circuit parameters using NN models has been dramatically reduced, while sufficient accuracy has been maintained. Furthermore, NNs provide an excellent mathematical tool for dealing with non-linear problems. In addition, NN behaviour in fault diagnosis is directly related to the quality and the nature of NN inputs (fault indicators) and it can learn the motor-incipient fault detection process to give accurate solutions to a particular fault (Liying et al. 2013). However, the response of a static NN at any instant in time depends only on the value of the input sequence at that same time instant, so that DNN suggested in this work. DNNs have a wide range of applications, such as system identification and control, time series prediction and classification.

This chapter is organised as follows: section 7.2 presents the DNN structures for fault classification and fault severities prediction; Section 7.3 describes the proposed DNN structure, while in section 7.4, the performance of the proposed structure in diagnosing

155

localised and generalised rolling element bearing faults under stationary and non-stationary operating conditions will be discussed. To validate the prosed structure, the severity of thruster blade faults will be introduced in Section 7.5, and a summary of the chapter will be given in section 7.6.

7.2 Dynamic Neural Network Structure

Most industrial systems are dynamic and non-linear in nature, and hence during fault identification it seems desirable to employ those models which can represent the dynamics of the system, to increase operational reliability and to optimise preventative maintenance.

NNs can be categorised into dynamic and static, in static NNs the output is calculated directly from the input through feed-forward connections there and are no delays and feedback. Whereas in DNN, the output depends on the current and past inputs, outputs, or states of the network. Generally, DNN are more active than static NN, and studies have shown that their use can help to improve the fault prediction accuracy of electrical motor condition monitoring systems (Hyun et al. 2010).

Furthermore, DNNs have a great capability for learning the dynamics of complicated non-linear systems, where conventional static NN cannot yield and perform acceptable modelling representation and mapping (Howard et al. 2006). The DNN is initially trained on past demand data, with the network input vector being a moving window on the load time series. As time progresses, the NN weights are dynamically adapted. It is common that once the networks are proven on the test data, it is concluded that they will perform consistently well for the foreseen demand trends.

For providing a NN with dynamic behaviour, one of the existing methods is the insertion of a filter before or after the activation function, This method based on the

structure where all input signals flow in one direction, from input to output (Li et al. 2005) i.e. NNs that have only feed forward connections, as mentioned in Chapter 2 and Figure 2.3. The filter can be applied to the network inputs only, keeping the network internally static as in the filtered multilayer perceptron (MLP), or at the input of each neuron, as in the MLP with FIR filter synapses. The main disadvantage of this approach is the limited past-history horizon, which needs to be used in order to keep the size of the network computationally manageable (Yousif 2012).

The EN is another commonly used dynamic network category. It consists of a two-layer network with feedback from the first-layer output to the first-layer input. This recurrent connection allows the EN to both detect and generate time-varying patterns. An EN might use BP for training, but it tends to proceed too rapidly.

The most general example of the implementation of feedbacks in a NN is the fully recurrent NN (FRNN) (Liu 2002). This is constituted by a single layer of neurons fully interconnected with each other or by several such layers. However, this network requires a large structure, so that in recent years growing efforts have been propounded to develop methods for implementing temporal dynamic feedback connections into the widely used multi-layered FFNN.

Recurrent neural network (RNN) connections can be added by using two main types of recurrence or feedback: DNN classifiers for non-linear output classification without exogenous data, and a nonlinear autoregressive classifier with exogenous data (NARX)

The first type has a delay line appear at only the input layer of a static MLP network, and is also known as a time delay neural network (TDNN), as shown in Figure 7.1, where $x(t)$ and $y(t)$ are the input and output respectively. Furthermore TDNN does not need dynamic BP to compute the network gradient static MLP network, and there are no feedback adjustable parameters (Huo and Poo 2013).
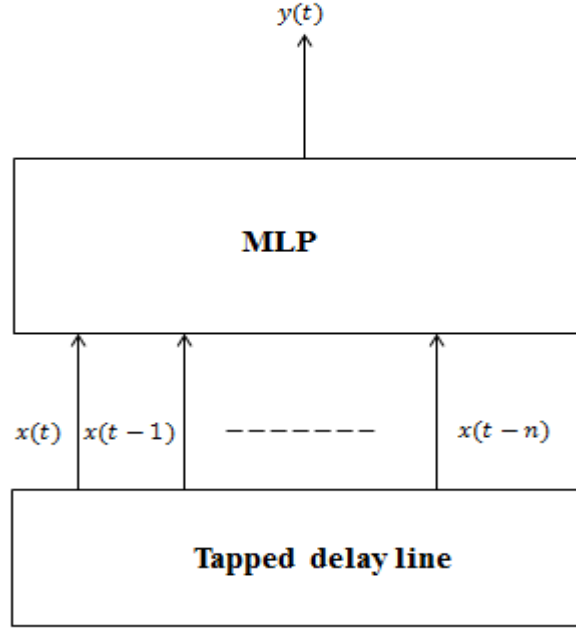
Figure 7.1 TDNN structure.

The second type, NARX has a similar architecture to feed forward MLP NNs, with a delay line on the input and the output being fed back to the input by another delay line (Chetouani 2013). NARX can be called (NARX – RNN) (Lin et al. 1996) or dynamic DRNN, based on the linear ARX model. NARX has a limited output feedback not from hidden neurons like other RNN networks, as shown in Figure.7.2. As part of the standard NARX architecture The output of the NARX is feed back to the input of the FFNN.

The network has tapped delay lines (d) to store previous values of the input, $u(t)$ and output, $y(t)$ sequences; the tapped delay line on the input has a maximum delay of 1. The defining equation for the NARX model is:

$$y(+1) = f(y(k) \dots \dots y(k - q + 1), u(k), \dots \dots u(k - q + 1)) \tag{7.1}$$

where f is the nonlinear approximation function, the next value of the dependent $y(t)$ output signal is regressed on the basis of an independent exogenous signal

$(u_{t-1} \dots u_{t-n})$. The next value of the dependent output signal $y(t)$ is regressed on previous values of the output signal and an independent (exogenous) input signal. NARX response at any given time depends not only on the current input, but on the history of the input sequence. If the network does not have any feedback connections, then only a finite amount of history will affect the response.
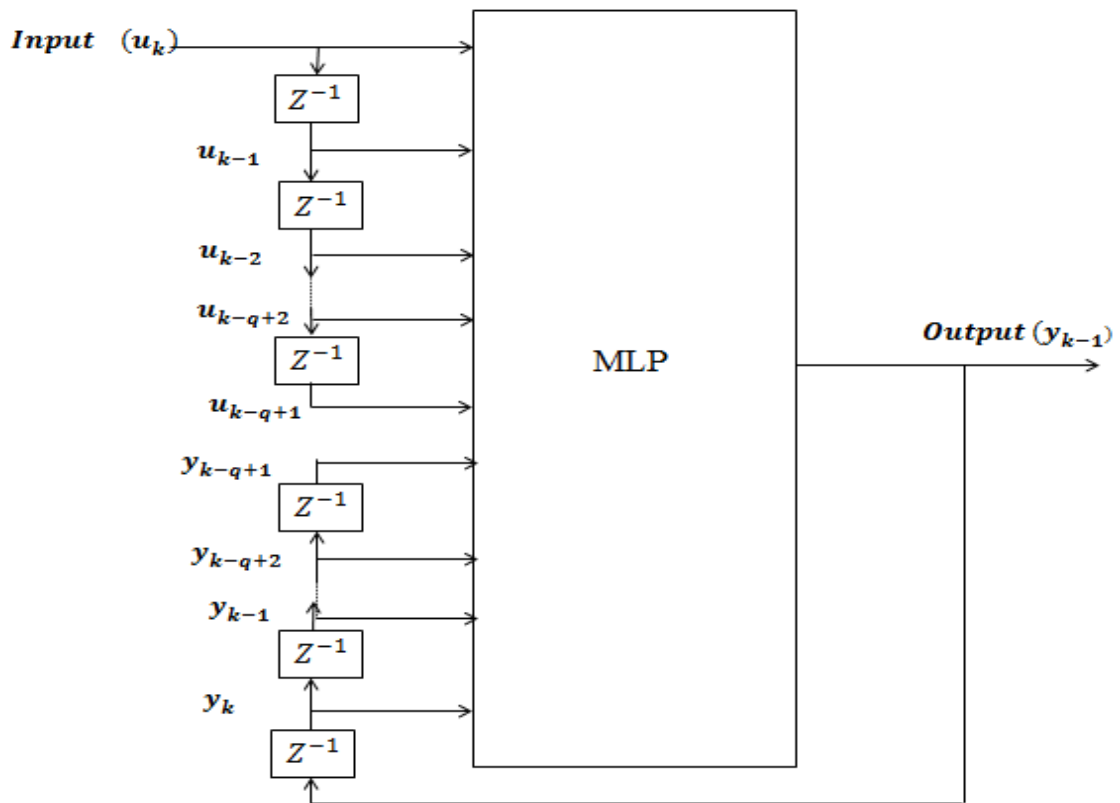
Figure 7.2 A DRNN with exogenous data.

Furthermore, NARX is commonly used in time series modelling, they have several advantages in practice. It has been reported that gradient-descent learning can be more effective in NARX networks than in other RNN architectures. In addition, the architecture of NARX will reduce the computational cost; this network will be discussed in detail in the next section.

7.3 The Proposed DRNN for PMDC Motor Fault Diagnosis

Diagnosis is the task of estimating a system's operating conditions to demine an accurate prediction technique, to predict behaviour that provides information about the remaining useful life of the components (Mohammadi et al. 2011).

In this study, NARX was trained to detect and classify PMDC motor faults during stationary and non-stationary operating conditions. NARX are a special type of DRNN with a large number of network layers connected via feedback connections, supported by an external exogenous input to improve calibration. In this work, five time-delayed selected from the input and output were feedback as inputs to the network and are often used as shown in Figure 7.3.
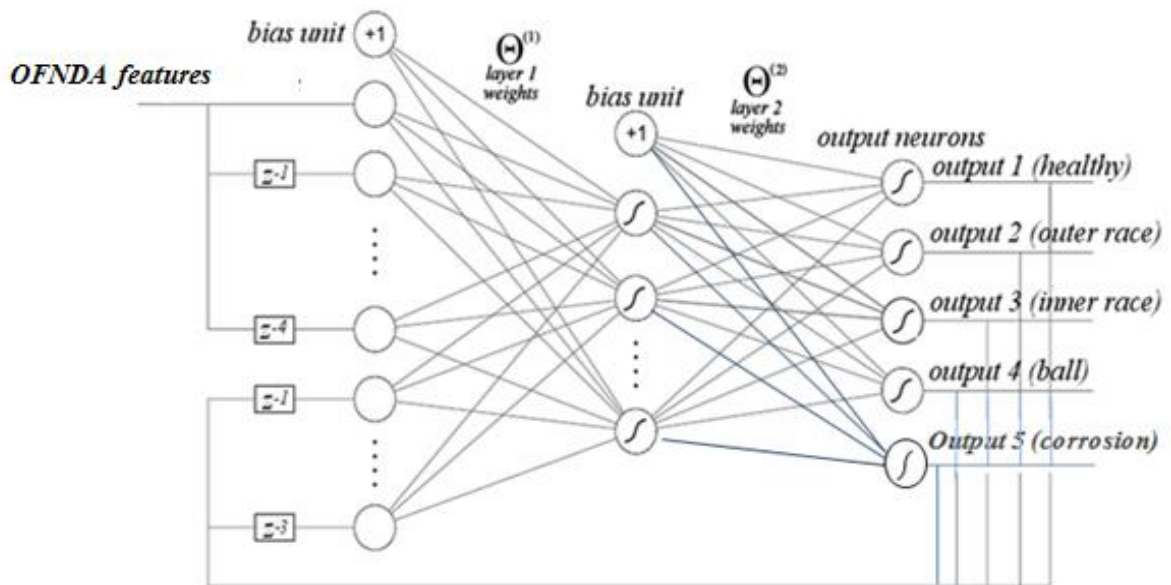
Figure 7.3 DRNN used for fault diagnosis

.

After the dimensionality reduction stage the wavelet features were reduced from 12 to 4 features that represent network inputs. The input pattern of the network (input layer) at each time k consists of the four input features (present and delayed values), as well as the output feedback, and is formed as:

$$x(k) = \begin{bmatrix} x_1^{OFNDA}(k) \\ \vdots \\ x_1^{OFNDA}(k - n_{di_1}) \\ \vdots \\ x_3^{OFNDA}(k) \\ \vdots \\ x_4^{OFNDA}(k - n_{di_2}) \\ \hat{y}_1(k - 1) \\ \vdots \\ \hat{y}_1(k - n_{do_1}) \\ \vdots \\ \hat{y}_4(k - 1) \\ \vdots \\ \hat{y}_5(k - n_{do_5}) \end{bmatrix}$$

(7.2)

where n_{di_j} and n_{do_j} are the number of delays of input feature j and output j respectively.
In this case, four input delays and three output delays were used for all input and output
features respectively. The network used is a logistic classifier that incorporates sigmoid
activations in all the hidden and output units. For each input pattern $x(k)$, the output of
each node is calculated by forward propagation according to

$$a^{(1)}(k) = \begin{bmatrix} 1 \\ x(k) \end{bmatrix};$$

(7.3)

$$a^{(2)}(k) = \begin{bmatrix} 1 \\ s(\Theta^{(1)} a^{(1)}(k)) \end{bmatrix};$$

(7.4)

$$\hat{y}(k) = a^{(3)}(k) = s(\Theta^{(2)} a^{(2)}(k)$$

(7.5)

where $a_i^{(l)}$ denotes the activation or output of the ith node of layer l, $\hat{y}$ is the output
vector of the network, $\Theta^{(1)}$ and $\Theta^{(2)}$ are the matrices of parameters of the network such
that $\Theta_{ij}^{(l)}$ represents the strength of the connection between the jth of layer l and node i^{th}
node of layer $(l+1)$, and $s(x)$ is the logistic function as shown in Figure 7.4, below.

$$s(x) = \frac{1}{1 + e^{-x}}$$

(7.6)
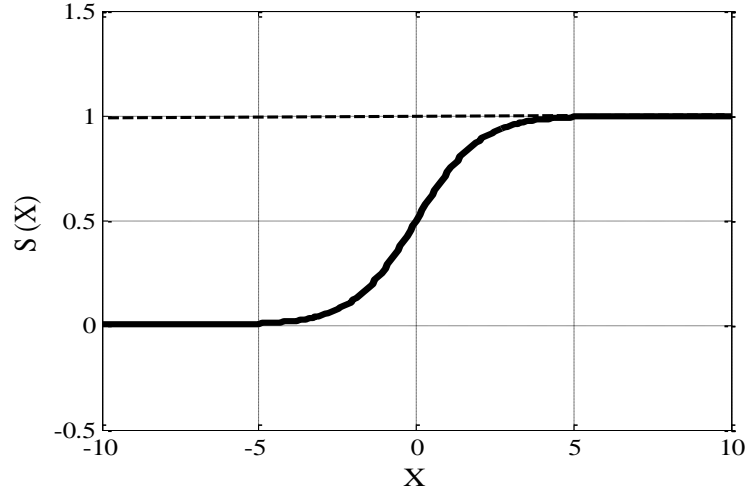
Figure 7.4 Sigmoid logistic function

For each input pattern, the network outputs four values:

$(\hat{\mathbf{y}}(k) = [\hat{\mathbf{y}}_1(k), \hat{\mathbf{y}}_2(k), \hat{\mathbf{y}}_3(k), \hat{\mathbf{y}}_4(k)]^T)$ between 0 and 1; these output values are

rounded to 0 or 1 to indicate a certain fault condition. Training consists of minimising

the cost function with regularization is given by Andrew (2014):

$$J(\theta) = \frac{1}{m} \sum_{i=1}^{m} \sum_{k=1}^{k} \left[-y_k \log\big((h\theta(x))\big) - (1 - y_k) \log\big((h\theta(x))\big) \right] + \frac{\gamma}{2m} \left[\sum_{i=1} \sum_{k=1} (\theta^2) \right]$$

(7.7)

γ is the regularization factor, with respect to the network parameters $\mathbf{\Theta}^{(1)}$ and $\mathbf{\Theta}^{(2)}$, where

m is the number of training samples, and $\mathbf{y}_t$ is the adequate target output for each one.

This process was carried out recursively using the Gradient Descent (GD) method

according to:

$$\mathbf{\Theta}_{ij}^{(l)} := \mathbf{\Theta}_{ij}^{(l)} - \alpha \Delta_{ij}^{(l)} \quad \text{For all } \mathbf{\Theta}_{ij}^{(l)}$$
(7.8)

Until convergence is reached, where $\Delta_{ij}^{(l)} = \frac{\partial J}{\partial \mathbf{\Theta}_{ij}^{(l)}}$ and α is the learning rate, in which the

initial network parameters were chosen randomly. In order to calculate the gradient

components $\Delta_{ij}^{(l)}$, BP method was used.

162

BP is an algorithm that uses the delta rule to compute the weights between connected processing elements, so that the difference between the actual and the desired output is minimised. The basic algorithm for back-propagation is presented by McClelland et al. (1986).

BP method:

For each training pattern $x(k)$,

1. Obtain $a^{(1)}(k), a^{(2)}(k)$, and $\hat{y}(k) = a^{(3)}(k)$ according to $\qquad$ (7-9)

2. $\delta^{(3)}(k) = y_t(k) - \hat{y}(k)$ $\qquad$ (7.10)

3. $\delta_i^{(2)}(k) = a_i^{(2)}(k)\left(1 - a_i^{(2)}(k)\right)\sum_{n=1}^{4}\Theta_{ni}^{(2)}\delta_n^{(3)}(k)$; $\qquad$ (7.11)

   $i = 1, \dots, n_h,$

   $$\Delta_{ij}^{(2)} = -\frac{1}{m}\sum_{k=1}^{m}\delta_i^{(3)}(k)a_j^{(2)}(k); \qquad (7.12)$$

   $i = 1, \dots, 4; \ j = 0, \dots, n_h$

   $$\Delta_{ij}^{(1)} = -\frac{1}{m}\sum_{k=1}^{m}\delta_i^{(2)}(k)a_j^{(1)}(k); \qquad (7.13)$$

   $i = 1, \dots, n_h; \ j = 0, \dots, n_i$

where n_h is the number of hidden units (not counting the bias unit) and n_i the number of input units (not counting the bias unit). The GD process was applied in two stages. During the first set of iterations, the (delayed) target values y_t were used to construct $x(k)$ for computation of $\hat{y}$ in the first step of the BP process, effectively training a network without feedback. During a second stage, (past) predictions of the network $\hat{y}$ were used to construct $x(k)$ in accordance with the true feedback architecture of the network.

The network is trained by an initially random weight, learning rate, and the regularisation parameter, and then presenting all training data repeatedly. The weights

are adjusted after each iteration until the weight convergence or the error is reduced to the desired value. Although the gradients computed with the BP algorithm in this case are approximations to the true gradient, the errors are small, as after the first set of iterations the network is sufficiently trained to output predictions close to the target values.

7.4 DRNN for Bearing Fault Analysis under Stationary and Non-stationary Operating Conditions

In order to reliably diagnose faults in a bearing, it is critical to select the number of feature (s) that can quantitatively describe the condition of the bearing vibrations and stator current, and use these features as inputs to the diagnosing NN. The number of features to be used as the input to the NN also affects the final performance: too many input features will result in high computational load and slow response, whereas too few features may not provide an accurate representation of the defect.
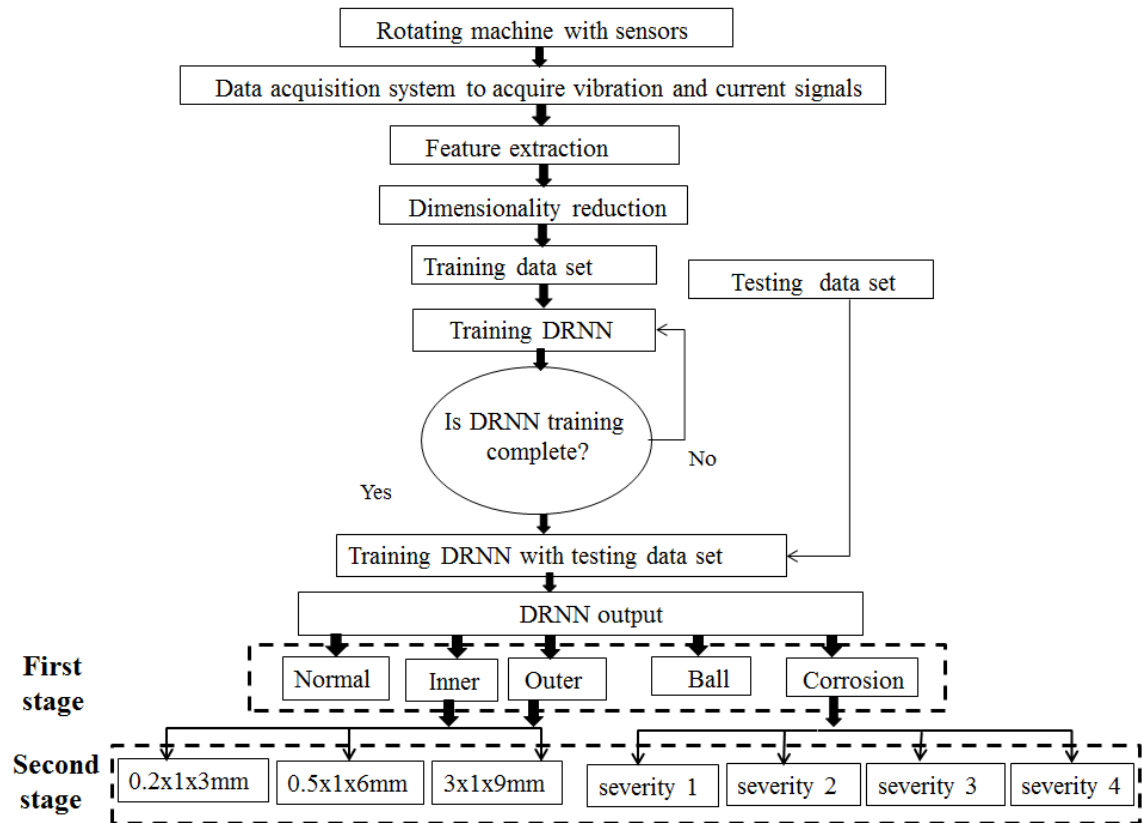
Figure 7.5 The process of DRNN performance for bearing fault diagnosing

Input consists of the OFNDA features, x_1^{OFNDA}, x_2^{OFNDA}, and x_3^{OFNDA} ....x_n^{OFNDA} and the output of the network consists of four units, used to indicate a particular bearing fault condition. 60% of the OFNDA was used as a training data asset and 20 % for testing and validation respectively. The proposed training DRNN methodology, as illustrated in Figure 7.5, contains training with both training and testing data sets, then in the first stage classifying bearing faults and in the second determining the level of fault.

7.4.1 Bearing fault classification

A total of fifteen tests with a length of 60 seconds each represent the motor under stationary and non-stationary conditions, with normal operation and three severities of local bearing faults (ball, inner race and outer race defects) and four severities of extended bearing fault (corrosion). This section will focus on the first stage mentioned in Figure 7.5 (bearing fault classification). So that a healthy condition should output a 1, an outer-race fault a 2, an inner-race fault a 3, a crushed ball fault a 4 and corrosion defects a 5, these outputs are compared with the correct output for each dataset, as shown in Table 7.1. It should be noted that misclassification only occurs when the rounded value does not coincide with the correct value.

Table 7.1 DRNN output signification

Output 1	Output 2	Output 3	Output 4	Output 5	Indication
1	0	0	0	0	healthy
0	1	0	0	0	inner-race fault
0	0	1	0	0	outer-race fault
0	0	0	1	0	crushed-ball
0	0	0	0	1	Corrosion fault

'Ninety-nine data sets' of raw vibration and stator current were recorded under stationary operating conditions for each of the three localised bearing defects (inner,

outer and ball) and the generalised bearing fault (corrosion), as well as normal condition being measured for comparison with fault cases. The data was collected at three different speeds (600, 900 and 1200) rpm and under no load, half load and full-rated load. Under the same operating conditions, 66 datasets were collected under variable speed and load conditions. After features extraction and the removal irrelevant of irrelevant features, the useful features will used to training, testing and validation of the DRNN. The learning algorithms of NN can be classified as:

➢ Supervised learning: both of input and output are provided during the learning process. The error can be calculated by comparing the actual output with the desired output. Weights are usually randomly adjusted and the overall objective is to minimise the error by modifying the connection weights until an acceptable level of accuracy is obtained.

➢ Unsupervised learning: the output is not provided to the network and the network learns by itself, by adapting to the structural features in input patterns.

In this work, supervised learning algorithms were implemented and the training was carried out for 4000 iterations. The initial random weights = 0.05, learning rate for gradient descent (α) = 0.03, regularisation parameter for the cost function λ = 0.05, feedback ratio (FR) = 0.7 with 6 input and output delays. A hidden layer with a different number of neurons has been tested to achieve the best training performance with a minimum number of neurons, for faster computation. The hidden layer size = 15, these parameters were selected based on network performance process.

The comparison accuracy of the classification tests are illustrated in Table 7.2 for bearings operating under stationary conditions while, Table 7.3 summarises the DRNN performance under non-stationary operating conditions.

Table 7.2 DRNN fault classification performance under stationary operating conditions

Operating conditions Load- speed	Defect Identified rate (%)							
	Training data set				Testing data set			
	1	2	3	4	1	2	3	4
No load and 1200 rpm	98.3	98.0	97.0	98.9	95.1	95.1	92.3	92.7
900 rpm	98.8	96.4	99.0	98.8	94.4	97.5	97.5	96.3
600 rpm	99.7	99.7	90.0	92.0	98.6	96.8	91.3	91.4
Half load and 1200 rpm	96.3	98.1	98.6	98.6	95.8	96.5	95.8	90.2
900 rpm	90.2	95.4	94.0	90.0	96.5	98.0	98.5	98.3
600 rpm	99.3	99.3	81.5	99.4	95.1	95.8	91.3	94.4
Full load and 1200 rpm	99.3	99.0	99.6	99.4	93.0	97.2	98.9	93.3
900 rpm	99.3	97.1	99.1	93.8	98.2	95.3	86.8	98.6
600 rpm	95.9	97.4	85.0	93.1	90.0	87.0	96.9	90.6

Finally, training applies the inputs to the network, calculates the outputs, compares them to the associated targets, and calculates a mean square error. If the error goal is met, or if the maximum number of epochs is reached, the training is stopped; otherwise training goes through another epoch. The DRNN is trained using OFNDA dataset (868,292,288) for training, testing set and validation respectively, to assesses DRNN performance for inner and outer bearing faults classification, while for corrosion bearing faults, training, validation and testing for (1085, 360 and 365) were used respectively.

Table 7.3 DRNN performance for rolling element bearing fault classification under non-stationary operating conditions

Operating conditions Load- speed	Defect Identified rate (%)							
	Training data set				Testing data asset			
	1	2	3	4	1	2	3	4
Variable load and 1200 rpm	97.4	98.5	98.8	99.5	97.9	92.0	90.2	98.6
900 rpm	97.2	98.1	98.5	99.2	97.2	90.2	90.0	98.0
600 rpm	98.3	99.8	99.2	99.0	94.3	96.3	95.3	93.3
Variable Speed and Full load	90.0	90.8	99.9	90.9	87.0	99.7	99.3	91.5
No load	97.6	98.9	96.6	99.2	93.7	95.4	90.9	95.5

Figures (7.6 - 7.8) show the performance of DRNN to isolate rolling element bearing faults under stationary condition at no-load and 1200 rotating speed, under variable load with 1200 rpm speed, and under variable speed with no-load condition
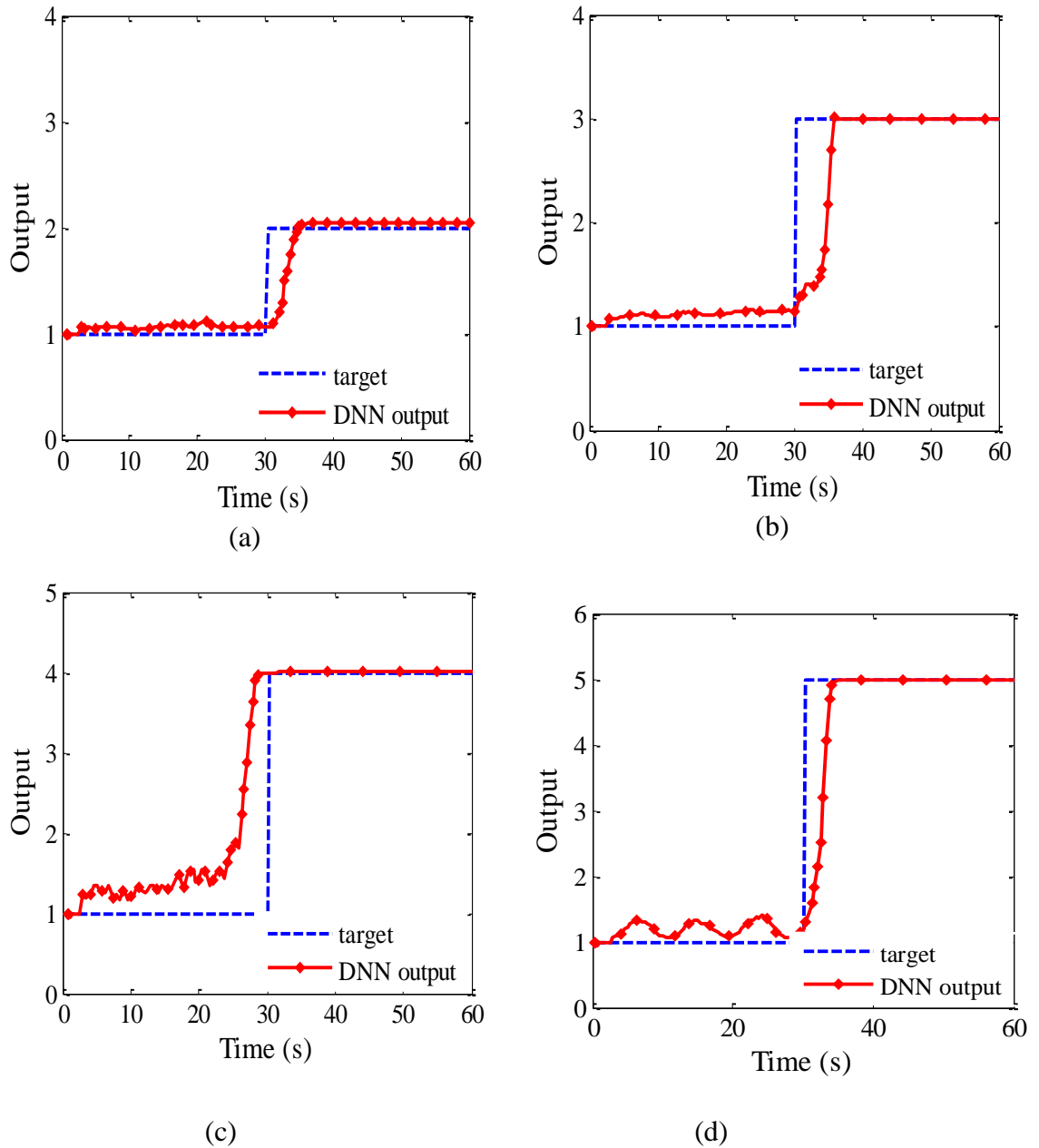
Figure 7.6 Bearing fault classifications for motor operating at no load and speed 1200 rpm (a) ball, (b) inner, (c) outer and (d) corrosion
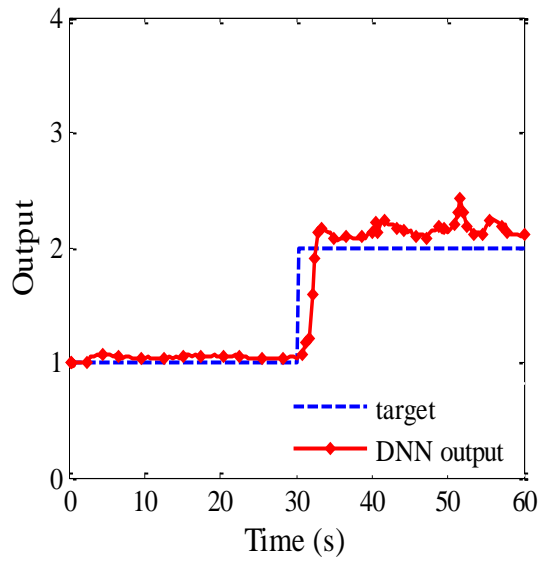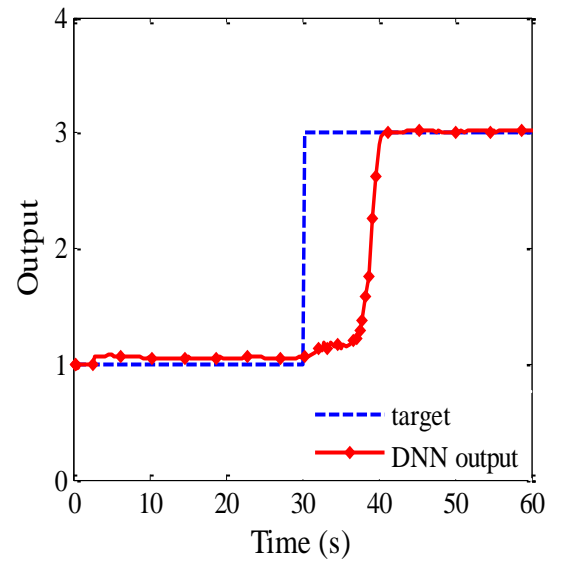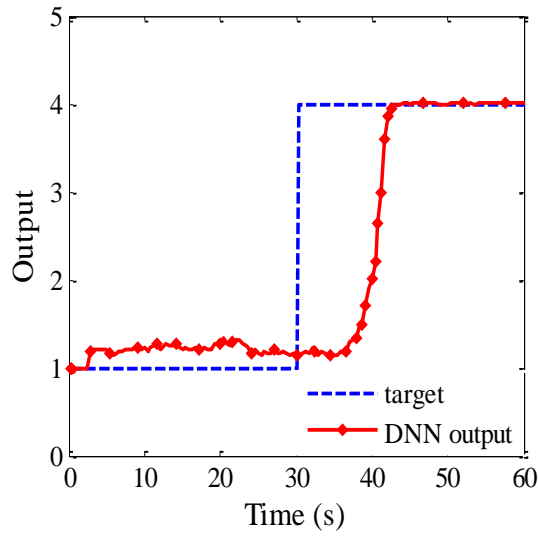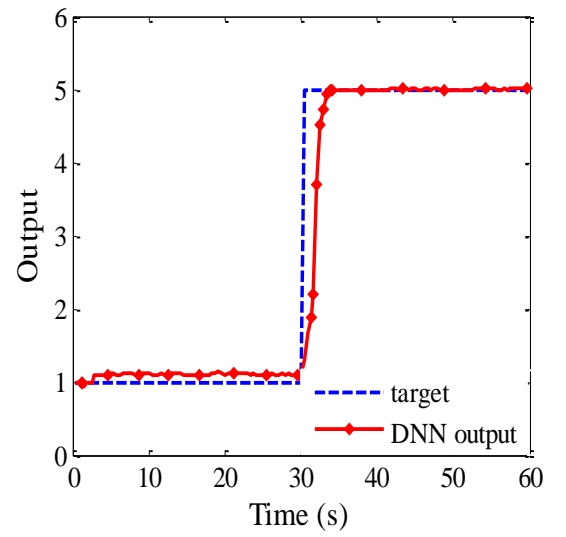
Figure 7.7 Bearing fault classification for motor operating at variable load and speed 1200 rpm (a) ball, (b) inner, (c) outer and (d) corrosion
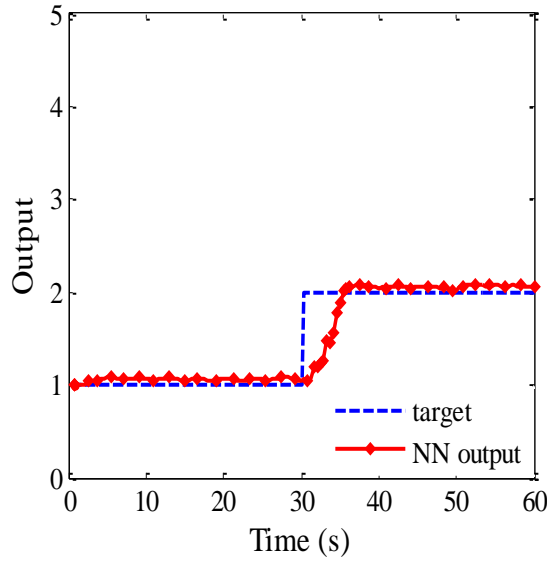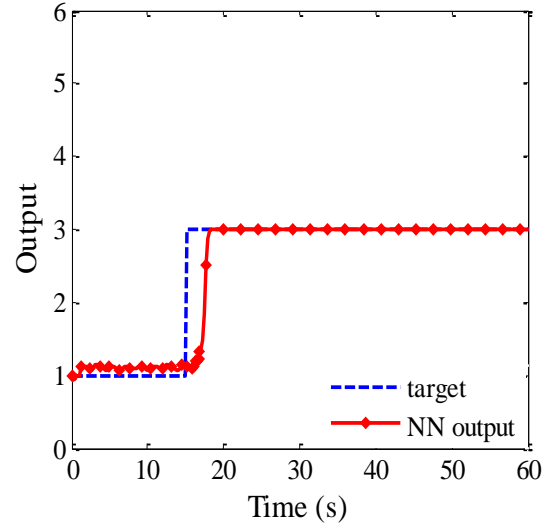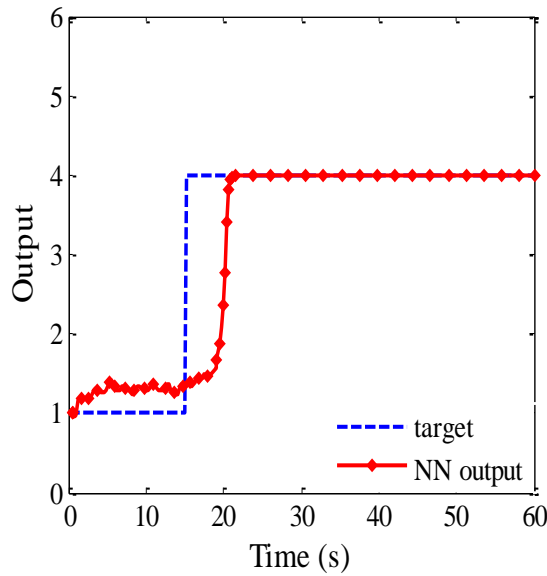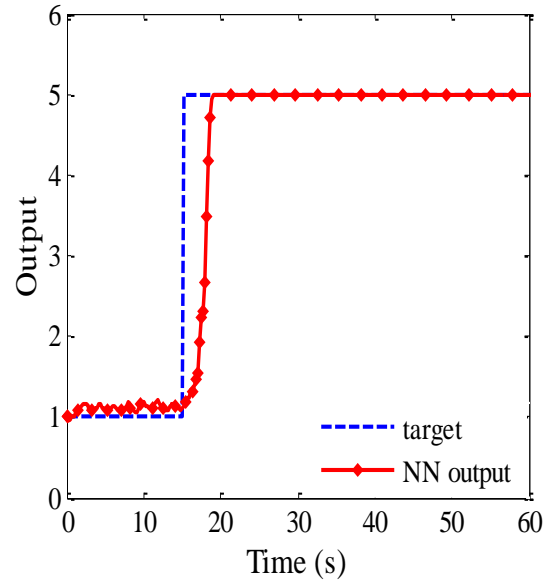
Figure 7.8 Bearing fault classification for motor operating at variable speed and no load conditions (a) ball, (b) inner, (c) outer and (d) corrosion

7.4.2 Bearing fault severity prediction

In the second stage of the proposed fault diagnosis approach (see Figure 7.5) fault severity prediction is included. 60% of OFNDA features were reserved for the trained DRNN and 20% for both testing and validation.
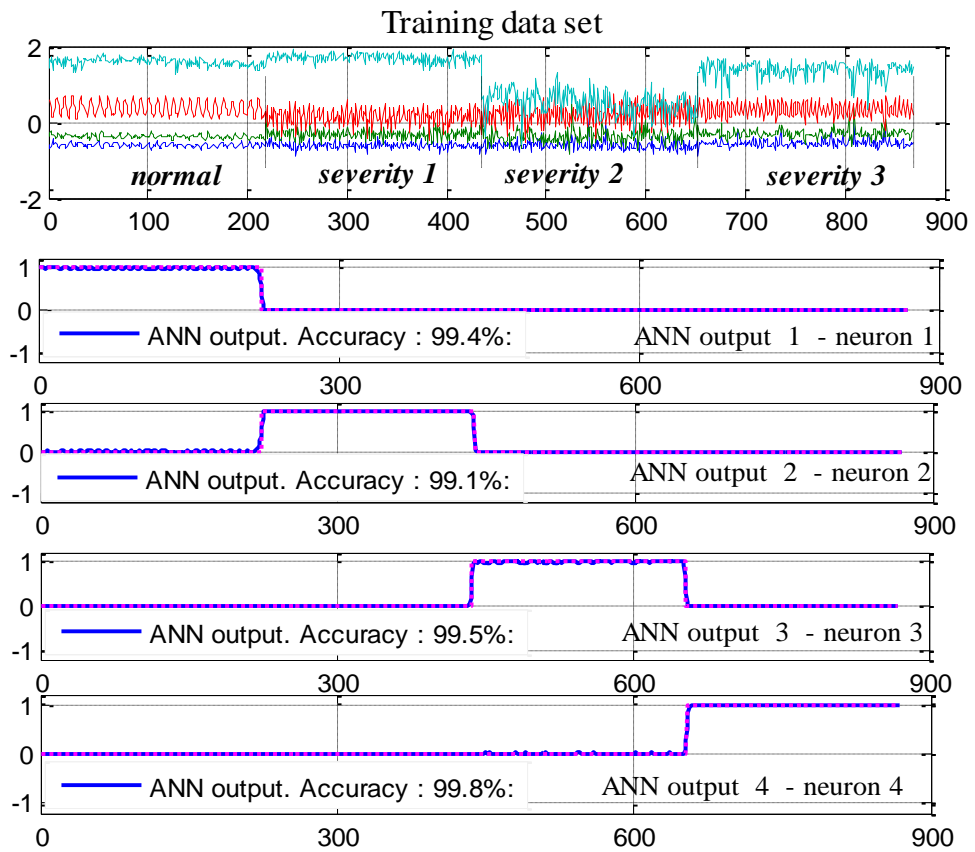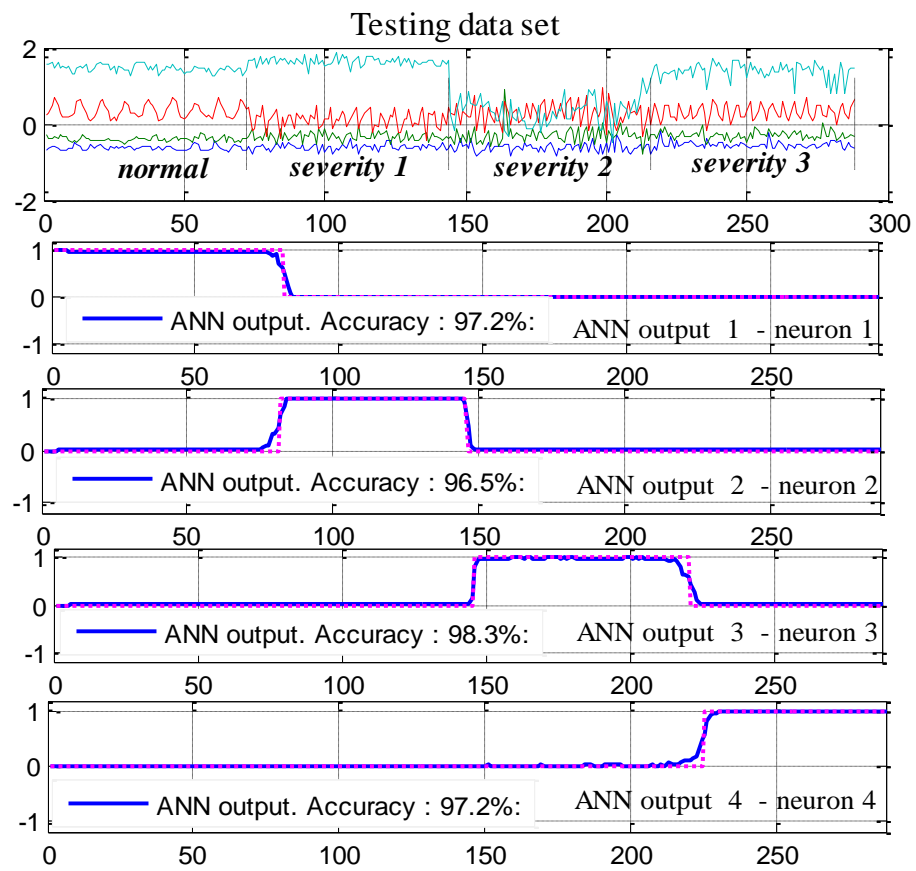
Figure 7.9 OFNDA features for inner race defect at full load and 1200 rpm speed
(a) training data set (b) testing data set

432 and 144 OFNDA data sets were used for training and testing. Figure 7.9 shows inner race defects at full load and 1200 rpm rotation speed. The overall performance of DRNN for bearing fault prediction at half load, full load and no-load conditions, and 1200 rpm rotation speed, is illustrated in Figures (7.10 - 7.12) respectively.

(a)

(b)

(c)
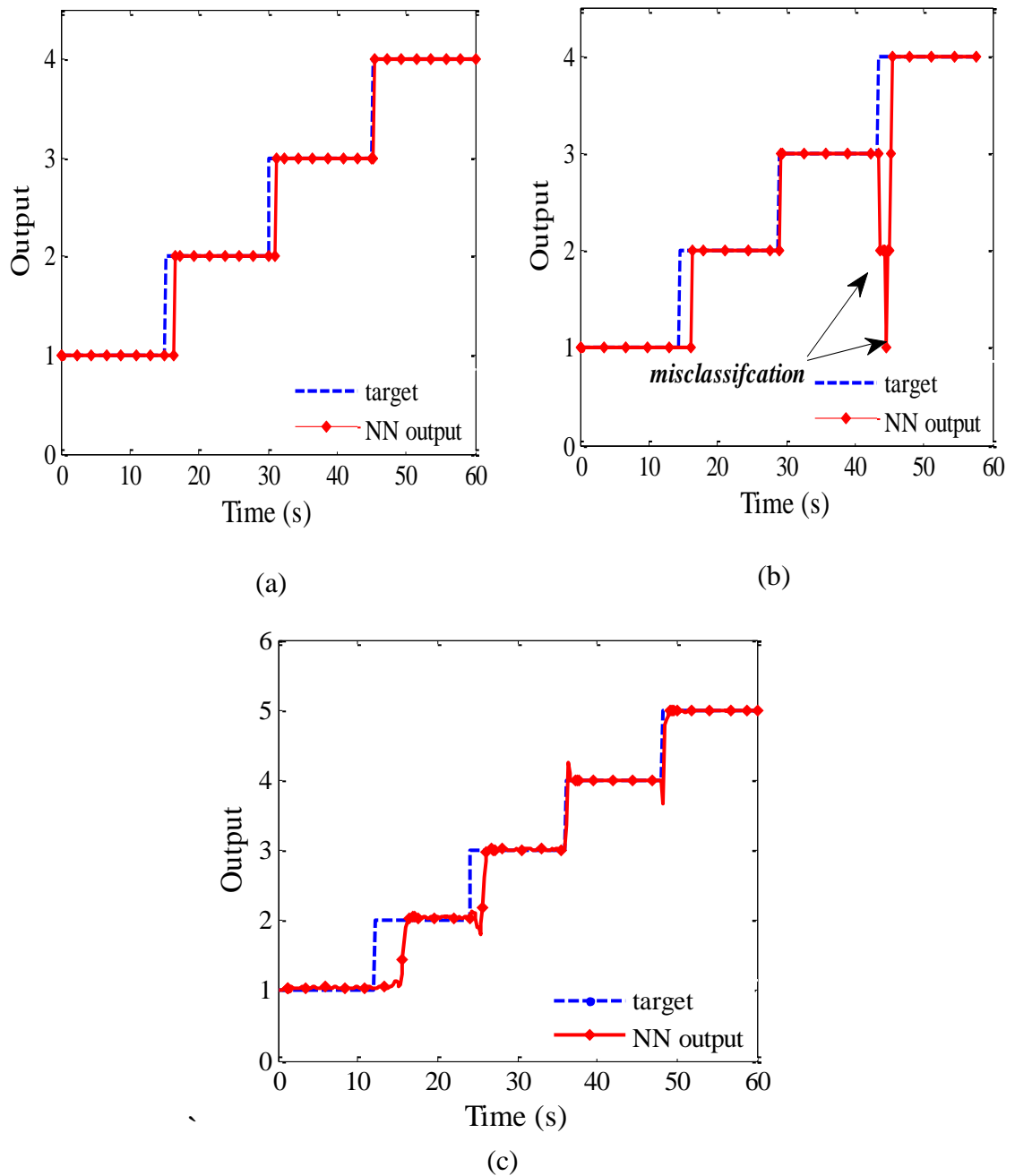
Figure 7.10 DRNN performance to predict bearing fault severity (a) outer, (b) inner and (c) corrosion under full load and 1200 rpm rotation speed
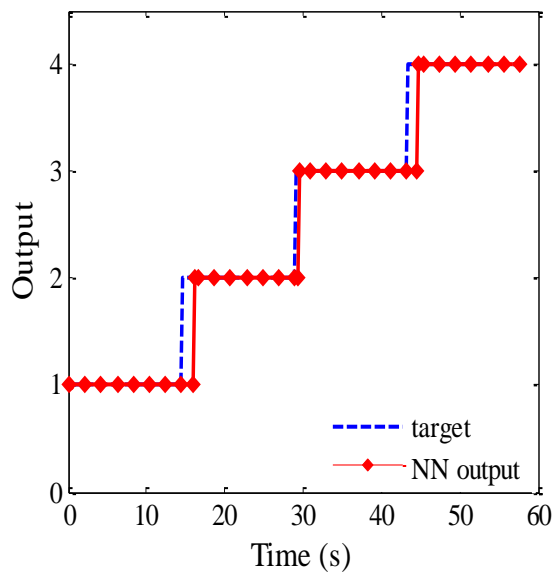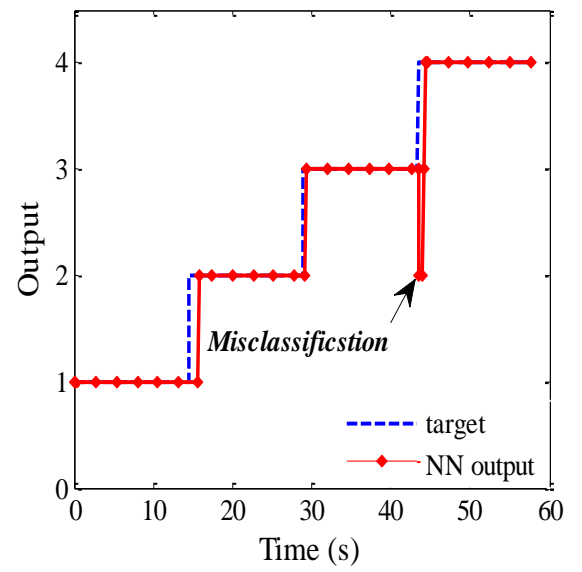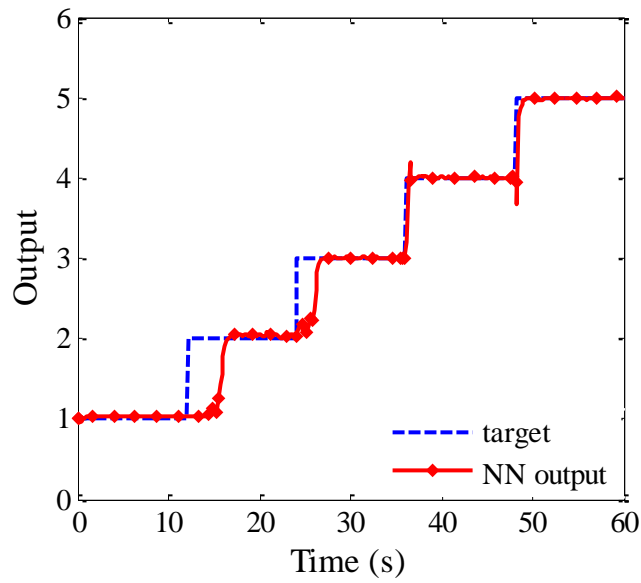
Figure 7.11 DRNN performance to predict bearing fault severity (a) inner, (b) outer and (c) corrosion under half rated load and 1200 rpm rotation speed
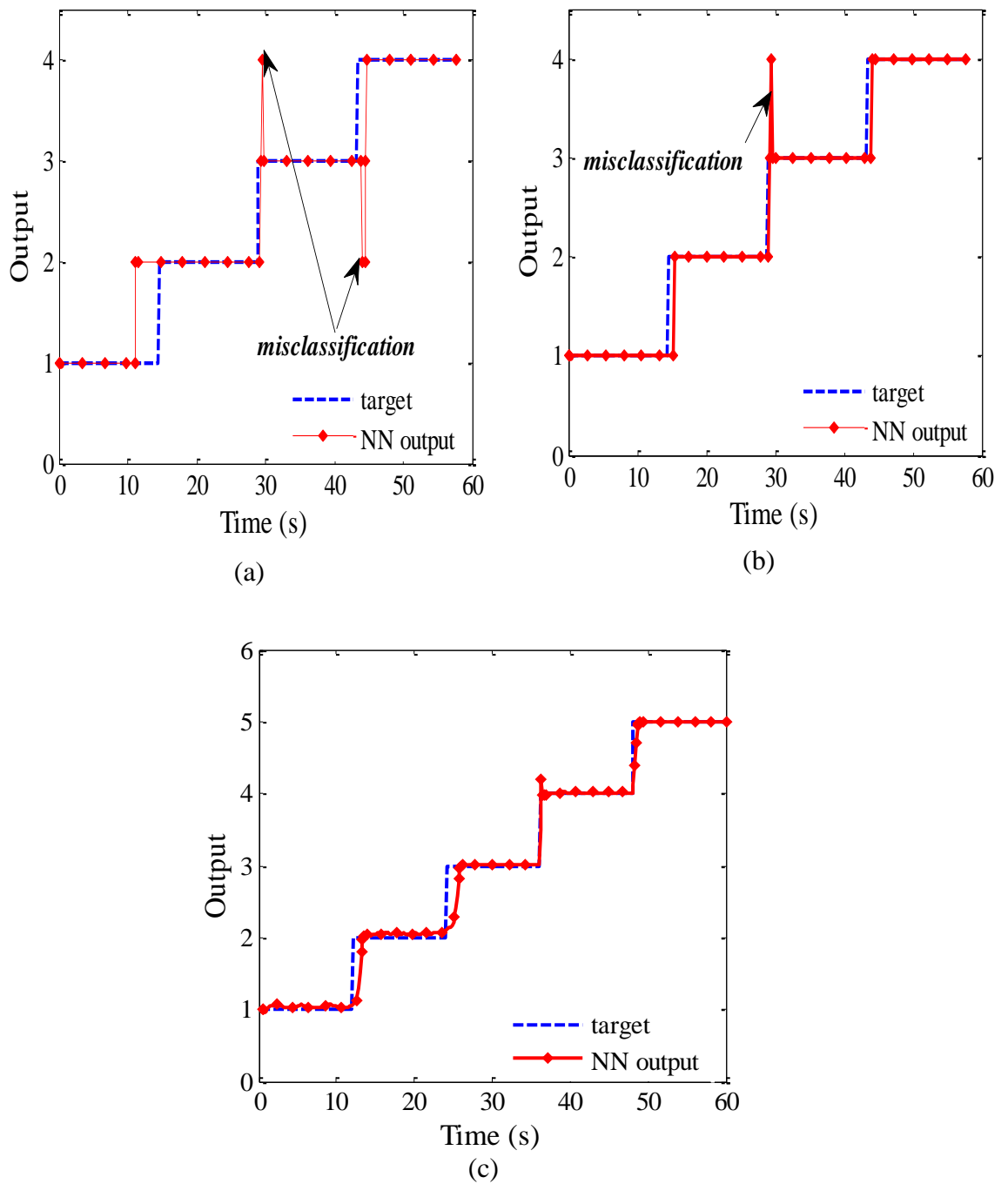
Figure 7.12 DRNN performance to predict bearing fault severity (a) outer, (b) inner and (c) corrosion under no load and 1200 rpm rotation speed

Table 7.4 is provides comparison of fault severities prediction accuracy for inner race,

outer brace and corrosion defect under different operating conditions.

Table 7.4 Fault severity accuracy prediction under stationary operating conditions

(a) Inner race defects

Operating conditions Load- speed	Inner race defect Identified rate (%)							
	Training accuracy for each DRNN output				Testing accuracy for each DRNN output			
No load and	**1**	**2**	**3**	**4**	**1**	**2**	**3**	**4**
1200 rpm	99.8	99.5	99.8	99.9	98.6	97.6	99.3	99.3
900 rpm	99.3	98.3	99.3	99.4	96.2	93.4	97.9	98.6
600 rpm	99.8	99.4	99.5	99.9	98.6	96.9	98.3	99.0
Half load and 1200rpm	99.8	99.4	99.7	99.8	98.6	97.2	98.6	98.6
900rpm	99.8	99.8	99.8	99.7	95.1	91.0	97.2	99.3
600rpm	98.5	97.9	99.4	99.7	93.8	92.5	97.9	97.9
Full load and 1200rpm	99.4	99.1	99.5	99.8	97.2	96.5	98.3	97.2
900rpm	99.9	99.7	100	99.9	98.3	97.9	96.9	99.3
600rpm	99.8	98.6	98.5	99.4	90.3	90.0	99.3	99.3

(b) Outer race defects

Operating conditions Load- speed	Outer race defect Identified rate (%)							
	Training accuracy for each DRNN output				Testing accuracy for each DRNN output			
No load and	**1**	**2**	**3**	**4**	**1**	**2**	**3**	**4**
1200 rpm	98.8	98.3	99.3	99.1	93.1	92.0	97.6	98.3
900 rpm	99.7	98.8	99.2	99.7	95.8	93.8	97.2	97.9
600 rpm	93.4	85.0	91.7	99.8	91.3	87.8	92.0	93.8
Half load and 1200rpm	99.7	98.5	99.0	99.5	98.3	95.1	96.9	97.9
900rpm	97.9	96.1	97.1	98.6	95.8	90.3	94.1	98.3
600rpm	98.8	97.9	99.1	99.3	96.2	94.9	98.6	98.6
Full load and 1200rpm	99.4	99.1	99.4	99.8	97.9	95.5	97.6	99.7
900rpm	97.9	96.3	97.1	98.6	95.8	91.0	94.1	98.3
600rpm	98.8	97.8	99.0	99.3	96.6	95.5	97.9	98.6

(c) Corrosion defects

Operating conditions Load- speed	Corrosion race defect Identified rate (%)									
No load	Training accuracy for each DRNN output					Testing accuracy for each DRNN output				
	1	2	3	4	5	1	2	3	4	5
and 1200 rpm	99.5	98.6	98.9	99.6	99.8	98.9	96.4	97.5	99.4	99.7
900 rpm	99.4	99.0	99.5	100	99.9	97.8	96.1	98.1	100	99.7
600 rpm	92.7	92.7	99.7	99.7	99.9	93.1	91.1	96.7	97.8	99.7
Half load and 1200rpm	99.5	99.0	99.0	99.6	99.8	93.4	91.2	96.4	98.6	99.5
900rpm	99.4	98.8	99.4	99.2	99.6	97.5	96.4	97.8	97.5	99.2
600rpm	99.5	99.3	99.2	99.1	99.7	96.4	95.3	97.2	97.2	99.2
Full load and 1200rpm	99.9	99.8	99.8	99.8	100	99.4	93.6	99.2	99.4	99.7
900rpm	99.8	99.7	99.7	99.5	99.7	99.2	98.6	98.1	89.7	90.3
600rpm	99.1	98.3	99.0	99.8	99.7	96.9	95.0	96.9	99.2	99.4

For non-stationary conditions, the bearing was tested under six variable speed and load conditions. From Figure 7.13 (a) it is clear that the network has learned properly and correctly produced the desired output. Figure 7.13 (b) provides a good indication about the performance of the DRNN with the testing data set, giving the test output with good accuracy.

Figures 7.14 and 7.15 show the overall fault diagnosis test for a motor operating at variable loads and speed of 600 rpm, and for variable speeds with no-load conditions. All the duration times of the misclassifications shown in Figures 7.10 - 7.12 are less than 0.7s. In practice, such misclassification times would not be noticeable. Hence, all the misclassifications can be considered spontaneous and can be ignored.

Training data set

(a)

Testing data set
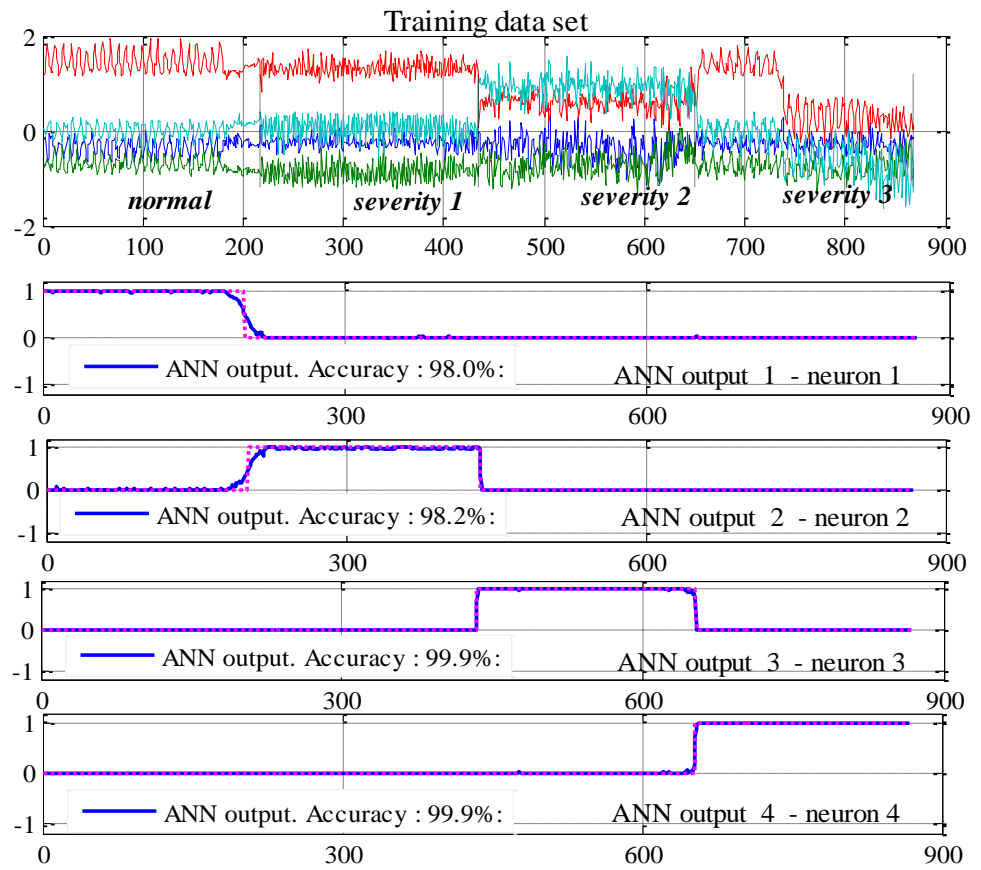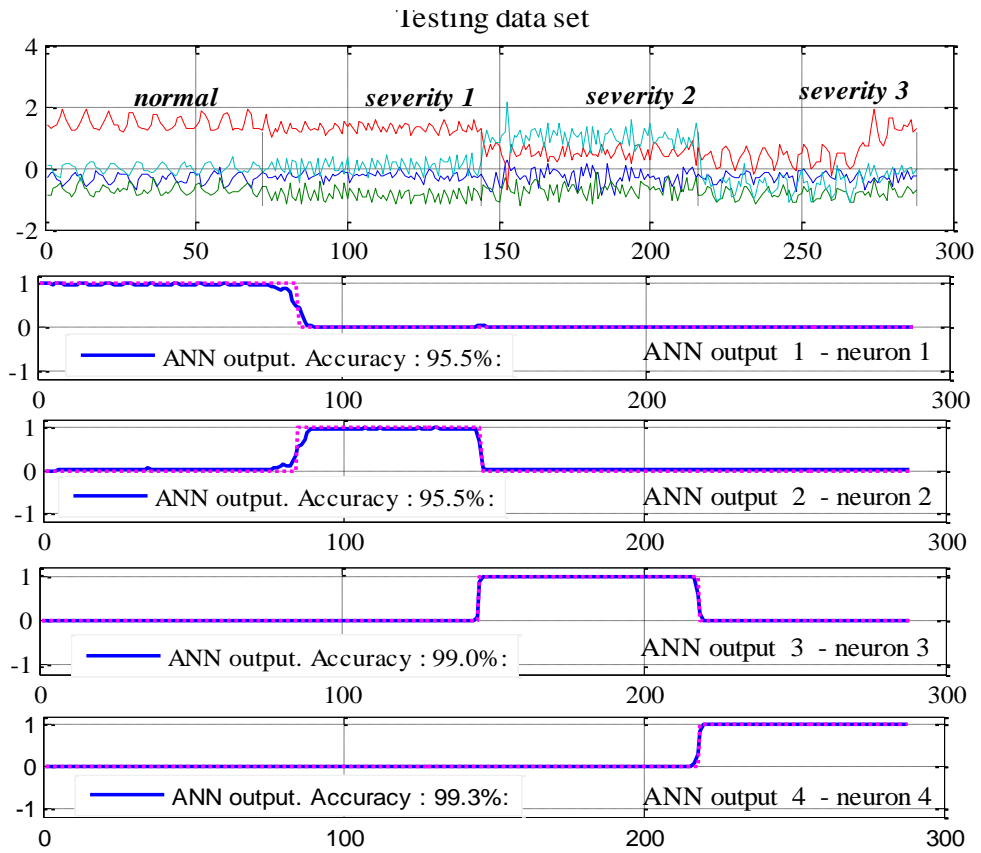
(b)

Figure 7.13 OFNDA features for inner race defect at variable load and 600 rpm speed (a) training and (b) testing

177
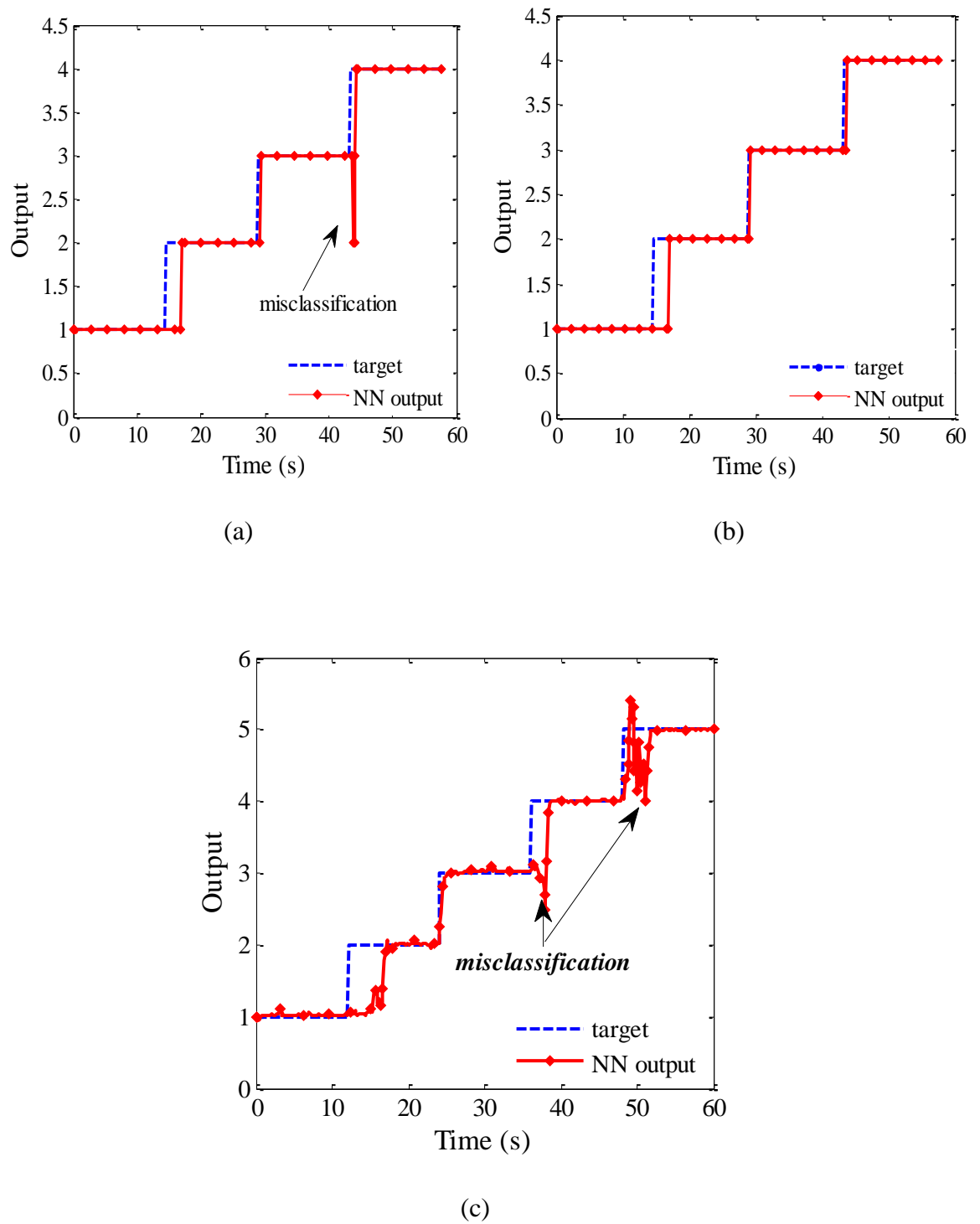
Figure 7.14 DRNN performance to predict bearing fault severity (a) outer, (b) inner and (c) corrosion under variable loads and 600 rpm rotation speed
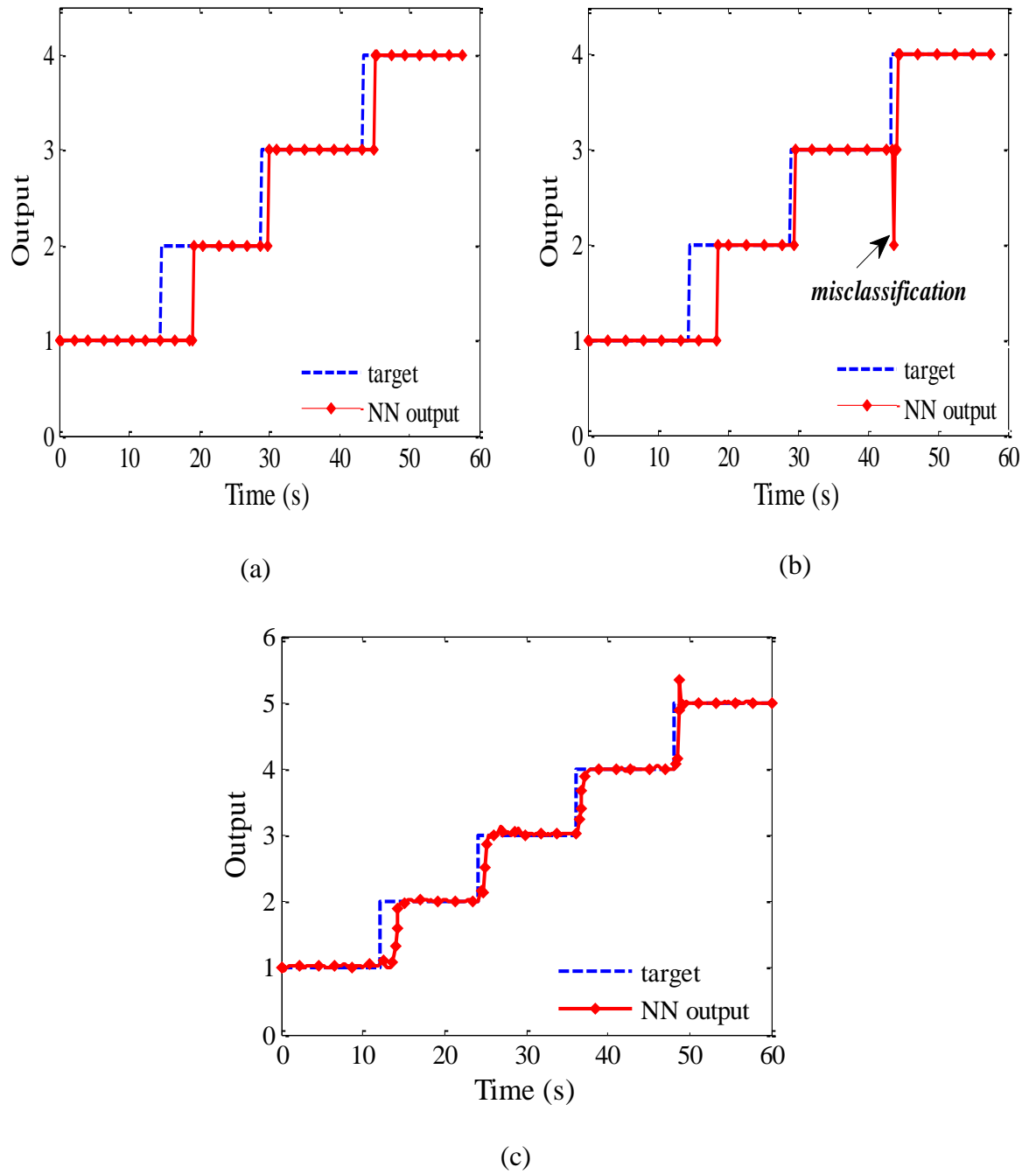
Figure 7.15 DRNN performance to predict bearing fault severity (a) outer, (b) inner and (c) corrosion under variable speed and no load

Table 7.5 shows the ability of the DRNN to diagnose bearing faults using training and testing data sets.

Table 7.5 Fault severity accuracy prediction under non-stationary operating conditions

(a) Inner race defects

Operating conditions Load- speed	Inner race defect Identified rate (%)							
Variable load and	Training accuracy for each DRNN output				Testing accuracy for each DRNN output			
	1	2	3	4	1	2	3	4
1200 rpm	98.8	95.4	96.3	97.5	95.8	94.4	94.4	100
900 rpm	99.0	97.7	99.0	99.9	96.5	94.1	97.2	97.2
600 rpm	98.0	98.2	99.9	99.9	95.5	95.5	99.0	99.3
Variable speed and full load	99.8	99.8	99.1	99.1	96.5	93.8	98.6	99.3
no load	99.0	98.0	99.0	99.2	93.8	91.3	97.6	99.0
half load	99.0	98.0	99.0	99.2	93.8	91.3	97.6	99.0

(b) Outer race defects

| Operating conditions Load- speed	Outer race defect Identified rate (%)							
Variable load and	Training accuracy for each DRNN output				Testing accuracy for each DRNN output			
1200 rpm	1	2	3	4	1	2	3	4
900 rpm	98.8	95.8	96.5	97.7	96.5	93.8	91.7	94.4
600 rpm	99.2	98.3	99.1	99.4	92.7	91.7	98.6	97.9
	98.8	98.3	99.2	99.5	96.2	94.1	97.9	98.6
Variable speed and full load	99.8	99.8	90.3	90.0	95.6	86.1	98.6	97.2
no load	94.1	90.0	96.2	97.6	99.7	98.8	99.2	99.3
half load	98.8	97.9	99.0	99.2	92.0	90.3	98.6	96.2

(c) Corrosion defect

Operating conditions Load- speed	Corrosion defect Identified rate (%)									
Variable load and	Training accuracy for each DRNN output					Testing accuracy for each DRNN output				
	1	2	3	4	5	1	2	3	4	5
1200 rpm	99.4	99.4	98.6	97.9	99.1	96.7	96.2	95.6	90.0	93.4
900 rpm	99.8	99.7	99.7	99.4	99.6	99.2	98.6	98.3	97.5	98.3
600 rpm	99.8	99.6	99.5	99.4	99.8	91.7	91.4	96.4	91.9	95.3
Variable speed and full load	98.3	97.7	98.4	93.4	95.4	88.0	88.0	94.5	91.5	96.4
no load	99.6	99.3	99.2	99.2	99.7	96.7	95.6	97.5	97.8	98.9
half load	99.1	85.1	96.5	94.2	99.8	91.4	94.3	85.7	93.6	95.7

7. 5 DRNN for Thruster motor Blades Fault Diagnosis

Automatic marine control systems for ships of all sizes have been and are being designed and developed, to meet the needs of both the military and civil marine industries. Although modern ships' automatic systems are endowed with highly sophisticated subsystems which are expensive, they also possess manual override facilities in case of emergencies and unforeseen occurrences.

USVs are now being employed by the scientific, offshore and naval sectors to perform a multitude of different tasks with great effect. As a consequence of their success, these sectors are now demanding longer mission lengths coupled with increasingly more vehicle autonomy. With an escalation in autonomy comes the need for higher reliability in order for them to better cope with unexpected events. Hence there is a growing interest in the use of fault detection and diagnostic techniques in USVs.

Thirty data sets were collected during experimental tests to represent thruster motors under four severities of blades fault at six rotation speeds, starting gradually from low to high speed. The extracted features from raw vibration and line current signals are optimised using OFNDA, and the same DRNN structure proposed in section 7.3 is implemented for thruster motor blade faults. The input consists of the eight OFNDA features, x_1^{OFNDA}, x_2^{OFNDA}, and x_3^{OFNDA}, ... x_8^{OFNDA} and the output of the network consists of five units used to indicate a particular thruster motor blade: normal and four severities (full, 50%, 25% and 10%) of blade cut.
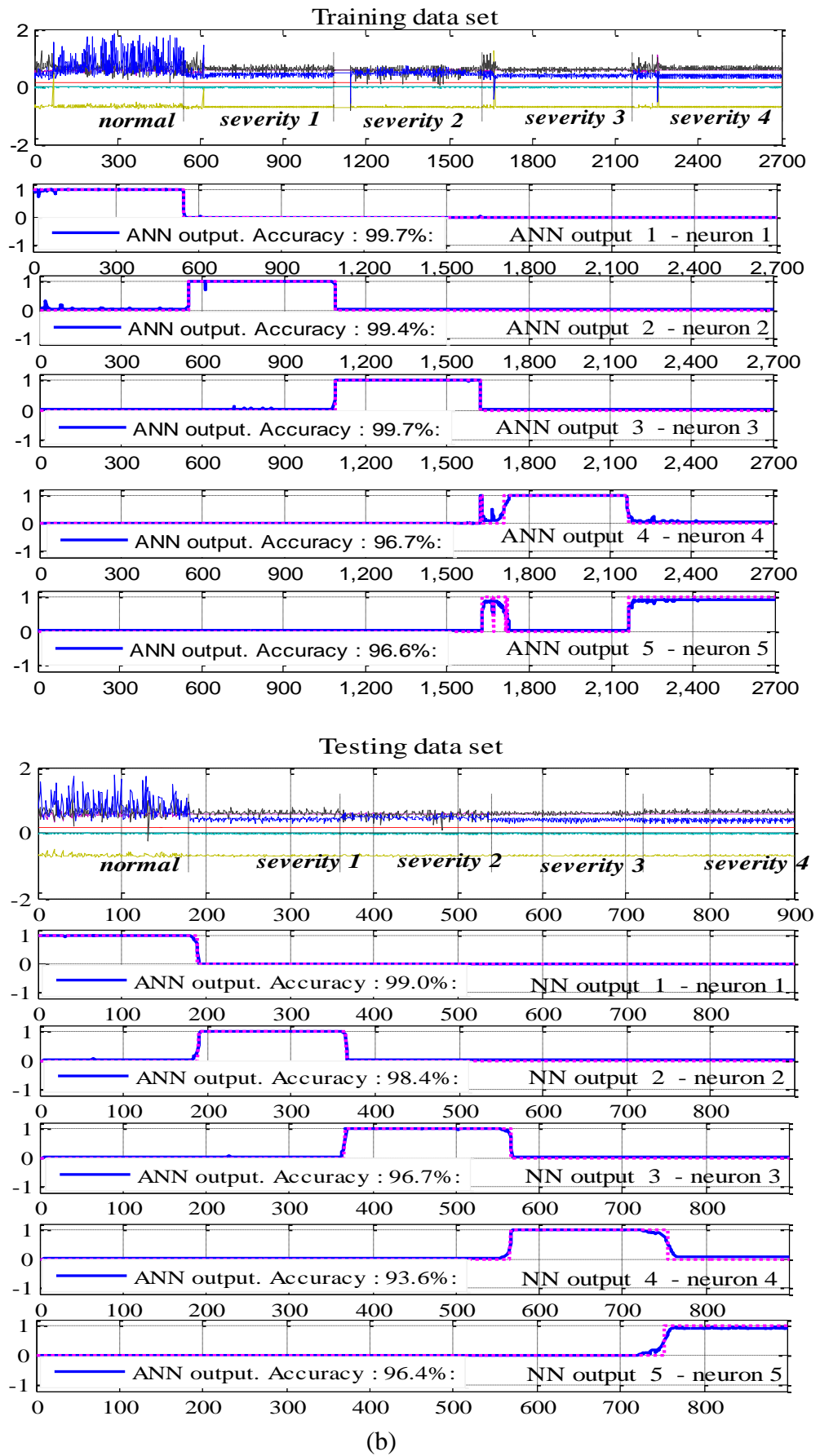
Figure 7.16 OFNDA features for blades defect at high speed

To ensure that its performance does not depend on specific data, OFNDA features (4500 x8) represents blades at normal and four levels of fault severity; these features are divided into three subsets 60% for supervised training and 20% for testing and validation respectively, as shown in Figure 7.16.

The performance of the DRNN should be consistently optimal over all the data sets with respect to classification accuracy. The network outputs four values between 0 and 1; these output values are rounded to 0 or 1 to indicate a certain fault condition, as shown in Table 7.6. Training of the NN involves trying several different values of λ, used to control the size of NN coefficients based on ridge logistic regression principles, number of input delays and number of hidden units, to achieve the optimised set for different parameters, Further, a small value of (α) would increases the time for setting up the network, while a large value may lead to instability.

A fast heuristic-based approach to set this parameter, according to minimal and maximal eigenvalues of the regression matrix and supervised learning, was implemented to calculate the error between the expected and the actual outputs, and this was used to strengthen the weights of the connections between the neurons.

Table 7.7 proves the DRNN parameters that had been implemented during training process. Using too few neurons in the hidden layers will result in under fitting. Under fitting occurs when there are too few neurons in the hidden layers to adequately detect the signals in a complicated data set, while using too many neurons in the hidden layers can result an over fitting.

Over fitting occurs when the NN has so much information processing capacity that the limited amount of information contained in the training set is not enough to train all of the neurons in the hidden layers. Furthermore, an inordinately large number of neurons

in the hidden layers can increase the time it takes to train the network. Several trial and error steps are used to optimise the suitable number of hidden neurons.

Table 7.6 DRNN output nodes

Output 1	Output 2	Output 3	Output 4	Output 5	Indication
1	0	0	0	0	healthy
0	1	0	0	0	Blades severity 1
0	0	1	0	0	Blades severity 2
0	0	0	1	0	Blades severity 3
0	0	0	0	1	Blades severity 4

Table 7.7 Network training parameters

α	λ	FB	Delay	No of iteration	Hidden unit
0.1	0.001	0.7	6	3000	25

Figure 7.17 indicates the performance of DRNN for a thruster motor operating under different severity of blades fault (F1, F2, F3, and F4). Also, Figure 7.17 shows a misclassification occurs when the actual value does not coincide with the desired value.

(a)

(b)
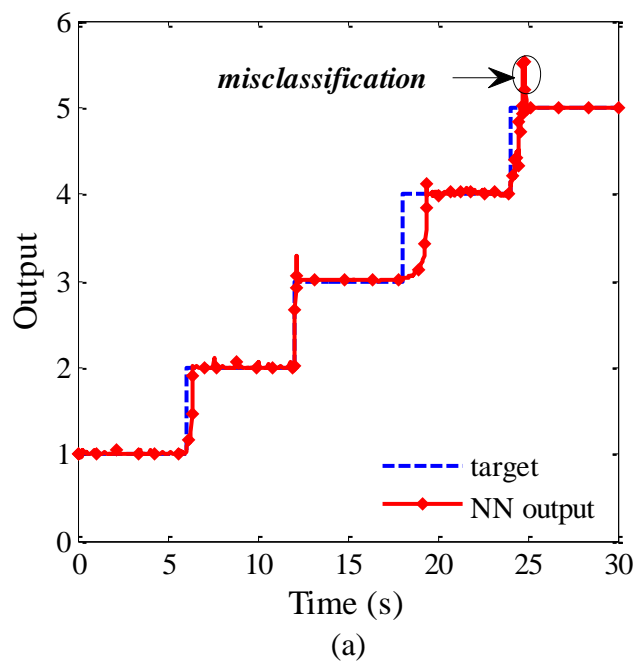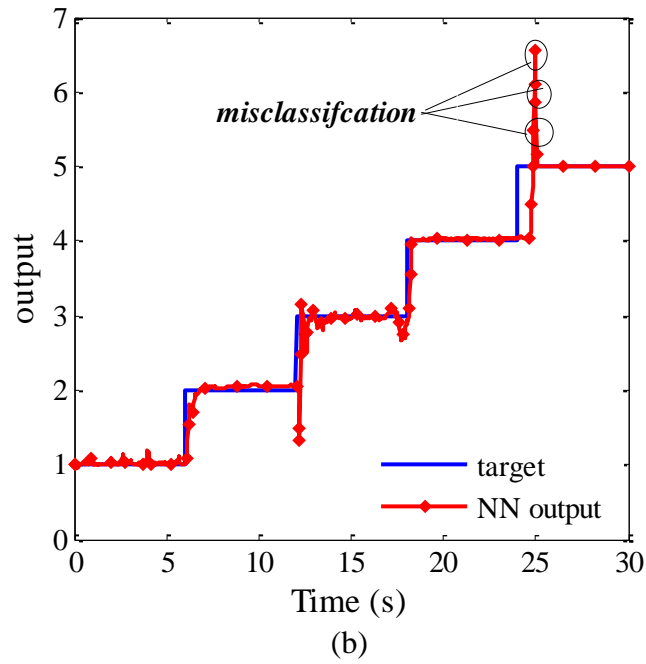
Figure 7.17 Overall fault diagnosis tests for motor operating under different severity of blades fault (F1, F2, F3, F4) at (a) high speed and (b) low speed

Table 7.8 lists the results of the comparisons between the thruster motor under different severity of blades fault with six speed rotating conditions.

Table7. 8 Thruster motor blade fault severities prediction

Speed	Number of OFNDA features	Blades identified rate %									
		Train data set					Testing data asset				
		1	2	3	4	5	1	2	3	4	5
High speed	8	99.7	99.4	99.6	93.1	93.1	98.4	94.0	94.3	92.3	93.0
Speed 2	8	96.3	96.3	98.4	97.8	99.8	99.7	98.9	97.6	96.4	98.7
Speed 3	8	97.1	97.2	97.9	98.0	99.8	99.3	98.3	98.3	91.6	98.3
Speed 4	8	96.3	96.3	98.4	97.8	99.8	99.7	98.9	97.6	96.4	98.7
Low speed	8	98.4	92.4	91.2	93.4	95.7	95.7	90.0	88.0	91.4	92.5

7.6 Chapter Summary

A fault diagnosis system based DRNN has been used to perform intelligent fault detection, classification and fault severity prediction. OFNDA features are used in training, validating and testing the DRNN, based on the sigmoid logistic transfer function that gives the optimal results.

For generalization, the network was trained and tested rigorously under different operating conditions, for both of bearing and thruster motor blades faults. The results demonstrated the capability of the proposed DRNN structure for fault classification and fault severities predication. The next chapter will discuss the results of the proposed diagnostic FA approach, and tests it with different data sets under different operating conditions.

CHAPTER 8

Results and Discussion

"This chapter summarises the proposed fault diagnosis approach, starting from an analysis of the data that was collected during experimental testing and processing, using DWT for feature extraction and OFNDA for dimensionality reduction, these features then being fed into the DRNN for fault classification and level of fault severity prediction."

8.1 Introduction

This chapter discusses the results obtained from tests carried out with the various diagnostic frameworks, in order to bring out their significance. It also reports on the successful implemented of a fault classification and fault severity prediction approach, based on the DRNN system. The results indicate that the proposed technique can be a suitable method for the detection, diagnosis and prediction of bearing and blade faults.

This chapter is organised as follows: Section 8.2 presents the initial data sets that were collected during experimental tests. The results and a discussion of tests on features extraction and dimensionality reduction are presented in section 8.3, with a comparison of the proposed technique with other linear and nonlinear dimensionality reduction approaches. In section 8.4, results for the performance of DRNN for fault classification and level of fault severity prediction are presented. Finally, section 8.5 gives a summary of the chapter's findings.

8.2 Initial Results and Discussion

Experimental tests carried out are described in Chapter 4, the experiment including two case studies. The first one involved, building a test rig to examine PMBLDC motor

performance under three single localised faults and corrosion bearing faults. 15 sets of data and 18112 data samples were collected during experimental tests, at 60s duration for each bearing fault. Results were acquired under stationary and non-stationary operating conditions.

In the second an experimental test was designed to measure PNBDC motor blade faults, and motor performance was tested at four levels of fault severity, with blades cut (10%, 25%, 50% and 100%), and at six speeds of operation.

Vibration measurement is the most widely used and effective way to detect rolling bearing faults such as cracks or corrosion. However, in many cases mechanical signals do not give a clear indication, especially in rugged environments and under low speed conditions. In addition, vibration signals always produce the sum of all the vibrations from other the machine components. Therefore, to increase fault diagnosis reliability in critical applications, the stator current signal can be used as another fault indicator.

Using a current sensor does not necessarily increase the cost of the system, as current sensors already form part of power protection circuits used in such systems. Furthermore, owing to the fact that bearing defects will cause eccentricity, and this will affect the electrical field and then the current, current signal analysis will be an effective indicator for bearing fault diagnosis. Raw vibration and stator current signals can be used as fault indicators, as explained in Chapter 5, to increase diagnostic reliability, especially under low speed conditions.

In order to summarise all the results that represent all data sets collected during the experiment, and for better understanding of the effects of faults, the root mean square (RMS) value of the stator current and raw vibration signals are calculated under different operating conditions.

A bar graph is given in Figure 8.1 that compares the RMS values of the stator current and raw vibration variations under constant load conditions (full load, half rated load and no load) and (600, 900, 1200) rpm rotation speeds, with different bearing faults (inner race, outer race, ball and corrosion).

The RMS value can be computed according to the following equation:

$$RMS = \sqrt{\frac{1}{n}\int_{i=1}^{n} X_i^2}$$

(8.1)

where n is the number of test patterns, and X_i is the sensor output (vibration and current).

Form Figure 8.1 it can be observed that the stator current changes much more when the load changes compared with the RMS value of the vibration signals, and it can also be seen that an inner race crack fault will cause significant changes in the RMS value of the stator current. Furthermore, there is a slight change in vibration when a fault occurs under no load condition (see Figure 8.1.c), while the stator gives good indication of an abnormal situation at low speed (see Figure 8.1.a).

(a)

(b)

(c)
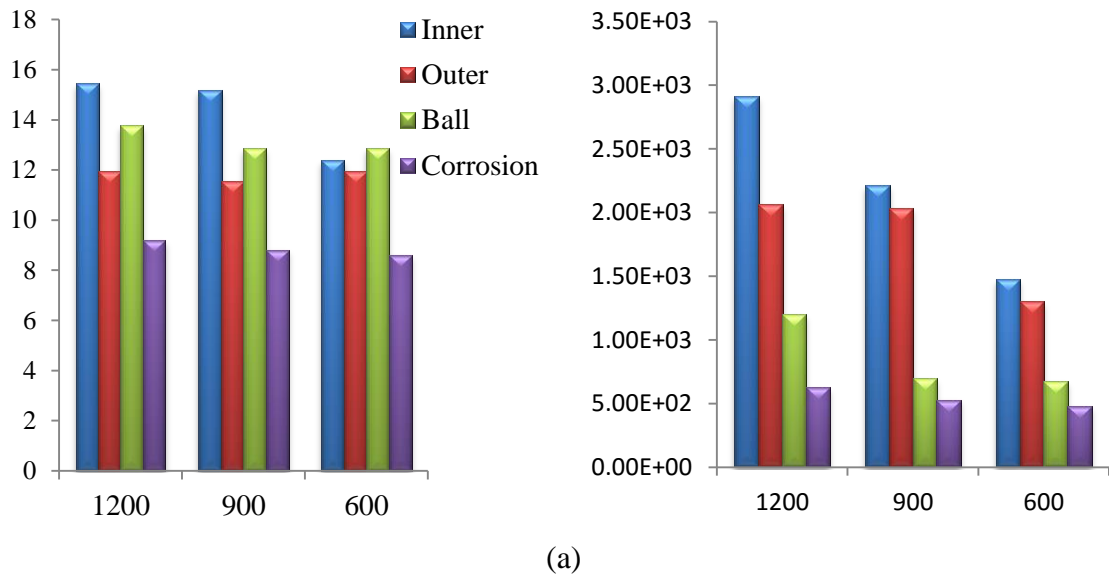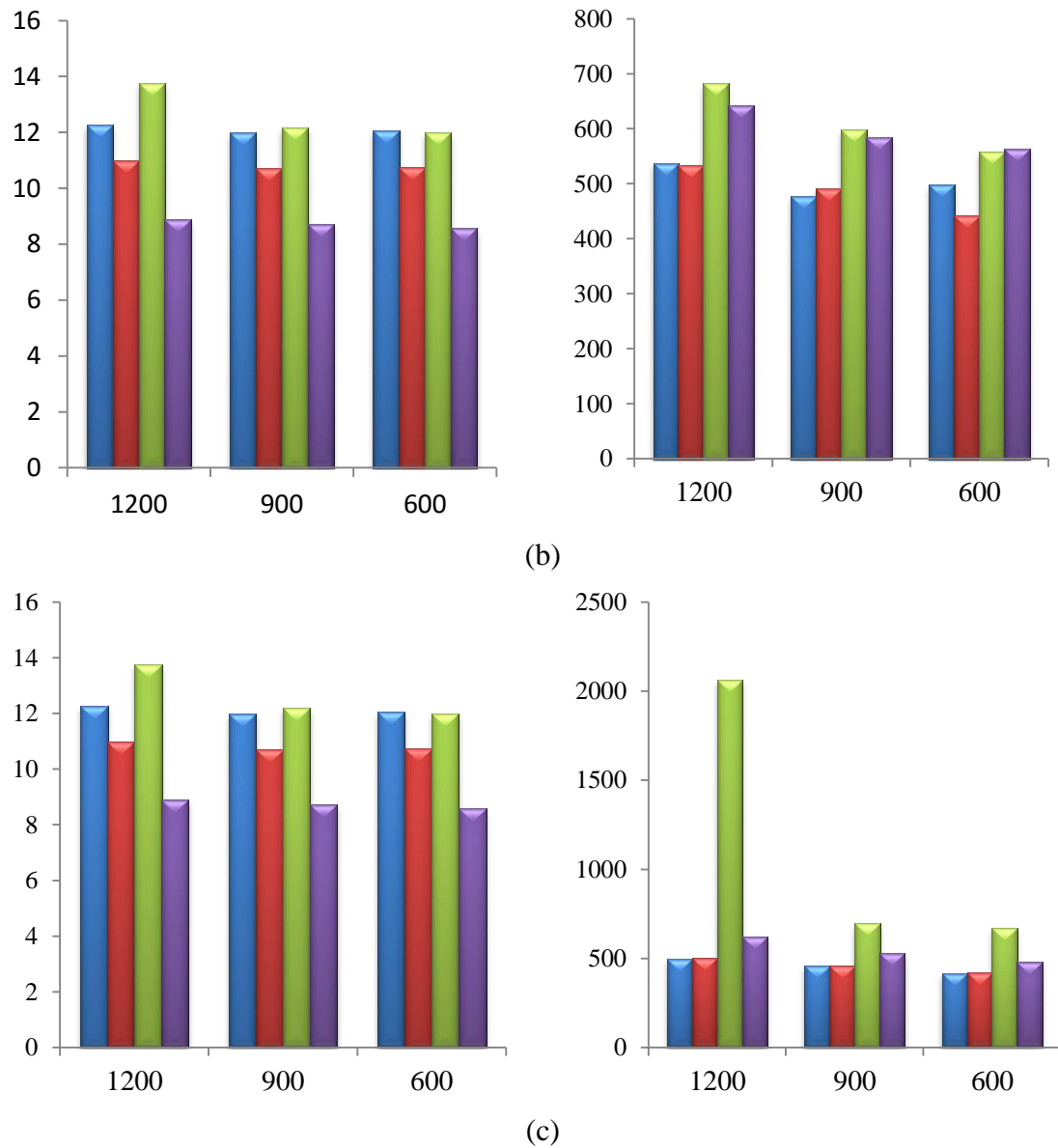
Figure 8.1 RMS value of stator current (left) and the raw vibration (right) at (a) full load, (b) half load and (c) no load, under stationary and various speed conditions.

In the same manner, Figure 8.2 shows the variation of stator current and raw vibration signals under variable load and speed conditions. It can be seen from Figure 8.2.a that the RMS value of the current and vibration are changed significantly at high speed (1200 rpm) compared with low speed (600 rpm), and that the current sensor give a good indication of bearing defects under all operating conditions.
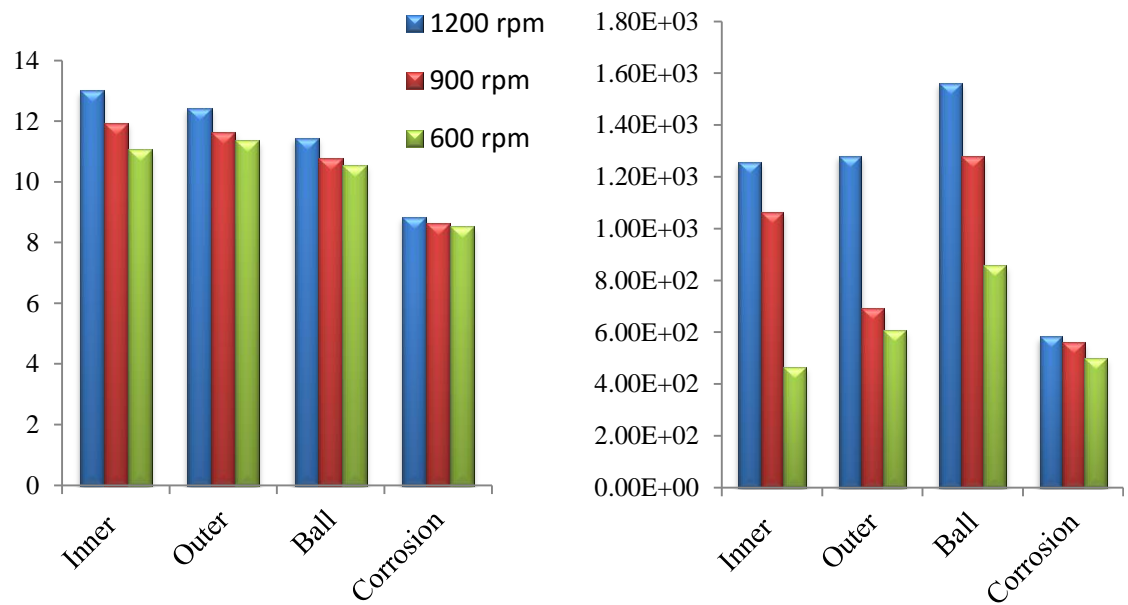
(a)
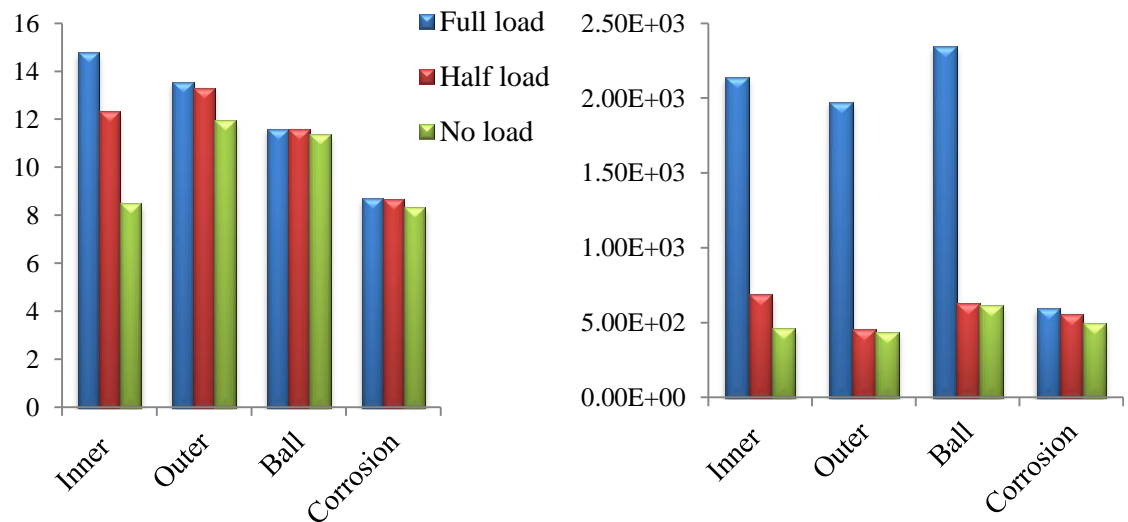
(b)

Figure 8.2 RMS value of stator current (left) vibration (right) under (a) variable load conditions and (b) variable speed conditions

In addition, under variable load conditions, when a fault occurs, the RMS value of the vibration level decreases rapidly (see Figure 8.2.b). Both Figures 8.1 and 8.2 indicate that the stator current is more effective than vibration at stationary and non-stationary operating conditions.

In the frequency domain, the presence of peaks in the stator current and raw vibration spectrum can be used to identify bearings under normal conditions (see Figure 5.1- 5.3)

with different speed and load conditions. In (Chapter 5), Table 5.3 shows single localised bearing defect frequencies and Figure 5.8 compares the spectrums of the raw vibration signal of the outer race defect under three different severities at no-load and 1200 rpm. Generally the level of spectrum increases alongside fault severity. Similarly, Figure 5.14 shows the corrosion defect spectrum under four severities, while Figure 5.15 shows the vibration and current signal with developed blades faults.

For nonlinear operating conditions such as loads and speeds, which have an effect on the vibration and current signals, it is very difficult to make an accurate evaluation of the working condition of faults through analysis in time or frequency domains only. Furthermore, the fault-induced fault signal is often too weak to be detected directly from the resonance sign. Thus, analysing resonance signals allows us to find the key to bearing fault diagnosis.

8.3 Discussion of results from features extraction and dimensionality reduction

Corresponding to different signal processing methods, the signal analysis method should be properly selected. Inaccurate and improper features reduce the overall reliability of fault diagnosis techniques and make them unable to predict actual condition.

T-FA techniques are needed to avoid the drawback of time-domain methods and frequency-domain features, as discussed in (chapter5). T-FA is the three-dimensional time, frequency and amplitude representation of a signal and is commonly implemented for rotating machine fault diagnosis, because it accurately extracts the useful features from a non-stationary signal.

DWT is one of the T-FA methods, and has the important and useful ability to detect and recognise stationary and non-stationary characteristics of signals. To extract the useful information, DWT was implemented to provide the time and frequency information. DWT has the ability to explore signal features with partial characteristics and analyse signals with different time and frequency resolutions. As explained in Chapter 6, DWT includes a large number of wavelet functions (see appendix C).

DWT was optimised before being implemented for features extraction, as mentioned in (Chapter 6). STD and MDL data criteria are used to select the suitable wavelet function and the DIS for the number of decomposition levels, optimising them. See Tables 6.1 and 6.10 for both of rolling element bearing and thruster motor blade defects, respectively.

DWT features were extracted for each operating condition and each type of fault. A sequence of data from the healthy case was prefixed to the data obtained from a faulty condition. 724, 1448, 1448 and 1810 wavelet features for ball, inner, outer and corrosion faults at DWT level five were extracted under stationary and non-stationary operating conditions. In the same way, 4500 features at DWT level 8 were extracted for blade faults under different speed conditions.

Tables 6.3 and 6.4 indicated DWT decomposition details and distribution of the outer race defect under stationary and variable load and speed conditions, with three levels of severities. Similarly, appendix.C.2 indicates these coefficients for ball, inner, and corrosion defects. Figures 6.5-6.8 plot the five levels of wavelet decomposition detail and approximate signal for vibration and current signals for the outer race defect. Wavelet details can be used to predict the probability of fault severity development, as shown in Figures 6.9 and 6.12 for stationary and non-stationary conditions, respectively.

In the same way, according to equations 6.19 and 6.21, for blade fault, the DWT functions and decomposition levels were optimised, as shown in Table 6.10 and energy details and approximate coefficients were calculated at six speeds conditions, as illustrated in Table 6.11. Figure 6.16 shows the comparison of wavelet energy under different levels of fault severities.

To overcome the redundancy features that affect diagnostic accuracy, a proper feature reduction technique can reduce the total fault diagnosis time without compromising the quality of classification. OFNDA is presented as a new approach for feature reduction. It works to maximise the distance between features belonging to different classes, whilst minimise the distance between features in the same class, and taking into account the contribution of the samples to the different classes.

OFNDA has been successfully applied to classify 4 classes of rolling element bearing defects and normal conditions (Chapter 6). For rolling element and blade faults (four and eight) OFNDA features respectively were fed into the DRNN. Figure 6.21 illustrates the step for OFNDA performance, and Figures 6.21-6.24 show OFNDA features used for fault classification and level of severity prediction at no-load and 1200 rpm speed.

In this section, a brief comparison is carried out of typical results obtained using OFNDA as a feature reduction technique, with PCA and LDA as linear and non- linear dimensionality reductions, respectively. PCA is one of the linear feature reduction techniques used to transfer data to a new orthogonal basis whose axes are oriented in the directions of the maximum variance of an input data set (Harmouche et al. 2015). To reduce dimensionality from d to m, PCA starts with centring the data matrix x_j and then calculates a covariance matrix C by subtracting the sampling mean from each row, as represented in the following equations:

$$C = \frac{1}{n-1} x_j x_j^T \qquad (8.2)$$

$$C_{jk=} \frac{1}{n-1} \sum_{j=1}^{n} \left(x_{ji} - x_i^* \right) \left(x_{jk} - x_k^* \right) \qquad (8.3)$$

$$j, k = 1, \dots \dots . p$$

where x_j denotes data matrix and n is the matrix dimension, the next step is to calculate the eigenvectors and eigenvalues of the matrix C by solving the following equation:

$$|C - lI| = 0 \qquad (8.4)$$

One of the main drawbacks of PCA is that it works to reduce feature redundancy only, without taking into account the relation of features or variables with the specific class labels, and this will affect the classification accuracy (Delgado et al. 2011). PCA also has the drawback of its limited ability to deal with non-linear behaviour of the data.

Figure 8.3 show the eigenvalues of the matrix C with indexes, and are based on the cut off values of the eigenvalues. Two principal components were found appropriate for feature reduction in this case. The cumulative percentages of variance using PCA for each feature are obtained as: 72.92, 89.7, 94.9, 98.0, 99.2, 99.6, 99.8, 99.9, 99.9, 100,100, 100, 100,100,100, and 100,100,100.

LDA is another supervised feature reduction technique which searches for the projection axes on which the distance between data points of different classes are increased and those between of the same class are minimised. Further details of the LDA can be found in [36].
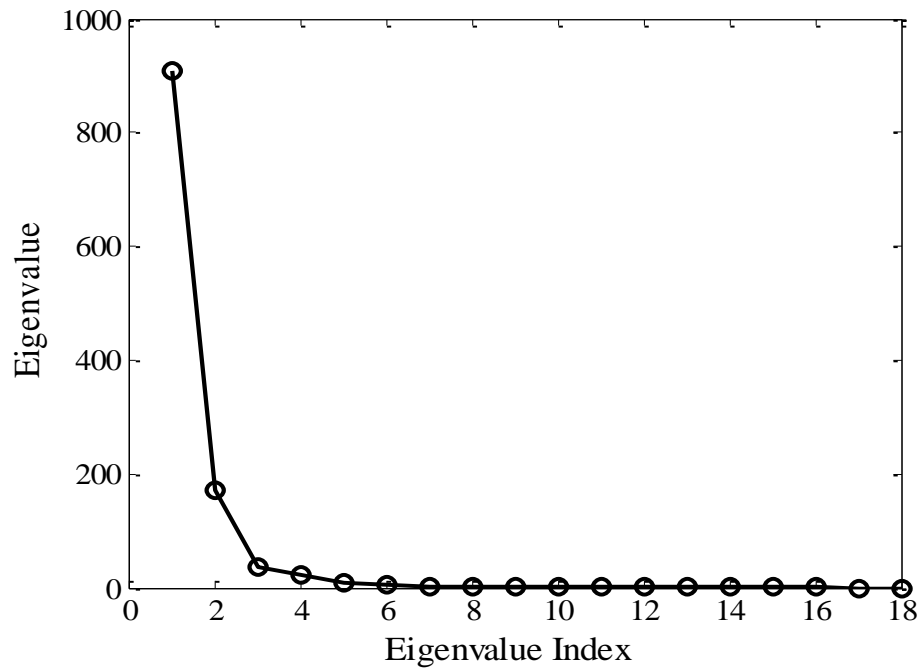
Figure 8.3 PCA performance

The main difference between LDA and PCA is that the former performs data classification whereas PCA does feature classification. In PCA, the shape and location of the original data set changes when transformed to a different space , whilst LDA does not change the location but only tries to provide more class separation and draws a decision region between the given classes.

The comparison (after using the same DRNN structure) indicated that feature reduction with the OFNDA technique provided better fault classification accuracy compared to PCA techniques. PCA reduces features by selecting the main 3 important features. One of the main drawbacks of PCA is that it works to reduce feature redundancy only, without taking into account the relation of features or variables with the specific class labels, and this will affect classification accuracy.

Table 8.1 Classification accuracy under variable load

Operating Conditions	Bearing Faults	Accuracy	
		OFNDA	PCA
1200 rpm	Inner race	98.2	97.7
	Outer race	96.8	98.4
	Ball	99.3	67.6
	Inner race	98.2	77.1
900rpm	Outer race	96.8	84.7
	Ball	97.2	90.5
600rpm	Inner race	93.8	87.8
	Outer race	95.4	86.9
	Ball	98.2	97.7

Table 8.2 Classification accuracy under variable speed

Operating Conditions	Bearing Faults	Accuracy	
		OFNDA	PCA
Full load	Inner race	98.2	92.2
	Outer race	98.8	81.3
	Ball	97.4	84.7
Half rated load	Inner race	94.7	82.4
	Outer race	94.0	72.9
	Ball	93.3	79.5
No- load	Inner race	95.4	96.9
	Outer race	97.8	71.3
	Ball	96.7	73.9

Furthermore, PCA's capability will decrease with nonlinear data (Jian et al. 2011). Tables 8.1 and 8.2 show the percentage diagnostic accuracy of DRNN with OFNDA and PCA. After applying PCA as a feature reduction tool, the overall percentage accuracy was reduced at variable loads, with 1200rpm, 900rpm, 600 rpm and variable speed with no-load conditions.

In a comparison with the classification accuracy obtained using OFNDA, the latter generally shows better fault prediction performance compared with PCA and LDA. Similarly, Table 6 indicates the comparison between the prediction accuracy of OFNDA, PCA and LDA for features reduction under low and high speed conditions. Figure 8.4 shows the prediction performance when PCA and LDA are implemented as features reduction tool. It can be seen from the prediction performance using OFNDA

(see Figure 7.17), that OFNDA is better than PCA and LDA in terms of misclassification and time needed to react to the presence of a fault.

Table 8.3 Comparison of the performance of different reduction methods

Speed (rpm)	Blades identified rate % Using Testing data set				
	1	2	3	4	5
PCA High speed	97.7	95.9	98.1	78.2	80.0
Low speed	99.1	82.8	77.9	64.2	96.0
LDA	95.6	95.8	99.2	85.6	85.8
High speed Low speed	51.4	72.4	80.0	80.0	80.0
OFNDA High speed	99.0	98.4	96.7	93.6	96.4
Low speed	99.7	98.9	97.6	96.4	98.7

(a)

(b)
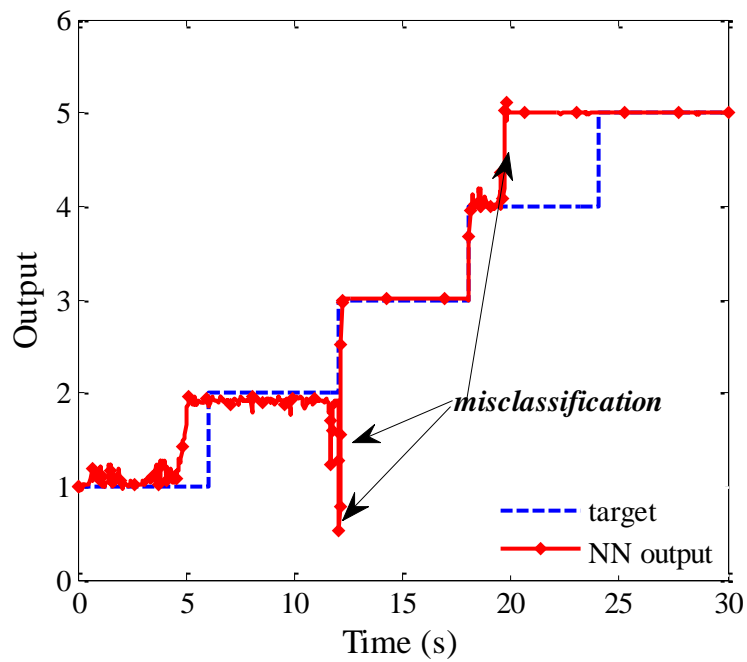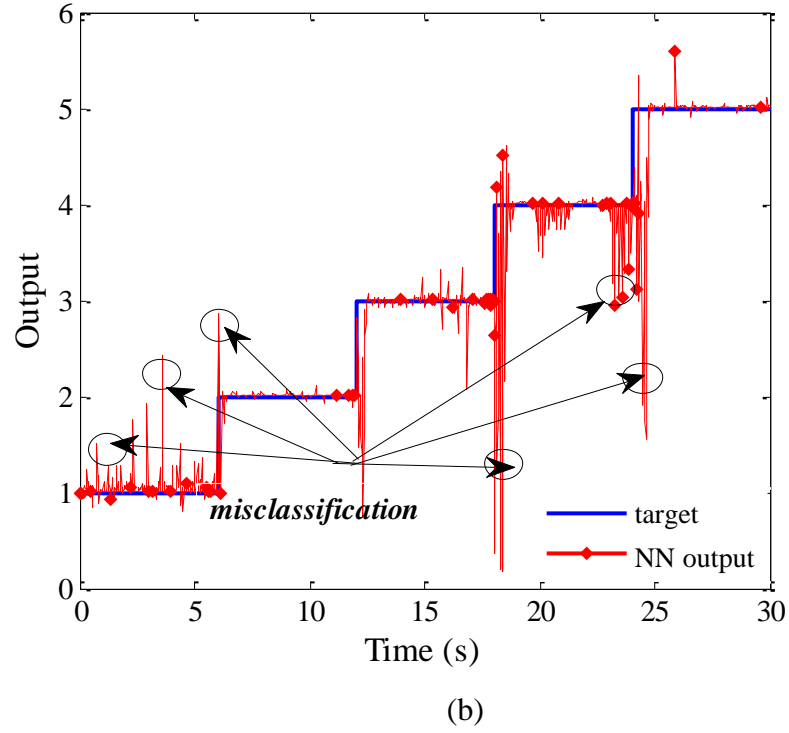
Figure 8.4 Overall fault diagnosis tests for motor operating under different severity of blade fault (F1, F2, F3 and F4) using (a) PCA features and (b) LDA feature

8.4 DRNN for Fault Classification and Level of Fault Severity Prediction

At any instant in time, the response of a static NN based on the value of the input sequence at that time instant. In real-life applications there are several circumstances where the motor is never operating at a constant speed or with a constant load.

18112x2 samples (represents motor vibration and current signals) were collected then DWT was selected to extracted features, DWT features were extracted for each operating condition under different type of faults: inner race, outer race, ball defects and corrosion. In the first stage, 724 wavelet features were obtained for ball defects, 1448 for both inner and outer race and 1810 for corrosion faults. In the second stage 70% and 30% of wavelet features were used for training and testing OFNDA respectively, OFNDA was implemented to remove the redundant wavelet features and nearly 50%

reduction was achieved. 60% of these OFNDA features were reserved as a training set for DRNN and 20% each for both testing and validation.

DNNs have been successfully applied for fault diagnosis, performing better than their static counter parts and providing the capability to learn the dynamics of complicated nonlinear systems, which conventional static NN cannot model. DRNN have been implemented for fault classification and level of fault severity prediction, as shown in Figure 7.4. OFNDA features are used as inputs into the DRNN for training and validation, and to test whether it was capable of detecting and classifying the different faults accurately. The measuring of misclassification ratios will give an indication about the classification algorithm; in this work the classification approach was tested with different operating conditions and different types of faults using many data sets.

A supervised learning algorithm was implemented and the training was carried out. NN parameters were selected based on the network performance process. The first stage focused on the bearing fault classification. Tables 7.2 and 7.3 indicate the classification accuracy under stationary and variable loads and speeds conditions.

The results show the ability of DRNN to classify bearing faults under different operating conditions, as shown in Figures 7.6 -7.8. The overall accuracy of the DRNN for bearing fault prediction at half load, full load and no-load conditions and 1200 rpm rotation speed is illustrated in Figures (7.10 - 7.12) respectively, and Table7.5 indicates the performance of DRNN for fault severity prediction under non-stationary operating conditions. The transition periods are not included in the misclassification count, but the delay is measured as a separate quantity in Table.8.4. The table measures the performance of the proposed approach, where NMC is the number of misclassifications and MMCT the maximum misclassification time. RT represents the network's response time to react to the presence of a fault.

Table 8.4 Test results for severity of fault under stationary operating conditions

Operating load	Bearing Faults	NMC	MMCT (s)	RT (s)
No load and 1200rpm	Inner race	1	0.4	1
	Outer race	3	0.2	2.5
	Corrosion	0	0	1
900rpm	Inner race	2	0.4	2.6
	Outer race	2	0.6	2.7
	Corrosion	2	0.27	2
600rpm	Inner race	0	0	2.5
	Outer race	4	0.6	4
	Corrosion	2	0.5	4
Half load and 1200rpm	Inner race	1	0.2	1
	Outer race	0	0	1.5
	Corrosion	0	0	4
900rpm	Inner race	1	0.4	4
	Outer race	0	0	3.5
	Corrosion	0	0	2
600rpm	Inner race	1	0.4	4
	Outer race	2	0.2	2.7
	Corrosion	1	0.8	3
Full load and 1200rpm	Inner race	4	0.4	2
	Outer race	0	0	1.5
	Corrosion	0	0	4
900rpm	Inner race	5	0.8	1.5
	Outer race	0	0	3.5
	Corrosion	3	0.5	5
600rpm	Inner race	1	0.2	3.5
	Outer race	1	0.4	2
	Corrosion	4	0.35	2.5

The maximum misclassification occurs with corrosion faults at variable load conditions (6 samples), with MMCT 2.5 S not exceeding 0.5 sec for both stationary and variable loads and speeds conditions. In practice, such misclassification times would not be noticeable. Hence, all the misclassifications can be considered spontaneous and can be ignored. Similarly, Table 8.5 indicates the fault severities prediction ability of the proposed approach under variable speed and load conditions (see appendix D).

Table 8.5 Test results under non-stationary operating conditions

Operating load	Bearing Faults	NMC	MMCT(s)	RT(s)
Variable load 1200rpm	Inner race	0	0	2.3
	Outer race	0	0	3
	Corrosion	0	0	1
900rpm	Inner race	5	0.3	3
	Outer race	2	0.4	4.5
	Corrosion	0	0	1
600rpm	Inner race	0	0	2.5
	Outer race	2	0.2	2.5
	Corrosion	6	2.5	4.75
Variable speed Full load	Inner race	0	0	1.8
	Outer race	3	3.5	3
	Corrosion	4.5	2	3.7
Half load	Inner race	0	0	3.2
	Outer race	2	2.7	3.0
	Corrosion	3	3.5	3
No load	Inner race	1	0.4	3.5
	Outer race	0	0	4.5
	Corrosion	0	0	2.5

For blade faults, 900 data sets were used for testing. Table 8.6 indicates the results for the level of fault severity under different speed conditions. From Table 8.6, it can be concluded that the number of misclassifications represents less than 1% of the data sample.

Table 8.6 Test results under non-stationary operating conditions

Rotation speed	NMC	MMCT (s)	RT(s)
Low speed	1	0.5	1.5
Speed 2	1	0.4	3.5
Speed 3	3	3.5	3
Speed 4	0	0	2.3
Speed 5	4	0.3	0.5
High speed	2	2.7	3.0

On-line testing for fault classification and severity of faults prediction has been done using training and testing data sets comprised of both normal and faulty data, using testing data sets that are different form the training data (see appendix E). This was done in Matlab environment with 4 GB of memory with an Intel dual core processor of 3.3 GHz speed. Owing to the delay introduced by the dynamics of the network architecture

(feedback loop), it should also be noted that the network cannot instantly respond to a faulty condition. Table 8.7 illustrates the time delay needed for fault classification purposes. The results show the ability of the current approach to analyse a fault and predict its severity at an early stage; the maximum time needed to diagnose a fault occurs with corrosion in both stationary and non-stationary conditions. It is clear from Tables 8.6 and 8.7 that the maximum time is needed to diagnose bearing faults under variable speed conditions with ball bearing faults, while corrosion faults can be diagnosed at an early stage.

Table 8.7 On-line testing performance

(a) On-line testing under stationary operating conditions

Operating condition	Type of fault	Time delay (s)
Stationary operating condition	Inner race	3.24
	Outer race	3.24
	Ball bearing	6.21
	Corrosion	3.14

(b) On-line testing under non-stationary operating conditions

Operating condition	Type ff fault	Time delay (s)
Non-stationary operating condition Variable load	Inner race	4.76
	Outer race	4.55
	Ball bearing	6.62
	Corrosion	2.48
Non-stationary operating condition Variable speed	Inner race	6.63
	Outer race	6.63
	Ball bearing	14.09
	Corrosion	2.48

To measure the performance of DRNNA at zero skill (without training), the probability of fault diagnosis is calculated under different operating conditions as illustrated in Table 8.8. It was found that ability of DRNN is almost less than 5% for fault classification and fault severity prediction.

Table 8.8 DRNN performance at zero skill

Test		Accuracy %
Fault classification	No load -1200 rpm	2
	Variable speed – no_ load	4
	Variable load -1200 rpm	1
Fault severity prediction	Full lad 1200 rpm (corrosion fault)	4
	Half load -1200 rpm	1.6
	No load -1200 rpm (corrosion fault)	2
	Variable speed- full load (corrosion fault)	5
	Variable load -1200 rpm (corrosion fault)	4

The binomial distribution is defined as the discrete probability distribution of the number of successes in a sequence of trail and can be described in the following equation is discrete as the following:

$$f(k) = \binom{n}{k} p^k (1-p)^{n-k} \tag{8.5}$$

Where k is the number of successes in n is the number of trails and p is the probability of success. 180 data sets were collected represents motor operating at normal and abnormal conditions with different level of fault severities at stationary and nonstationary operating conditions.

When n=180, k=n-11, the success rate of a "null hypothesis" for fault classification (p=0.2). So that the binomial probability distribution at zero skill is calculated according to the above equation is (7.5778e-103), the smaller value provides that the proposed approach is more skilful to classify and predict severity of faults.

According to MacKay (2005) the Bayesian approach helps detect poor underlying assumption in learning model and the system that was more complex will have large Occam factor and will have small evidence. So that the calculated value of the

binomial probability distribution should be less than the Occam factor that can be defined as the following equation (MacKay, 1992):

$$occam\ factor = (2\pi)^{2k} det^{-1/2}\ A \exp(-\alpha E_W^{MP})\ /Z_w(\alpha) \qquad (8.6)$$

where α is the decay rate, E_w is the regularization function, Z_w Gaussian integral, A is the network architecture and MP is the most probable parameter. The Occam factor for a model is straightforward to evaluate (MacKay, 2005):

8.5 Chapter Summary

A number of tools have been employed to obtain a reliable industrial fault diagnosis system. Confidence in the proposed fault diagnostics approach has been backed up by testing the motor under different operating conditions (stationary and non-stationary), and for different of levels of fault severity. Furthermore, the proposed approach has been tested with different types of fault for two types of PMDC motors. The combination of current and vibration as fault indicators helps to exploit the advantages of both. OFNDA was applied to obtain the best features for fault classification, and the results show that better classification accuracy was obtained across different data sets and a number of classes.

These features were fed into a DRNN for fault classification, enabling the fault classifier to incorporate a dynamic component. The application of these techniques to real data has shown that they constitute an effective fault classifier in practice, capable of detecting and classifying bearing and blade faults under stationary and non-stationary operating conditions fairly accurately.

DRNN has demonstrated a great capability in learning the dynamics of complicated non-linear systems during online testing, to classify and predict levels of fault severity

at an early stage, where conventional static neural networks cannot yield comparable results or perform an acceptable modelling representation and mapping. To increase confidence in the fault analysis results, the developed framework has been tested under multiple operating points. The current approach has proven its capability to diagnose different types of fault belonging to two types of motor, under constants and variable loads and speeds conditions.

CHAPTER 9

Conclusion and Recommendations for Future Research

"This chapter summarises the proposed fault analysis approach on different bearing and thruster motor blade faults. Conclusions are drawn on the progress made on developing a method, using the proposed approach to discriminate fault locations and level of severity predictions, and suggestions for possible future work are presented."

9.1 Summary and Conclusions

Electric machines are important components for specific industrial applications. The continuous healthy operations of machines are critical for the reliability of the entire system. Robust FA including the diagnosis of faults and predicting their level of severity is necessary to optimise maintenance and improve reliability.

Early diagnosis of faults that might occur in the supervised process renders it possible to perform important preventative actions, especially important for critical applications such as aircrafts aerodynamic surfaces. Condition monitoring thus renders it possible to perform important preventative actions, thereby avoiding economically damaging losses of elements and parts, through an adequate maintenance management system, as well as avoiding stalled production.

In this research a new approach for PMDC motor fault analysis (fault classification and level of fault severity prediction) has been proposed. The proposed approach is based on data collection, feature extraction and feature subset reduction, fault classification and level of faults severities prediction, and it is implemented to analyse single localised and

generalised bearing faults of PMBLDC motors and unbalanced rotor (blade faults) of PMBDC motors.

The literature review (Chapter 2) showed the limitations of conventional methods such as a model based and signal processing techniques. Recently, AI has been introduced into the fault diagnosis process for condition monitoring. AI aims to generate classifying expressions simple enough to be understood easily by humans.

In the available literature there were also no researchers dealing with both types of bearing fault (localised and generalised) under both stationary and non-stationary conditions. In addition, thruster motor blades defect with different levels of fault severities under different speeds conditions are not covered in the available literature. Some background about PMDC motor characteristics applied to high performance applications is provided, and common electrical and mechanical faults are described in Chapter 3.

Localised, corrosion rolling element bearing as well as blades fault experimental tests have been constructed to validate the proposed fault analysis approach. To test the performance of the proposed techniques with different types of motor and fault, an experimental rig was designed and used to diagnose thruster blade faults with different severities and under several rotation speed conditions, as detailed in Chapter 4. Data was logged under healthy operating conditions as well as with the motor running for each type of defect

To investigate the effects of speed and load conditions, data acquisition software was developed to acquire both raw vibration and current signals during experimental tests under constant and variable speeds and load conditions.

Vibration measurement is the most widely used and effective way to detect rolling bearing faults, but does not give a clear indication of faults at low speed. Vibration can

be picked up from other mechanical parts, thus leading to false positives. The stator current signal can be used as another fault indicator. It has been shown to be an effective fault indicator, especially at low motor speeds.

The combined use of both vibration and current signals will provide a more robust fault detection and diagnosis system without a significant increase in cost, and this is the approach used in this work. The ability of the vibration and current signals acquired during experimental tests to be indicators of the motor situation has been discussed in Chapter 5.

To extract the useful information, DWT, a signal analysis method that provides the time and frequency information of the signal was applied. The information that cannot be readily seen in the time domain can be observed in the frequency domain. It has the ability to explore signal features with partial characteristics and analyse signals with different time and frequency resolutions.

DWT was optimised for level and mother wavelet function. In this work, for optimal wavelet analysis selection, STD and MDL data criteria are used. The proposed features extraction methods were proven in terms of their accuracy, and the efficiency of the proposed extraction method on various datasets compared with time and frequency, as well as its ability to overcome irrelevant features that effect diagnostic performance (Chapter 6).

 OFNDA has not previously been used in electrical motor fault diagnosis system, but her has been implemented as a new approach for feature reduction. It works to maximise the distance between features belonging to different classes while minimizing the distance between features in the same class, and taking into account the contribution of the samples to the different classes (see Chapter 6).

Finally these features were fed into the fault classification and severity prediction algorithm. DNNs have been implemented for fault detection and diagnosis and fault severity prediction, based on OFNDA features used for training, validation and testing, as well as accurately diagnosing results. DRNN as a type of DNN has been successfully applied for fault diagnosis of nonlinear system compared with static NNs (Chapter 7).

The results showed the ability of the proposed diagnostics approach to recognise bearing and thruster motor blade defects under a variety of operating conditions (Chapter 8). The application of these techniques to real data has shown that they constitute an effective fault classifier in practice, capable of detecting and classifying bearing and blades faults under different operating conditions fairly accurately.

9.2 Recommendations for Future Research

Although this work has made contributions to the areas of localised and generalised rolling element bearing faults, and unbalanced load faults in thruster motors under a variety of operating conditions, there is still additional work required to prepare these new condition monitoring schemes for application in industry. Some of this work, which could initiate interesting research in the future is as follows:

> **Detailed fault modelling**

PMDC motor fault modelling is still inadequate. During the development of the fault model, several assumptions were made for simplicity, such as the assumption of infinite magnetic permeability of iron, sinusoidal distribution of magnetic motive force and flux, and the lack of consideration of magnetic saturation and higher order harmonics. All these assumptions will affect diagnostic reliability. Thus, advanced modelling techniques are needed to overcome this problem.

➤ Fault prognosis and useful life time

For improving reliability and reducing overall maintenance costs, an important area of condition monitoring research is the prediction of the remaining life of a bearing, which many bearing manufacturers take into account. However, relatively little work has been done on bearing prognosis, because of the difficulty of estimating the remaining life of a bearing, even with an accurate vibration history. Methods such as particle filtering show great promise for remaining useful life time prediction.

➤ Extension to other faults

The proposed approach can be extended to diagnose different types of rolling element faults, such as misalignment, unbalance, looseness, and lack of lubrication, as well as electrical faults such as stator winding faults and rotor eccentricity defects.

➤ DNN optimisation setup

DNN parameters have been selected based on trial and error and this is difficult in real life. Instead, a genetic algorithm could be implemented to optimise DNN structure parameters. This will reduce the DNN training time and limit the possibility of sub-optimisation via convergence in a local minimum.

➤ Develop fault tolerant techniques

There is a need to extend the proposed approach by developing a fault tolerant system, to increase the reliability of electrical power systems, especially for critical applications.

References

Abdusslam, A. (2012) 'Detection and Diagnosis of Rolling Element Bearing Faults Using Time Encoded Signal Processing and Recognition', *Ph.D. thesis*, University of Huddersfield.

Abed, W., Sharma, S. and Sutton, R. (2013) 'Fault diagnosis of brushless DC motor for an aircraft actuator using a neural wavelet network', *IET conference,* pp.1-6, doi: doi:10.1049/cp.2013.0020.

Abed W, Sharma SK, Sutton R, and Amit Motwani (2015)'A robust bearing fault detection and diagnosis technique for brushless DC motors under non-stationary operating conditions' *Journal of Control, Automation and Electrical Systems*, doi: 10.1007/s40313-015-0173-7

Administrator.(2005), available on line at: *http://blog.savel.org/2005/05/25/checking-power-mosfet-with-simple-tester/comment-page-1/*

Ah Chung, T. and Back, D. (1994) 'Locally recurrent globally feedforward networks: a critical review of architectures', *IEEE Transactions on Neural Networks,* vol.5, no 2, pp. 229-239.

Ahmadi, H., Sakhaei, B. and Labbafi, R. (2014) 'Support vector machine and K-nearest neighbour for unbalanced fault detection', *ournal of Quality in Maintenance Engineering,*volume, vol 20 , no 1, pp. 65-75.

Ahmed, A., Sozer, Y. and Hamdan, M. (2014) 'Maximum torque per ampere control for interior permanent magnet motors using DC link power measurement', *29th Annual IEEE Applied Power Electronics Conference and Exposition,* USA, pp.826-832, doi:10.1109/APEC.2014.6803403.

Alessandri, A., Caccia, M. and Veruggio, G. (1999) 'Fault detection of actuator faults in unmanned underwater vehicles', *Control Engineering Practice,* vol 7, no3,pp.357-368.

Allegro MicroSystems. (2013) ' Fully Integrated, Hall Effect-Based Linear Current Sensor ACS712'. *online available at:http://www.allegromicro.com/en/Products/ Current-Sensor-ICs/Zero-To-Fifty-Amp-Integrated-Conductor-Sensor-ICs/ACS7 12.aspx.*

Alok, S., Kuldip, K. and Godfrey, C. (2006) 'Class-dependent PCA,MDC and LDA: Acombined classifier for pattern classification', Pattern Recognition, vol.39, no.7, pp1215 - 1229.

Amar, M., Gondal, I. and Wilson, C. (2014) 'Vibration spectrum imaging: A novel bearing fault classification approach', *IEEE Transactions on Industrial Electronics,*vol. 62, no. 1, pp.494-50.

Analog Devices, I. (2009) 'ADXL325 Data Sheet' *available online at http://www.analog.com/static/ imported-files/ data_sheets/ADXL325.pdf.*

Andrew N.(2014).'Machine Learning, CS229 Lecture notes, Stanford University, USA

Angelo, V., Palhares, M., Cosme, B., Aguiar, A., Fonseca, S. and Caminhas, M. (2014) 'Fault detection in dynamic systems by a Fuzzy Bayesian network formulation', *Applied Soft Computing,* vol. 21, pp. 647–653, doi:10.1016/j.asoc.2014.04.007.

Antoni, J. and Randall, R. (2002) 'Differential Diagnosis of Gear and Bearing Faults Research Associate ', J*ournal of Vibration and Acoustics*, vol.124, no. 2, pp. 165-171.

Antonino, J., Riera, M., Roge, J., Martínez, F. and Peris, A. (2006) 'Application and optimisation of the discrete wavelet transform for the detection of broken rotor bars in induction machines', *Applied and Computational Harmonic Analysis*, vol .21, no 2, pp.268-279.

Antonino, J., Riera, M., Folch, R. and Molina , M. (2006) 'Validation of a new method for the diagnosis of rotor bar failures via wavelet transform in industrial induction machines', *IEEE Transactions on Industry Applications*, vol.42, no.4, pp. 990-996.

Antonino, J., Aviyente, S., Strangas, G. and Riera, M. (2013) 'Scale Invariant Feature Extraction Algorithm for the Automatic Diagnosis of Rotor Asymmetries in Induction Motors', *IEEE Transactions on Industrial Informatics*, vol. 9, no.1, pp.100-108.

Balaban, E., Saxena, A., Bansal, P., Goebel, F. and Curran, S. (2009) 'Modeling, Detection, and Disambiguation of Sensor Faults for Aerospace Applications', *IEEE Sensors Journal,* vol. 9, no. 12, pp. 1907-1917.

Barakat, M., El Badaoui, M. and Guillet, F. (2013) 'Hard competitive growing neural network for the diagnosis of small bearing faults', *Mechanical Systems and Signal Processing,* vol.37, no. 1-2, pp.276-292.

Barzegaran, M., Mazloomzadeh, A. and Mohammed, A. (2013) 'Fault Diagnosis of the Asynchronous Machines Through Magnetic Signature Analysis Using Finite-Element Method and Neural Networks', *IEEE Transactions on Energy Conversion,* vol.28, no. 4, pp. 1064-1071.

Bediaga, I., Mendizabal, X., Arnaiz, A. and Munoa, J. (2013) 'Ball bearing damage detection using traditional signal processing algorithms', *IEEE Instrumentation & Measurement Magazine,* vol. 16, no. 2, pp. 20-25.

Bellini, A., Filippetti, F., Tassoni, C. and Capolino, A. (2008) 'Advances in Diagnostic Techniques for Induction Machines', *IEEE Transactions on Industrial Electronics,* vol. 55, no. 2, pp. 4109-4126

Bhavaraju, M., Kankar, P., Sharma, C. and Harsha, S. (2010) 'A Comparative Study on Bearings Faults Classification by Artificial Neural Networks and Self-Organizing Maps using Wavelets', *International Journal of Engineering Science and Technology*, vol.2, no.5, pp.1001-1008.

Bianchini, C., Immovilli, F., Cocconcelli, M., Rubini, R. and Bellini, A. (2011) 'Fault Detection of Linear Bearings in Brushless AC Linear Motors by Vibration Analysis', *IEEE Transactions on Industrial Electronics,* vol. 58, no. 5, pp. 1684-1694.

Biet, M. (2013) 'Rotor faults diagnosis using feature selection and nearest neighbors rule: Application to a turbogenerator', Industrial Electronics, IEEE Transactions on, vol.6, no.9, pp.4063-4073.

Bin, Z., Sconyers, C., Byington, C., Patrick, R., Orchard, M. and Vachtsevanos, G. (2011) 'A Probabilistic Fault Detection Approach: Application to Bearing Fault Detection', *IEEE Transactions on Industrial Electronics,* vol. 58, no. 5, pp. 2011-2018.

Bindu, S. and Thomas, V. (2014) 'Diagnoses of internal faults of three phase squirrel cage induction motor A review', *International Conference on Advances in Energy Conversion Technologies*, India, pp.48-54, doi:10.1109/ICAECT.2014.6 757060.

Blodt, M., Chabert, M., Regnier, J., Faucher, J. and Dagues, B. (2005) 'Detection of mechanical load faults in induction motors at variable speed using stator current time-frequency analysis', *5th IEEE International Symposium on* Diagnostics for *Electric Machines, Power Electronics and Drives*, Austria, pp.1-6, doi:10. 1109/ DEMPED.2005.4662496.

Bouzida, A., Touhami, O., Ibtiouen, R., Belouchrani, A., Fadel, M. and Rezzoug, A. (2011) 'Fault Diagnosis in Industrial Induction Machines Through Discrete Wavelet Transform', *IEEE Transactions on Industrial Electronics*, vol.58, no. 9, 4385-4395.

Camarena, D., Valtierra, M., Garcia, A., Osornio, A. and Romero, J. (2014) 'Empirical Mode Decomposition and Neural Networks on FPGA for Fault Diagnosis in Induction Motors', *The Scientific World Journal*, vol.14, pp. 1-17, doi: 10.1155/ 2014/908140.

Cevikalp, H. (2005) 'Feature Extraction Techniques in High Dimension Spaces :Linear and Nonlinear Approaches' *PhD thesis in Electrical Engineering*, Vanderbilt University,USA.

Climente, V., Antonino, J. A., Riera, M. and Vlcek, M. (2014) 'Induction Motor Diagnosis by Advanced Notch FIR Filters and the Wigner Ville Distribution', *IEEE Transactions on Industrial Electronics*, vol.61, no.8, pp.4217-4227.

Changning, L. and Gang, Y. (2010) 'A New Statistical Model for Rolling Element Bearing Fault Signals Based on Alpha-Stable Distribution', *Second International Conference on* Computer Modelling and Simulation, China, pp. 386-390,doi:10.1109/ICCMS.2010.309.

Chen, Z. and Gao, L. (2013) 'Fault Diagnosis of Roller Bearing Using Dual-Tree Complex Wavelet Transform, Rough Set and Neural Network', *Advances in Intelligent Systems Research*, pp.1196-1199, doi:10.2991/iccsee.2013.301.

Chetouani, Y. (2014) 'Model selection and fault detection approach based on Bayes decision theory: Application to changes detection problem in a distillation column', *Process Safety and Environmental Protection*,vol.92, no. 3, pp.215 – 223.

Chiang, L. H., Kotanchek, M. E. and Kordon, K. (2004) 'Fault diagnosis based on Fisher discriminant analysis and support vector machines', Computers and Chemical Engineering, vol.28, no.8, pp. 1389-1401.

Chiementin, X., Bolaers, F., Cousinard, O. and Rasolofondraibe, L. (2008) 'Early detection of rolling bearing defect by demodulation of vibration signal using adapted wavelet', *Journal of Vibration and Control,* vol.14, no.11, pp.1675-1690.

Cho,C., Knowles, J., Fadali, M. and Lee, S. (2010) 'Fault detection and isolation of induction motors using recurrent neural networks and dynamic bayesian modeling', *IEEE Transactions on Control Systems Techn*ology,vol.18, no. 2, pp. 430-437.

Choy, F., Mugler, D. and Zhou, J. (2003) 'Damage identification of a gear transmission using vibration signatures', *Journal of Mechanical Design*, vol.125, no. 2, pp.394-403

Choudhury, A., Tandon, N. (1999) 'A theoretical model to predict vibration response of rolling bearings to distributed defects under radial load', *ASME, Journal of Vibration and Acoustics,* vol.120, no. 1, pp.214-220.

Christophe, C., Cocquempot, V. and Jiang, B. (2002) 'Link between high gain observer-based residual and parity space one'*, Proceedings of the American Control Conference,* vol. 3, pp. 2100-2105, doi:10.1109/ACC.2002.1023946.

Cruz, A. and Cardoso, M. (2005) 'Multiple Reference Frames Theory: A New Method for the Diagnosis of Stator Faults in Three-Phase Induction Motors', *IEEE Transactions on Energy Conversion,* vol.20, no. 3, pp. 611-619.

Cusido, J., Romeral, L., Ortega, A., Rosero, A. and Garcia Espinosa, A. (2008) 'Fault Detection in Induction Machines Using Power Spectral Density in Wavelet Decomposition', *IEEE Transactions on Industrial Electronics,* vol. 55, no. 2, pp. 633-643.

Daqi, Z. and Bing, S. (2013) 'Information fusion fault diagnosis method for unmanned underwater vehicle thrusters', *Electrical Systems in Transportation, IET,* vol 3, no.4, pp.102-111.

Davoodi, R., Meskin, N. and Khorasani, K. (2013) 'Simultaneous fault detection and control design for an autonomous unmanned underwater vehicle', 7th IEEE *GCC Conference and Exhibition,* pp.529-534, doi:10.1109/IEEEGCC.2013.6705835.

Delgado, M., Cusido, J. and Romeral, L. (2011) 'Bearings fault detection using inference tools,Vibration Analysis and Control New Trends and Developments'*, InTech*, pp. 263-280, doi:10.5772/22696.

Delgado, M., Urresty, J. , Albiol, L., Ortega, A., Garcia, A., Romeral, L. and Vidal, E. (2011) 'Motor fault classification system including a novel hybrid feature reduction methodology'*,37th Annual Conference on IEEE Industrial Electronics Society* , Australia, pp. 2388-2393, doi:10.1109/IECON.2011.6119683.

Ding, S., Xiao , C., and Wu, H. (2013) 'Application of Probabilistic Neural Networks in Fault Diagnosis of Three-Phase Induction Motors', *Applied Mechanics and Materials,* vol.705, pp. 433-435,doi:10.4028/www.scientific.net/AMM.433-435.705.

Ding, X. (2013) 'Model-Based Fault Diagnosis Techniques: Design Schemes, Algorithms and Tools'*,* 1st Edition, Springer verlage Germany.

Doguer, T. and Strackeljan, J. (2009) 'Vibration analysis using time domain methods for the detection of small roller bearing defects',8th International Conference on Vibrations in Rotating Machines, pp.23-25, *available online at: http://www.ovgu.de/ifme/l-dynamik/quellen/SIRM_Paper16.pdf.*

Dunn, S. (2002) 'Condition Monitoring in the 21st Century', *Plant Maintenance Resource Center,available online at: http://www.conditionmonitoringintl.com/re sources/TLT_columns/09-11%2021st%20Century%20CM.pdf.*

Farag, A. A. 2008 'A Tutorial on Data Reduction Linear Discriminant Analysis (LDA)'. Available at: *http://www.cvip.uofl.edu/wwwcvip/education/ECE523/LDA%20 Tutorial.pdf.*

Farshad, S., Naser, M., and Mahdi, K. (2013)'Turbine Rotor Vibration Failures: Causes and Solutions'. Available online at: http://www.powermag.com/steam-turbine-rotor-vibration-failures-causes-and-solutions/.

Faucher, J. (2010) 'Comparison between vibration and stator current analysis for the detection of bearing faults in asynchronous drives', *IET Electric Power Applications,* vol.4, no. 2, pp. 90- 100.

Feng, Z., Liang, M. and Chu, F. (2013) 'Recent advances in time–frequency analysis methods for machinery fault diagnosis: A review with application examples', Mechanical Systems and Signal Processing,vol. 38, no.1, pp.165-205.

Feng, G., Zhen, D., Tian, X., Gu, F. and Ball, D. (2015) 'A Novel Method to Improve the Resolution of Envelope Spectrum for Bearing Fault Diagnosis Based on a Wireless Sensor Node' *Springer in Vibration Engineering and Technology of Machinery*, pp.765-775, doi:10.1007/978-3-319-09918-7_68.

Fitzgerald, E., Charles , J. and Umans, D. (2003) 'Electric Machinery', Sixth Edition, McGraw-Hill Higher Education, USA.

Freescale Semiconductor (2008) 'Micro machined Accelerometer MMA7361L'. *available online at: http://imall.iteadstudio.com/im120712010.html.*

Frosini, L. and Bassi, E. (2010) 'Stator Current and Motor Efficiency as Indicators for Different Types of Bearing Faults in Induction Motors', *IEEE Transactions on Industrial Electronics,* vol.57, pp, 244-251.

Ece, G. and Başaran, M. (2011) 'Condition monitoring of speed controlled induction motors using wavelet packets and discriminant analysis', *Expert Systems with Applications,* vol.38, no. 7, pp. 8079-8086.

Eleyan, A. and Demirel, H. (2007) 'PCA and LDA based Neural Networks for Human Face Recognition' , *InTech chine*, pp.93-106, http://cdn.intechopen.com/pdfs-wm/197.pdf.

Emerson bearing (1996) 'Bearing failure analysis', *available online at: http://www. emer sonbearing.com/technical-toolbox.html.*

Esfahani, T., Wang, S. and Sundararajan, V. (2014) 'Multisensor Wireless System for Eccentricity and Bearing Fault Detection in Induction Motors', *Mechatronics, IEEE/ASME Transactions on,* vol.19,no.3, pp. 818-826.

Garcia, A., Cusido, J., Rosero, J. A., Ortega, A. and Romeral, L. (2008) 'Reliable electro-mechanical actuators in aircraft', *IEEE Aerospace and Electronic Systems Magazine,* vol. 23, no. 8, pp.19-25.

Germen, E., Başaran, M. and Fidan, M. (2014) 'Sound based induction motor fault diagnosis using Kohonen self-organizing map', *Mechanical Systems and Signal Processing,* vol.46, no. 1, pp. 45-58.

Gieras, F. (2009) 'Permanent Magnet Motor Technology Design and Appications' , *1st Edition ,CRC Press is an imprint of the Taylor & Francis Group*, USA.

Gohshi, S. (2012) 'A new signal processing method for video: reproduce the frequency spectrum exceeding the Nyquist frequency', in *3rd Multimedia Systems Conference*, USA, pp.47-52,doi:10.1007/978-1-4614-3501-3_49.

Gritli, Y., Di Tommaso, O., Miceli, R., Rossi, C. and Filippetti, F. (2013) 'Diagnosis of mechanical unbalance for double cage induction motor load in time-varying conditions based on motor vibration signature analysis', *International Conference on Renewable Energy Research and Applications* ,Spain, pp.1157-1162, doi:10.1109/ICRERA.2013.6749927.

Gritli, Y., Filippetti, F. and Casadei, D. (2014) 'Diagnosis and Fault Detection in Electrical Machines and Drives based on Advanced Signal Processing Techniques', *Ph.D thesis* in Electrical Engineering, University of Bologna, Italy

Hai, H., Lei, W., Wen, C., Yong-jie, P. and Shu, J. (2014) 'A Fault-tolerable Control Scheme for an Open-frame Underwater Vehicle', *International Journal of Advanced Robot System,* vol. 11, doi:10.5772/58578.

Haixian, W., Xuesong, L., Zilan, H. and Wenming, Z. (2014) 'Fisher Discriminant Analysis With L1-Norm', *IEEE Transactions on Cybernetics*, vol.44, no 6, pp.828-842.

Hamid, Y. and Kawasaki, I. (2002) 'Wavelet-based data compression of power system disturbances using the minimum description length criterion', *IEEE Transactions on Power Delivery*, vol.17, no. 2, pp.460-466.

Harmouche, J., Delpha, C. and Diallo, D. (2014) 'Improved Fault Diagnosis of Ball Bearings Based on the Global Spectrum of Vibration Signals', I*EEE Transactions on Energy Conversion*, vol.30, no.1, pp.363-383.

Harmouche, J., Delpha, C. and Diallo, D. (2015) 'Improved Fault Diagnosis of Ball Bearings Based on the Global Spectrum of Vibration Signals', *Energy Conversion, IEEE Transactions on,* vol.30, no.1, pp.376-383.

Harris, W. (2013) 'Anomaly Detection in Rolling Element Bearings via Two-Dimensional Symbolic Aggregate Approximation', MSc of Science In Mechanical Engineering, Virginia Polytechnic Institute and State University, USA.

He, D., Ruoyu, L., Junda, Z. and Zade, M. (2011) 'Data Mining Based Full Ceramic Bearing Fault Diagnostic System Using AE Sensors', *IEEE Transactions on Neural Networks,* vol. 22, no.12, pp. 2022-2031.

Henao, H., Capolino, G., Fernandez, M., Filippetti, F., Bruzzese, C., and Strangas, E. (2014) 'Trends in Fault Diagnosis for Electrical Machines: A Review of Diagnostic Techniques', *IEEE Industrial Electronics Magazine,* vol. 8, no. 2, pp. 31-42.

Hill, C. (2004) 'An Introduction to Low Voltage DC Motors', *Philips Semiconductors*, avialble online at: ftp://ftp.dei.polimi.it/outgoing/Massimo.Ghioni/Power%20 Electronics%20/Motor%20control/DC/DC%20-%20motors.pdf.

Hocine, B., Salah Bouhouche and Boucherit, M. (2012) 'Application of Wavelet Transform for Fault Diagnosis in Rotating Machinery ', *International Journal of Machine Learning and Computing*, vol.2, no.1, pp.82-87.

Honeywell datasheet CSLA1DJ, 2014 available on line at: http//www. kosmodrom. com.ua/pdf/CSLA_2.pdf.

Howard, D., Mark, B. and Martin, H. (2006) 'Neural Network Toolbox For Use with MATLAB', *The Mathowrks User's Guide,* Version 5.

Huang, Y, Hsiung, W., Yang, Y. and Loh, C. (2014). 'Application of image analysis and time-frequency analysis for tracking the rotating blades vibration*', Sensors and Smart Structures Technologies for Civil, Mechanical, and Aerospace Systems Conference*, USA, pp.1-6,doi:10.1117/12.2044353.

Hui, Z. and Shou, H. (2010) 'Fault diagnosis of rolling bearing vibration based on particle swarm optimisation-RBF neural network*', The 2nd International Conference on Computer and Automation Engineering*, Singapore, pp. 632-634,doi:10.1109/ICCAE.2010.5451320.

Huo ,F. and Poo, A. (2013) 'Nonlinear autoregressive network with exogenous inputs based contour error reduction in CNC machines', *International Journal of Machine Tools and Manufacture,* vol.67, pp.45-52. doi:10.1016/ jijmachtools.20 12.12.007.

Hyun , C., Knowles, J., Fadali, S. and KWon, L. (2010) 'Fault Detection and Isolation of Induction Motors Using Recurrent Neural Networks and Dynamic Bayesian Modeling', *IEEE Transactions on Control Systems Technology,* vol.18, no.2, pp. 430-437.

Immovilli, F., Cocconcelli, M., Bellini, A. and Rubini, R. (2009) 'Detection of Generalised -Roughness Bearing Fault by Spectral-Kurtosis Energy of Vibration or Current Signals', *Industrial Electronics, IEEE Transactions on,* vol.56, no. 11, pp.4710-4717.

Immovilli, F., Bellini, A., Rubini, R. and Tassoni, C. (2010) 'Diagnosis of Bearing Faults in Induction Machines by Vibration or Current Signals: A Critical Comparison', *IEEE Transactions on Industry Applications,* vol. 46, pp. 1350-1359,doi: 10.1109/08IAS.2008.26.

Immovilli, F., Bianchini, C., Cocconcelli, M., Bellini, A. and Rubini, R. (2013) 'Bearing Fault Model for Induction Motor With Externally Induced Vibration', *IEEE Transactions on Industrial Electronics,* vol.60, no. 8, pp. 3408-3418.

Isermann, R. (2005) 'Model Based fault Diagnosis Fault Detection-status and Applications' and Diagnosis Systems*' , Annual Review In control,*vol 29, pp.71-85,doi :10.1016/j.arcontrol.2004.12.002.

Isermann, R. (2006) 'Fault Diagnosis Systems: An Introduction from Fault Detection to Fault Tolerance', *1st Edition* , SpringerSCience and Business Media, Germany.

Isermann, R.(2011) 'Fault Diagnosis applications*', 1st Edition*, Springer Heidelberg Dordrecht, UK.

Ivan, V. Peter, F., Mária K. (2013). 'Friction Effect Analysis of a DC Motor'. A*merican Journal of Mechanical Engineering*, vol. 1, no. 1, pp.1-5.

Jacek. F. 'Permanent magnet motor technology: design and applications', *3rd Edition*, CRC press, Taylor and Francis Group,2013, *London, UK*

Jayaswal, P.,Verma, S. and.adhwani, A. (2010) 'Application of ANN, Fuzzy Logic and Wavelet Transform in machine fault diagnosis using vibration signal analysis', *Journal of Quality in Maintenance Engineering*, vol.16, no. 2, pp.190-213.

Jens ,H. 'Rolling Element Bearings' Available online at: http://www.snipview.com/q/ Rolling-element_bearings.

Jiang, L., Yin, K. and Tang, W. (2013) 'Fault Diagnosis of Rolling Bearing Based on Feature-Level Fusion Method', *Applied Mechanics and Materials,* vol. 273, pp.260-263,doi:10.4028/www.scientific.net/AMM.273.260.

Jiang, L., Xuan, J. and Shi, T. (2013) 'Feature extraction based on semi-supervised kernel Marginal Fisher analysis and its application in bearing fault diagnosis', *Mechanical Systems and Signal Processing*, vol. l41, no.1–2, pp.113-126.

Jiang, j., Yin, k., Li, j. and Tang, w. (2014) 'Fault Diagnosis of Rotating Machinery Based on Multi sensor Information Fusion Using SVM and Time-Domain Features', *Journal of Shock and Vibration,*doi:418178.

Jian , Z,. Yangwei, Y. (2011).'Brushless DC Motor Fundamentals Application Note' Available online at: *https://www.monolithicpower. com/Portals/0/Documents/ Products/Documents/ appnotes/Brushless%20DC%20Motor%20Fundamentals .pdf.*

Jiancheng, F., Wenzhuo, L. and Haitao, L. (2014) 'Self-Compensation of the Commutation Angle Based on DC-Link Current for High-Speed Brushless DC Motors With Low Inductance', *IEEE Transactions on Power Electronics,* vol. 29, no. 1, pp. 428-439.

Jieping, Y., Janardan, R., Cheong Hee, P. and Haesun, P. (2004) 'An optimisation criterion for generalised discriminant analysis on under sampled problems', *IEEE Transactions on Pattern Analysis and Machine Intelligence*, vol. 26, no.8, pp. 982-994.

Jin, X., Zhao, M., Chow, T. and Pecht, M. (2014) 'Motor Bearing Fault Diagnosis Using Trace Ratio Linear Discriminant Analysis'. *IEEE Transactions on Industrial Electronics*, vol.62, no.1, pp.2441-2451.

Jha, B., Yadav, B., Rao, M. and Yadav,. L. (2013) 'Selection of Optimal Mother Wavelet for Fault Detection Using Discrete Wavelet Transform', *International Journal of Advanced Research in Electrical, Electronics and Instrumentation Engineering,* vol. 2, no. 6, pp.2338-2343.

Joyce, C., Skikne, S., Simpson, E. and Nee, J. (2014) 'Brushed DC Motor Theory and Operation', avilable online at: *http://c31joyce.herokuapp.com/static/PDFs/E-M_proj.pdf.*

Jun, H., Jianzhong, Z., Ming, C. and Zheng, W. (2013) 'Fault diagnosis of mechanical unbalance for permanent magnet synchronous motor drive system under nonstationary condition', *IEEE Energy Conversion Congress and Exposition* , USA, pp. 3556-3562,doi:10.1109/ECCE.2013.6647169.

Jung, S., Jin, P., Hag, K., KWan, C. and Myung, Y. (2013) 'An MRAS-Based Diagnosis of Open-Circuit Fault in PWM Voltage-Source Inverters for PM Synchronous Motor Drive Systems', *IEEE Transactions on Power Electronics,* vol. 28, no.6 , pp. 2514-2526.

Kankar, K., Sharma, C. and Harsha, P. (2011) 'Fault diagnosis of ball bearings using machine learning methods', *Expert Systems with Applications,* vol. 38, no.3, pp.1876-1886.

Kankar, K., Sharma, C. and Harsha, P. (2011) 'Fault diagnosis of ball bearings using continuous wavelet transform', *Applied Soft Computing,* vol. 11, no.2, pp.2300-2312.

Keskes, H., Braham, A. and Lachiri, Z. (2013) 'Broken rotor bar diagnosis in induction machines through stationary wavelet packet transform and multiclass wavelet SVM', *Electric Power Systems Research*, vol. 97, no.8, pp.151-157.

Khan, M. and Rahman, A. (2009) 'Development and Implementation of a Novel Fault Diagnostic and Protection Technique for IPM Motor Drives', *IEEE Transactions on Industrial Electronics,* vol. 56, no.1, pp.85-92.

Kharche, P. and Kshirsagar, V. (2014) 'Review of Fault Detection in Rolling Element Bearing', *Engineering Asset Lifecycle Management*, pp.596-602, doi:10.1007/9 78-0-85729-320-6_69.

Khushaba, N., Al-Ani, A. and Al-Jumaily, A. (2010) 'Orthogonal Fuzzy Neighborhood Discriminant Analysis for Multifunction Myoelectric Hand Control', *IEEE Transactions on Biomedical Engineering*, vol. 57, no. 6, pp.1410-1419.

Kim, T., Lee, W. and KWak, S. (2009) 'The internal fault analysis of brushless dc motors based on the winding function theory', *IEEE Transactions on Magnetics,* vol .45, no.5, pp. 2090-2096.

Krishnan, R. (2001) 'Electric Motor Drives Modeling, Analysis and Control*',* Prentice Hall, Inc. 1st Edition, USA.

Krishnan, R. (2010) 'Permanent Magnet synchronous and Brushless DC Motor Drives' Taylor & Francis groube,1St Edition, USA.

Kurfess, T., Billington, S. and Liang, S. (2006) *'Advanced Diagnostic and Prognostic Techniques for Rolling Element Bearings' Condition Monitoring and Control for Intelligent Manufacturing,Springer Series in Advanced Manufacturing,* pp.137165, doi:10.1007/1-84628-269-1_6.

Kuphaldt, R. (2009) 'Lessons In Electric Circuits*',* A free series of textbooks on the subjects of electricity and electronics *available on line at: http://www. ibiblio. org/kuphaldt/electricCircuits/.*

Kyung, K., Seung, L. and Jin, H. (2014) 'Diagnosis Technique Using a Detection Coil in BLDC Motors With Inter turn Faults', *IEEE Transactions on Magnetics,* vol. 50, no.2, pp. 885-888.

Lau, C. and Ngan, W. (2010) 'Detection of Motor Bearing Outer Raceway Defect by Wavelet Packet Transformed Motor Current Signature Analysis', *IEEE Transactions on Instrumentation and Measurement,* vol. 59 , no.10, pp. 2683-2690.

Lee, J., Wu, F., Zhao, W., Ghaffari, M., Liao, L. and Siegel, D. (2014) 'Prognostics and health management design for rotary machinery systems Reviews, methodology and applications', *Mechanical Systems and Signal Processing,* vol. 42, no.1-2, pp. 314-334.

Lemos, A., Caminhas, W. and Gomide, F. (2013) 'Adaptive fault detection and diagnosis using an evolving fuzzy classifier', *Information Sciences,* vol. 220, pp.64-85, doi:10.1016/j.ins.2011.08.030.

Li, K., Ping, X., Wang, H., Chen, P. and Cao, Y. (2013) 'Sequential Fuzzy Diagnosis Method for Motor Roller Bearing in Variable Operating Conditions Based on Vibration Analysis', *Sensors,* vol. 13, pp. 8013-8041, doi:10.3390/s130608013.

Li, L., Ma, L. and Khorasani, K. (2005) 'A Dynamic Recurrent Neural Network Fault Diagnosis and Isolation Architecture for Satellite's Actuator/Thruster Failures' *in Advances in Neural Networks,* Springer Berlin Heidelberg, pp.574-583.

Li, H., Zhao, J., Zhang, X., Teng, H., Yang, R. and Hao, L. (2014) 'Bearing Fault Diagnosis Method Using Envelope Analysis and Euclidean Distance', *TELKOMNIKA Indonesian Journal of Electrical Engineering,* vol.12, no.3, pp.1887-1894.

Lin, J. and Qu, L. (2000) 'Feature Extraction Based on Morlet Wavelet and Its Application for Mechinecal Fault Diagnosis', *Journal of Sound and Vibration,* vol.234, no.1, pp.135-148.

Lin, T., Horne, G., Tino, P. and Giles, L. (1996) 'Learning long-term dependencies in NARX recurrent neural networks', *Neural Networks, IEEE Transactions on,* vol.7, no.6, pp.1329-1338.

Lindh, T. (2003) 'On The condition monitoring of induction motors', *Ph.D Thesis*, Lappeenranta University of Technology, Finland.

Liu, G. (2002) 'Nonlinear identification and control: a neural network approach', *Industrial Robot: An International Journal,* vol.29, no.5, pp.469-470.

Liu, P. (2010) 'Robust fault detection observer and fault estimation filter design for LTI systems based on GKYPLemma ', *European Journal of Control*, pp.366-383.doi:10.3166/EJC.16.336-383.

Liu, W., Liu, L., Chung, Y., Cartes, A. and Zhang, W. (2012) 'Modeling and detecting the stator winding fault of permanent magnet synchronous motors', *Simulation Modelling Practice and Theory,* vol. 27, pp.1-16,doi:10.1016/j.simpat.2012.04.007.

Liu, X., Ma, L. and Mathew, J. (2009) 'Machinery fault diagnosis based on fuzzy measure and fuzzy integral data fusion techniques', *Mechanical Systems and Signal Processing,* vol.23, no.3, pp. 690-700.

Liying, J., Xinxin, F., Jianguo, C. and Zhonghai, L. (2013) 'Rolling element bearing fault diagnosis using recursive wavelet and SOM neural network'*,* 25th Chinese Conference on Control and Decision, pp. 4691, doi:4696.doi:101109/ CCDC. 20 13.656178.

Lu, M., Masrur, A., Zhihang, C. and Baifang, Z. (2006) 'Model-based fault diagnosis in electric drives using machine learning', *IEEE/ASME Transactions on Mechatronics,*vol.11, no.3, pp.290-303.

MacKay, C. (1992). 'A practical Bayesian framework for backprop networks', available on line at: http://citeseerx.ist. psu.edu/viewdoc/download? doi=10.1.1.29.274& rep=rep1 &type=pdf*Neural Comp.* 4, 448472.

MacKay, C. (2005).'Information Theory, Inference, and Learning Algorithms', Version 7.2, Cambridge University Press, UK.

Mahammed, A. and Hiyama, T. (2011) 'Fault Classification Based Artificial Intelligent Methods of Induction Motor ', *International journal of Innovative computing information and Control,* vol. 7, no. 9, pp. 5477-5493.

Mao, K. and Wu, Y. (2011) 'Fault Diagnosis of Rolling Element Bearing Based on Vibration Frequency Analysis'*, Third International Conference on Measuring Technology and Mechatronics Automation* , China, pp. 198-201, doi:10.1109/I CMTMA.2011.337.

Mathew, M., Jayakumar, M. and Jaleel, A. (2012) 'Fault detection in brushless DC motors using Discrete Square Root Filtering and fuzzy logic*',* international Conference on Computing, Electronics and Electrical Technologies , India, pp. 12-17, doi:10.1109/ICCEET.2012.6203736.

Nakhaeinejad, M., Choi, J. and Bryant, M. (2011) 'Model-Based Diagnostics and Fault Structural Health Monitoring', *Shock and Vibration*, Springer New York, vol.11, pp. 439-449, doi:10.1007/978-1-4419-9428-8_37.

Martin, B., Marie, C., Jérémi, R. and Jean, F. (2006) 'Mechanical Load Fault Detection in Induction Motors by Stator Current Time-Frequency Analysis', *IEEE Transactions on Industry Applications,* vol. 42, pp. 1454-1463,doi:10.1109/IEM DC.2005.195977.

McClelland, L., Rumelhart, E. and Group, R. (1986) 'Parallel distributed processing', Explorations in the microstructure of cognition*', A Bradford Book* , vol.2.

Mcbain, J. and Timusk, M. (2011) 'Feature extraction for novelty detection as applied to fault detection in machinery', Pattern Recognition Letters, vol.32, no. 7, pp.1054-1061.

Merzouki, R., Samantaray, A., Pathak, P. and Ould , B. (2013) 'Model-Based Fault Diagnosis and Fault Tolerant Control' in *Intelligent Mechatronic Systems*, Springer London, pp. 577-617 ,doi:10.1007/978-1-84882-653-3_1.

Misiti, M., Misiti, Y., Oppenheim, G. and Poggi, J. (2014) 'Wavelet Toolbox User's Guide (R2014b)', available online at: http://www.ltu.se/cms_fs/1.51590! /wavelet%20toolbox%204%20user's%20guide%20(introduction%20+%20p.%2 02-5%20 to%202-58%20only).pdf.

Mitoma, T., Wang, H. and Chen, P. (2008) 'Fault diagnosis and condition surveillance for plant rotating machinery using partially-linearized neural network', *Computers and Industrial Engineering*, vol.55, no.4, pp.783-794.

Mohammed, A., Liu, S. and Liu, Z. (2005) 'Physical modeling of Permanent Magnet synchronous motors for integrated coupling with machine drives', *IEEE Transactions on Magnetics,* vol. 41, no.5, pp. 1628-1631.

Mohammed, A., Liu, S. and Liu, Z. (2006) 'FE-based Physical Phase Variable Model of PM Synchronous Machines with Stator Winding Short Circuit Fault*',IET Science, Measurement and Technology*,vol. 1, no.1, pp. 12 -16.

Mohammadi, R., Naderi, E., Khorasani, K. and Hashtrudi, S. (2011) 'Fault diagnosis of gas turbine engines by using dynamic neural networks', *IEEE International Conference on Quality and Reliability*, Thailand, pp.25-30, doi:101109/CQR. 2011.6031675.

Moseler, O., Juricic, D., Rakar, A. and Muller, N (1999). 'Model-based fault diagnosis of an actuator system driven by the brushless DC motor*',* Proceedings of the American Control Conference, vo.6, pp. 3779-3783, doi:10.1109/ACC.1999. 786214.

Moosavian, A., Ahmadi, H., Sakhaei, B. and Labbafi, R. (2014) 'Support vector machine and K-nearest neighbour for unbalanced fault detection', *Journal of Quality in Maintenance Engineering,* vol. 20, no.1, pp. 65-75.

Maxon, m. (2010) 'DC and BLDC Motors with Permanent Magnets', online available at: http://www.electromate.com/ftp/public/Maxon%20DC%20Moto or%20Sizing% 20Made%20Easy%20Presentation%20English%20Version%20March%202010/ 2_DcBldcMotor.pdf.

Motion Control Products Ltd (2009) 'DSD806 Digital Servo Drive data Sheet' *online available online at: http://www.motioncontrolproducts.com/pdfs/DSD806-digit al- servo- drive.pdf.*

Niang, O., Deléchelle, É. and Lemoine, J. (2010) 'A spectral approach for sifting process in empirical mode decomposition', *IEEE Transactions on Signal Processing,* vol. 58, no, 11, pp. 5612-5623.

Ngui, K., Leong, S., Hee, M. and Abdelrhman, M. (2013) ' Classification and Analysis of Speech Abnormalities ', *Applied Mechanics and Materials*, vol.26, no5, pp.953-958.

Obuchowski, J., Wyłomańska, A. and Zimroz, R. (2014) 'The local maxima method for enhancement of time–frequency map and its application to local damage detection in rotating machines', *Mechanical Systems and Signal Processing*, vol.46, no.2, pp.389-405.

Olivier, O., Emmanuel, B., Eric, B. and Guy, C. (2012) 'Coupling Pattern Recognition With State Estimation Using Kalman Filter for Fault Diagnosis', *IEEE Transactions on Industrial Electronics,* vol. 59 , no. 11, pp. 4293-4300.

Olsson, E. (2009) 'Fault Diagnosis of industrial Machines using Sensor Signals and Case Based Reasoning' *PhD thesis*, School of Innovation, Design and Engineering, Mälardalen University, Sweden.

Ojaghi, M., Sabouri, M. and Faiz, J. (2014) 'Diagnosis methods for stator winding faults in three-phase squirrel-cage induction motors', *International Transactions on Electrical Energy Systems*, vol. 24, no.6, pp.891–912.

Ovedo, S., Quiroga, J. and Borras, C. (2011) 'Motor current Signature Analysis and Negative Sequence Current Based stator Winding Short Fault Detection In an Induction Motor ', *DYNA,* vol.78, no.170, pp.214-220.

Oyvind S, 2006'Control of Marine Propellers from Normal to Extreme Conditions. *PhD-thesis*, University of Science and Technology, Department of Marine Technology, Norway

Pandya, H., Upadhyay, H. and Harsha, P. (2013) 'Fault diagnosis of rolling element bearing with intrinsic mode function of acoustic emission data using APF-KNN', *Expert Systems with Application*s, vol.40, no.10, pp.4137-4145.

Pandya, H., Upadhyay, H. and Harsha, P. (2014) 'Fault diagnosis of rolling element bearing by using multinomial logistic regression and wavelet packet transform', *Soft Computing,* vol.18, pp. 255-266, doi:10.1007/s00500-013-1055-1.

Patan, K. (2008) 'Artificial Neural Networks for the Modelling and Fault Diagnosis of Technical Processes ABC*', 1st Edition Springer-Verlag Berlin Heidelberg,* doi:*10.1007/978-3-540-79872-9*.

Patil, M., Mathew, J., Rajendrakumar, P. and Desai, S. (2010) 'A theoretical model to predict the effect of localised defect on vibrations associated with ball bearing', *International Journal of Mechanical Sciences,* vol. 52, no. 9, pp. 1193-1201.

Peng, K. and Chu, L. (2004) 'Application of the wavelet transform in machine condition monitoring and fault diagnostics: a review with bibliography', *Mechanical Systems and Signal Processing*, vol.18, no.2, pp.199-221.

Perrier, V., Philipovitch, T. and Basdevant, C. (1995) 'Wavelet spectra compared to Fourier spectra', *Journal of Mathematical Physics*, vol.36, no.3, pp.1506-1519.

Phinyomark, A., Nuidod, A., Phukpattaranont, P. and Limsakul, C. (2012) 'Feature Extraction and Reduction of Wavelet Transform Coefficients for EMG Pattern Classification', *Electrical and Electronics Engineering*, vol.122, no. 6, pp.27-32.

Ping, Z. A., Juan, Y. and Ling, W. (2013) 'Fault Detection of Stator Winding Interturn Short Circuit in PMSM Based on Wavelet Packet Analysis', Fifth International Conference on Measuring Technology and Mechatronics Automation , pp.566-569, doi:10.1109/ICMTMA.2013.141.

Prieto, D., Roura, J. and Martínez, R. (2011) 'Bearings Fault Detection Using Inference Tools' '*Vibration Analysis and Control New Trends and Developments'* Chapter 13,open access, *InTech*, pp.307-433, doi:10.5772/22696.

Prieto, D., Cirrincione, G., Espinosa, G., Ortega, A. and Henao, H. (2013) 'Bearing Fault Detection by a Novel Condition-Monitoring Scheme Based on Statistical-Time Features and Neural Networks', *IEEE Transactions on Industrial Electronics*, vol.60, no.8, pp.3398-3407.

Progovac, D., Wang Y. and Yin, G. (2014) 'Parameter estimation and reliable fault detection of electric motors', *Control Theory and Technology,* vol.12, no.2, pp. 110-121.

Qian , L. and Daqi , Z. (2009) 'Fault-tolerant Control of Unmanned Underwater Vehicles with Continuous Faults: Simulations and Experiments', *International Journal of Advanced Robotic Systems,* vol 6, no.4, pp.301-308.

Qin, H., Luo, H. and Eklund, N. (2009) 'On-Board Bearing Prognostics in Aricraft Engine, Enveloping Analysis or FFT', *ninth International Design Engineering Technical Conferences*, USA, pp. 1-7,doi:10.1115/DETC2009-86141.

Qing, Z, Qin, S, and Qin, A. (2013) 'Concurrent Fault Diagnosis for Rotating Machinery Based on Vibration Sensors', *International Journal of Distributed Sensor Network*,vol.2013 pp. 1-10, doi: org/10.1155/2013/472675.

Rafiee, J., Tse, P., Harifi, A. and Sadeghi, M. (2009) 'A novel technique for selecting mother wavelet function using an intelli gent fault diagnosis system', *Expert Systems with Applications*, vol.36, no.3, pp.4862-4875.

Rajagopalan, S., Habetler, G., Harley, G., Aller, M. and Restrepo, A. (2005) 'Diagnosis of rotor faults in brushless DC (BLDC) motors operating under non-stationary conditions using windowed Fourier ridges'*, Fourtieth IAS Annual Meeting. Conference on Industry Applications,* vol.1, pp. 26-33, doi:10.1109/TAS.2005. 1518287.

Rajagopalan, S., Aller, M., Restrepo, A., Habetler, G. and Harley, G. (2006) 'Detection of Rotor Faults in Brushless DC Motors Operating Under Nonstationary Conditions', *IEEE Transactions on* Industry Applications, vol.42 , no.6,pp.1464-1477.

Riera, M., Antonino, A., Pineda, M., Puche, R. and Perez, J. (2008) 'A General Approach for the Transient Detection of Slip-Dependent Fault Components Based on the Discrete Wavelet Transform', *IEEE Transactions on Industrial Electronics*, vol.55, no.12, pp.4167-4180.

Roy, S., Mohanty,R. and Kumar, S. (2014) 'Fault detection in a multistage gearbox by time synchronous averaging of the instantaneous angular speed', *Journal of Vibration and Control*, pp. 1-13, doi:10.1177/1077546314533582.

Sadough, N., Khorasani, K. and Meskin, N. (2014) 'Fault detection and isolation of a dual spool gas turbine engine using dynamic neural networks and multiple model approach', *Information Sciences,* vol. 259, pp.234-251, doi:10.1016/j.ins .2013.05.032.

Sakthivel, N., Nair, B., Elangovan, M., Sugumaran, V. and Saravanmurugan, S. (2014) 'Comparison of dimensionality reduction techniques for the fault diagnosis of mono block centrifugal pump using vibration signals', *Journal,of Engineering Science and Technology, an International* vol.17, no.1, pp.30-38.

Saleh, A. and Rahman, A. (2005) 'Modeling and protection of a three-phase power transformer using wavelet packet transform', *IEEE Transactions on Power Delivery*, vol.20, no.2, pp.1273-1282.

Salah, M., Bacha, K. and Chaari, A. (2013) 'Load torque effect on diagnosis techniques consistency for detection of mechanical unbalance*',* International Conference on Control, Decision and Information Technologies, Tunisia, pp. 770-775,doi :10. 1016/j.ins.2013.05.032.

Sawalhi, N. (2007) 'Diagnostics, prognostics and fault simulation for rolling element bearings', PhD thesis, School of Mechanical and Manufacturing Engineering, University of New South Wales, UK.

Sawalhi, N. and Randall, B. (2011) 'Vibration response of spalled rolling element bearings: Observations, simulations and signal processing techniques to track the spall size', *Mechanical Systems and Signal Processing,* vol.25, no.3, pp.846-870.

Schröder, J. (2006) 'Diagnosis and Fault-Tolerant Control*',* 2nd Edition Springer Verlag Berlin Heidelberg, doi:10.1007/978-3-540-35653-0.

Seshadrinath, J., Singh, B. and Panigrahi, K. (2014) 'Investigation of Vibration Signatures for Multiple Fault Diagnosis in Variable Frequency Drives Using Complex Wavelets', *IEEE Transactions on Power Electronic*s, vol.29, no.2 pp.936-945.

Shakouhi, M., Mohamadian, M. and Afjei, E. (2012) 'Torque control of permanent magnet BLDC motor during static eccentricity fault*', 3rd IEEE Power Electronics and Drive Systems Technology Conference,* Iran, pp. 284-289, doi:10.1109/PEDSTC.2012.6183342.

Sharma, R., Kumar, A. and Kankar, P. (2014).'Ball Bearing Fault Diagnosis Using Continuous Wavelet Transforms with Modern Algebraic Function', Advances in Intelligent Systems and Computing , Springer, vol. 236 , pp.313-322, doi:10. 10 07/978-81-322-1602-5_35.

Sharma, A., Amarnath, M. and Kankar, P. (2014) 'Feature extraction and fault severity classification in ball bearings', *Journal of Vibration and Control,* pp. 1-17, doi:10.1177/1077546314528021.

Shen, Y., Hao, L. and Ding, X. (2014) 'Real-Time Implementation of Fault-Tolerant Control Systems With Performance Optimisation', *IEEE Transactions on Industrial Electronics,* vol 61, no. 5, pp. 2402-2411.

Sina , Sadough , N. and Khorasani, K. (2014) 'Dynamic neural network-based fault diagnosis of gas turbine engines', *Neurocomputing,* vol.125, pp. 153-165, doi: 10.1016/j.neucom.2012.06.050.

Sobhani, E. and Khorasani, K. (2009) 'Fault Diagnosis of Nonlinear Systems Using a Hybrid Approach'*,* Series: Lecture Notes in Control and Information Sciences, Springer. doi:10.1007/978-0-387-92907-1.

Spyropoulos, D. and Mitronikas, E. (2013) 'A Review on the Faults of ElectricMachines Used in Electric Ships', *Advances in Power Electronics,* vol 2013, pp. 1-8, doi:org/10.1155/2013/216870.

Subhasis., N., Hamid , T. and Xiaodong, L. (2005) 'Condition Monitoring and Fault Diagnosis of Electrical Motors A Review', *IEEE Transactions on Energy Conversion,* vol. 20, no.4, pp. 719-729.

Sun, J., Chai, Y., Su, C., Zhu, Z. and Luo, X. (2014) 'BLDC motor speed control system fault diagnosis based on LRGF neural network and adaptive lifting scheme', *Applied Soft Computing,* vol. 14, no.4, pp. 609-622,doi:10.1016/j.asoc.2013. 10.010.

Taher, A., Malekpour, M. and Farshadnia, M. (2014) 'Diagnosis of broken rotor bars in induction motors based on harmonic analysis of fault components using modified adaptive notch filter and discrete wavelet transform', S*imulation Modelling Practice and Theory*, pp.26-41,doi:101016/j.simpat.2014.02.006.

Tashakori, A. and Ektesabi, M. (2013) 'A simple fault tolerant control system for Hall Effect sensors failure of BLDC motor'*, 8th IEEE Conference on Industrial Electronics and Applications*, Australia, pp. 1011-1016, doi:10.1109/ICIEA. 2013.6566515.

Tavner, P., Ran, L., Penman, J. and Sedding, H. (2008) 'Condtion Monitoring of Rotating Electrical Machines', *2nd Edition, The Institution of engineering and Technology*, UK.

Tavner, J. (2008) 'Review of condition monitoring of rotating electrical machines', Electric Power Applications'*, IET Journal ,* vol. 2, no.4, pp.215-247.

Tehrani, E. and Khorasani, K. (2009) 'Fault diagnosis of nonlinear system using hybrid model' *Lecture Notes in Control and Information Sciences*,1st ed, springer Dordrecht Heidelberg.

Tenconi, A., Vaschetto, S. and Vigliani, A. (2014) 'Electrical Machines for High-Speed Applications: Design Considerations and Tradeoffs', *IEEE Transactions on Industrial Electronics,* vol. 61, no.6, pp. 3022-3029.

Tiwari, R., Kankar, P. and Gupta, V. (2014) 'Fault Diagnosis of Ball Bearings Using Support Vector Machine and Adaptive Neuro Fuzzy Classifier', *Proceedings of the Second International Conference on Soft Computing for Problem Solving*, Springer India, pp. 1477-1482,doi:10.1007/978-81-322-1602-5_148.

Toliyat, A. (2002) 'Condition Monitoring and Fault Diagnosis of Electric Machinery', Texas A and M University, USA, available online at: http://groups. engine.umd .umich.edu/vi/w2_workshops/fault_diagnosis_Toliyat_w2.pdf.

Torkaman, H., Moradi, R., Hajihosseinlu, A. and Toulabi, S. (2014) 'A comprehensive power loss evaluation for Switched Reluctance Motor in presence of rotor asymmetry rotation: Theory, numerical analysis and experiments', *Energy Conversion and Management,* vol. 77, pp. 773-783.

Trajin, B., Regnier, J. and Faucher, J. (2009) 'Comparison Between Stator Current and Estimated Mechanical Speed for the Detection of Bearing Wear in Asynchronous Drives', *IEEE Transactions on Industrial Electronics,* vol. 56, no.11, pp. 4700-4709.

Utthiyuung, T., Premrudeepreechacharn., S., Utthiyuung, T., Kruepengkul., K. and Puongkaew, P. (2002) 'Induction motor fault detection and diagnosis using supervised and unsupervised neural network*',* *IEEE International Conference on Industrial Technology* Thailand, vol.1, pp. 93-96, doi:10.1109/ICIT.2002.11 89869.

Valéria L., Jonas, S., Giscard, V., Luiz, S, Erik Leandro, B., and Levy, O (2015). 'Detection of Localized Bearing Faults in Induction Machines by Spectral Kurtosis and Envelope Analysis of Stator Current', *IEEE Transaction on Industrial Electronics*, vol. 62, no. 3, pp.1855-1865.

Van, J., Postma, O. and van , J. (2009) 'Dimensionality reduction: A comparative review', *Journal of Machine Learning Research*, vol.10, no.1-41, pp.66-71.

Villa, F., Reñones, A., Perán, R. and de Miguel, J. (2012) 'Statistical fault diagnosis based on vibration analysis for gear test-bench under non-stationary conditions of speed and load', *Mechanical Systems and Signal Processing,* vol 29, pp.436-446 ,doi:10.1016/j.ymssp.2011.12.013.

Villani, M., Tursini, M., Fabri, G. and Castellini, L. (2012) 'High reliability permanent magnet brushless motor drive for aircraft application', *IEEE Transactions on Industrial Electronics,* vol. 59, no.5, pp. 2073-2081.

Walker, B., Vayanat, R., Perinpanayagam, S. and Jennions, K. (2014) 'Unbalance localization through machine nonlinearities using an artificial neural network approach', *Mechanism and Machine Theory,* vol. 75, pp. 54-66, doi:10.1016/j.m echmachtheory.2014.01.006.

Wang, T., Liang, M., Li, J. and Cheng, W. (2014) 'Rolling element bearing fault diagnosis via fault characteristic order (FCO) analysis', *Mechanical Systems and Signal Processing*, vol.45, no. 1, pp.139-153.

Wang, X., Ma, L. and Wang, T. (2014) 'An optimised nearest prototype classifier for power plant fault diagnosis using hybrid particle swarm optimisation algorithm', *International Journal of Electrical Power & Energy Systems,* vol 58, pp. 257-265, doi:10.1016/j.ijepes.2014.01.016.

Weilin, L., Monti, A. and Ponci, F. (2014) 'Fault Detection and Classification in Medium Voltage DC Shipboard Power Systems With Wavelets and Artificial Neural Networks', *IEEE Transactions on Instrumentation and Measurement*, vol.63, no.11, pp.2651-2665.

Wen, X. (2011) 'A hybrid intelligent technique for induction motor condition monitoring', *PhD thesis, Institute of Industrial Research, University of Portsmouth*, UK.

Wenping, C., Mecrow, C., Atkinson, J., Bennett, W. and Atkinson, J. (2012) 'Overview of Electric Motor Technologies Used for More Electric Aircraft (MEA)', *IEEE Transactions on Industrial Electronics,* vol. 59, no.9, pp. 3523-3531.

Wu, D. and Liu, H. (2008) 'Investigation of engine fault diagnosis using discrete wavelet transform and neural network', *Expert Systems with Applications*, vol. 35 , no.3, pp.1200-1213.

Wu, Y., Lai, H. and Lin, S. (2013) 'Featur Extracrtion for Bearing detection Iden-Tification Under variable Rotation Speed', in *20th International Congress on sound and Vibration,* Thailand, pp.1-6.

Xiangli, K., Ma, R., Zhang, Q. and Wang, W. (2014) 'Modeling and Simulation of Short Circuit Faults in Stator Coils of Brushless DC Motor' *Mechatronics and Automatic Control Systems*, *Springer International Publishing, Springer*, vol. 237, pp. 35-45, doi:10.1007/978-3-319-01273-5_4.

Xiaohang, J., Mingbo, Z. and Tommy , C. (2013) 'Motor Bearing Fault Diagnosis Using Trace Ratio Linear Discriminant Analysis ', *IEEE Industrial Electronics Society*, vol 61, no.5, pp. 1-11.

Xiaohang, J., Tommy, S. and KWo , T. (2014) 'Online Anomaly Detection of Brushless DC Motor Using Current Monitoring Technique', *International Journal of Performability,* vol. 10, no.3, pp. 263-271.

Xiao,W., Xiao, L.and Yao, L. (2013) 'Fault Diagnosis of Drilling Process Based on Rough Set and Support Vector Machine', *Advanced Materials Research,* vol.709, pp. 266-272 ,doi:10.4028/www.scientific.net/AMR.709.266.

Xuhong, W. and Yigang, H. (2005) 'Diagonal recurrent neural network based on-line stator winding turn fault detection for induction motors*' , Proceedings of the Eighth International Conference on Electrical Machines and Systems,* vol.3, pp.2266-2269, doi:10.1109/ICEMS.2005.202972.

Yahia, K., Cardoso, A., Ghoggal, A. and Zouzou, S. (2014) 'Induction motors airgap-eccentricity detection through the discrete wavelet transform of the apparent power signal under non-stationary operating conditions', *ISA Transactions*, vol.53, no.2, pp.603-611.

Yan, R., Gao, X. and Chen, X. (2014) 'Wavelets for fault diagnosis of rotary machines: A review with applications', *Journal of Signal Processing*, vol.96, pp.1-15, doi:10.1016/j.sigpro.2013.04.015.

Yan, D., Liang, X., Huang, J. and Guo, H. (2014) 'No Coupling Test Method for Brushless DC Motor Based on Model Identification', *Unifying Electrical Engineering and Electronics Engineering*, Springer, USA, pp.775-782,doi:10.1007/978-1-4614-4981-2_84.

Yang, Y., Wang, H., Cheng, J. and Zhang, K. (2013) 'A fault diagnosis approach for roller bearing based on VPMCD under variable speed condition', *Measurement,* vol. 46, no.8, pp. 2306-2312.

Yao, D. and Toliyat, H. (2012) 'A review of condition monitoring and fault diagnosis for permanent magnet machines'*, IEEE Coinference on Power and Energy Society General Meeting,* USA, pp. 1-4, doi:10.1109/PESGM.2012.6345545.

Yedamale, P. (2003) ' Brushless DC (BLDC) Motor Fundamentale', *Microchip.avilable online at:http://electrathonoftampabay.org/www/Documents/Motors/Brushless %20DC%20(BLDC)%20Motor%20Fundamentals.pdf.*

Yilmaz, S. and Ayaz, E. (2009) 'Adaptive neuro-fuzzy inference system for bearing fault detection in induction motors using temperature, current, vibration data', *IEEE EUROCON, Russia*, pp.1140-1145,doi:10.1109/EURCON.2009.5167779.

Yizhuo, Z., Guanghua, X., Lin, L. and Jing, W. (2009) 'Feature Extraction Methods for 'Fault Classification of Rolling Element Bearing Based on Nonlinear Dimensionality Reduction and SVMs', *International Conference on Artificial Intelligence and Computational Intelligence*, China pp. 228-234, doi:10.1109/AICI.2009.253.

Yousif, M. (2012) 'Recurrent Neural Network with Human Simulator Based Virtual Reality', *Intech*, pp.1-27, doi:10.5772/35538.

Yun, L., Yan, G., Jun, G. and Xian, J. (2013) 'Fault Diagnosis of Metallurgical Machinery Based on Spectral Kurtosis and GA-SVM', *Advanced Materials Research*, pp. 3958-3961, doi:10.4028/www.scientific.net/AMR.634-638.3958.

Yusuf, A., Brown, J., Mackinnon, A. and Papanicolaou, R. (2009) 'Application of Dynamic Neural Networks with Exogenous Input to Industrial Conditional Monitoring', *International joint Conference on Neural Networks*, USA, vol. 50, pp. 1-8, doi:10.1109/IJCNN.2013.6706762.

Zanardelli,. G., Strangas, G. and Aviyente, S. (2007) 'Identification of Intermittent Electrical and Mechanical Faults in Permanent-Magnet AC Drives Based on Time and Frequency Analysis', *IEEE Transactions on Industry Applications,* vol. 43, no.4, pp. 971-980.

Zarei, J., Tajeddini, A. and Karimi, R. (2014) 'Vibration analysis for bearing fault detection and classification using an intelligent filter', *Mechatronics,* vol. 24, no.2, pp. 151-157.

Zhang, Y., Zuo, H. and Bai, F. (2013) 'Classification of fault location and performance degradation of a roller bearing', *Measurement,* vol.46, no. 3, pp.1178-1189.

Zhenyu, Y., Uffe, M., and Morten, R. (2009) 'A Study of Rolling-Element Bearing Fault Diagnosis Using Motor's Vibration and Current Signatures', in *Preprints of the 7th IFAC Symposium on Fault Detection, Supervision and Safety of Technical Processes*, Spain, pp. 354-359, doi:10.3182/20090630-4-ES-2003.00059.

Zhou, H., Xiao, H., Zidong, W., Guo, L. and Ji, D. (2012) 'Leakage Fault Diagnosis for an Internet-Based Three-Tank System: An Experimental Study', *IEEE Transactions on Control Systems Technology,* vol.20, no.4, pp.857-870.

Zhu, J. (2008) 'Modelling, 'Simulation and Implemantation of a Fault Tolerant Permanent Magnet AC Motor Drive with Redudancy', PhD thesis, school of electrical and electronic engineering, University of Adelaide, Australia.

Ziaja, A., Antoniadou, I., Barszcz, T., Staszewski, J. and Worden, K. (2014) 'Fault detection in rolling element bearings using wavelet-based variance analysis and novelty detection', *Journal of Vibration and Control*, pp.1-15, doi:10.1177/1077 546314532859.

Ziani, R., Zegadi, R., Felkaoui, A. and Djouada, M. (2012) 'Bearing Fault Diagnosis Using Neural Network and Genetic Algorithms with the Trace Criterion' *Springer Berlin Heidelberg*, pp.89-96, doi:10.1007/978-3-642-28768-8_10.

Zouzou, E., Sahraoui, M., Ghoggal, A. and Guedidi, S. (2010) 'Detection of inter-turn short-circuit and broken rotor bars in induction motors using the Partial Relative Indexes: Application on the MCSA', International Conference on Electrical MAchines, Italy, pp. 1-6, doi:10.1109/ICELMACH.2010.5607874.

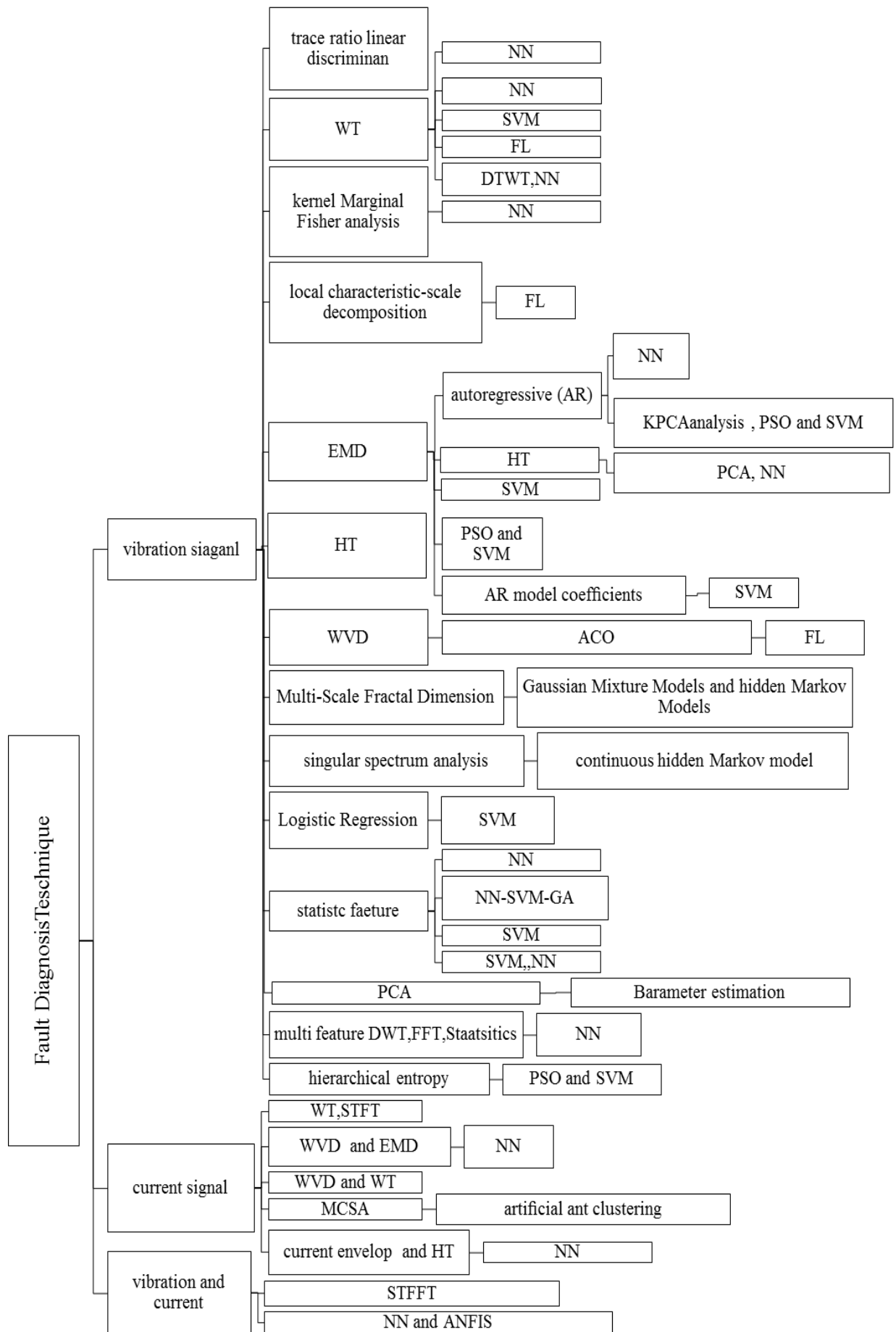# A: Fault diagnosis techniques based on available literature

Figure A-1 Electrical motor fault diagnosis approaches based on the available literature

B: Corrosion fault LAB simulator

Corrosion fault was simulated in the lab, including bearing de-lubrication and then measure the effect of chemical material on bearing surface that usual happen in industrial components

Figure B.1 bearing cleaning and remove lubrication for experimental test

Figure B.2 Measure the effect of chemical material on bearing structure
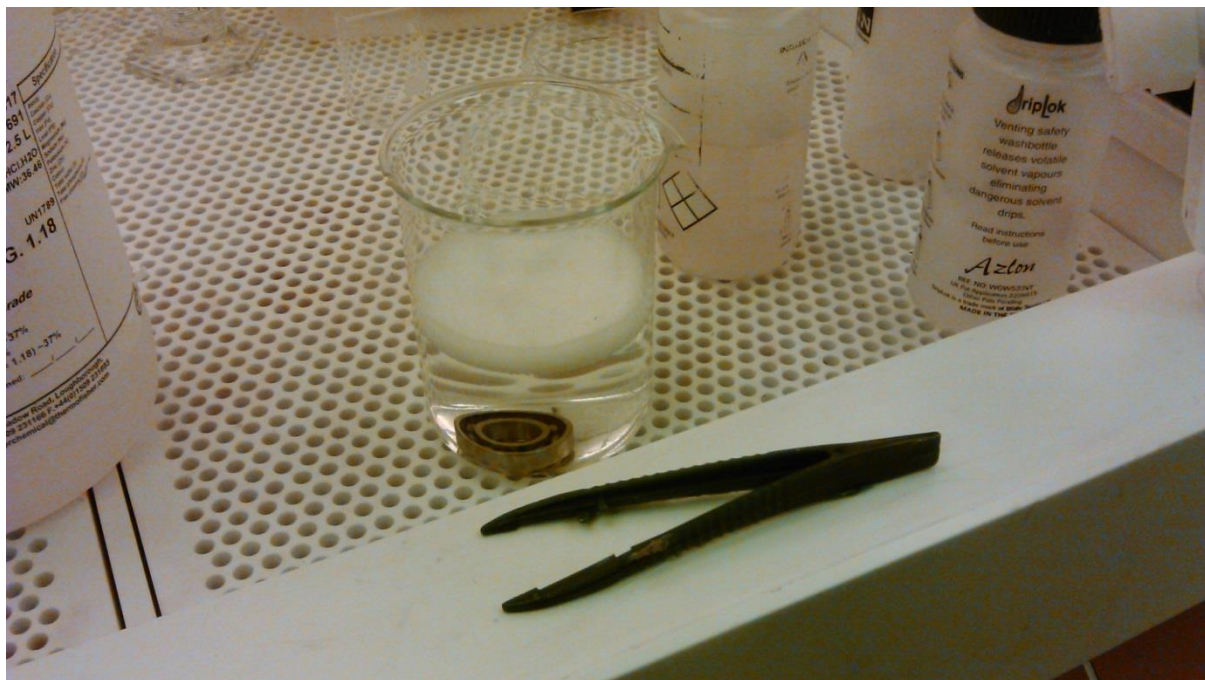
Figure B.3 Simulate bearing corrosion fault with different severities

Figure B.4 prepare bearing for experimental test
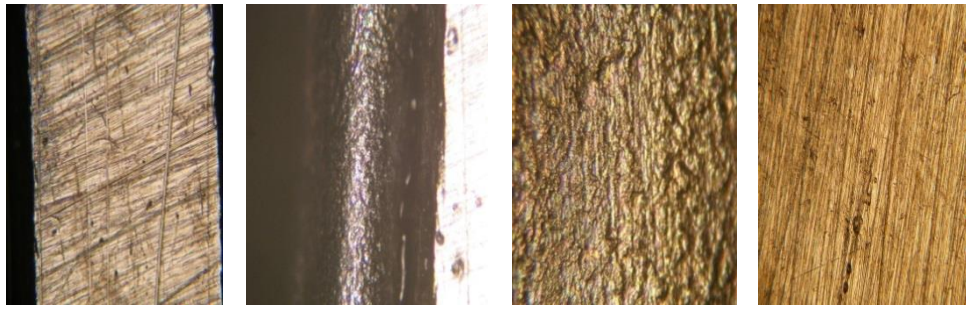
Normal
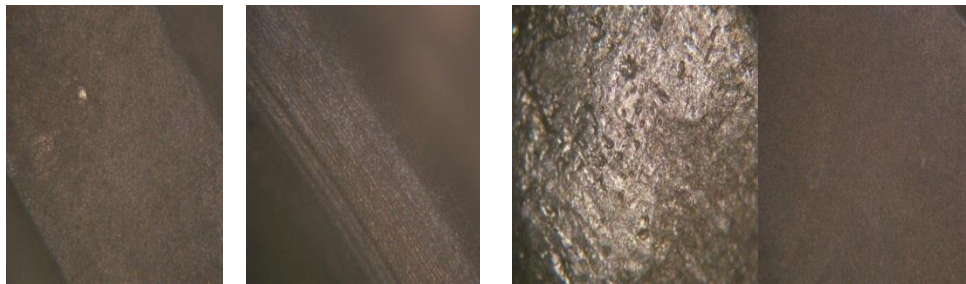
Severity 1
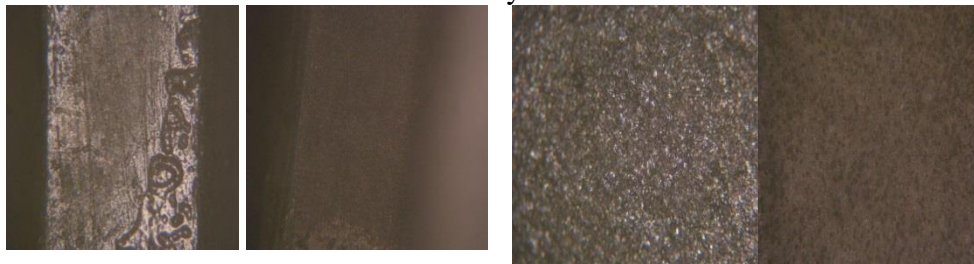
Severity 2

Severity 3

Severity 4

Figure B.5 different severities of the corrosion fault

C: Wavelet Transform

Table C-1 Wavelet transforms families

Wavelet family Name	Wavelet family (short name)	Order
Haar wavelet	$'haar'$	db_1
Daubechies wavelet	$'db'$	$db_2 - db_{45}$
Symlets	$'sym'$	$sym_2 - sym_{20}$
Coiflets	$'coif'$	$coif_1 - coif_5$
Biorthogonal wavelets	$'bior'$	$bior_{1.1} - bior_{6.8}$
Reverse biorthogonal wavelets	$'rbio'$	$rbio_{1.1} - rbio_{6.8}$
Meyer wavelet	$'meyr'$	$'meyr'$
Discrete approximation of Meyer	$'dmey'$	$'dmey'$
Gaussian wavelets	$'gaus'$	$gaus_1 - gaus_8$
Mexican hat wavelet	$'mexh'$	
Morlet wavelet	$'morl'$	$morl'$
Complex Gaussian wavelets	$'cgau'$	$cgau_1 - cagu_5$
Shannon wavelets	$'shan'$	$shan_{1-1.5}$ $shan_{1-1}$ $shan_{1-0.5}$ $shan_{1-0.1}$ $shan_{2-3}$
Frequency B-Spline wavelets	$'fbsp'$	$fbsp_{1-1-1.5}$ $fbsp_{1-1-1}$ $fbsp_{1-1-0.5}$ $fbsp_{2-1-1}$ $fbsp_{2-1-0.5}$ $fbsp_{2-1-0.1}$
Complex Morlet wavelets	$'comr'$	$cmor_{1-1.5}$ $cmor_{1-1}$ $cmor_{1-0.5}$ $cmor_{1-0.1}$

Table C.2 Wavelet energy (J) for different DWT decomposition details and distribution

(a) Inner race with defect size 0.2x1x3 mm at different loads (KW) and speeds (rpm) conditions

Load - speed	A	D1	D2	D3	D4	D5
No load - 600	49.9426	16.5860	33.2572	0.1310	0.0499	0.0334
No load - 900	51.2805	3.7726	42.1815	2.4608	0.2645	0.0401
No load - 1200	46.1757	17.3596	36.2472	0.1267	0.0572	0.0337
Half load - 600	59.9101	0.6067	12.6353	26.6153	0.1915	0.0412
Half load - 900	54.2367	3.4859	39.6218	2.3533	0.2623	0.0400
Half load - 1200	49.9426	16.5860	33.2572	0.1310	0.0499	0.0334
Full load- 600	16.5405	0.5161	26.9588	55.6328	0.3219	0.0299
Full load- 900	7.3913	7.1982	81.3613	3.5524	0.4884	0.0085
Full load-1200	4.2694	32.2635	63.3807	0.0645	0.0163	0.0056

(b) Inner race with defect size 0.5x1x6 mm at different loads (KW) and speeds (rpm) conditions

Load - speed	A	D1	D2	D3	D4	D5
No load - 600	10.5558	28.6206	60.4903	0.1995	0.0908	0.0429
No load - 900	15.8862	6.3541	72.8685	4.3614	0.4748	0.0550
No load - 1200	13.6850	28.5165	57.5193	0.1598	0.0796	0.0398
Half load - 600	15.9689	1.2501	28.0294	54.3413	0.3477	0.0626
Half load - 900	12.8014	6.5886	75.2766	4.7486	0.5000	0.0847
Half load - 1200	10.5558	28.6206	60.4903	0.1995	0.0908	0.0429
Full load- 600	4.5427	0.6492	34.7642	59.8127	0.2125	0.0187
Full load- 900	2.0807	7.3997	86.0884	3.9210	0.5006	0.0096
Full load-1200	2.6797	31.4408	65.7977	0.0547	0.0182	0.0088

(c) Inner race with defect size 3x1x9mm at different loads (KW) and speeds (rpm) conditions

Load - speed	A	D1	D2	D3	D4	D5
No load - 600	1.7403	34.9685	62.8872	0.2425	0.1040	0.0575
No load - 900	4.0098	6.5637	82.1207	6.8055	0.4018	0.0985
No load - 1200	3.1829	32.1487	64.2804	0.2369	0.0976	0.0536
Half load - 600	3.3386	1.5470	33.1371	61.6105	0.2942	0.0726
Half load - 900	1.9533	7.3789	84.4128	5.6596	0.5086	0.0868
Half load - 1200	1.7403	34.9685	62.8872	0.2425	0.1040	0.0575
Full load- 600	0.2821	0.5765	33.8741	65.1373	0.1087	0.0213
Full load- 900	0.0645	7.7618	87.8442	3.8003	0.5199	0.0093
Full load-1200	0.0592	34.3821	65.5115	0.0322	0.0102	0.0047

Table C.3 Energy (J) for different DWT decomposition details and approximation under non-stationary operating conditions for inner race defect

Speed	A	D1	D2	D3	D4	D5
Inner race with defect size 0.5x1x3 mm at variable load conditions						
600	55.6261	0.5288	13.5415	30.0590	0.2069	0.0376
900	44.3083	3.8649	48.2867	3.2501	0.2539	0.0361
1200	27.3136	23.5519	49.0068	0.0858	0.0273	0.0146
Inner race with defect size 0.5x1x6 mm at variable load conditions						
600	10.088	0.8815	30.0745	58.3943	0.4983	0.0616
900	4.3400	7.6323	83.9986	3.4823	0.5296	0.0173
1200	7.6460	30.023	62.1257	0.1207	0.0556	0.0290
Inner race with defect size 1x3x9 mm at variable load condition						
600	2.0993	13.1747	68.1087	16.1833	0.3686	0.0653
900	0.3374	7.6825	87.3806	4.0611	0.5212	0.0172
1200	0.1765	34.1775	65.5493	0.0695	0.0187	0.0084

Table C.4 Energy (J) for different DWT decomposition details and approximation under variable speeds conditions for inner race defect

Load	A	D1	D2	D3	D4	D5
Inner race with defect size 0.2x1x3 mm at variable speeds conditions						
No load	59.6051	5.2910	28.0593	6.8315	0.1749	0.0382
Half load	7.2061	14.7889	68.5869	9.1694	0.2324	0.0162
Full load	7.4611	7.0560	77.0741	8.3878	0.0142	0.0068
Inner race with defect size 0.5x1x6 mm at variable speeds conditions						
No load	15.5743	10.9015	58.0487	15.0535	0.3564	0.0656
Half load	14.2714	11.5026	58.6813	15.1228	0.3532	0.0686
Full load	4.6993	15.7725	68.3142	10.9454	0.2490	0.0197
Inner race with defect size 1x3x9 mm at variable speeds conditions						
No load	0.6324	12.3843	66.2816	19.9790	0.6404	0.0823
Half load	1.6200	0.9218	34.6751	62.5130	0.2341	0.0360
Full load	0.0763	17.9148	71.2402	10.4938	0.2638	0.0111

Table C.5 Energy (J) for different DWT decomposition details and approximation for ball defect

(a) Ball defect under stationary operating conditions

Operating conditions	A	D1	D2	D3	D4	D5
Half load _600	33.0603	0.8356	21.4121	44.2874	0.3680	0.0366
Half load _900	26.6720	23.8964	49.1833	0.1619	0.0598	0.0265
Half load_1200	20.0009	13.9543	65.6833	0.2476	0.0796	0.0344
Nooad_600	31.6185	5.4199	58.5096	4.0283	0.3808	0.0429
Noload_900	8.3416	30.9423	60.6441	0.0566	0.0107	0.0047
Noload_`1200	6.9315	7.7652	80.9522	3.7852	0.5576	0.0084
Fullload_600	12.7763	0.5626	28.6682	57.9124	0.0593	0.0212
Fullload_900	6.9315	7.7652	80.9522	3.7852	0.5576	0.0084
Fullload_900	8.3416	30.9423	60.6441	0.0566	0.0107	0.0047

(b) Ball defect under non-stationary operating conditions

Variable load	A	D1	D2	D3	D4	D5
600	18.8982	0.6709	27.1168	53.0933	0.1898	0.0311
900	8.9347	7.1224	78.4854	4.9253	0.5091	0.0231
1200	6.2987	32.3988	61.2128	0.0698	0.0135	0.0064
Variable speed	A	D1	D2	D3	D4	D5
Full load	3.7200	18.1163	69.6958	8.1872	0.2719	0.0088
Half load	32.8643	9.2137	45.6615	11.9508	0.2738	0.0359
No load	34.2632	8.8974	44.7409	11.7507	0.3044	0.0434

Table C.6 Energy (J) for different DWT decomposition details and approximation for corrosion defect

(a) Corrosion with defect severity 2 at different loads (KW) and speeds (rpm) conditions

Load - speed	A	D1	D2	D3	D4	D5
No load - 600	9.5977	0.6168	17.3160	70.8929	1.1593	0.4173
No load - 900	65.5136	0.4957	33.5268	0.3605	0.0660	0.0374
No load - 1200	62.4882	7.0193	30.3116	0.1010	0.0572	0.0227
Half load - 600	9.5977	0.6168	17.3160	70.8929	1.1593	0.4173
Half load - 900	65.5136	0.4957	33.5268	0.3605	0.0660	0.0374
Half load- 1200	62.4882	7.0193	30.3116	0.1010	0.0572	0.0227
Full load- 600	7.0150	1.8201	87.3358	3.5778	0.2176	0.0337
Full load- 900	7.0150	1.8201	87.3358	3.5778	0.2176	0.0337
Full load-1200	5.9477	29.6753	62.3549	1.8421	0.1469	0.0330

(b) Corrosion with defect severity 3 at different loads (KW) and speeds (rpm) conditions

Load - speed	A	D1	D2	D3	D4	D5
No load - 600	0.3462	0.7970	19.9104	77.9788	0.8438	0.1238
No load - 900	2.6137	0.9719	95.7453	0.5136	0.0988	0.0567
No load - 1200	2.1889	17.8393	79.6589	0.1748	0.0810	0.0572
Half load - 600	0.3462	0.7970	19.9104	77.9788	0.8438	0.1238
Half load - 900	2.6137	0.9719	95.7453	0.5136	0.0988	0.0567
Half load - 1200	2.1889	17.8393	79.6589	0.1748	0.0810	0.0572
Full load- 600	0.0731	1.8613	94.6213	3.2056	0.1755	0.0632
Full load- 900	0.0731	1.8613	94.6213	3.2056	0.1755	0.0632
Full load-1200	0.2467	0.5782	21.4097	76.0065	1.5551	0.2038

(c) Corrosion with defect severity 4 at different loads (KW) and speeds (rpm) conditions

Load - speed	A	D1	D2	D3	D4	D5
No load - 600	0.3024	0.8917	17.9696	`80.0994	0.5885	0.1485
No load - 900	65.195	0.4098	34.0946	0.2304	0.0464	0.0228
No load - 1200	61.9384	6.7352	31.1768	0.0840	0.0447	0.0208
Half load - 600	0.3024	0.8917	17.9696	80.0994	0.5885	0.1485
Half load - 900	65.1959	0.4098	34.0946	0.2304	0.0464	0.0228
Half load - 1200	61.9384	6.7352	31.1768	0.0840	0.0447	0.0208
Full load- 600	0.1058	1.8069	94.3671	3.2796	0.3815	0.0591
Full load- 900	0.1058	1.8069	94.3671	3.2796	0.3815	0.0591
Full load- 1200	0.0846	9.6698	89.4236	0.7042	0.0907	0.0270

D: Fault severities prediction

DRNN have been tested under different operating conditions figures below illustrates the overall level of fault severities prediction under stationary and non -stationary operating conditions
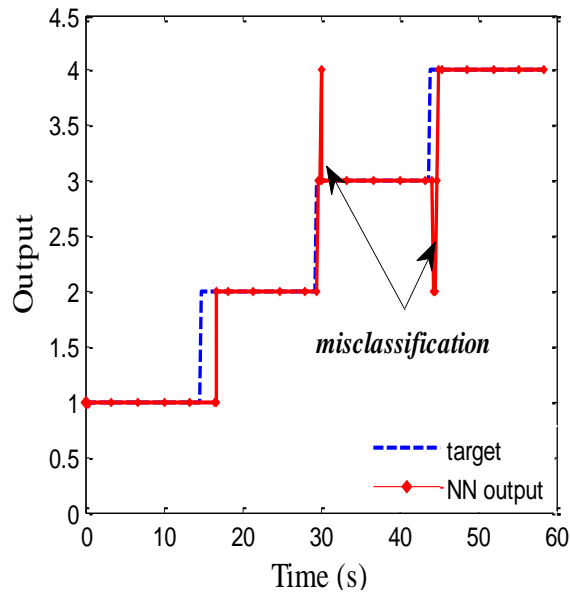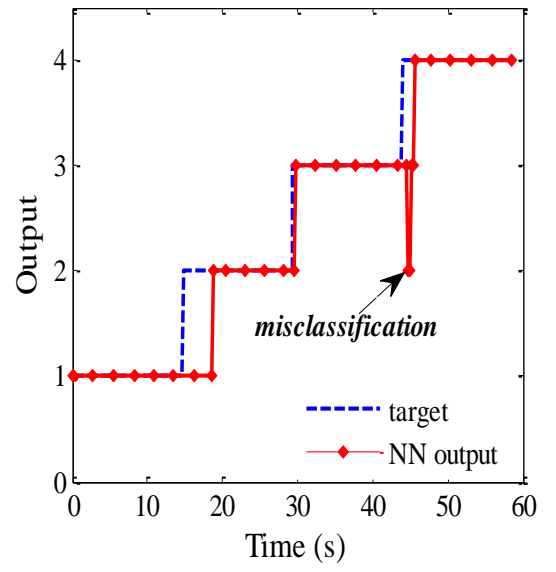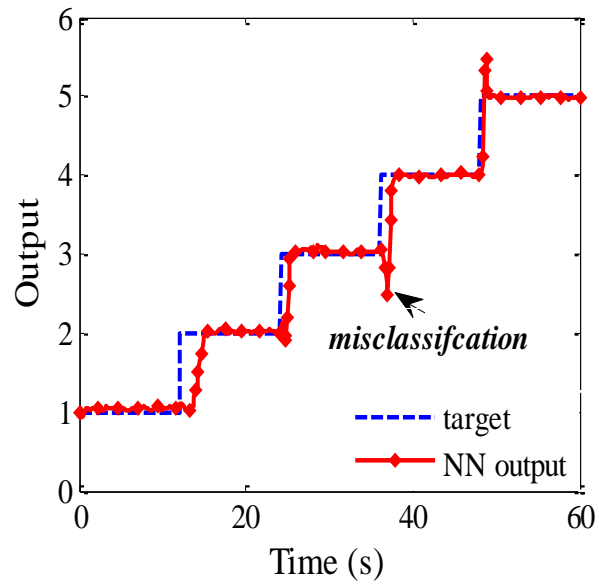
Figure D.1 DRNN performance to predict bearing fault severity (a) outer, (b) inner and (c) corrosion half load and 600rpm speed
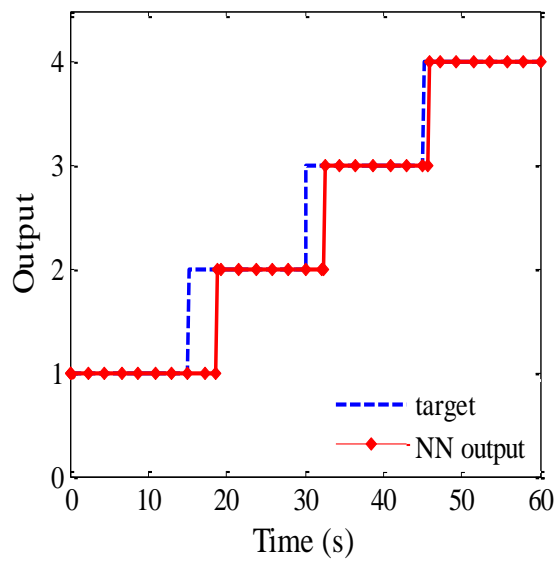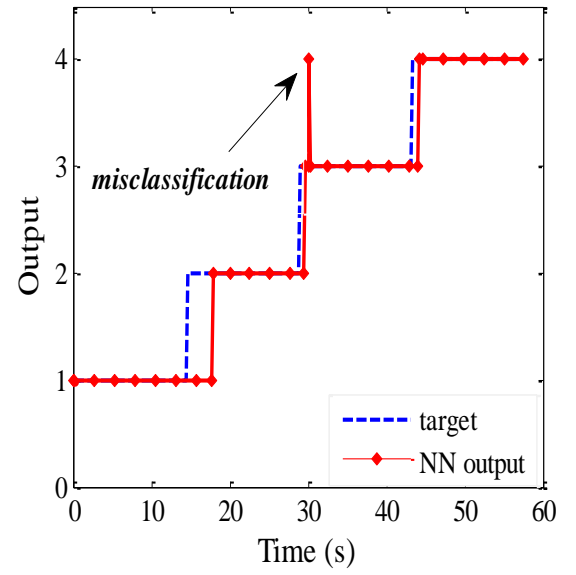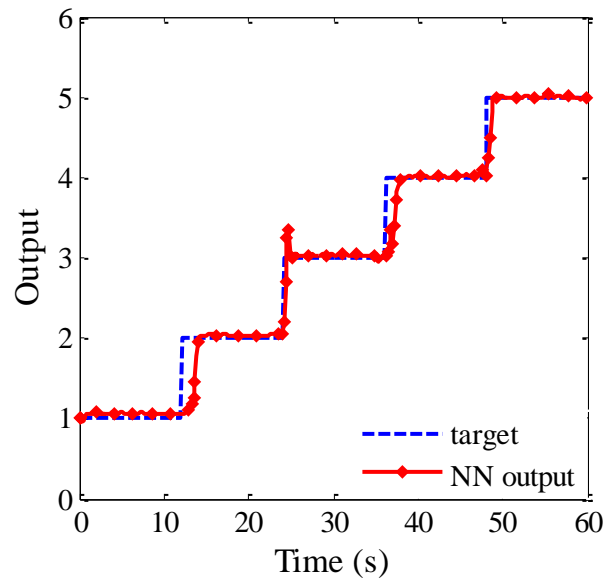
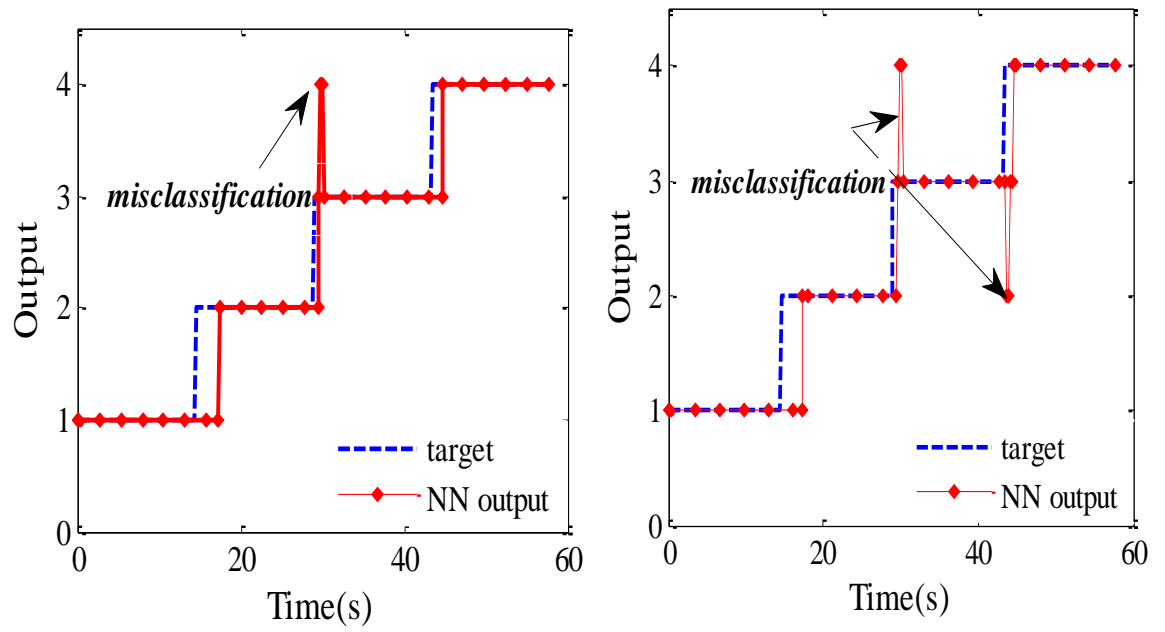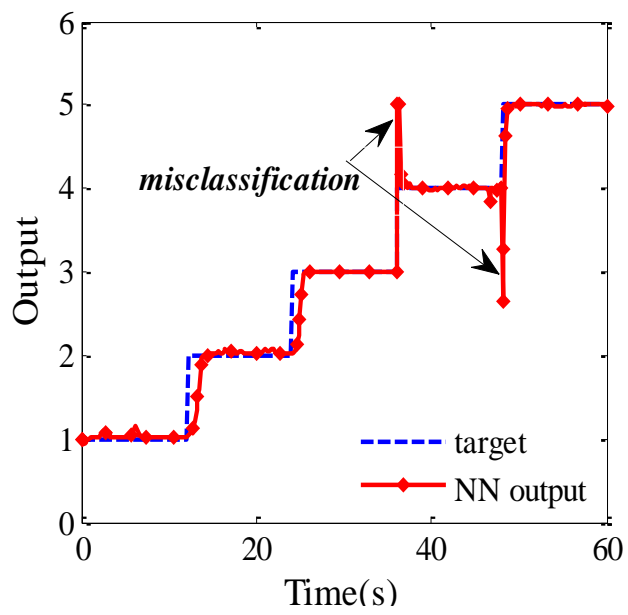Figure D.2 DRNN performance to predict bearing fault severity (a) outer, (b) inner and (c) corrosion half load and 900rpm speed
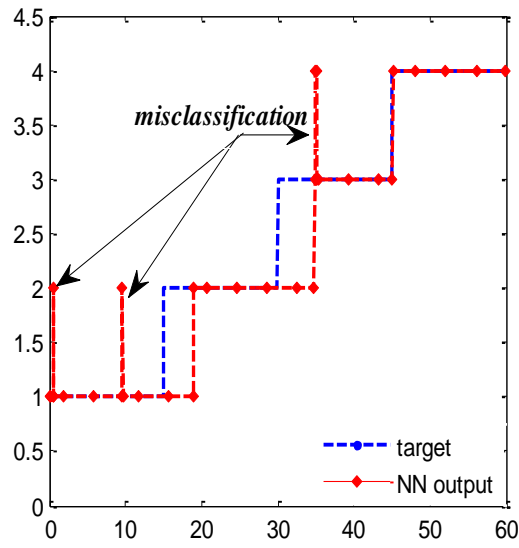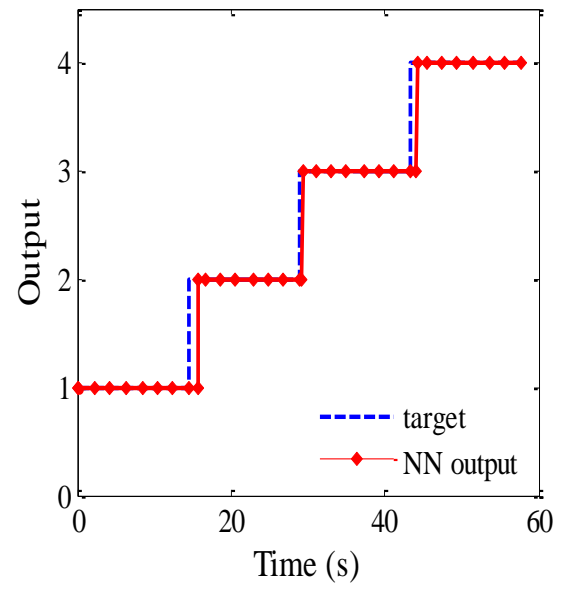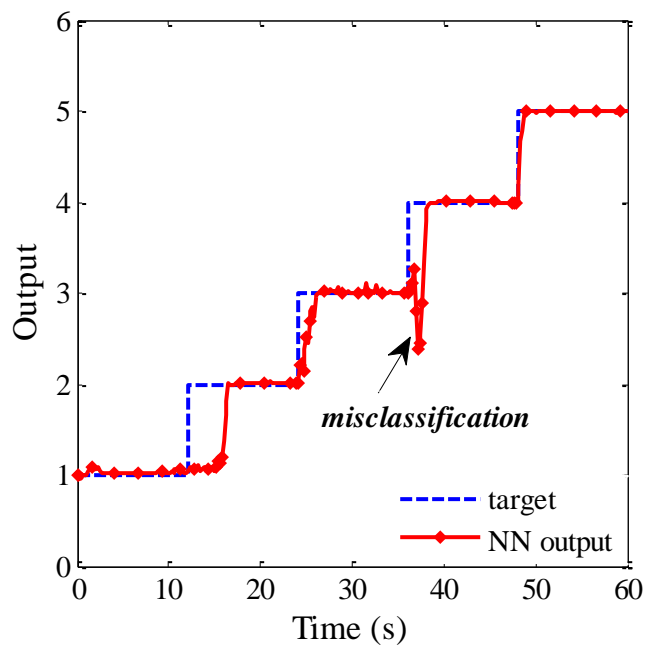
Figure D.3 DRNN performance to predict bearing fault severity (a) outer, (b) inner and (c) corrosion at no load and 600 (rpm) speed
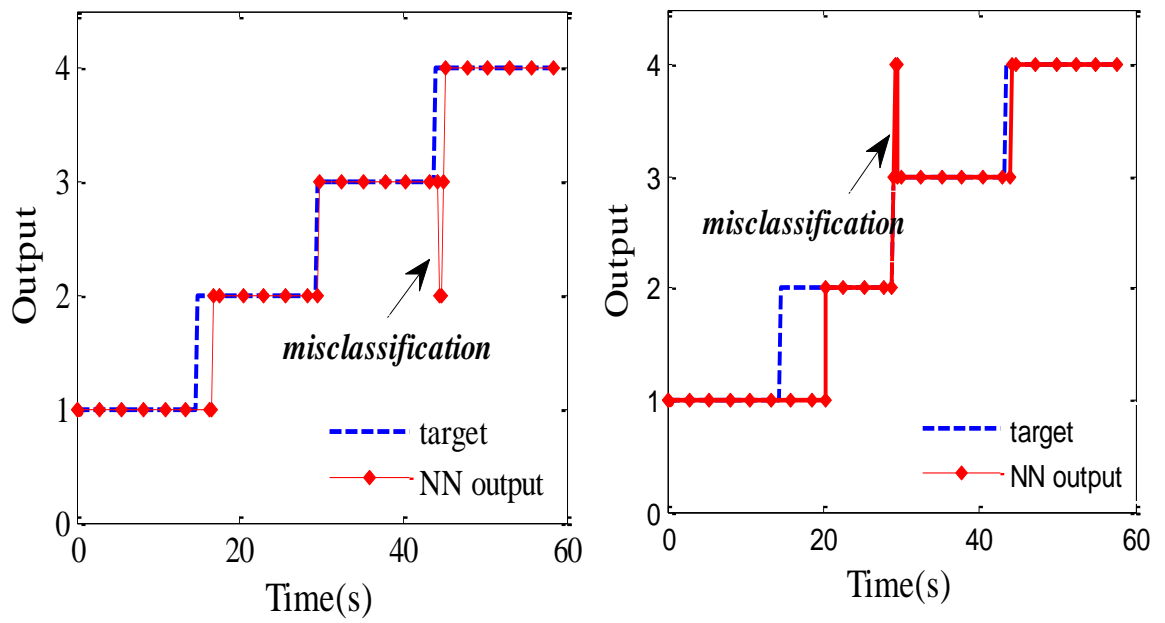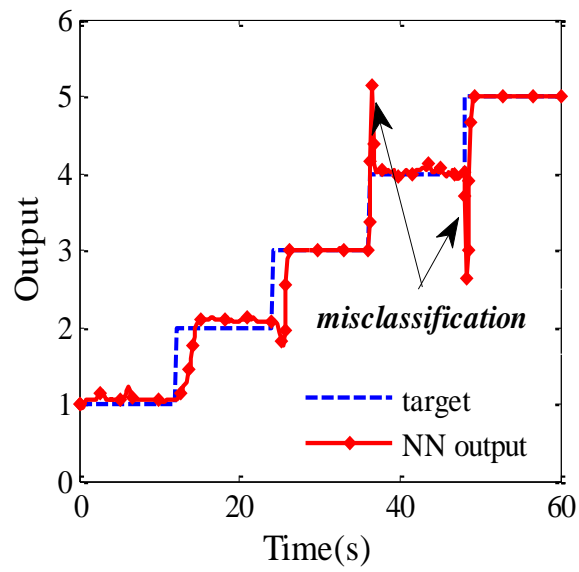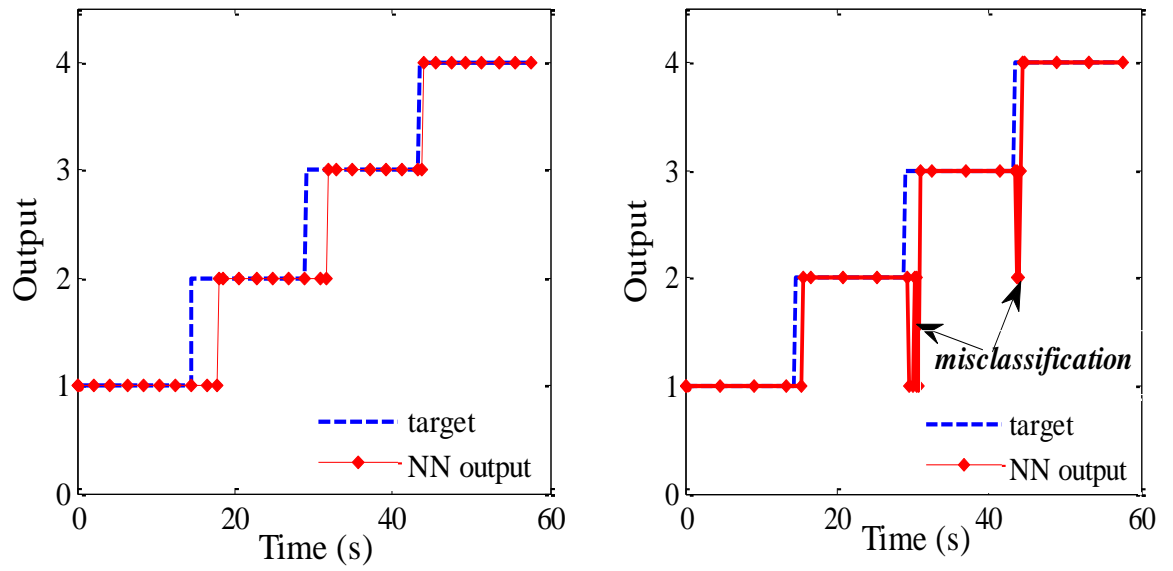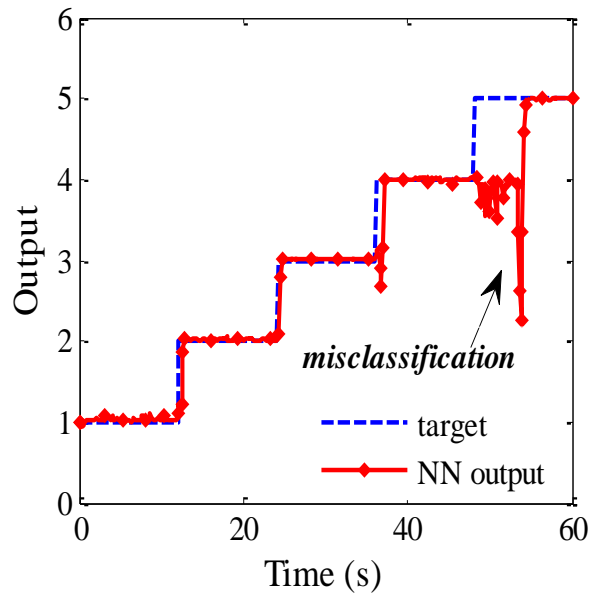
misclassification

misclassification

(a)

(b)

misclassification

(c)

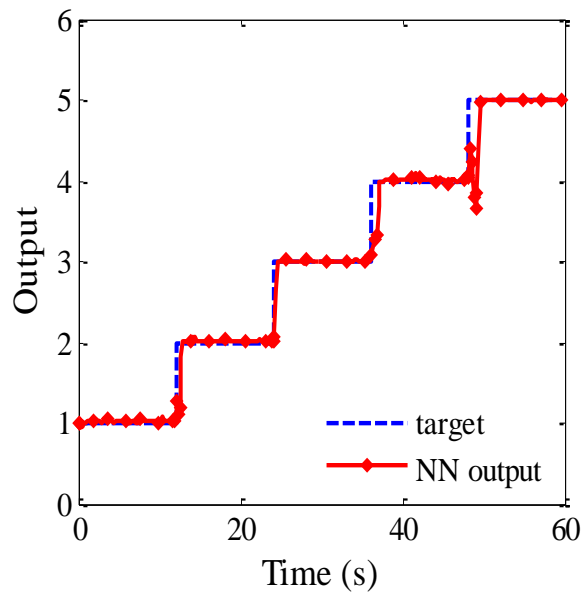Figure D.4 DRNN performance to predict bearing fault severity (a) outer, (b) inner and (c) corrosion at no load and 900rpm speed

Figure D.5 DRNN performance to predict bearing fault severity (a) outer, (b) inner and (c) corrosion at full load and 600 rpm speed

Figure D.6 DRNN performance to predict bearing fault severity (a) inner,
(b) outer and (c) corrosion at full load and 900rpm speed
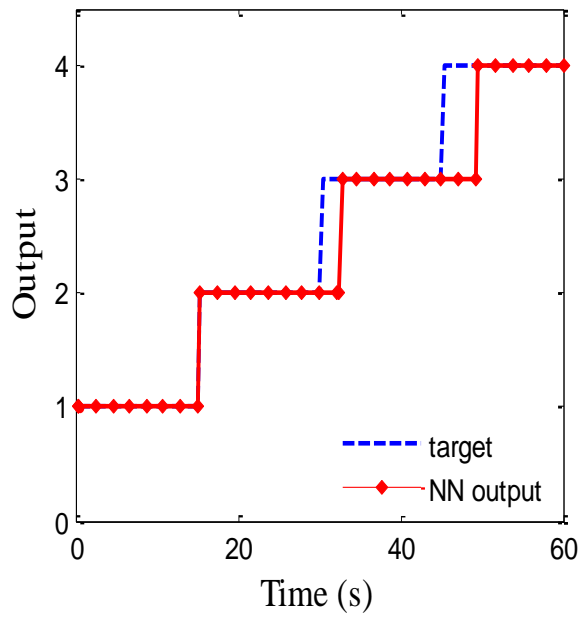
(a)
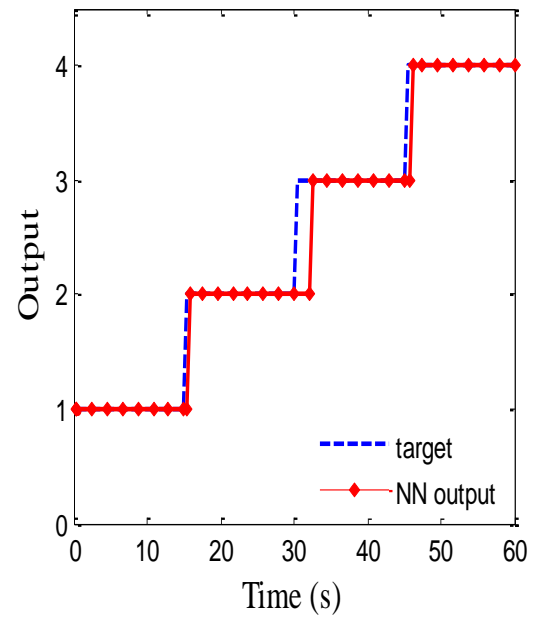
(b)
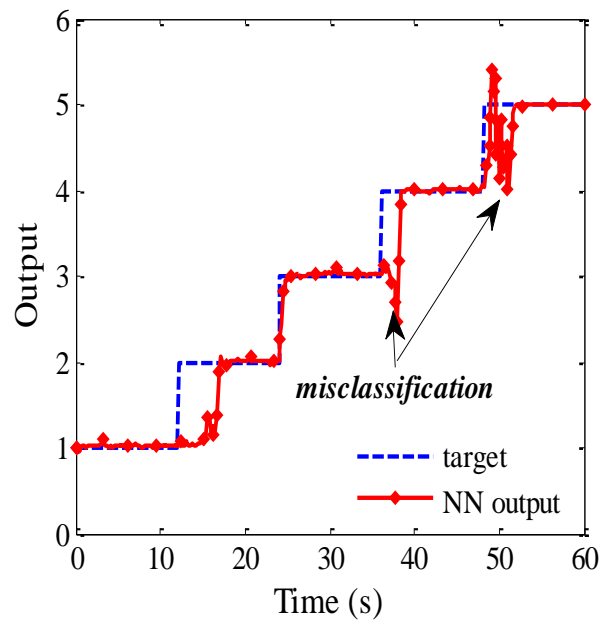
(c)

Figure D.7 DRNN performance to predict bearing fault severity (a) inner, (b) outer and (c) corrosion at variable load and 1200 rpm speed
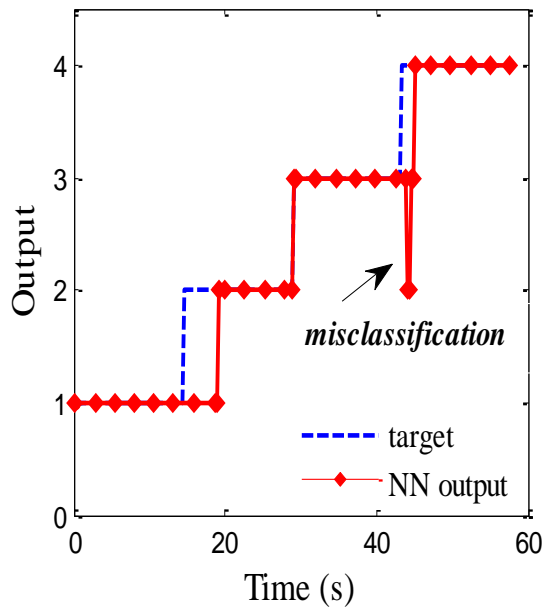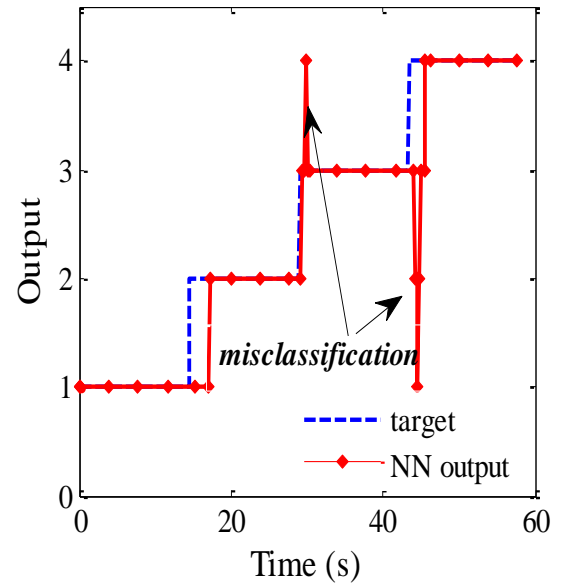
Figure D.8 DRNN performance to predict bearing fault severity (a) inner, (b) outer and (c) corrosion at variable load and 900rpm speed

E: On line testing

To measure the performance p of DRNN, online testing using test data sets different

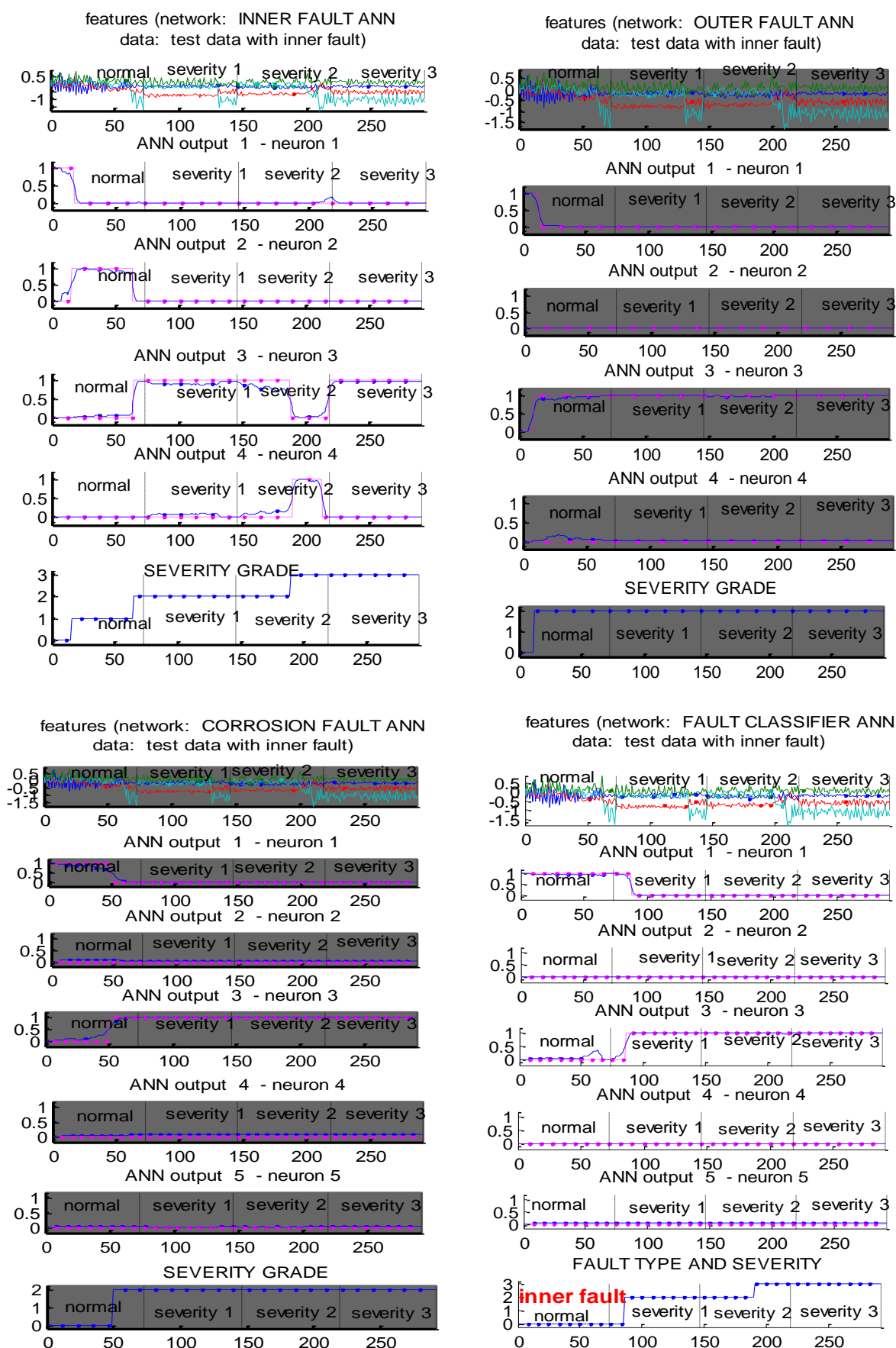form training and validation data set to calculate the time need to diagnosis fault

Figure E1 on line testing for variable speed and half load condition-inner race fault
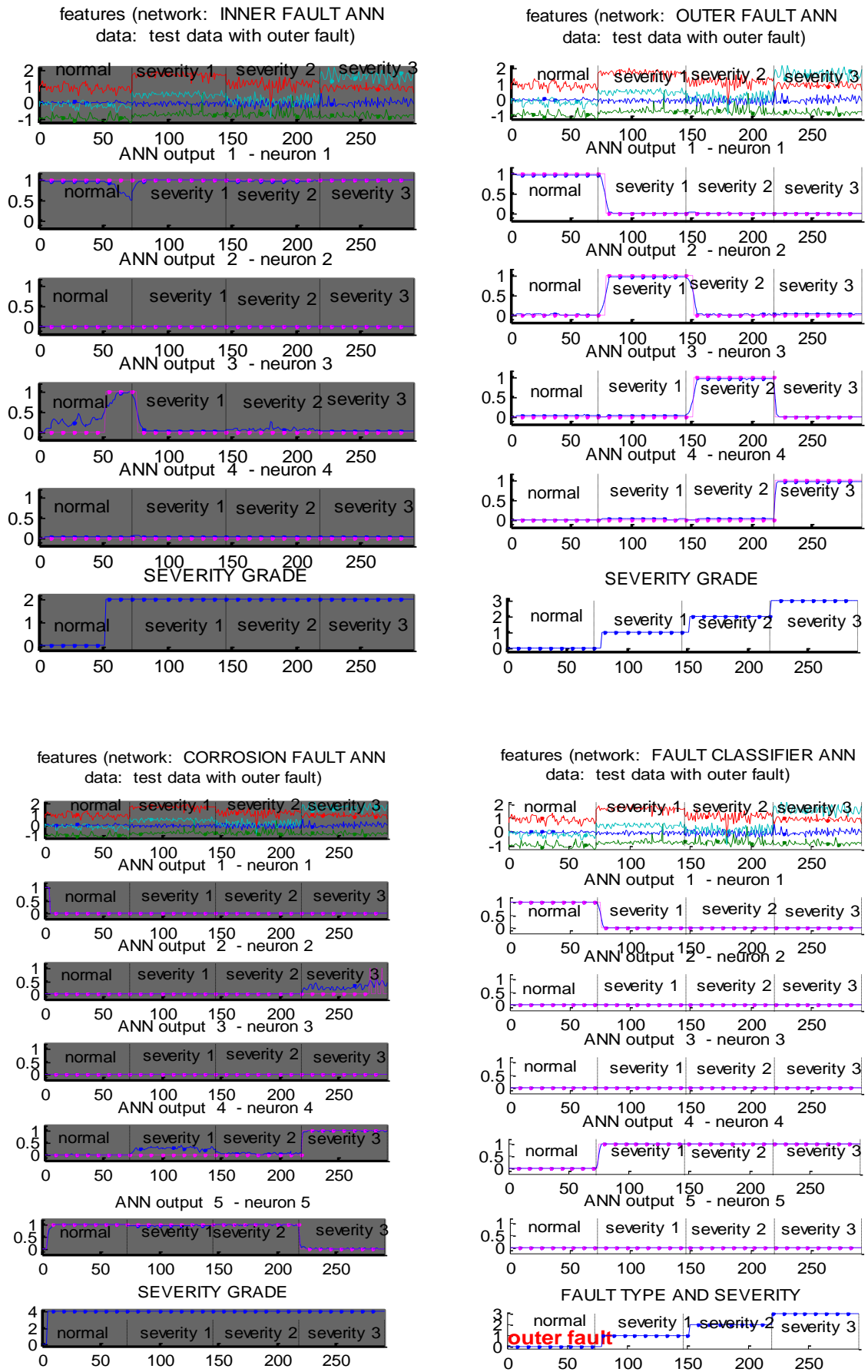
Figure E.2 on line testing for variable speed and half load condition-outer race fault
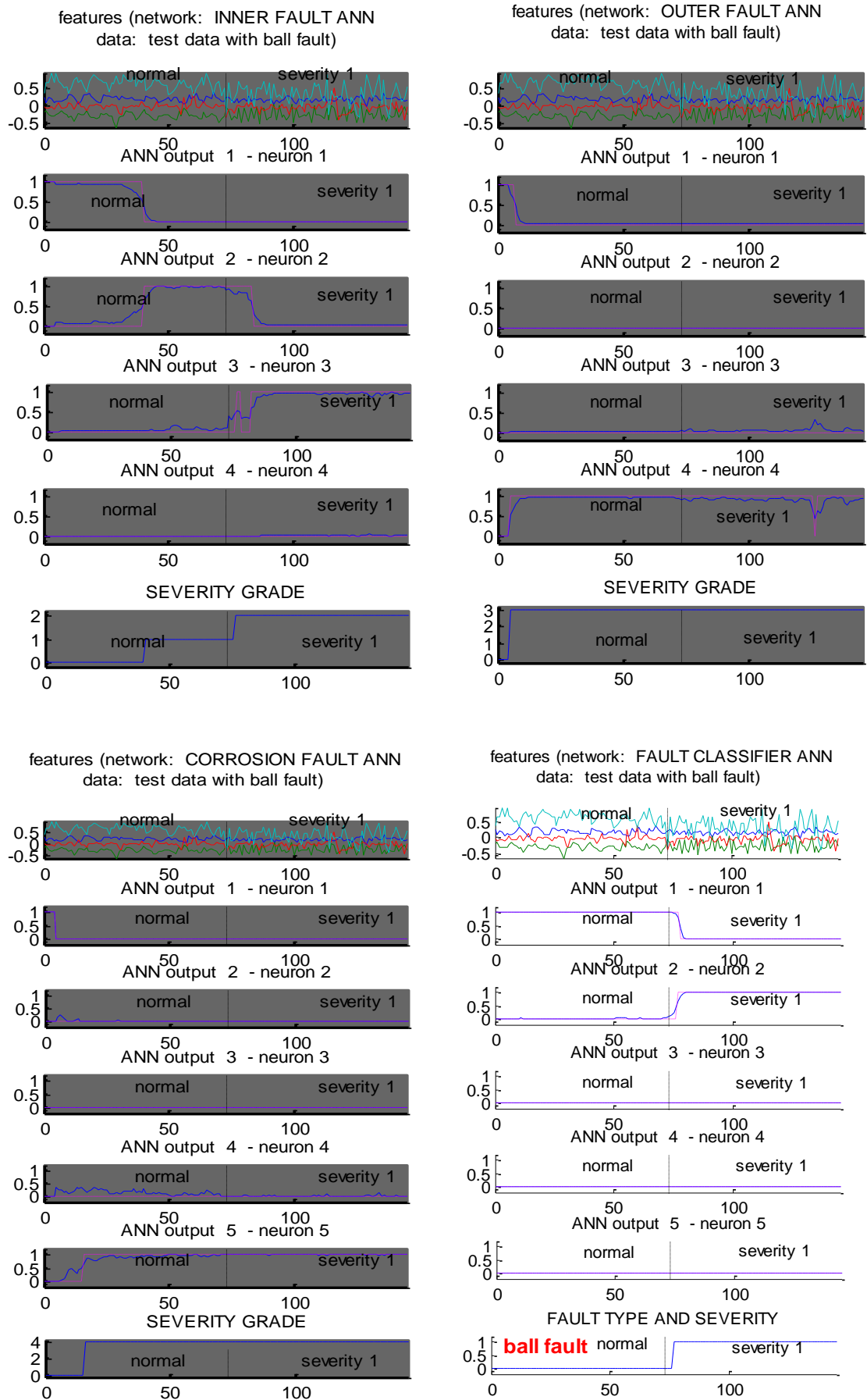
Figure E.3 on line testing for variable speed and half load condition-ball fault
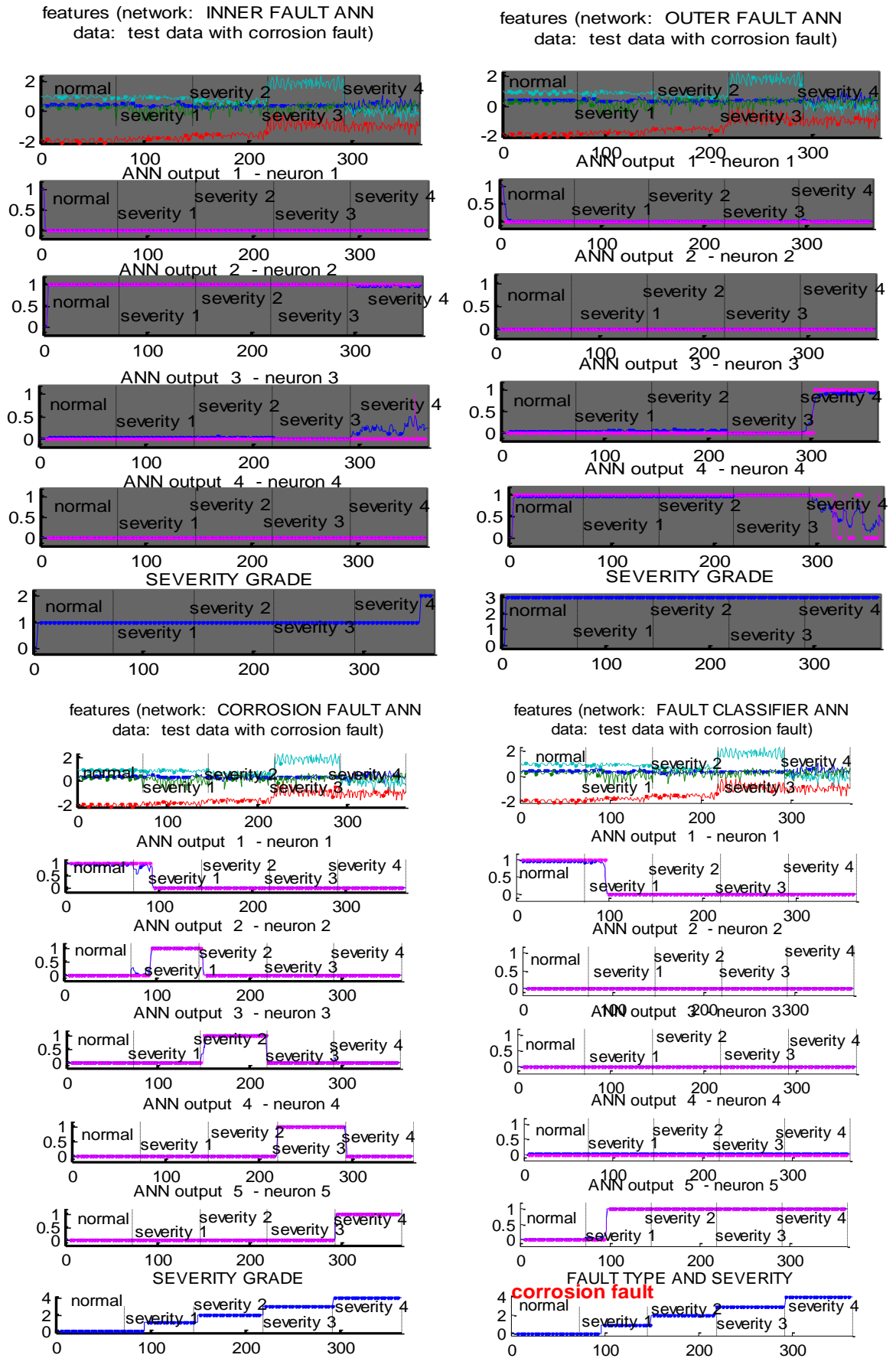
Figure E.4 on line testing for variable speed and half load condition-corrosion fault

F: Selected Publications

1- Abed W, Sharma SK, Sutton R, and Amit Motwani (2015). 'A robust bearing fault detection and diagnosis technique for brushless DC motors under non-stationary operating conditions' *Journal of Control, Automation and Electrical Systems*, doi:10.1007/s40313-015-0173-7.

2- Abed W, Sharma SK, Sutton R (2015)'Neural network fault diagnosis of a trolling motor based on feature reduction techniques for an unmanned surface vehicle', *Proceedings of the Institution of Mechanical Engineers, Part I: Journal of Systems and Control Engineering* doi: 10.1177/0959651815581095.

3- Abed W, Sharma SK, Sutton R. (2013) 'Fault diagnosis of brushless DC motor for an aircraft actuator using a neural wavelet network' *Proceedings of the 1st IET Control and Automation Conference*, Conference Aston Lakeside Centre, Birmingham, UK, 4 - 5 June, pp.1-6, doi: org/10.1049/cp.2013.0020.

4- Abed W Sharma SK, Sutton R. (2014) 'Intelligent Fault Diagnosis of an Unmanned Underwater Vehicle Electric Thruster Motor', *the Global Event for Undersea Defence and Technology (UDT)*, Liverpool, UK, 10-12 June.

5- Abed W, Sharma SK, Sutton R. (2104) 'Diagnosis of bearing fault of brushless DC motor based on dynamic neural network and orthogonal fuzzy neighborhood discriminant analysis', *10th International Conference of the United Kingdom, Automatic Control Council (UKACC)*, Loughborough University, UK, 9 - 11 July, pp. 378-382, doi: 10.1109/CONTROL.2014.6915170.

6- Abed W, Sharma SK, Sutton R.(2015)'Corrosion Fault Diagnosis on Rolling Element Bearing under variable load and speed conditions' , *9th IFAC Symposium on Control of Power and Energy Systems (CPES)*, New Delhi, India, 9-11 December.